Fachbereich Medizin der Justus-Liebig-Universität Gießen

Physiologisches Institut

Charakterisierung von Funktionen der mitochondrialen Atmungskette in Mäusen durch xenotope Expression einer alternativen Oxidase (AOX)

Habilitationsschrift
zur Erlangung der *Venia legendi* des Fachbereichs Medizin
der Justus-Liebig-Universität Gießen

für das Fach
Physiologie

vorgelegt von
Dr. med. Marten Szibor

Gießen (2021)

Diese kumulative Habilitationsschrift basiert auf den folgenden Publikationen.

Bypassing mitochondrial complex III using alternative oxidase inhibits acute pulmonary oxygen sensing

Sommer, N., Alebrahimdehkordi, N., Pak, O., Knoepp, F., Strielkov, I., Scheibe, S., Dufour, E., Andjelković, A., Sydykov, A., Saraji, A., Petrovic, A., Quanz, K., Hecker, M., Kumar, M., Wahl, J., Kraut, S., Seeger, W., Schermuly, R. T., Ghofrani, H. A., Ramser, K., Braun, T., Jacobs, H. T., Weissmann, N. & **Szibor, M.**

Sci Adv **6,** eaba0694 (**2020**)

Respiratory chain signalling is essential for adaptive remodelling following cardiac ischaemia

Szibor, M., Schreckenberg, R., Gizatullina, Z., Dufour, E., Wiesnet, M., Dhandapani, P. K., Debska-Vielhaber, G., Heidler, J., Wittig, I., Nyman, T. A., Gärtner, U., Hall, A. R., Pell, V., Viscomi, C., Krieg, T., Murphy, M. P., Braun, T., Gellerich, F. N., Schlüter, K.-D. & Jacobs, H. T.

J Cell Mol Med **24,** 3534–3548 (**2020**)

Bioenergetic consequences from xenotopic expression of a tunicate AOX in mouse mitochondria: Switch from RET and ROS to FET

Szibor, M., Gainutdinov, T., Fernández-Vizarra, E., Dufour, E., Gizatullina, Z., Debska-Vielhaber, G., Heidler, J., Wittig, I., Viscomi, C., Gellerich, F. & Moore, A. L.

Biochim Biophys Acta Bioenerg **1861,** 148137 (**2020**)

Alternative Oxidase Attenuates Cigarette Smoke-induced Lung Dysfunction and Tissue Damage

Giordano, L., Farnham, A., Dhandapani, P. K., Salminen, L., Bhaskaran, J., Voswinckel, R., Rauschkolb, P., Scheibe, S., Sommer, N., Beisswenger, C., Weissmann, N., Braun, T., Jacobs, H. T., Bals, R., Herr, C. & **Szibor, M.**

American Journal of Respiratory Cell and Molecular Biology **60,** 515–522 (**2019**)

Perturbed Redox Signaling Exacerbates a Mitochondrial Myopathy

Dogan, S. A., Cerutti, R., Benincá, C., Brea-Calvo, G., Jacobs, H. T., Zeviani, M., **Szibor, M.** & Viscomi, C.

Cell Metabolism **28,** 764–775.e5 (**2018**)

Broad AOX expression in a genetically tractable mouse model does not disturb normal physiology

Szibor, M., Dhandapani, P. K., Dufour, E., Holmström, K. M., Zhuang, Y., Salwig, I., Wittig, I., Heidler, J., Gizatullina, Z., Gainutdinov, T., German Mouse Clinic Consortium, Fuchs, H., Gailus-Durner, V., de Angelis, M. H., Nandania, J., Velagapudi, V., Wietelmann, A., Rustin, P., Gellerich, F. N., Jacobs, H. T. & Braun, T.

Dis Model Mech **10,** 163–171 (**2017**)

Inhaltsverzeichnis

Abkürzungen

$\Delta\psi$	Mitochondriales Membranpotential (elektrochemischer Protonengradienten)
AMPK	Adenosinmonophosphat-aktivierte Proteinkinase
AOX	Alternative Oxidase
AOX^{Rosa26}	AOX Mauslinie mit Transgen Integration im *Rosa26*-Lokus
BN-PAGE	Blau-native (BN) Polyacrylamid-Gelelektrophorese (PAGE)
COPD	*Chronic Obstructive Pulmonary Disease* (chronisch obstruktive Lungenerkrankung)
CoQ	Coenzym Q
COX	Cytochrom *c*-Oxidase oder Komplex IV der mitochondrialen Atmungskette
DNA	*Deoxyribonucleic Acid* (Desoxyribonukleinsäure, DNS)
ETK	Elektronentransportkette (mitochondrial)
ESR	Elektronenspinresonanz(-Spektroskopie)
$FADH_2$	Flavin-Adenin-Dinukleotid (FAD) + Hydrogen (H)
FET	*Forward Electron Transport* (vorwärts-gerichteter Elektronentransport)
GTP	Guanosintriphosphat
HIF-1α	Hypoxie-induzierbarer Faktor 1α
HPV	Hypoxische pulmonale Vasokonstriktion
iMEF	Immortalisierte embryonale Mausfibroblasten
IR	Ischämie-Reperfusion
KO	*Knockout* (genetische Ablation)
Komplex I	NADH:Ubichinon-Oxidoreduktase
Komplex II	Succinat:Ubichinon-Oxidoreduktase oder Succinat-Dehydrogenase (SDH)
Komplex III	Cytochrom *bc1*-Komplex
Komplex IV	Cytochrom *c*-Oxidase (COX)
Komplex V	F_1F_0 ATPase (mitochondrial)
LAD	Links-anteriore absteigende Koronararterie (*left anterior descending artery*)
LVDP	Linksventrikulärer Druck (*left-ventricular-developed pressure*)
MitAOX	AOX Mauslinie mit zufälliger genomischer Transgen Integration
mRNA	*Messenger Ribonucleic Acid* (Boten-Ribonukleinsäure, RNS)
mtDNA	*Mitochondrial Deoxyribonucleic Acid* (mitochondriales Genom)
NADH	Nicotinamid-Adenin-Dinukleotid (NAD) + Hydrogen (H)
Ndi1	NADH Dehydrogenase aus *Saccharomyces cerevisiae*
nPG	n-Propylgallat (AOX-Inhibitor)
OXPHOS	Oxidative Phosphorylierung
PAP	pulmonal-arterieller Druck
PASMC	*Pulmonary Artery Smooth Muscle Cells* (pulmonal-arterielle glatte Muskelzellen)
PH	Pulmonale Hypertonie
P_{syst}	*Systolic Pressure* (systolischer Druck)
RCI	Respiratorische Kontrollindex
RET	*Reverse Electron Transport* (reverser Elektronentransport)
RNA	*Ribonucleic Acid* (Ribonukleinsäure)
RNS	*Reactive Nitrogen Species* (reaktive Stickstoffspezies)
ROS	*Reactive Oxygen Species* (reaktive Sauerstoffspezies)
rRNA	*Ribosomal Ribonucleic Acid* (ribosomale Ribonukleinsäure, rRNS)
tRNA	*Transfer Ribonucleic Acid* (Transfer-Ribonukleinsäure, tRNS)
SDH	Succinat-Dehydrogenase oder Komplex II der mitochondrialen Atmungskette
SOD	Superoxiddismutase
WT	Wildtyp

„Life is a chemical reaction. Metabolism and life move forward only if energy is released in the overall reaction, as stipulated by the second law of thermodynamics, which permits no exceptions."[1]

1 Einleitung

1.1 Entwicklung des Begriffs der metabolischen Flexibilität

Der Begriff „Stoffwechsel" umschreibt die Summe aller chemischen Reaktionen, die in den Zellen eines Organismus ablaufen. Der Stoffwechsel liefert sowohl die Energie für lebenswichtige Prozesse als auch Bausteine für die Neusynthese von organischem Material[2]. Die Anpassungsfähigkeit des Stoffwechsels an die Verfügbarkeit von Substraten auf der einen Seite und den eigentlichen Bedarf auf der anderen Seite ist fundamental wichtig für die Lebensfähigkeit eines Organismus. Diese macht ihn widerstandsfähig gegen Schwankungen in Energieangebot und -nachfrage wie sie bei Nahrungsüberschuss oder Hunger, Ruhe oder erhöhter Aktivität auftreten. Sie wird durch Substraterkennung sowie dessen Transport, Speicherung und angepasste Verwertung erreicht[3–6]. Die metabolische Anpassungsfähigkeit markiert dabei einen schmalen Grat zwischen Gesundheit (Funktion) und Krankheit (Dysfunktion)[3–6]. Die molekularen Zusammenhänge zwischen regulärem Stoffwechsel und der Entwicklung einer krankhaften Störung werden bisher nur unzureichend verstanden und sind im Kern Gegenstand der hier vorgestellten Untersuchungen.

Schon 1983 wurde das Prinzip der metabolischen Anpassungsfähigkeit als „metabolische Plastizität" im Skelettmuskel beschrieben und dessen Bedeutung für den Erhalt der Gesundheit herausgestellt[7]. Aus diesem Konzept entwickelte sich später, ebenfalls in Bezug auf Stoffwechselvorgänge im Skelettmuskel, der Begriff „metabolische Flexibilität"[8]. Der wesentliche Befund war, dass Skelettmuskeln von schlanken Personen die Fähigkeit besitzen, die jeweilige Substratoxidation flexibel an Fastenzustände und alternierende Insulinlevel (hier eingestellt durch Infusionen) anzupassen. Im Vergleich dazu zeigten Übergewichtige generell eine geringere Abhängigkeit von Fettsäureoxidation und waren nicht in der Lage, diese nach Fasten zu erhöhen (oder nach Insulininfusionen zu reduzieren). Die Beschreibung „metabolisch unflexibel" charakterisiert diese eingeschränkte metabolische Anpassungsfähigkeit[8,9]. Inzwischen weiß man, dass schlanke Personen im Gegensatz zu übergewichtigen mittels metabolischer Flexibilität nach einer fettreichen Diät in der Lage sind, die Fettsäureoxidation auf Kosten der Glukoseoxidation zu erhöhen[10]. Es muss also maladaptive Mechanismen als Teil eines pathophysiologischen Vorgangs geben, die für den Verlust der metabolischen Flexibilität verantwortlich sind. Das ist insofern erstaunlich, weil sich der Mensch entwicklungsgeschichtlich sehr gut daran angepasst hat, Kohlenhydrate, Fettsäuren und Aminosäuren variabel zu verwerten. Insbesondere das Leben in entwickelten Ländern ist allerdings geprägt von einem permanenten Nahrungsüberangebot. Bei gleichzeitigem Bewegungsmangel führt dies zu einer metabolischen Ausnahmesituation, die evolutionär betrachtet beispiellos ist und in der Summe für die Entwicklung sogenannter metabolischer Erkrankungen verantwortlich gemacht wird[11,12]. Welche molekularen Mechanismen metabolische Erkrankungen jedoch steuern, ist in weiten Teilen unklar. Ein interessanter Ansatz geht davon aus, dass chronische Nährstoffüberlastung insbesondere auf der Ebene der Mitochondrien zum Verlust der metabolischen Flexibilität führt[13]. Damit treten Mitochondrien aus ihrem Nischendasein in

Ätiologien seltener Erkrankungen und erscheinen als mögliche Treiber in der Entwicklung sogenannter Volkskrankheiten.

1.2 Mitochondrien, die Kraftwerke der Zelle

Der Begriff Mitochondrion wurde erstmals im Jahr 1898 von Carl Benda verwendet und setzt sich aus zwei griechischen Wörtern zusammen, *„mitos"* (Faden) und *„chondrion"* (Körnchen)[14]. Als intrazelluläre Strukturen wurden Mitochondrien aber schon früher in den 1840er Jahren beschrieben[14]. Um 1890 erkannte Richard Altmann deren ubiquitäres Vorkommen und nannte sie zunächst „Bioblasten". Interessanterweise ging Altmann davon aus, dass Bioblasten „Elementarorganismen" seien, d.h. Organismen, die im Inneren einer Zelle „leben" und dort besondere Funktionen übernehmen[14]. Tatsächlich geht eine weit verbreitete Theorie davon aus, dass Mitochondrien ehemalige Endosymbionten sind. Diese sogenannte Endosymbiontentheorie wurde vor allem durch Lynn Margulis bekannt gemacht[15] und sieht einen engen zeitlichen Zusammenhang zwischen der Ausbildung von Mitochondrien und der Entstehung von eukaryotischem Leben[16]. Eine Kernaussage der Endosymbiontentheorie ist, dass Archaeen, als die Sauerstoffkonzentration in der Atmosphäre durch die Photosynthese anstieg, zuvor freilebende Alphaproteobakterien phagozytierten, weil diese in einer Reihe von Redoxreaktionen den molekularen Sauerstoff sicher zu Wasser entgiften konnten. Die Nachkommen dieser Alphaproteobakterien sind unsere heutigen Mitochondrien. Ein bislang fehlendes Bindeglied (*„missing link"*) für diese Endosymbiontentheorie wurde kürzlich entdeckt und die Archaeen-Art nach ihrem Fundort Lokiarchaeota genannt[16]. Obwohl die ursprüngliche Aufgabe der Alphaproteobakterien möglicherweise also darin bestand, die Archaeen vor der Bildung von potenziell schädlichen Sauerstoffradikalen (*reactive oxygen species*, ROS) zu schützen, werden Mitochondrien heute häufig als Kraftwerke der Zelle bezeichnet. Dies geht auf ihre zentrale Fähigkeit zurück, Energie in Form von Adenosintriphosphat (ATP) durch die sogenannte oxidative Phosphorylierung (OXPHOS) bereitzustellen. Interessanterweise ist die ATP-Generierung durch OXPHOS an die Funktion eben jener Redoxreaktionen gekoppelt, welche molekularen Sauerstoff entgiften. Die entscheidenden Redoxreaktionen laufen in einer Elektronentransportkette (ETK) ab, welche häufig auch als die mitochondriale Atmungskette bezeichnet wird.

Die Endosymbiontentheorie und nachfolgend abgelaufene Anpassungsvorgänge erklären auch eine Reihe biologischer Besonderheiten der Mitochondrien. Mitochondrien sind von einer doppelten Membran umgeben, wodurch sie vier distinkte Kompartimente bilden: (i) die äußere Membran, (ii) die innere Membran, (iii) den intermembranären Raum und (iv) die Matrix. Mitochondrien vermehren sich zytosolisch unabhängig von der Zelle und besitzen ein eigenes, zirkuläres Genom, die mitochondriale DNA (mtDNA)[17–19]. Die humane mtDNA ist 16.569 Basenpaare lang[20] und kodiert 22 tRNAs, 2 rRNAs und 13 mRNAs (essentielle Untereinheiten von Komplexen der ETK)[17–19]. Damit kodiert die mtDNA aber nur einen Bruchteil dessen, was unabhängiges Leben möglich macht. Im Laufe der Evolution wurden die meisten der anfänglich mtDNA-kodierten Gene in die Kern-DNA transferiert, während es keine Hinweise für einen Transfer regulatorischer Kern-kodierter Gene in entgegengesetzter Richtung gibt. Wenn das Vorhandensein mtDNA-kodierter Gene also keine evolutionäre Momentaufnahme ist, muss es einen ausreichenden Selektionsdruck für beides geben, den Gentransfer von den Mitochondrien in den Kern aber eben auch den Verbleib einzelner Gene in den

Mitochondrien. Dies wird seit langem als Hinweis darauf gedeutet, dass die verbliebenen Gene nicht nur essentielle Strukturproteine darstellen, sondern durch ihre räumliche Nähe zum Ort des Bedarfs (ETK) möglicherweise einer Redox-abhängigen Regulation unterliegen[21]. Der mito-nukleäre Gentransfer hat als weitere Konsequenz, dass sämtliche Regulatoren mitochondrialer Funktionen einschließlich der mitochondrialen Biogenese und der ETK-Komplex-Assemblierung von Kern-kodierten Faktoren abhängig sind. Diese Tatsache bedingt, dass metabolische Homöostase/Flexibilität, d.h. bedarfsgerechte Energiebereitstellung, nur durch fein abgestimmte, intergenomische Regulation möglich ist. Die Kern-gesteuerte Anpassung mitochondrialer Stoffwechselaktivitäten wird dabei oft auch als „anterograde Regulation" bezeichnet. Eukaryotischen Zellen stellen durch die anterograde Regulation sicher, dass der mitochondriale Stoffwechsel funktionsfähig ist, bevor komplexe zelluläre Prozesse initiiert werden (wie z. B. Differenzierung). Aufgrund der reziproken Abhängigkeit muss der Informationsaustausch allerdings bidirektional funktionieren. Tatsächlich können Mitochondrien über sogenannte „retrograde Signale"[22,23] wie die Freisetzung von Cytochrom *c* den geordneten Zelltod (Apoptose) auslösen[24,25], durch Aktivierung der Adenosinmonophosphat-aktivierten Proteinkinase (AMPK) die mitochondriale Fission und Fusion anpassen[26,27], durch veränderte ROS-Produktion die nukleärer Genexpression beeinflussen[28,29] oder durch Freisetzung von mtDNA Immunantworten modulieren[30,31]. Mitochondrien spielen ebenfalls eine wichtige Rolle in der Ionenhomöostase[32–35]. Eine herausragende Rolle spielt dabei Kalzium, das nicht nur zytosolische Funktionen reguliert (wie z. B. die elektromechanische Kopplung in kontraktilen Geweben), sondern zugleich die mitochondriale Energiebereitstellung steuert. Diese wird oft als Bioenergetik bezeichnet[35].

Der zentrale Baustein für die Energiebereitstellung, die mitochondriale ETK, ist in die innere Membran eingebettet. Die ETK wird im Wesentlichen aus vier Proteinkomplexen und zwei integrierten Redoxpartnern (Coenzym Q, CoQ, und Cytochrom *c*) gebildet[36]. NADH:Ubichinon-Oxidoreduktase (Komplex I) und Succinat:Ubichinon-Oxidoreduktase (auch Succinat-Dehydrogenase oder Komplex II) oxidieren spezifische Substrate und reduzieren den CoQ-Pool. Die funktionell in Reihe geschalteten Komplexe Cytochrom *bc1*-Komplex (Komplex III) und Cytochrom *c*-Oxidase (COX oder auch Komplex IV) und Redoxpartner Cytochrom *c* oxidieren den CoQ Pool und reduzieren am Komplex IV molekularen Sauerstoff kontrolliert zu Wasser. Diese Funktion der ETK wurde bereits in den 1940er und 1950er Jahren ganz wesentlich durch Arbeiten von Lehninger, Racker, Chance, Boyer, Ernster und Slater geprägt[37]. Dabei ging man anfangs davon aus, dass der Elektronenfluss durch die ETK selbst an die ATP-Synthese gekoppelt ist, die sogenannte „chemische Kopplungshypothese"[37]. Inzwischen weiß man jedoch, dass der Elektronenfluss durch die ETK nur indirekt die ATP-Synthese beeinflusst. Tatsächlich koppeln die Komplexe I, III und IV den Elektronenfluss an einen Protonenexport aus der mitochondrialen Matrix in den intermembranären Raum. Durch diesen Protonentransport entsteht ein elektrochemischer Protonengradient ($\Delta\psi$). Da die innere mitochondriale Membran für Protonen weitestgehend undurchlässig ist, wird dieser Gradient (oft nur als Membranpotential bezeichnet) zur Triebkraft für die ATP-Erzeugung am Komplex V (F_1F_0 ATPase). Dieser Zusammenhang ist bekannt als die „chemiosmotische Hypothese" und wurde 1961 von Peter Mitchell dargestellt[38], wofür er 1978 den Nobelpreis in Chemie

bekam *„for his contribution to the understanding of biological energy transfer through the formulation of the chemiosmotic theory"*[a].

Aus der beschriebenen anatomischen Anordnung der ETK-Komplexe ergibt sich, dass eine Störung des Elektronenflusses durch die ETK die Flexibilität der mitochondriale ATP-Gewinnung einschränkt. Dies geht häufig einher mit einem veränderten Redoxstatus der ETK und ist von pathophysiologischer Bedeutung. Mechanistisch verursacht ein hoher Reduktionsgrad des CoQ-Pools bei gleichzeitig hohem $\Delta\psi$ eine Umkehr des Elektronenflusses vom Komplex II zu Komplex I. Diese Richtungsumkehr des Elektronenflusses (auch bekannt als *„reverse electron transport"*, RET) verursacht die exzessive Bildung von reaktiven Sauerstoffspezies (ROS) an der ETK[39,40], welche Zellschäden verursachen und dadurch Organfunktionen einschränken können. Gleichzeitig beeinträchtigt ein verminderter Elektronenfluss durch die ETK indirekt (z. B. durch Substrat-Akkumulation) oder auch direkt (z. B. durch Hemmung von Schlüsselenzymen) Stoffwechselkreisläufe wie den Zitronensäurezyklus und verursacht veränderte Stöchiometrien von Stoffwechselintermediaten. Das erklärt, warum sowohl ROS als auch Stoffwechselintermediate als Signale des mitochondrialen Stoffwechsels erkannt werden und zur bidirektionalen Konfiguration des zellulären Stoffwechsels beitragen.

1.3 Der Zitronensäurezyklus (Krebs-Zyklus)

Einzelne Komponenten und Reaktionen des Zitronensäurezyklus (von hier an als Krebs-Zyklus bezeichnet) wurden schon in den 1930er Jahren durch die Forschung von Albert von Szent-Györgyi Nagyrápolt beschrieben, der dafür 1937 den Nobelpreis für Physiologie oder Medizin *„for his discoveries in connection with the biological combustion processes, with special reference to vitamin C and the catalysis of fumaric acid"*[b] erhielt. Der Krebs-Zyklus, wie wir ihn heute kennen, wurde schließlich 1937 von Hans Adolf Krebs und William Arthur Johnson identifiziert[41]. Hans Adolf Krebs erhielt für seine Arbeit gemeinsam mit Fritz Albert Lipmann 1953 den Nobelpreis für Physiologie oder Medizin *„for his discovery of the citric acid cycle"* (Hans Adolf Krebs) und *„for his discovery of co-enzyme A and its importance for intermediary metabolism"* (Fritz Albert Lipmann)[c]. Inzwischen weiß man, dass der Krebs-Zyklus eine integrative Stellung in Bezug auf eine Vielzahl biochemischer Stoffwechselvorgänge hat[42]. Wie auch bei Mitochondrien ist seine evolutionäre Herkunft äußerst interessant, da der Krebs-Zyklus abiogene Vorläufer besitzt. Einzelne Komponenten, Citrat und andere Intermediate, wurden sogar auf einem kohlenstoffhaltigen Meteoriten nachgewiesen und konnten in Gegenwart von Sulfatradikalen nicht-enzymatisch umgesetzt werden[43]. Der Krebs-Zyklus könnte somit den Beginn des Lebens selbst darstellen[44–46].

Anatomisch ist der Krebs-Zyklus in eukaryotischen Zellen im Inneren der Mitochondrien, der sogenannten Matrix, lokalisiert. Die Gesamtausbeute des Krebs-Zyklus an energiehaltigen Verbindungen beträgt 3 NADH, 1 $FADH_2$ und 1 GTP. Die sogenannten Reduktionsäquivalente NADH und $FADH_2$ werden durch die Komplexe der ETK oxidiert und dienen somit ebenfalls der ATP-Gewinnung durch OXPHOS. GTP hingegen kann durch eine Nukleosiddiphosphat-Kinase in ATP überführt werden[42]. Der Krebs-Zyklus verbindet dabei anabole und

[a] The Nobel Prize in Chemistry 1978. <https://www.nobelprize.org/prizes/chemistry/1978/summary/>
[b] The Nobel Prize in Physiology or Medicine 1937. <https://www.nobelprize.org/prizes/medicine/1937/summary/>
[c] The Nobel Prize in Physiology or Medicine 1953. <https://www.nobelprize.org/prizes/medicine/1953/summary/>

katabole Reaktionen des Kohlenhydrat-, Fett- und Proteinstoffwechsels miteinander[42]. Die teilweise reversiblen oder irreversibel verlaufenden biochemischen Reaktionen werden von allen aeroben Organismen genutzt, um die in Nährstoffen gespeicherte Energie freizusetzen. Katalysiert werden die Reaktionen durch acht Enzyme bzw. Enzymkomplexe. Die Vielseitigkeit des Krebs-Zyklus ergibt sich aus der Tatsache, dass es mehrere Eintrittsstellen für verschiedene Stoffwechselwege gibt, wobei ein aus Kohlenhydraten, Fetten oder Proteinen abgeleitetes Zwei-Kohlenstoff-Molekül, das Azetyl-CoA, vollständig zu Kohlendioxid und Wasser oxidiert wird. Die Funktionalität und Plastizität des Krebs-Zyklus ist damit eine Grundvoraussetzung für die oben beschriebene metabolische Flexibilität eines Organismus. Obwohl im Krebs-Zyklus jedes Produkt einer Reaktion ein Substrat für die nächste darstellt, was zur Regeneration jeder dieser Reaktionen führt, ist das Wort „Zyklus" teilweise irreführend. Unter bestimmten Bedingungen, z. B. während einer Hypoxie, können einzelne Segmente des Krebs-Zyklus aktiv bleiben, obwohl die nachgeschaltete mitochondriale ETK keine Reduktionsäquivalente oxidiert. Unter solchen Bedingungen laufen einzelne Reaktionen in entgegengesetzter Richtung ab[47]. Die Segmentierung des Krebs-Zyklus, das adaptive Verzweigen oder Umkehren metabolischer Abläufe, beeinflusst die Entstehung und Akkumulation von Stoffwechselintermediaten und erklärt deren Wirkung als retrograde Signale auf die metabolische Flexibilität[23].

1.4 Retrograde Signale des Krebs-Zyklus

Krebs-Zyklus-Intermediate haben Signalfunktionen außerhalb von Mitochondrien. Für Citrat, zum Beispiel, ist bekannt, dass es zytosolisch für die *de novo* Synthese von Fettsäuren benötigt wird[48]. Citrat kann im Zytosol ebenfalls genutzt werden, um Azetyl-CoA zu generieren. Extramitochondriale Azetylgruppen sind wichtig für Azetylierungsreaktionen, eine wichtige post-translationale Proteinmodifikation z. B. an Histonen. Dadurch nehmen Mitochondrien über Azetyl-CoA-Level Einfluss auf die epigenetische Kontrolle von Genexpressionen und verändern in diesem Zusammenhang Zellfunktionen[49,50]. Ein weiteres Krebs-Zyklus-Intermediat mit zellulärer Funktion ist α-Ketoglutarat (auch bekannt als 2-Oxoglutarat). α-Ketoglutarat ist ein obligatorisches Co-Substrat für 2-Oxoglutarat-abhängige Dioxygenasen. Zu diesen Dioxygenasen gehören die Prolylhydroxylasen[51]. Prolylhydroxylierungen ermöglichen die Interaktion des Hypoxie-induzierbaren Faktors-1α (HIF-1α, ein wichtiger Modulator der zellulären Hypoxie-Antwort) mit weiteren Faktoren und nachfolgend die Rekrutierung in den E3-Ubiquitin-Protein-Ligase-Komplex. HIF-1α Ubiquitinierung führt dann zu dessen Abbau im 26S-Proteasom[52]. Indirekt steuert α-Ketoglutarat somit ebenfalls Genexpressionen im Kern[52] aber auch mitochondriale Anpassungsvorgänge an eine veränderte Sauerstoffverfügbarkeit[53–55]. Im Gegensatz zu α-Ketoglutarat inhibieren andere Krebs-Zyklus Intermediate (Citrat, Isocitrat, Succinat, Fumarat, Malat, Oxalacetat) aber auch Pyruvat die Aktivität von Prolylhydroxylasen (auch unter normoxischen Bedingungen)[56]. Succinat übernimmt darüber hinaus wichtige Funktionen bei der Regulation der angeborenen Immunität. Eine Behandlung von Makrophagen mit Lipopolysacchariden (LPS, Bestandteil der äußeren Membran gramnegativer Bakterien) erhöht z. B. die Abundanz von Succinat und führt dadurch über HIF-1α-Stabilisierung zu verstärkter Transkription pro-inflammatorischer Zytokine[57,58]. Succinat wird auch als Onkometabolit bezeichnet, nachdem bei verschiedenen Krebsarten gefunden wurde, dass sie auf Mutationen im Komplex II und nachfolgender Akkumulation von Succinat basieren[59–62]. Daraus ergibt sich, dass die Aktivität des Krebs-Zyklus eine zentrale Funktion für den

Erhalt der metabolischen Flexibilität zugeschrieben werden muss, dessen zentraler Regulator die mitochondriale ETK ist.

1.5 Mitochondriale Dysfunktionen in humanen Erkrankungen

Mitochondriale Dysfunktionen werden für eine ganze Reihe von Pathologien verantwortlich gemacht, einschließlich neurodegenerativer[63] und kardiovaskulärer Erkrankungen[64], Adipositas, Diabetes mellitus[65,66] und maligner Zelltransformation[67–69]. Allgemein werden nur Erkrankungen, die auf einer OXPHOS Störung basieren, als mitochondriale Erkrankungen definiert[70,71]. Mitochondrialen Erkrankungen variieren dabei stark in ihrer klinischen Ausprägung. Es können einzelne Organe genauso betroffen sein wie eine Kombination verschiedener Organe. Mitochondriale Erkrankungen können prinzipiell in jedem Lebensalter auftreten[70,71]. Bei Beginn im Kindesalter liegt oft eine rezessiv vererbte Erbkrankheit zugrunde, welche in der Regel durch einen schweren und progressiven Verlauf gekennzeichnet ist[72]. Bekannte Syndrome sind das Leigh-Syndrom und das Alpers-Syndrom, bei denen hauptsächlich das zentrale Nervensystem, die Skelettmuskulatur (seltener das Herz) aber auch andere Organe betroffen sein können. Bei Auftreten im Erwachsenenalter sind häufiger Mutationen in der mtDNA verantwortlich[70,71]. Zu den bekannten Syndromen im Erwachsenenalter gehören die chronisch progressive externe Ophthalmoplegie, LHON (*Leber's hereditary optic neuropathy*), das MELAS (*mitochondrial encephalopathy, lactic acidosis, and stroke-like episodes*) Syndrom und MERRF (*myoclonic epilepsy with ragged red fibers*). Generell gilt, dass es nur einen schwachen Zusammenhang gibt zwischen dem eigentlichen genetischen Defekt und der klinischen Präsentation. Darüber hinaus lassen sich viele Mutationen nicht klar definierten Syndromen zuordnen. Dies gilt auch für Patienten mit der sogenannten m.3243A>G-Mutation[73], die bei fast einem Drittel der erwachsenen Patienten mit mitochondrialer Erkrankung vorhanden ist. Aufgrund der großen klinischen und genetischen Heterogenität ist es schwierig, die genaue Prävalenz der mitochondrialen Erkrankung zu schätzen. Die Geburtsprävalenz bei Kindern beträgt etwa 6.2/100,000, wobei es bei in einigen Fällen aufgrund von Häufung autosomal rezessiver Erkrankungen höher sein kann[74]. Nimmt man pathogene Mutationen sowohl des mitochondrialen als auch des nukleären Genoms zusammen, liegt das Auftreten bei Erwachsenen in etwa bei 1 zu 4,300. Mutationen der mtDNA werden dabei in mehr als 75% aller Fälle beobachtet[75].

Mitochondriale Dysfunktionen können aber auch auftreten, ohne dass eine bestimmte Untereinheit der ETK primär mutiert ist. Besonders offensichtlich wird dies bei septischem Organversagen[76]. Sepsis ist gekennzeichnet durch eine „lebensbedrohliche Organdysfunktion, die durch eine dysregulierte Reaktion des Wirts auf eine Infektion verursacht wird“[77] und ist mit weltweit hoher Inzidenz[78] und Krankenhaussterblichkeit (41.1 % in Europa) assoziiert[79]. Obwohl im Verlauf einer Sepsis prinzipiell jedes Organ funktionelle Beeinträchtigungen entwickeln kann, zeigen Organe, die auf den oxidativen Stoffwechsel angewiesen sind, wie das Herz, eine besondere Anfälligkeit. Tatsächlich ist eine kardiale kontraktile Dysfunktion (Sepsis-induzierte Kardiomyopathie) eine häufige Sepsis-bedingte Komplikation[79], die eng mit einem schweren klinischen Verlauf korreliert[80–82]. Ein besonderes Merkmal des Organversagens bei Sepsis ist es, dass es zu funktionellen Einschränkungen bei bioenergetischen und metabolischen Prozessen trotz ausgezeichneter Oxygenierung des Gewebes kommt[83], eine sogenannte zytopathische Hypoxie. Sowohl die bioenergetischen Störungen als auch eine darauf

basierende kontraktile Dysfunktion bilden sich bei Überlebenden einer Sepsis trotz ihrer negativen Auswirkungen auf den Krankheitsverlauf in der Regel komplett zurück[84], was darauf hindeutet, dass während der Sepsis lediglich eine transiente Störung des Elektronenflusses durch die mitochondriale ETK der wesentliche Auslöser für die kontraktile Dysfunktion ist[76,85]. Tatsächlich konnten wir in einem Endotoxämie-Modell der Maus durch Wiederherstellen des Elektronenflusses durch die ETK die Überlebenswahrscheinlichkeit erhöhen[58]. Unsere Daten erlauben den Schluss, dass Sepsis ätiologisch eine Mitochondriopathie infolge einer ETK-Dysfunktion darstellt. Darüber hinaus lässt sich vermuten, dass ETK-Dysfunktionen (und damit eine eingeschränkte metabolische Flexibilität) weit häufiger für Erkrankungen verantwortlich sind, als die oben beschriebenen Zahlen zur Prävalenz mitochondrialer Erkrankungen nach klassischer Definition vermuten lassen. Wir haben diese Annahme in den vorliegenden Arbeiten vor allem in Krankheitsmodellen des kardiopulmonalen Systems untersucht.

1.6 Die mitochondriale Elektronentransportkette (ETK) in Anpassungsvorgängen der Lunge

Mitochondriale Funktionen (und Dysfunktionen) wurden im Zusammenhang mit verschiedenen Vorgängen in der Lunge diskutiert. Die hypoxische pulmonale Vasokonstriktion (HPV) beispielsweise ist ein lebenswichtiger physiologischer Mechanismus, der den pulmonalen Blutfluss von schlecht belüfteten zu gut belüfteten Lungenalveolen umleitet. Durch HPV wird somit die arterielle Oxygenierung unter Bedingungen lokaler alveolärer Hypoxie optimiert[86,87]. Eine gestörte HPV kann umgekehrt zu lebensbedrohlichem Sauerstoffmangel führen, z. B. im Rahmen einer Pneumonie, bei Sepsis oder Leberversagen. HPV trägt ebenfalls zur Entwicklung eines Höhenlungenödems bei. Im Falle einer globalen alveolären Hypoxie kann die HPV einen Anstieg des pulmonal-vaskulären Drucks verursachen. Ganz natürlich tritt dieses Phänomen in den hypoxischen Lungen des ungeborenen Fötus auf. Eine Fortsetzung der HPV nach der Geburt verursacht dagegen die sogenannte persistierende pulmonale Hypertonie (PH) des Neugeborenen. Wenn es zur Persistenz einer PH nach Geburt kommt, ist dies mit deutlich erhöhter Mortalität und Morbidität verbunden[88]. Deshalb wurde vermutet, dass die HPV auch zur Entwicklung einer PH bei Erwachsenen beitragen kann. In diesem Fall könnte es infolge von Hypoxie-induzierten pulmonalen Gefäßumbildungen zur Bildung eines Rechtsherzversagens kommen[89]. Welche Rolle Mitochondrien in der Entwicklung der HPV spielen, war lange Zeit unklar. Kürzlich wurde gezeigt, dass akute HPV durch einen Sauerstoffsensor innerhalb der mitochondrialen ETK reguliert wird. Eine zentrale Rolle kam dabei der Isoform 2 der Untereinheit 4 (COX4I2) des Komplex IV zu[90]. Mechanistisch soll eine akute Hypoxie dabei eine COX4I2-abhängige mitochondriale Hyperpolarisation induzieren, die mitochondriales ROS am Komplex III und/oder Komplex I freisetzt. Diese ROS wurden verantwortlich gemacht für eine Kaskade von Ereignissen wie die Hemmung zellulärer Kaliumkanäle (K_V), die zelluläre Membrandepolarisation und Aktivierung spannungsabhängiger Kalziumkanäle. Der resultierende Anstieg intrazellulären Kalziums verursacht dann die HPV. In bisherigen Versuchen blieb insbesondere unklar, ob eine Hypoxie-vermittelte Inhibition des Komplex IV oder ein verminderter Elektronenfluss durch die ETK der eigentliche Auslöser für HPV war, da HPV bereits bei Sauerstoffwerten ausgelöst wurde, bei denen die Sauerstoffaffinität des Komplex IV eine Inhibition verhindern sollte. Darüber hinaus stand eine verringerte ROS-Freisetzung aus Komplex I[91] während akuter Hypoxie im Gegensatz zu einem Konzept, dass erhöhte ROS aus Komplex III als Hauptursache für die Entwicklung einer HPV sieht[92]. In der

Tat wird angenommen, dass chronische Hypoxie-Änderungen von Genexpressionen durch mitochondriale ROS-vermittelte Stabilisierung von HIF-1α beeinflusst werden. Wir wollten daher untersuchen, (i) wie HPV, PH und HIF-1α-Stabilisierung durch Hypoxie-induzierte Hemmung der mitochondrialen ETK ausgelöst werden, (ii) welche Mechanismen und Signalwege der ETK-Hemmung nachgeschaltet sind und (iii) ob eine Wiederherstellung des mitochondrialen Elektronenflusses durch die ETK HPV und/oder PH verhindern kann.

Ein anderes Krankheitsbild der Lunge mit wahrscheinlich mitochondrialer Beteiligung ist die chronisch obstruktive Lungenerkrankung (COPD), ein globales Gesundheitsproblem und eine der häufigsten Todesursachen[93]. Als ein wesentlicher Faktor für die Entwicklung einer COPD wurde Rauchen erkannt. Klinische Kennzeichen der COPD sind Einschränkungen des Luftstroms und die Zerstörung von Lungengewebe. Die schlechte Regenerationsfähigkeit der humanen Lunge insbesondere im Erwachsenenalter und der Mangel an therapeutischen Interventionen, die die Gewebedestruktion aufzuhalten oder umzukehren könnten, machen die COPD zu einem unheilbaren Zustand. Verschiedene Mechanismen, wie Zigarettenrauch, wurden als Pathomechanismen diskutiert. Beispielsweise sollen lokale Entzündungen und Zigarettenrauch-induzierte ROS-Produktion einen maladaptiven Umbau der Lunge initiieren[94]. Die pro-oxidative Natur von Zigarettenrauch ist gut dokumentiert und unterstützt diese Hypothese[95]. Die komplexe Zusammensetzung von Zigarettenrauch aus mehr als 5,000 Verbindungen[96], von denen viele als Toxine oder Karzinogene bekannt sind, erschwert jedoch die mechanistische Untersuchung. Zwei prominente Verbindungen im Zigarettenrauch sind dabei potente Inhibitoren des mitochondrialen Komplex IV, nämlich Kohlenmonoxid und Zyanid. Jedes dieser Gifte kann zu einer Störung des Elektronenflusses durch die ETK führen und so das zelluläre Redoxgleichgewicht stören und die ROS-Produktion verursachen. Da Zyanid eine systemische Halbwertszeit von bis zu 25 h hat[97], kann die mitochondriale Beeinträchtigung also nicht von vornherein als Nebenbefund bei der Entwicklung der COPD abgetan werden. Wir wollten daher testen, (i) ob eine Hemmung der ETK als Auslöser für einen maladaptiven Umbau der Lunge verantwortlich sein kann, (ii) wie Zigarettenrauch die Funktion der ETK einschränkt, (iii) ob Zigarettenrauch ROS-Produktion an der ETK erhöht und (iv) welchen Einfluss eine Zigarettenrauch-vermittelte ETK-Dysfunktion auf die zelluläre Viabilität hat.

1.7 Dysfunktionen der mitochondrialen ETK in kontraktilen Geweben

Kontraktiles Gewebe, insbesondere aber Kardiomyozyten, zeigen eine hohe Anfälligkeit für Sauerstoffmangel, was lange Zeit allein auf ihre Abhängigkeit von OXPHOS zur ATP-Produktion zurückgeführt wurde[98]. Etwa 30% des kardiomyozytären Zellvolumens werden von Mitochondrien eingenommen. Trotzdem wurde in isolierten Kaninchenherzmitochondrien[99] sowie an intakten Kaninchenherzen[100] gezeigt, dass ein kardialer ATP-Verlust allein nicht ausreicht, um alle post-ischämischen Gewebeschäden zu erklären[99]. Es wurde vermutet, dass möglicherweise während der Reperfusion große Mengen schädlicher ROS an der ETK produziert werden, die dann Gewebeschäden verursachen[99], deshalb auch als Schaden nach Ischämie-Reperfusion (IR) bezeichnet. Paradoxerweise hat der therapeutische Einsatz von Antioxidantien wie Vitamin C zur post-ischämischen Kardioprotektion zu widersprüchlichen Ergebnissen geführt[101–106] und teilweise selbst schädliche Nebenwirkungen hervorgerufen[107]. Eine mögliche Erklärung für das widersprüchliche Verhalten von Antioxidantien könnte sein, dass diese nicht immer ausreichende Konzentrationen im mitochondrialen Kompartiment erreichen, um

kardioprotektiv wirksam zu sein. Daneben sind Antioxidantien wie Vitamin C nicht spezifisch für mitochondriale ROS. Tatsächlich zeigen mitochondriale und zytoplasmatische ROS teilweise gegensätzliche Effekte[108]. Zudem gibt es wirksame Schutzmechanismen, die speziell mitochondriale ROS sicher entgiften (z. B. die mitochondrial-exprimierte Mangan-abhängige Superoxid-Dismutase, MnSOD oder SOD2), die sowohl für eine normale Herzfunktion essentiell sind[109] als auch die post-ischämische Funktionserholung des Herzens beeinflussen[110,111].

Um diese Annahme zu testen, wurden verschiedene Antioxidantien zur therapeutischen Entgiftung von mitochondrialen ROS entwickelt. MitoQ, das wohl bekannteste Beispiel, besteht aus reduziertem CoQ, das kovalent an lipophiles Triphenylphosphonium (TPP) gebunden ist und das durch eine positive Ladung von Mitochondrien aufgenommen wird[112]. In einem Rattenmodell für kardiale IR verringerte MitoQ, aber nicht ein nicht-mitochondriales Antioxidans oder TPP allein, die kontraktile Dysfunktion, den Zelltod und mitochondriale Schädigungen[112]. Positive Effekte von MitoQ wurden auch in anderen Studien gesehen, die sich mit Posttransplantationsschäden[113] oder drucküberlastungsinduzierter Herzinsuffizienz befassten[114]. Szeto-Schiller (SS)-Peptide[115] wirken ebenfalls antioxidativ, reichern sich allerdings Membranpotential ($\Delta\psi$)-unabhängig in Mitochondrien an. SS-Peptide bewirkten phänotypische Verbesserungen nach Angiotensin-II-induzierter mitochondrialer ROS-Produktion und kontraktiler Dysfunktion[116] sowie nach experimenteller Aortenkonstriktion[117]. Sowohl MitoQ als auch SS-Peptide erwiesen sich als biologisch sicher, auch wenn sie langfristig verabreicht wurden[118,119]. Darüber hinaus wurden Moleküle identifiziert, welche die ROS-Produktion am Komplex I unterdrücken, sogenannte S1QELs[120]. Auch die Verwendung von S1QELs schützte das perfundierte Mausherz vor IR-vermittelten Schäden[120]. Ein Mechanismus, der übergreifend die positiven Wirkungen der verschiedenen mitochondrialen Antioxidantien erklärt, wurde kürzlich beschrieben[121]. Demnach akkumuliert Succinat, z. B. während einer kardialen Ischämie, und wird während der Reperfusion sehr schnell oxidiert. Dieser Prozess führt zur Produktion von exzessiven Mengen an ROS durch RET und Gewebeschäden[121,122]. Das Entgiften von RET-induzierten ROS könnte daher der entscheidende Mechanismus sein, um post-ischämische Zell- und Organschäden zu verhindern. Allerdings gibt es verschiedene nicht-mitochondriale ROS-Quellen, die alle in reziproker Abhängigkeit zu einander stehen[123], sodass man andere Ursachen für das Versagen von Vitamin C (und anderen nicht-gerichteten Antioxidantien) nicht ausschließen kann.

Ein weiterer Erklärungsansatz für die scheinbar widersprüchlichen Ergebnisse zielt auf mögliche biphasische Effekte von ROS ab, wonach hohe ROS-Konzentrationen zu Schäden führen und niedrigere Konzentrationen adaptive Reaktionen auslösen[124,125]. Der Begriff „Mitohormesis" beschreibt diesen Ansatz[126]. Unter physiologischen Bedingungen wirken geringe Mengen an ROS demzufolge als Signalmoleküle, die homöostatische Wege im Zusammenhang mit der mitochondrialen Bioenergetik regulieren, während sie bei hohen Konzentrationen (exzessive Produktion) als toxische Substanzen wirken und Schäden an Nukleinsäuren, Proteinen und Lipiden verursachen[126]. Tatsächlich sind ROS, die an verschiedenen Stellen der ETK erzeugt werden[127], im Skelettmuskel essentiell für Reparaturvorgänge[128] und wirken im Herzen nach IR sogar kardioprotektiv[129]. Wir wollten deshalb an kontraktilen Geweben testen, (i) welchen Einfluss die ETK auf die Induktion von Signalkaskaden hat, die einen adaptiven Organumbau regulieren, (ii) unter welchen Bedingungen mitochondrial produziertes ROS als adaptives Signal oder schädigend wirkt und (iii) welchen Einfluss die Wiederherstellung des

Elektronenflusses durch die ETK auf die Entwicklung und den Verlauf von verschiedenen Krankheitszuständen hat.

1.8 Verzweigung der Atmungskette durch alternative Enzyme

Viele Spezies, darunter Pflanzen und einige Metazoen, aber nicht Insekten und Säugetiere, exprimieren alternative Atmungskettenenzyme. In ihren Wirtsorganismen verzweigen diese Enzyme die ETK unter Bedingungen, wenn der Elektronenfluss durch die ETK gestört ist (**Abb. 1**). Somit stellen alternative Atmungskettenenzyme einen Mechanismus zur Bewältigung mitochondrialer Stresssituationen dar[130]. Alternative Atmungskettenenzyme übernehmen somit eine wichtige Funktion bei der Wiederherstellung gestörter metabolischer Prozesse bzw. gewährleisten die metabolische Flexibilität. Im Rahmen der Entwicklung komplexer Tiere ist die Expression alternativer Atmungskettenenzyme verloren gegangen, was möglicherweise auf einen Selektionsnachteil hinweist.

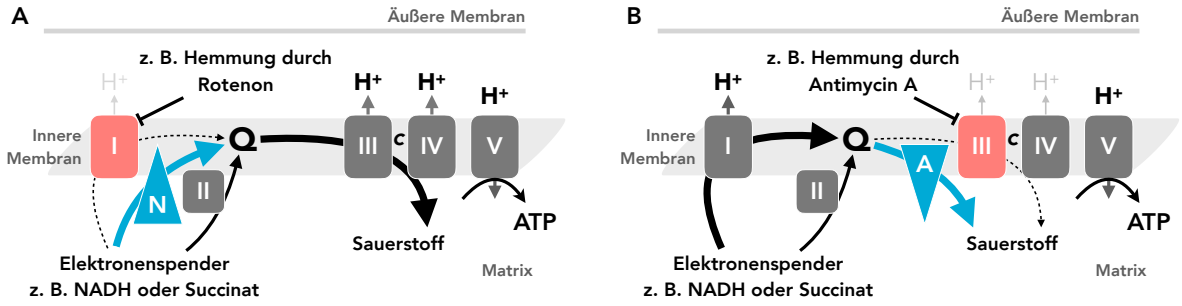

Abb. 1 *Schematische Darstellung der mitochondrialen Elektronentransportkette (ETK). Elektronen von Atmungskettensubstraten (z. B. NADH oder Succinat) werden durch die ETK geschleust und reduzieren am Komplex IV Sauerstoff zu Wasser. Dabei werden Protonen über die innere Membran an den Komplexen I, III und IV in den intermembranären Raum gepumpt. Dieser elektrochemische Gradient (H^+-Gradient) ist die Antriebskraft für die ATP-Produktion am Komplex V. Defekte (rote Markierung) innerhalb der ETK stören die metabolische Flexibilität, verursachen ROS-Produktion und lösen Erkrankungen aus. Alternative Atmungskettenenzyme wie Ndi1 aus Saccharomyces cerevisiae (**A**) oder AOX aus Ciona intestinalis (**B**) umgehen Teile der ETK, pumpen aber selbst keine Protonen. I-IV, ETK-Komplexe; V, F_1F_0-ATPase; c, Cytochrom c; Q, CoQ-Pool; N, Ndi1; A, AOX. Die Abbildung wurde adaptiert von Giordano et al., 2020[131].*

Im Allgemeinen unterscheidet man zwei Hauptvertreter bei alternativen Atmungskettenenzymen. Erstens gibt es alternative Dehydrogenasen (z. B. NADH-Dehydrogenase in der Hefe, Ndi1), die unter Umgehung des Komplex I den NADH-Pool oxidieren und den CoQ-Pool reduzieren[132–134]. Zweitens gibt es alternative Oxidasen (AOX, z. B. in *Ciona intestinalis*), die unter Umgehung der Komplexe III und IV, den Elektronentransfer vervollständigen und Sauerstoff zu Wasser reduzieren[135–137]. Mechanistisch wichtig ist, dass alternative Atmungskettenenzyme wie Ndi1 und AOX Protonenpumpen (Komplexe I, III, IV) umgehen, während sie selbst keine Protonenpumpen sind[134,137]. Daraus ergibt sich, dass alternative Enzyme den Elektronenfluss durch die ETK zwar wiederherstellen, dabei aber die Effizienz der OXPHOS vermindern. Indirekt ermöglichen Ndi1 und AOX allerdings sehr wohl die mitochondriale ATP-Produktion, da sie den Elektronenfluss durch die jeweils verbliebenen Komplexe (Komplex I bei AOX sowie Komplexe III und IV bei Ndi1) wiederherstellen. Vor diesem Hintergrund wurden alternative Enzyme als Werkzeuge zur Untersuchung mitochondrialer Erkrankungen und als mögliche Therapeutika diskutiert[130,135,138–140].

Wir haben in den hier vorgestellten Arbeiten ausschließlich AOX aus *Ciona intestinalis* benutzt. Wie alle AOXs, vermittelt diese Zyanid-resistente Atmung, ist ein membrangebundenes mitochondriales Enzym und besteht (im Gegensatz zu den klassischen Enzymen) aus nur einem Genprodukt (mit einer Größe von ca. 37 kDa)[141]. Voraussetzung für katalytische AOX-Aktivität ist ein mindestens zu 35-40% reduzierter CoQ-Pool[142], ein ausreichendes mitochondriales Membranpotential ($\Delta\psi$) sowie ein hohes ATP/ADP-Verhältnis[40,137], also Bedingungen, unter denen die mitochondriale ETK RET-vermittelt ROS produziert[40,137]. Da AOX Elektronen direkt auf Sauerstoff überträgt, handelt es sich wie bei der klassischen Atmung um eine thermogene Reaktion. AOX verhindert also durch Reaktivierung einer gestörten ETK eine übermäßige Reduktion des mitochondrialen CoQ-Pools und dadurch die exzessive RET-vermittelte ROS-Produktion[39,40,137]. Gleichermaßen wichtig ist dabei, dass ein Aufrechterhalten des Elektronenflusses durch die ETK ebenfalls die Aktivität des Krebs-Zyklus (und damit die metabolische Flexibilität) aufrechterhält. Wir betrachten deshalb xenotop exprimiertes AOX als ein exzellentes Mittel, um Ätiologien von humanen Pathologien zu charakterisieren und möglicherweise deren Verlauf zu beeinflussen, wenn der jeweilige Zustand auf einer Störung des Elektronenflusses durch die ETK basiert. In diesem Fall könnte durch AOX-vermittelte Wiederherstellung des Elektronenflusses durch die ETK den Stoffwechsel wiederherstellen wodurch eine Pathologie korrigiert werden kann. Die Validität dieser Annahme wurde in kultivierten Säugetierzellen[138,139,143], in der Fruchtfliege[144–147] aber auch in einem Mausmodell[148] nachgewiesen. Insbesondere das bisherige Mausmodell hatte allerdings technische Schwächen (zufällige genomische Integration von AOX), die eine weitere Verwendung in Krankheitsmodellen verhinderten und deshalb durch ein besser geeignetes Modell ersetzt werden sollte. In den hier vorgestellten Arbeiten wollten wir testen, (i) ob AOX aus *Ciona intestinalis* mit einfacher genomischer Integration gefahrlos in der Maus exprimiert werden kann, (ii) welchen Einfluss AOX auf den Elektronenfluss durch die ETK und den allgemeinen Stoffwechsel unter regulären und unter Stressbedingungen hat und (iii) welchen Einfluss AOX auf den Verlauf ausgewählter Krankheitszustände nimmt.

1.9 Zielsetzung der Arbeit

In der vorliegenden Arbeit sollte zunächst der Einfluss von xenotoper AOX-Expression auf die allgemeine Physiologie der Maus unter Basalbedingungen untersucht werden, um eventuelle negative Einflüsse eines solchen Gentransfers auf Säuger zu erkennen. In den nachfolgenden Arbeiten wurde die xenotope AOX-Expression in den Kontext relevanter physiologischer und pathophysiologischer Zustände gesetzt.

Nach Phänotypisierung des neu-generierten AOX^{Rosa26}-Mausmodells[136] haben wir folgende Fragestellungen untersucht:

- wie beeinflusst AOX den mitochondrialen Elektronenfluss und die ROS-Produktion in isolierten Herzmitochondrien[137],
- welche Rolle spielt die ETK in der pulmonalen Vaskulatur für die Sauerstoffwahrnehmung bei akuter und chronischer Hypoxie[149],
- welchen Einfluss nimmt die ETK auf Zigarettenrauch-induzierte pulmonale Gewebeschäden und Dysfunktion[150],
- welche Rolle spielen Signale der ETK bei adaptivem Organumbau nach kardialer Ischämie-Reperfusion (IR)[111] und
- welcher Zusammenhang besteht zwischen mitochondrialen Redox-Signalen und der Entwicklung einer mitochondrialen Myopathie[39]?

Unsere Arbeiten belegen, dass eine xenotope Expression von AOX im Grundsatz möglich ist, ohne mitochondriale Funktionen basal zu stören. Die Arbeiten zeigen auch, dass man durch AOX Prozesse wie Rauch-induzierte Lungenschäden oder pulmonale Sauerstoffwahrnehmung positiv beeinflussen kann. Bei anderen Zuständen wie beispielsweise im post-ischämischen Herzen oder bei bestimmten mitochondrialen Myopathien bietet AOX keine Vorteile oder verschlechtert Prozesse des adaptiven Organumbaus.

Wir konnten kürzlich zwar zeigen, dass AOX therapeutisch anwendbar ist[131]. Auf der Grundlage unserer Experimente erscheint eine gezielte Beeinflussung des Elektronentransfers im Sinne einer alternativen Oxidase allerdings nur bei bestimmten Erkrankungen sinnvoll zu sein. Die therapeutische Verwendung von AOX stellt somit kein allgemein gültiges Prinzip dar, weil den Ätiologien der unterschiedlichen Erkrankungen an Lunge und Herz ganz unterschiedliche molekulare Mechanismen zugrunde liegen.

2 Ergebnisse und Diskussion

2.1 Generierung und Phänotypisierung einer Maus mit xenotoper Expression einer alternativen Oxidase (AOX) aus *Ciona intestinalis*

In diesem Teilabschnitt wird die Generierung und Charakterisierung eines Mausmodells beschrieben (AOX^{Rosa26}), welches in allen nachfolgenden Teilabschnitten eingesetzt wurde. AOX^{Rosa26}-transgene Mäuse sollten AOX aus *Ciona intestinalis* ubiquitär exprimieren und, idealerweise, unter physiologischen Bedingungen phänotypisch unauffällig sein. Ziel war es, mit AOX^{Rosa26} ein Mausmodell zu etablieren, mit dem die Rolle der mitochondrialen ETK bei Anpassungsvorgängen nach metabolischem Stress (Verlust metabolischer Flexibilität) untersucht werden kann. Resultate und Diskussion dieses Teilabschnittes entstammen in wesentlichen Teilen aus Szibor *et al.*, *Dis Model Mech*. **10**, 163–171 (2017)[136]. AOX^{Rosa26} ist ein AOX-Mausmodell mit singulärer genomischer Integration von AOX aus *Ciona intestinalis* in den *Rosa26*-Lokus. AOX wird in fast allen Geweben stark exprimiert. Dennoch zeigt die AOX^{Rosa26}-Maus nur subtile phänotypische Effekte hinsichtlich der Zusammensetzung der mitochondrialen Atmungskettenkomplexe, des mitochondrialen Sauerstoffverbrauchs oder des globalen Metaboloms. Insbesondere zeigten AOX^{Rosa26}-Mäuse keine wesentlichen Abweichungen von der regulären Physiologie. AOX vermittelte eine robuste Resistenz gegen Inhibitoren der Atmungskette *in organello* sowie gegen eine systemisch applizierte LD50-Dosis Zyanid (**Abb. 2**). Die AOX^{Rosa26}-Maus eignet sich deshalb als Werkzeug zur Untersuchung von Kontrollmechanismen der ETK und von Ätiologien mitochondrialer Erkrankungen.

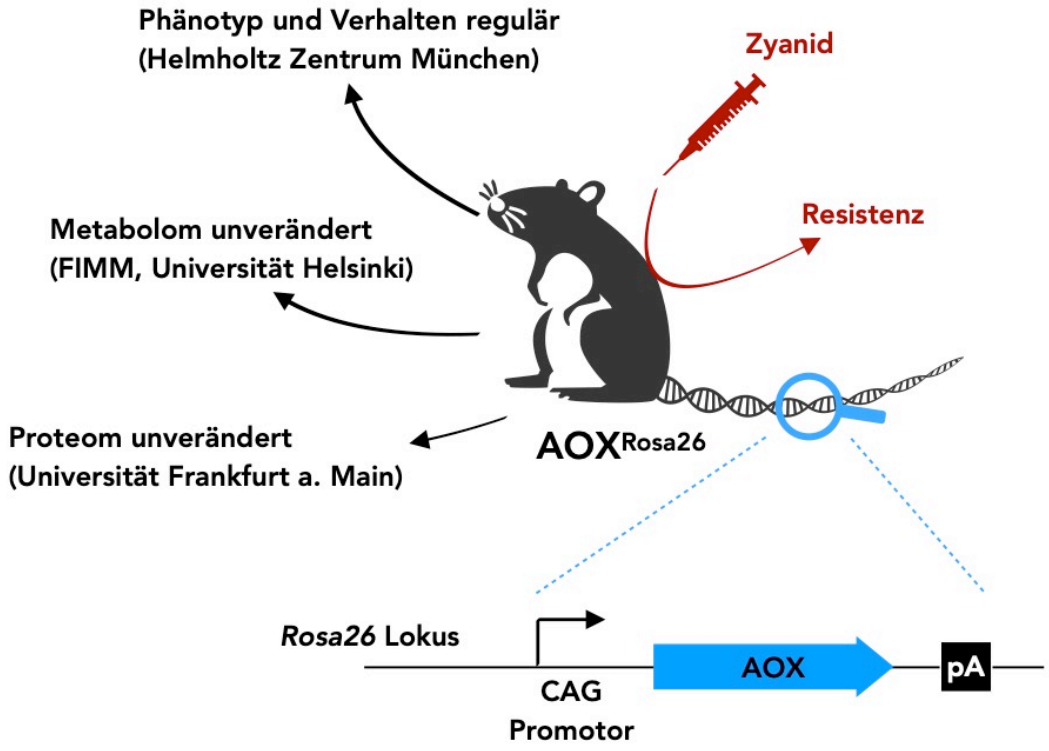

Abb. 2 *Generierung und Charakterisierung von AOX^{Rosa26}-Mäusen. Die kodierende Sequenz von AOX aus Ciona intestinalis wurde in den Rosa26-Lokus integriert. Ein CAG-Promoter kontrolliert die ubiquitäre AOX-Expression. AOX^{Rosa26}-Mäuse sind unauffällig hinsichtlich metabolischer, verhaltensbezogener, morphologischer,*

immunologischer, kardialer und neurologischer Parameter. Sie sind zudem resistent gegen Schäden durch Zyanidintoxikation.

2.1.1 Generierung des AOX^{Rosa26}-Mausmodells

Zunächst wurde die kodierende Sequenz von *Ciona intestinalis* AOX mittels homologer Rekombination[151] in das Kerngenom von embryonalen Stammzellen (ES Zellen) der Maus integriert. Als Integrationsstelle haben wir den *Rosa26*-Lokus ausgewählt, der einerseits ubiquitär aktiv ist und sich andererseits bei zielgerichteter Integration von Genen bewährt hat[152,153]. Der *Rosa26*-Lokus wurde auch deshalb ausgewählt, weil in früheren Arbeiten keine phänotypischen Veränderungen der Maus durch Insertionen in diesen Lokus beschrieben wurden und Transgene stabil exprimiert werden konnten[154,155]. Für die Expression von AOX haben wir den sogenannten CAG-Promotor ausgewählt, ein synthetischer Promotor, der ubiquitär aktiv ist und dessen Aktivität die des endogenen *Rosa26*-Promotors um ein Vielfaches übersteigt[156–159]. Selektion positiver ES-Zellklone erfolgte durch Nutzung einer Neomycin-Selektionskassette. Die korrekte Insertion des AOX-Selektionskassetten-Konstrukts in das ES-Zellgenom wurde durch Southern Blot-Analysen verifiziert[160]. Anschließend wurden chimäre Mäuse durch Blastozysteninjektion positiver ES-Zell-Klone etabliert[151]. Die Neomycin-Selektionskassette wurde durch FLP-vermittelte Rekombination *in vivo* nach Keimbahnübertragung eliminiert[161]. Der neue AOX^{Rosa26}-Stamm wurde nachfolgend auf den C57BL/6J Hintergrund zurückgekreuzt, wobei das Vorhandensein des Transgens bei jedem Schritt mittels PCR überprüft wurde. Unsere Untersuchungen zeigten, dass die Vererbung von AOX streng Mendel'schen Regeln folgt und keine Einschränkung der Lebensfähigkeit oder phänotypische Auffälligkeiten bei den Nachkommen verursacht. Unauffällig waren ebenso Wurfgrößen und das Geschlechterverhältnis bei den Nachkommen.

2.1.2 AOX wird in verschiedenen Geweben der AOX^{Rosa26}-Maus exprimiert

Im Rahmen der Phänotypisierung von AOX^{Rosa26} haben wir zunächst die Expression von AOX in verschiedenen Geweben sowohl auf Transkript- als auch auf Proteinebene untersucht. Eine Northern Blot-Analyse bestätigte eine breite, wenngleich ungleichmäßige, mRNA-Expression mit höchsten Werten im Herzgewebe und Skelettmuskel. Die relativ gesehen geringste AOX-Expression fanden wir im Gehirn. Eine Western Blot-Analyse ergab für AOX-Expression auf Proteinebene etwas einheitlichere Werte, die aber prinzipiell ähnlich verteilt waren. Die AOX-Expression war allerdings nicht stabil niedrig im Gehirn. Die höchsten Werte fanden wir postnatal. Innerhalb des ersten Monats nach der Geburt, also im Zuge der Reifung, nahm die AOX-Expression bis hin zur Western Blot-Nachweisgrenze kontinuierlich ab. Dieser Verlust an AOX-Expression im adulten Gehirn lässt sich wahrscheinlich nicht durch technische Schwächen, z. B. des Konstruktdesigns, erklären. Der hier verwendete CAG-Promotor findet breite Verwendung insbesondere auch für Transgenexpressionen im Gehirn der Maus, sowohl während der Entwicklung[162] als auch im adulten Gehirn[163,164]. Auch die Integrationsstelle, der *Rosa26*-Lokus, ist prinzipiell für effiziente Expression von Transgenen im Gehirn geeignet[165–167]. Ebenfalls die Expression eines mitochondrialen Proteins an sich oder die Nutzung eines CAG-Promotors stellen keine limitierenden Faktoren dar. In einer anderen Studie wurde zudem AOX aus *Ciona intestinalis* in der Maus exprimiert (MitAOX-Mauslinie)[148] mit substanzieller AOX-Expression im Gehirn. Allerdings gibt es wesentliche Unterschiede zwischen dem

MitAOX- und dem hier etablierten AOX^{Rosa26}-Modell. Im MitAOX-Modell wurde erstens die AOX-Sequenz vor der genomischen Integration für Expression in Säugerzellen Kodon-optimiert. Zweitens wurde die Verwendung des CAG-Promotors gepaart mit der Nutzung eines post-transkriptional-regulatorischen Elements des Woodchuck-Hepatitis-Virus (WPRE). Diese Kombination soll unter bestimmten Voraussetzungen geeignet sein, Genexpressionen zu steigern[168]. Drittens erfolgte die genomische Integration in MitAOX-Mausembryonen zufällig durch lentivirale Keimbahntransduktion. Untersuchungen ergaben, dass im Gegensatz zur singulären Integration beim AOX^{Rosa26}-Modell 4-8 Konstrukt-Kopien im MitAOX-Genom vorliegen. Daraus ergibt sich, dass posttranskriptionelle oder posttranslationale Regulationsmechanismen für das unterschiedliche Expressionsverhalten verantwortlich sein könnten. Ob der Verlust von AOX-Expression in AOX^{Rosa26}-Mäusen funktionell relevante Nachteile bringt, ist noch nicht abschließend geklärt. Wir konnten beispielsweise zeigen, dass AOX^{Rosa26}-Mäuse vor Letalität durch systemisch verabreichtes Zyanid geschützt sind. Das ist insofern erstaunlich, weil Zyanid die Blut-Hirn-Schranke passiert und im zentralen Nervensystem für toxische Effekte verantwortlich gemacht wird[169,170]. Zudem verhindert AOX die Entwicklung einer Astrogliose im adulten Gehirn einer Maus mit globalem Komplex III Defekt[171]. Die molekularen Mechanismen, die AOX im adulten Gehirn möglicherweise stabilisieren oder seine katalytische Aktivität fördern, müssen zukünftige Studien aber erst noch näher untersuchen. Andererseits ist ebenfalls unklar, wie viele Kopien von AOX pro Mitochondrion/ETK wirklich nötig sind, um Zyanid-resistente Atmung zu ermöglichen. Die relativ geringen Mengen AOX im adulten Gehirn von AOX^{Rosa26}-Mäusen ist unter Umständen ausreichend, einen sicheren Schutz vor Schäden durch Unterbrechung des Elektronenflusses durch die ETK zu bieten. Eine Möglichkeit die AOX-Expression auch in AOX^{Rosa26}-Mäusen zu erhöhen, wäre die Nutzung homozygoter Tiere. In Organen mit guter AOX-Expression konnten wir feststellen, dass bei homozygoten Tieren die AOX-Expression höher ausfiel als bei hemizygoten Tieren. Systematische Vergleiche zwischen hemizygoten und homozygoten AOX^{Rosa26}-Mäusen wurden jedoch nicht durchgeführt.

2.1.3 AOX beeinflusst die Zusammensetzung der Atmungskettenkomplexe nicht

Als Nächstes wollten wir herausfinden, ob sich das xenotop exprimierte AOX ordnungsgemäß in die mitochondriale Innenmembranen der Maus integriert. Dazu nutzten wir die sogenannte Karbonatextraktionsmethode[172–174]. Wir konnten zeigen, dass AOX mit der mitochondrialen Membranfraktion assoziiert ist, wenngleich weniger fest als integrale Membranproteine der ETK (z. B. die Untereinheit 1 des Komplex IV). Wir haben ebenfalls untersucht, ob die Expression von AOX die Assemblierung oder die Stöchiometrie der klassischen Atmungskettenkomplexe und/oder Superkomplexe beeinträchtigt[175–177]. Mithilfe von blau-nativer Gelelektrophorese (BN-PAGE) gefolgt von in-Gel-Färbungen von mitochondrialen Präparationen aus verschiedenen Geweben konnten wir zeigen, dass sowohl die Expression repräsentativer Untereinheiten der fünf Atmungskettenkomplexe (I-V) als auch ihre Organisation in Superkomplexe im Wesentlichen unbeeinflusst sind. AOX selbst migrierte hauptsächlich in der Größe eines Dimers oder aber als Multimer von Dimeren. Das lässt den Schluss zu, dass AOX nicht mit einem der anderen Atmungskomplexe oder Superkomplexe assoziiert. Die Tatsache, dass AOX keinen Einfluss hat auf die allgemeine Zusammensetzung der Atmungskettenkomplexe hat, sagt allerdings nichts über seine katalytische Funktion und mögliche Anpassungsvorgänge des zellulären Metabolismus aus. Deshalb analysierten wir

das Niveau verschiedener Metabolite im Herzgewebe und im Skelettmuskel. Die Analyse von mehr als 100 Einzelmetaboliten erbrachte keine signifikanten Unterschiede zwischen WT- und AOX^{Rosa26}-Mäusen. Das gibt einen indirekten Hinweis darauf, dass AOX unter nicht-gestressten Bedingungen nicht signifikant in den generellen Zellstoffwechsel eingreift.

2.1.4 AOX ist in Geweben der AOX^{Rosa26}-Maus katalytisch aktiv

Um eine mögliche katalytische Aktivität von AOX festzustellen, haben wir Mitochondrien aus verschiedenen Geweben isoliert und respirometrisch analysiert. Komplex-spezifische Substratkombinationen und Inhibitoren kamen dabei zum Einsatz. Unsere Untersuchungen ergaben keine Substrat-spezifischen Unterschiede des Sauerstoffverbrauchs von Mitochondrien in Abhängigkeit von AOX. In Gegenwart des Komplex III-Inhibitors Antimycin A zeigten die getesteten Gewebe mit Ausnahme des Gehirns eine signifikant höhere (AOX-vermittelte) Atmung. In isolierten Herzmitochondrien konnten wir zudem zeigen, dass AOX die Succinat-getriebene mitochondriale ROS-Produktion stark herabsetzt. Der Einfluss von AOX auf die mitochondriale ROS-Produktion war insbesondere dann sichtbar, wenn der Komplex I nicht durch den Komplex I-Inhibitor Rotenon gehemmt wurde. Das deutet darauf hin, dass AOX RET effektiv unterbindet[40]. Diesen Befund haben wir in einer nachfolgenden Studie näher untersucht und bestätigt[137].

2.1.5 AOX^{Rosa26}-Mäuse sind physiologisch unauffällig

Die beobachtete hohe AOX-Expression und die Tatsache, dass AOX einen großen Teil des Elektronenflusses abzweigen kann, wenn die Komplexe III und/oder IV gehemmt sind, warf die Frage nach potentiell schädlichen Folgen unter normalen physiologischen (ungestressten) Bedingungen auf. Überraschenderweise waren hemizygote und homozygote AOX^{Rosa26}-Mäuse beiderlei Geschlechts phänotypisch von ihren Wildtyp (WT)-Wurfgeschwistern nicht zu unterscheiden. AOX^{Rosa26}-Mäuse nahmen während der Entwicklung regulär an Gewicht zu. Muskel- und Herzfunktionen wiesen zu verschiedenen Zeitpunkten hinsichtlich Haltekraft, Laufbandleistung und kardialer Auswurffraktion keine signifikanten Unterschiede auf. Um diese Daten zu ergänzen, führten wir in Kooperation mit der Deutschen Mausklinik[d] (Helmholtz Zentrum München) eine umfassende Phänotypisierung durch. Diese Analyse umfasste sowohl metabolische, verhaltensbezogene, morphologische, immunologische, kardiale und neurologische Parameter. Keiner der getesteten Parameter zeigte wesentliche oder systematische Abweichungen in AOX^{Rosa26}-Mäusen im Vergleich mit WT-Wurfgeschwistern. Diese Befunde deuten darauf hin, dass AOX trotz katalytischer Aktivität *in organello* unter physiologischen Standardbedingungen in der Maus *in vivo* funktionell inaktiv und somit biologisch inert ist. Frühere Arbeiten unterstützen diese Schlussfolgerung[138,144,148]. Indirekte Unterstützung für fehlende AOX-Aktivität unter nicht-gestressten Bedingungen kommt zudem von den folgenden Beobachtungen. (i) Ein wesentlicher Beitrag des nicht-Protonen-pumpenden AOX zum mitochondrialen Elektronenfluss sollte sich in einem signifikant erniedrigten respiratorischen Kontrollindex (RCI) widerspiegeln. Diesen Nachweis konnten wir in unserer Gewebeuntersuchung zumindest für Komplex I-verknüpfte Substrate nicht erbringen. (ii) Eine ineffiziente Mobilisierung von Nahrungsressourcen in AOX-exprimierende Mäuse müsste weitere metabolische Parameter in Mitleidenschaft ziehen. Wir konnten jedoch keine Unterschiede feststellen

[d] <https://www.mouseclinic.de>

im Gesamtkörpergewicht und physiologischen Parametern, die mittels indirekter Kalorimetrie bestimmt wurden wie Nahrungsaufnahme, Körpertemperatur oder Sauerstoff/CO_2-Austausch. (iii) Wir fanden keine signifikanten Unterschiede in der Herzfunktion ermittelt durch Echokardiographie oder Magnetresonanztomographie. Das Herz, als ein Gewebe mit hohem Energiebedarf aus OXPHOS, sollte aber sehr sensibel auf Ineffizienzen der Atmungskette reagieren.

Welche molekularen Mechanismen für die katalytische Inaktivität von AOX letztlich verantwortlich sind, ist gegenwärtig Gegenstand von Untersuchungen. Möglicherweise verhindert die starke Kompartimentierung der inneren mitochondrialen Membran mit unterschiedlichen Strukturen, Proteinzusammensetzungen und biochemischen Funktionen[178] eine effektive Interaktion von AOX mit der ETK. Insbesondere die supramolekulare Organisation von Atmungskettenkomplexen in Superkomplexe, allgemein als Maximierung der Effizienz des Elektronenflusses angesehen[179,180], könnte AOX-Atmung unter physiologischen Bedingungen verhindern. Auch die Funktion der beobachteten AOX-Multimere ist unklar, obwohl unsere Ergebnisse den Schluss zulassen, dass diese Multimere in der Maus „gutartig" sind. In welcher Form AOX in seinem natürlichen Wirt, *Ciona intestinalis*, vorliegt, ist genauso wenig bekannt, wie deren Einfluss auf seine katalytische Aktivität. Andererseits ist bekannt, dass AOX erst dann katalytisch aktiv werden kann, wenn der CoQ-Pool in der inneren Membran zu mindestens 35-40% reduziert vorliegt[142]. In Abwesenheit einer Atmungskettenstörung wird dieser Wert wahrscheinlich nicht erreicht. Nur bei Hemmung oder Überlastung der klassischen ETK (in Situationen mit Verlust der metabolischen Flexibilität) könnte der CoQ-Pool ausreichend reduziert vorliegen. Diese Annahme wird gestützt durch Experimente in isolierten Zellen[143] und stimmt auch mit unserer Beobachtung überein, dass AOX-Expression die mitochondriale ROS-Produktion in Herzmitochondrien in Gegenwart von hohen Succinat-Werten wie im ischämischen Herzen[121,122] drastisch verringert.

2.1.6 AOX verleiht Schutz gegen systemisch verabreichtes Zyanid

Trotz des Fehlens eines aussagekräftigen Phänotyps, der auf AOX-Aktivität unter physiologischen Standardbedingungen hinweist, wollten wir testen, ob die die ubiquitäre AOX-Expression eine Resistenz des Gesamtorganismus gegen ein Atmungskettengift zulässt. Dazu wurde AOX^{Rosa26}-Mäusen Zyanid als LD_{50} verabreicht[181] und die Überlebensrate nach bis zu 48 h ermittelt. LD (letale Dosis) ist eine in der Toxikologie verwendete Menge, wobei die Zahl (hier 50) die Letalität in Prozent in definierter Zeit nach Behandlung angibt. Alle fünf getesteten AOX^{Rosa26}-Mäuse überlebten die Zyanidgabe, während drei von sechs Kontrollmäusen erwartungsgemäß starben. Obwohl die Stichprobengröße klein und daher eher indikativ als definitiv ist, ist das Ergebnis konsistent mit einem Schutz gegen Zyanid auf der Ebene des Gesamtorganismus und bestätigt frühere Experimente an MitAOX-Mäusen[148].

2.2 Untersuchung des Einflusses xenotoper AOX-Expression auf Elektronenfluss und ROS-Bildung in isolierten Herzmitochondrien

In diesem Teilabschnitt wird beschrieben, wie sich eine xenotope AOX-Expression auf Atmungskettenfunktionen in isolierten Herzmitochondrien auswirkt. Ziel war es dabei, besser zu verstehen, warum AOX^{Rosa26}-Mäuse unter physiologischen Bedingungen phänotypisch weitestgehend unauffällig sind. Insbesondere wollten wir herausfinden, inwieweit möglicherweise die Nutzung unterschiedlicher Atmungskettensubstrate durch AOX diesen Befund beeinflusst. Außerdem hat uns interessiert, unter welchen Bedingungen die ROS-Produktion durch AOX vermindert wird und welche biochemischen Voraussetzungen für katalytische AOX-Aktivität erfüllt sein müssen. Resultate und Diskussion dieses Teilabschnittes entstammen in wesentlichen Teilen aus Szibor *et al.*, *Biochimica Et Biophysica Acta Bba - Bioenergetics*. **1861**, 148137 (2020)[137]. Unsere Ergebnisse zeigen, dass xenotop in der Maus exprimiertes AOX aus *Ciona intestinalis* als frei diffusibler Redoxpartner in der mitochondrialen Innenmembran agiert. AOX ist aber nur katalytisch aktiv, wenn der CoQ-Pool stark reduziert ist. Wir konnten zeigen, dass AOX vor allem unter nicht-phosphorylierenden Bedingungen aktiv ist, ein Zustand der allgemein als respiratorischer Stress beschrieben wird. AOX umgeht somit bei Stress respiratorische Kontrollmechanismen während es unter physiologischen Bedingungen kaum nennenswert in die mitochondriale Atmung eingreifen kann (**Abb. 3**). AOX könnte aufgrund dieser fehlenden Nebenwirkung in der Tat eine Behandlungsoption für Pathologien werden, bei denen die Einschränkung der metabolischen Flexibilität auf eine fehlerhafte Funktion der ETK zurückzuführen ist.

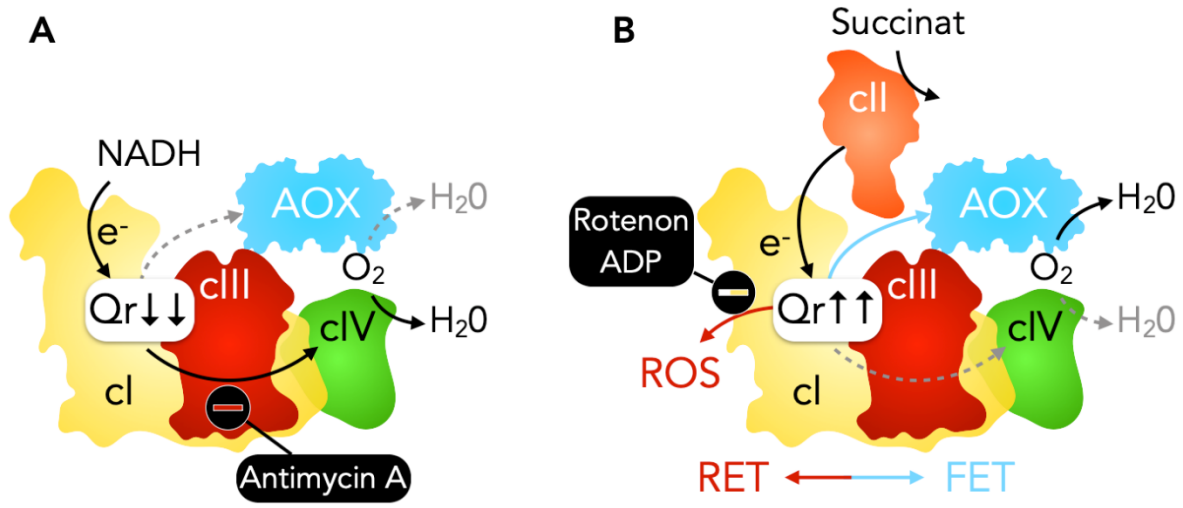

Abb. 3 *Grafische Darstellung des Eingreifens von AOX in den Elektronenfluss durch die ETK. (**A**) Komplex I-Substrate ermöglichen die AOX-Atmung nur, wenn Komplex III und/oder IV inhibiert werden. Der CoQ-Pool ist nur gering reduziert (Qr). Antimycin A, Komplex III-Inhibitor, blockt den Elektronenfluss durch die Komplexe III und IV. (**B**) Komplex II-Substrat Succinat aktiviert AOX-Atmung. Der CoQ-Pool ist stark reduziert. Rotenon oder ADP aktivieren die klassische Atmungskette (Elektronenfluss durch Komplexe III und IV). RET, reverse electron transport. FET, forward electron transport. Die Abbildung wurde adaptiert von Szibor et al., 2019[137].*

2.2.1 AOX interagiert nicht mit Proteinuntereinheiten der Atmungskette

In Ergänzung der oben beschriebenen Untersuchungen[136] wollten wir mit höherer Auflösung feststellen, ob AOX mit spezifischen Proteinuntereinheiten der ETK interagiert. Wir untersuchten diese Fragestellung zunächst unter Verwendung von Digitonin-solubilisierten Herzmitochondrien, die mittels BN-PAGE aufgetrennt wurden[182,183]. Da die Digitonin-vermittelte Solubilisierung von mitochondrialen Membranen ein relativ mildes Verfahren darstellt, das Superkomplexe und individuelle ETK-Komplexe weitestgehend intakt lässt, wird durch BN-PAGE in erster Dimension das sogenannte mitochondriale Komplexom abgebildet[177]. Ein Interaktionspartner aus der ETK (oder anderer Partner aus der inneren Membran) würde bei dieser Methode durch sein überlappendes Migrationsprofil auffallen. Danach kamen zwei, sich ergänzende Anwendungen, zum Einsatz. Zum einen wurde die Gel-Spur der ersten Dimension mit einem Skalpell fraktioniert und die einzelnen Fraktionen mit Trypsin verdaut. Dieser Verdau der einzelnen Fraktionen erlaubt massenspektrometrische Analysen. Parallel dazu inkubierten wir eine separate Gel-Spur der ersten Dimension mit dem stringenteren Detergens (n-Dodecyl β-Maltosid, DDM), um hochmolekulare Komplexe und Superkomplexe zu dissoziieren und in einer zweiten Dimension aufzutrennen (BN/BN)[175]. In keinem der beiden Ansätze fanden wir, abgesehen der bereits beschriebenen AOX-Multimere[136], Hinweise auf eine Interaktion zwischen AOX und einem der ETK-Komplexe. Alle ETK-Komplexe zeigten zudem regelmäßige Migrationsmuster und Zusammensetzung aus Untereinheiten. Dies lässt den Schluss zu, dass xenotop exprimiertes AOX in der Maus als frei diffusibler Redoxpartner agiert.

2.2.2 AOX erlaubt phosphorylierende Atmung in Gegenwart von Komplex I-Substraten

Ein frei diffusibler Redoxpartner der ETK stellt potenziell eine metabolische Bedrohung dar, wenn dadurch Teile der Atmungskette unkontrolliert umgangen werden. Das ist insbesondere dann problematisch, wenn der Redoxpartner, wie für AOX bekannt, nicht zum Aufbau des Protonengradienten beiträgt[184]. Dass bei Untersuchungen mit trypanosomaler AOX maximale NADH-Oxidationsraten in submitochondrialen Partikeln aus Rinderherzen erreicht wurden, scheinen diese Befürchtung zu unterstützen[185]. Wir haben beobachtet, dass selbst eine globale Expression von AOX aus *Ciona intestinalis* trotz katalytischer Aktivität keine schädlichen Auswirkungen auf die allgemeine Mausphysiologie hat[136]. Dies hängt unter Umständen mit der Unfähigkeit von AOX aus *Ciona intestinalis* im Gegensatz zu AOX aus *Trypanosoma brucei brucei* zusammen, effektiv mit dem Komplex III der Atmungskette der Maus um Elektronen aus dem reduzierten CoQ-Pool zu konkurrieren[186]. Wir testeten diese Annahme in isolierten intakten Mitochondrien und fanden, dass AOX bei Gabe von Komplex I-Substraten wenig in die mitochondriale Atmung eingreift. Zwar sinkt der respiratorische Kontrollindex (RCI) leicht von 6.9 ± 1.7 (Mittelwert ± SD) in WT-Mitochondrien auf 4.9 ± 1.5 in AOX-Mitochondrien, was auf eine leicht erhöhte Rate der nicht-phosphorylierenden Atmung (State 4) hinweist. Man kann aber anhand dieser Daten schlussfolgern, dass bei ungehemmter Atmungskette nur ca. 7% des Elektronenflusses aus Komplex I-Substraten durch AOX umgeleitet werden. Wir vermuteten, dass die Unfähigkeit von AOX, trotz optimaler Bedingungen als terminale Oxidase eingesetzt zu werden, auf seine hohe K_M für reduziertes CoQ zurückzuführen ist[187]. Deshalb bestimmten wir den Anteil von reduziertem CoQ am Gesamt-CoQ (in %) während Komplex I-getriebener Atmung in isolierten Herzmitochondrien mithilfe einer

selbstgefertigten CoQ-Elektrode[188]. Das Verhältnis von reduziertem zu Gesamt-CoQ blieb bei Komplex I-getriebener Atmung überraschend niedrig (≈13%) und zwar unabhängig davon, ob es sich um phosphorylierende oder nicht-phosphorylierende Atmung handelte. Eine mögliche Erklärung für diesen Befund ist, dass die kritische Schwelle für Aktivierung der AOX Atmung (ca. 35-40% reduziertes CoQ)[142] bei ungehemmter Komplex I Atmung nicht erreicht wird. Antimycin A erhöht hingegen die mitochondriale CoQ-Reduktion[187]. In der Tat konnten wir nach Hemmung der Atmungskette durch Antimycin A eine starke AOX-getriebene Atmung nachweisen. Die Tatsache, dass Antimycin A und Azid (ein potenter Komplex IV-Inhibitor) in ähnlicher Weise die AOX-Atmung stimulierten, macht unspezifische Inhibitor-Effekte unwahrscheinlich. Inhibitor-Titrationsexperimente gepaart mit BN-PAGE haben zudem ergeben, dass diese AOX-Atmung nicht auf einem Verlust der ETK-Komplexintegrität und unkontrollierter Freisetzung von reduziertem CoQ beruht. Ein weiteres wichtiges Ergebnis war, dass AOX in Gegenwart von Antimycin A, obwohl selbst nicht Protonen-pumpend[184], durch Komplex I-vermittelte Atmung $\Delta\psi$ aufrechterhalten kann (Rotenon unterbindet diesen Effekt). Basierend auf diesen Ergebnissen konnten wir schlussfolgern, dass AOX, auch wenn es aufgrund seiner katalytischen Eigenschaften OXPHOS weniger effizient macht, unter bestimmten Voraussetzungen ATP-Spiegel indirekt erhält.

2.2.3 AOX erhöht die Succinat-abhängige Atmung in Gegenwart von Rotenon

Der Komplex II der Atmungskette ist wie AOX keine Protonenpumpe und nicht Bestandteil von respiratorischen Superkomplexen. Dennoch erhöht die Oxidation von Succinat durch den Komplex II den Anteil des reduzierten CoQ am Gesamt-CoQ schnell auf ca. 90%[187]. Ein solcher Wert liegt deutlich über der angenommenen Schwelle für AOX-Aktivierung[142] und würde den Schluss zulassen, dass Komplex II und AOX bei Koexpression eine Kurzschlussatmung verursachen. Das würde aber, im Umkehrschluss, die Lebensfähigkeit von Zellen und Organismen erheblich einschränken. Unsere Untersuchungen in AOX^{Rosa26} deuten darauf hin, dass die Aktivierung einer solchen Kurzschlussatmung unter nicht gestressten Bedingungen in der Maus nicht stattfindet[136]. Um die mechanistische Grundlage für dieses Paradoxon zu verstehen, haben wir in isolierten Herzmitochondrien Atmungsraten von Succinat in Gegenwart von Rotenon gemessen. Unsere Daten bestätigen, dass Succinat den CoQ-Pool schnell zu über 90% reduziert[187], ohne dabei relevante Mengen mitochondrialer reaktiver Sauerstoffspezies (ROS) zu erzeugen. Wie erwartet steigert AOX mitochondriale Atmungsraten sowohl unter phosphorylierenden als auch nicht-phosphorylierenden Bedingungen. Eine solche Umleitung des Elektronenflusses durch AOX spiegelt sich auch in einer Abnahme des RCI wider, der von 3.2 ± 0.5 (Mittelwert ± SD) in WT- auf 1.3 ± 0.1 in AOX-Mitochondrien sinkt. Interessanterweise hat die Atmungsrate und AOX-Aktivität, wenn überhaupt, nur einen relativ geringen Einfluss auf den CoQ-Redoxstatus. Ähnlich wie bei der Komplex I-Atmung wird $\Delta\psi$ auch während der Succinat-getriebenen Atmung aufrechterhalten, was darauf hindeutet, dass selbst in Anwesenheit von AOX ein signifikanter Anteil des Elektronenflusses über die Aktivitäten der Komplexe III und IV (beides Protonenpumpen) vermittelt wird.

2.2.4 AOX verhindert den reversen Elektronentransport

Die Hemmung des Komplex I durch Rotenon *in organello* spiegelt keinen metabolischen Zustand wider, wie er *in vivo* vorkommt. Deshalb wollten wir wissen, ob die Hemmung des Komplex I für die widersprüchlichen Befunde verantwortlich sein könnte, dass AOX einerseits

die Succinat-getriebene Atmung *in organello* steigert, andererseits aber AOX^{Rosa26}-Mäuse phänotypisch unauffällig sind[136]. Ein besseres Verständnis der zugrunde liegenden Mechanismen ist wichtig, weil Succinat-Akkumulation zusammen mit hohen $\Delta\psi$ und reduziertem CoQ unter pathologischen Bedingungen (z. B. kardiale IR und Endotoxämie)[58,122] die mitochondriale ROS-Produktion stimulieren soll[40]. Wir untersuchten deshalb die Succinat-Atmung erneut in isolierten Herzmitochondrien allerdings in Abwesenheit von Rotenon und somit mit funktionsfähigem Komplex I. Unter diesen Bedingungen erlaubte AOX Succinat-Atmung vor allem unter nicht-phosphorylierenden Bedingungen. Obwohl die Zugabe kleiner Mengen von ADP die Atmung in WT-Mitochondrien erhöhte, hatte die Anwesenheit von AOX hier keinen nennenswerten additiven Effekt. Die Zugabe von ADP im Überschuss konnte sowohl in WT- als auch in AOX-Herzmitochondrien keine anhaltende phosphorylierende Atmung induzieren. Dieses Phänomen wurde in einer anderen Arbeit auf den Verlust von $\Delta\psi$ und die Bildung des potenten Komplex II-Inhibitors Oxalacetat zurückgeführt[189]. Diese Schlussfolgerungen werden durch unsere Ergebnisse nicht gestützt. Obwohl die Zugabe von ADP die Größe des $\Delta\psi$ stark verringerte, stellte eine Hemmung der ATP/ADP-Translokase (ANT) $\Delta\psi$ wieder her. Das deutet darauf hin, dass die beobachtete Depolarisation auf einen mitochondrialen Austausch von ATP und ADP beruht und nicht auf einer Hemmung des Komplex II. Darüber hinaus zeigten Messungen des Redox-Gleichgewichts des CoQ-Pools, dass dieser unabhängig von der An- oder Abwesenheit von ADP und/oder AOX durch Succinat stark reduziert wird. Die Zugabe von Komplex I-Substraten und/oder Rotenon erhöhte die Succinat-getriebenen Atmungsraten zwar deutlich, führte aber nur zu einer vernachlässigbaren Oxidation des CoQ-Pools. Wichtig hinsichtlich der oben beschriebenen Bedeutung als Krankheitsmechanismus ist die Beobachtung, dass AOX auch in Abwesenheit von Rotenon die mitochondriale ROS-Produktion erheblich reduzierte. Dies schien insbesondere bei Succinat-Atmung unter nicht-phosphorylierenden Bedingungen der Fall zu sein. Dabei hat AOX nie maximale Atmungsraten erreicht, was darauf hindeutet, dass es eine Einschränkung des Elektronenflusses unabhängig vom CoQ-Redoxstatus gibt. Wenn AOX jedoch aktiv ist, unterstützt es die Atmung und hebt die mitochondriale ROS-Produktion durch RET in ähnlicher Weise auf wie die Zugabe von ADP. Aus unserer Sicht spricht das gegen die Oxalacetat-Hypothese. Wir nehmen deshalb an, dass Succinat *in vivo* möglicherweise kein wichtiges Atmungssubstrat ist, da ein nicht-phosphorylierender respiratorischer Komplex II-AOX-Shunt unweigerlich zu einem schweren, nicht lebensfähigen, Phänotyp führen würde, was offensichtlich nicht der Fall ist[136]. Interessant ist, dass wir bei Zugabe von Komplex I-Substraten zu den Mitochondrien einen Anstieg der phosphorylierenden, Oligomycin-sensitiven Atmung und eine Abnahme der ROS-Produktion beobachteten. Diese Stimulation ist jedoch nicht allein von einer Erhöhung des $\Delta\psi$ oder des Elektronenflusses durch Komplex I abhängig, da die Zugabe von Rotenon ein ähnliches Ergebnis zeigte. Dieser Befund wirft weitere Fragen bezüglich der wahren Funktion des Komplex II und seiner Regulation durch andere Komplexe der ETK auf. Im Gegensatz zum Komplex I, der zu mindestens 84% in respiratorischen Superkomplexen organisiert ist[182], ist der Komplex II nicht Teil höherer Organisation. Unsere Daten lassen den Schluss zu, dass der Komplex I eine Art Flusskontrolle von Elektronen durch den CoQ-Pool übernimmt. Komplex II kann zwar den CoQ-Pool fast komplett reduzieren, für maximale Atmung bedarf es jedoch der Zugabe von Rotenon. Die eigentliche Funktion der Superkomplexe ist also möglicherweise ein effektiver Schutz vor ungewollter CoQ-Oxidation.

2.3 Charakterisierung der Funktion der mitochondrialen ETK in der pulmonalen Vaskulatur bei akuter und chronischer Hypoxie

In diesem Teilabschnitt wird beschrieben, welchen Einfluss die mitochondriale Atmungskette auf die intrazelluläre Detektion von Sauerstoffkonzentrationen hat und wie dadurch die kontraktile Funktion in glatten Muskelzellen von Pulmonalarterien beeinflusst wird. Insbesondere hat uns interessiert, ob mitochondriale Signale die Kontraktion von glatten Muskelzellen induzieren und an welcher Position in der Signalkaskade sie gegebenenfalls stehen. Resultate und Diskussion dieses Teilabschnittes entstammen in wesentlichen Teilen aus Sommer *et al.*, *Sci Adv.* **6**, eaba0694 (2020)[149]. Unsere Daten weisen darauf hin, dass die Hemmung der mitochondrialen Atmungskette sehr hoch in der HPV-Signalhierarchie steht. Superoxidradikale, die in der ETK entstehen, sind für die Induktion einer akuten HPV essentiell obwohl andere Hypoxie-empfindliche Komponenten existieren (**Abb. 4**). Diskutiert werden die unterschiedlichen Wirkungen von AOX bei akuter und chronischer Hypoxie in der Lunge, was einmal mehr den Wert von AOX als genetisches Werkzeug zur Untersuchung von Krankheitsmechanismen unterstreicht. Für bestimmte Formen der HPV stellt AOX möglicherweise einen neuartigen therapeutischen Ansatz dar.

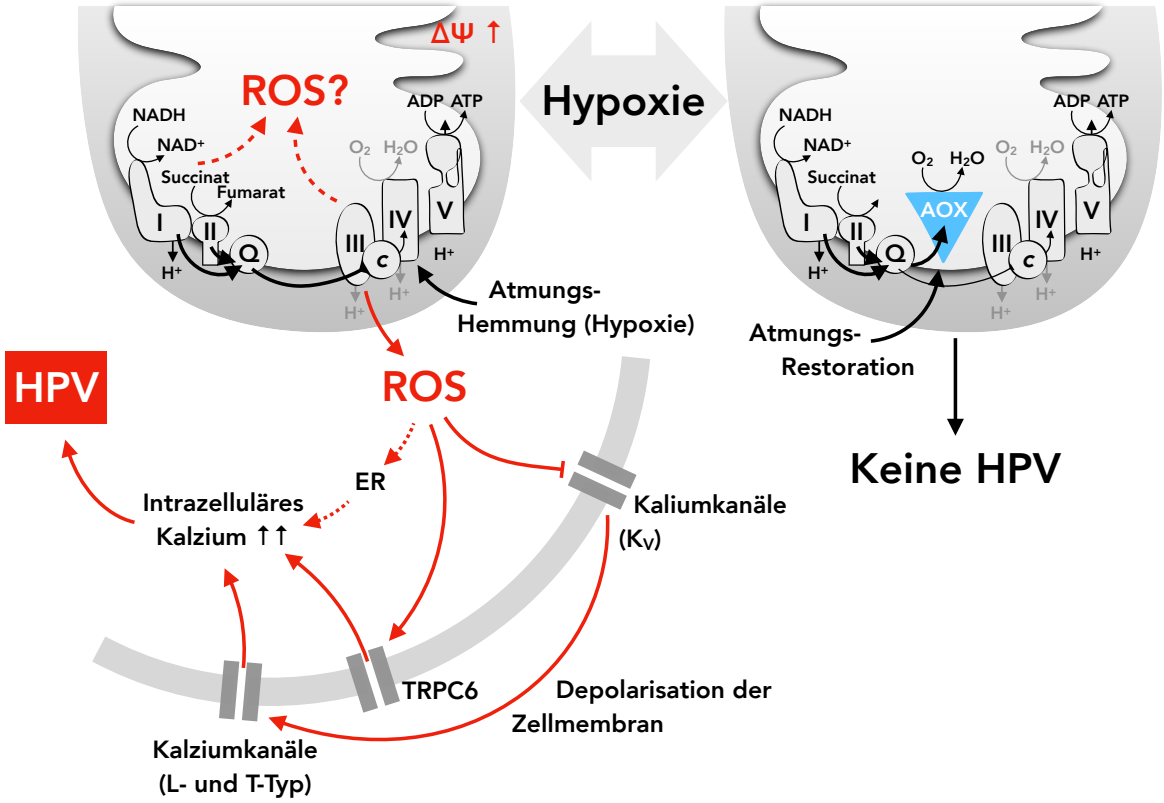

Abb. 4 *Darstellung des Zusammenhangs zwischen Hypoxie-Signalen der ETK und HPV in der Lunge der Maus. Akute HPV hängt von einem zentralen Sauerstoffsensor innerhalb der mitochondrialen Atmungskette ab (wahrscheinlich lokalisiert am Komplex IV). Hypoxie induziert eine Hyperpolarisation der mitochondrialen Membran, einen Anstieg der mitochondrialen ROS-Freisetzung und eine anschließende Hemmung der zellulären Kaliumkanäle (Kv), was zu einer zellulären Membrandepolarisation und Aktivierung von spannungsabhängigen Kalziumkanälen führt. Diese Abfolge von Ereignissen führt zur HPV. AOX verhindert HPV in der Maus, indem es die mitochondriale ROS-Produktion und -Freisetzung verhindert. Dies stellt die Mitochondrien und den Elektronenfluss*

durch die mitochondriale Atmungskette auf die oberste Ebene in der Hierarchie des Hypoxiesignalwegs, der die HPV kontrolliert. Die Abbildung wurde adaptiert von Sommer et al., 2020[149].

2.3.1 AOX hemmt die hypoxische pulmonale Vasokonstriktion (HPV)

Zunächst haben wir die Expression von AOX in verschiedenen Abschnitten der Lunge, einschließlich des Gefäßsystems und der Atemwege, überprüft und eine breite Expression in verschiedenen Zellen und Kompartimenten der Lunge bestätigt. Das war notwendig, weil bei der Erstbeschreibung von AOX^{Rosa26} lediglich nach AOX-Expression in verschiedenen Geweben gesucht wurde[136]. Wir konnten zeigen, dass AOX breit in Zellen der Lunge exprimiert wird, insbesondere jedoch in den Zellen der pulmonalen Vaskulatur wie Endothelzellen und glatten Muskelzellen. Damit eignet sich das AOX^{Rosa26}-Modell für Untersuchungen zur Hypoxie-induzierten pulmonalen Vasokonstriktion (HPV). Kürzlich wurde gezeigt, dass Signale der mitochondrialen ETK die HPV steuern[90,190], ohne die darunter liegenden Mechanismen vollends aufzuklären. Wir wollten mithilfe von AOX^{Rosa26}-Mäuse testen, ob die Wiederherstellung des Elektronenflusses durch die ETK die Entwicklung der HPV beeinflusst. Vasokonstriktion wurde in unseren Untersuchungen als Anstieg des pulmonal-arteriellen Drucks (ΔPAP) in isolierten, hypoxisch beatmeten und mit Puffer perfundierten Lungen gemessen. In WT-Lungen erreichte ΔPAP nach ungefähr 10 min hypoxischer Beatmung (akute HPV) einen kurzzeitigen Maximalwert, der zunächst wieder abfiel bevor er unter längerer Hypoxie von bis zu 3 h (anhaltende HPV) wieder anstieg (ohne jedoch den Maximalwert wieder zu erreichen). AOX-exprimierende Lungen zeigten eine nahezu komplette Hemmung der HPV unter akut-hypoxischer Beatmung. Um zu testen, ob dieses Ergebnis wirklich auf die katalytische Aktivität von AOX zurückzuführen ist, haben wir PAP in Gegenwart von Zyanid gemessen. Auch Zyanid induzierte HPV in WT- aber nicht in AOX-Lungen. Ein weiterer Hinweis auf einen kausalen Zusammenhang mit der Expression von AOX ergab sich aus Versuchen mit einem AOX-spezifischen Inhibitor, n-Propylgallat (nPG). AOX-Hemmung durch nPG während akut-hypoxischer Beatmung stellte die HPV wieder her. Um sicherzugehen, dass der AOX-Effekt nicht auf einer unspezifischen Lungenschädigung basiert oder beispielsweise auf ein gestörtes Kalzium-Signal zurückzuführen ist, stimulierten wir isolierte Lungen mit dem Hypoxie-unabhängigen Vasokonstriktor U46619, einem Thromboxan-Mimetikum. WT- und AOX-Lungen reagierten mit einem vergleichbaren Anstieg des PAP, was auf eine intakte pulmonale Gefäßphysiologie hinweist. Im Unterschied zur HPV haben wir keinen Einfluss von AOX auf eine post-ischämische Endothelschädigung gefunden, was routinemäßig als Anstieg der kapillaren Filtrationsrate (Kfc) und der Gewichtszunahme der Lunge gemessen wird. Diese Ergebnisse stützen die Schlussfolgerung, dass die AOX-Expression in der Mauslunge die Reaktion des Lungengefäßsystems auf akute und anhaltende Hypoxie spezifisch hemmt. Darüber hinaus lassen unsere Daten den Schluss zu, dass Schäden durch Ischämie-Reperfusion anderen Mechanismen unterliegen.

2.3.2 AOX vermindert die Hypoxie-induzierte zelluläre Membrandepolarisation in isolierten pulmonal-arteriellen glatten Muskelzellen (PASMC)

Wir untersuchten die Hypoxie-Reaktion in isolierten pulmonal-arteriellen glatten Muskelzellen (PASMC). In früheren Untersuchungen wurde diskutiert, dass die zelluläre Membrandepolarisation ein essentieller Schritt in der Entwicklung der HPV ist. Konkret wurde gezeigt, dass ein

Teil der Membrandepolarisation durch die Aktivierung von ROS-abhängigen Signalwegen erreicht wird. Dabei sollen (mitochondriale) ROS die Aktivität von bestimmten Ionenkanälen in der Zellmembran beeinflussen[87], z. B. über eine Wasserstoffperoxid-vermittelte Hemmung von K_V-Kanälen[90]. Hemmung der K_V-Kanäle führt demnach zu einer Depolarisation der Zellmembran und einer anschließenden Aktivierung von L- und T-Typ-Kalziumkanälen, wodurch der intrazelluläre Kalziumspiegel steigt und HPV ausgelöst wird[191,192]. Der Schwellenwert für die Aktivierung von spannungsabhängigen Kalziumkanälen wurde für Maus PASMC in einer früheren Arbeit bei einem Membranpotential zwischen -30 und -20 mV festgestellt[193]. Um zu testen, ob die AOX-Effekte über diesen Mechanismus funktionieren, nutzten wir die *Patch-Clamp*-Technologie. Wir fanden zunächst in isolierten Maus PASMC, dass das basale Membranpotential in WT- und AOX-PASMC ähnlich war. Wie erwartet, erhöhte sich das zelluläre Membranpotential graduell in WT-PASMC nach Hypoxie-Exposition. Im Gegensatz dazu war die Hypoxie-Antwort in AOX-PASMC abgestumpft, d.h. die Depolarisation stoppte beim Erreichen eines niedrigeren (unterschwelligen) Niveaus. Zugabe von nPG vervollständigte die Membrandepolarisation. Die nur teilweise Inhibierung der Membrandepolarisation durch AOX deutet allerdings darauf hin, dass mehrere Mechanismen zum Erreichen einer Schwelle der zellulären Membrandepolarisation beitragen, die für die endgültige Ausführung der HPV notwendig ist[194], beispielsweise Hypoxie-sensitive Kaliumkanäle[195,196]. Wir wollten testen, ob die Abschwächung der Membrandepolarisation auch die Entwicklung der HPV beeinflusst. Um diese Frage in einem physiologischeren Kontext zu testen, untersuchten wir die Hypoxie-induzierte Vasokonstriktion in isolierten pulmonal-arteriellen Gefäßen. Auch in diesem Modell wurde die HPV durch AOX verhindert. Wir haben als nächstes die Höhe des Membranpotentials durch Zugabe von Kaliumchlorid experimentell verschoben. Damit konnten wir das mitochondriale Hypoxie-Signal umgehen und die HPV auslösen. Einen ähnlichen Effekt hatte die Zugabe von Kaliumchlorid zum Perfusat in isolierten AOX-Lungen. Dies deutet darauf hin, dass Mitochondrien, insbesondere der Elektronenfluss durch die ETK, in der Hierarchie der akuten HPV-Signalkaskade über einer ROS-vermittelten Hemmung von Kaliumkanälen liegt.

2.3.3 AOX hemmt Hypoxie-induzierte mitochondriale Superoxid-Freisetzung und Membran-Hyperpolarisation in PASMC

Ein allgemeiner Hinweis für einen gestörten Elektronenfluss durch die Atmungskette ist die Produktion von ROS und reaktiven Stickstoffspezies (RNS). Deshalb haben wir getestet, ob ROS und RNS das eigentliche mitochondriale Signal sind, das die HPV auslöst. Wir untersuchten deren Freisetzung in Hypoxie-exponierten, tiefgefrorenen Maus-PASMC mithilfe von spezifischen Sonden für Elektronenspinresonanz-(ESR)-Spektroskopie. Um den Anteil des Superoxids am Gesamt-ROS/RNS zu bestimmen, inkubierten wir Kontrollproben mit Polyethylenglykol-konjugierter Superoxiddismutase (pSOD). Wir fanden, dass die Superoxid-Konzentration unter hypoxischen Bedingungen in WT-PASMC, aber nicht in AOX-PASMC, anstiegen. Um diesen Befund zu validieren, exprimierten wir entweder natives AOX oder eine katalytisch inaktive AOX-Mutante[197] in WT-PASMC. In diesem Versuchsaufbau zeigte nur die inaktive AOX-Mutante einen Hypoxie-abhängigen Anstieg der Superoxidproduktion. Um den Mechanismus hinter der erhöhten Superoxidproduktion näher zu untersuchen, haben wir ebenfalls das mitochondriale Membranpotential ($\Delta\psi$) gemessen. In WT-PASMC, aber nicht in AOX-PASMC, kam es unter Hypoxie zu einer Erhöhung des Membranpotentials. Um herauszufinden, ob AOX während der akuten Hypoxie ausreichend katalytisch aktiv ist, untersuchten wir

als Nächstes Atmungsraten bei abnehmenden Sauerstoffmengen. Dazu haben wir PASMC aus der Ratte isoliert und mit einem AOX-kodierenden Plasmid transfiziert. WT- und AOX-transfizierte Ratten-PASMC zeigten verringerte Atmungsraten bei Sauerstoffabnahme. Besonders bei niedrigen Sauerstoffkonzentrationen hatten AOX-exprimierende PASMC jedoch einen geringfügig (aber signifikant) höheren Sauerstoffverbrauch als die WT-Kontrollen. Dieser Befund stützt unsere Annahme, dass AOX auch unter hypoxischen Bedingungen in die mitochondriale Signalkaskade eingreifen kann. In früheren Arbeiten wurde diskutiert, dass eine ROS-Freisetzung speziell am Komplex III ein wesentlicher Schritt im Prozess der HPV sein könnte[198,199]. Die Identifizierung einer Komplex IV Untereinheit in diesem Hypoxie-Signalweg[90] stimmt mit der Komplex III-Hypothese prinzipiell überein. Bislang blieb der initiale Auslösemechanismus der akuten Hypoxie aber unklar. Mithilfe von AOX, das katalytisch nur aktiv ist, wenn der CoQ-Pool ausreichend reduziert ist[142] und eine mitochondriale Membran-Hyperpolarisation vorliegt[40], konnten wir zeigen, dass die Hemmung der mitochondrialen Atmungskette und Störung des Elektronenflusses der erste Schritt für die Induktion einer HPV sein könnte. Leider gibt unsere Studie keinen Hinweis auf die genaue Quelle der ROS-Produktion am Komplex I oder III (oder beiden). Allerdings ist uns keine Studie bekannt, die eine erhöhte ROS-Bildung am Komplex I als Auslöser von HPV überzeugend beschreibt. Außerdem können wir nicht ausschließen, dass eine Hypoxie-induzierte Zunahme oder Abnahme von Krebs-Zyklus Intermediaten ebenfalls zur Hemmung der hypoxischen Reaktion in Gegenwart von AOX beiträgt. Eine herausragende Rolle der Hypoxie-induzierten Superoxid-Freisetzung am Komplex III wurde allerdings bereits zuvor mit dem spezifischen Komplex III-abhängigen ROS-Inhibitor S3QEL2[200] nachgewiesen, der nachweislich HPV verhindert[90]. Darüber hinaus wurde gezeigt, dass ein Knockdown von Komplex III-Untereinheiten akute Hypoxie-induzierte Reaktionen des Lungengefäßsystems hemmt[199]. Diese Befunde werden nun durch unsere Untersuchung unter Verwendung von AOX untermauert.

2.3.4 AOX beeinflusst den mitochondrialen Redoxstatus unter Hypoxie

In Mitochondrien ist der Redoxstatus der einzelnen ETK-Komplexe hochdynamisch und hängt insbesondere von der Sauerstoffversorgung ab. Dementsprechend sollte eine hypoxische Inhibition des Komplex IV durch Hemmung des Elektronenflusses die vorgeschalteten ETK-Komplexe reduzieren. Als Konsequenz müsste sich ebenfalls das NADH/NAD^+-Verhältnis erhöhen. Da AOX die mitochondriale Kette verzweigt, wenn der Elektronenfluss unterhalb des CoQ-Pools beeinträchtigt ist[137], stellten wir die Hypothese auf, dass sowohl der Redoxstatus der ETK als auch das NADH/NAD^+-Verhältnis unter Hypoxie in AOX-PASMC unverändert bleiben würden. Um diese Hypothese zu testen, führten wir eine Raman-Spektroskopie durch, die es erlaubt, den Redoxstatus einzelner ETK-Komponente und das NADH/NAD^+-Verhältnis in lebenden PASMC zu untersuchen[201–205]. Wie erwartet, führte akute Hypoxie zu einer verstärkten Reduktion von NADH, CoQ und Cytochrom *c* in isolierten PASMC aus WT-Mäusen. Interessanterweise war der Redoxstatus von Cytochrom *b* unverändert, was möglicherweise auf ein Elektronenleck am Komplex III hindeutet. In Übereinstimmung mit unserer Hypothese wurden keine Veränderungen des Redoxstatus an Cytochrom *c* und Cytochrom *b* in AOX-PASMC beobachtet. Außerdem stiegen die Spiegel von NAD^+ aber nicht von NADH unter Hypoxie in AOX-PASMC an. Diese Befunde unterstützen unsere vorherige Beobachtung, dass AOX bei akuter Hypoxie katalytisch aktiv ist, und legen nahe, dass NADH (ein Komplex I-Substrat) ein wesentlicher Elektronendonor für die AOX-Atmung ist.

2.3.5 AOX hat keinen Einfluss auf Adaptationsprozesse bei chronischer Hypoxie

Interessanterweise wurde die mitochondriale Beeinträchtigung auch als zugrundeliegender Mechanismus für die chronische Hypoxie-induzierte pulmonale Hypertonie (PH) beschrieben[206], eine lebensbedrohliche Erkrankung, die z. B. in großer Höhe auftritt. Um zu testen, ob die AOX-Expression auch die nachteiligen Auswirkungen einer generalisierten chronischen Hypoxie verhindern kann, haben wir WT- und AOX-Mäuse einer 4-wöchigen Hypoxie (10% O_2) ausgesetzt. Entgegen unserer Erwartungen entwickelten sowohl WT- als auch AOX-Mäuse eine ausgeprägte PH mit ähnlichen Veränderungen des rechtsventrikulären systolischen Drucks, der rechtsventrikulären Hypertrophie, des Herzzeitvolumens und der Muskularisierung der pulmonalen Gefäßmuskulatur. Auch bei anderen kardialen und/oder systemischen Parametern, die die Reaktion auf Hypoxie charakterisieren, konnten wir keinen Vorteil der Expression von AOX finden. Auch die HIF-1α-Expression war in PASMC beider Stämme nach 3 Tagen Hypoxie (1% O_2) ähnlich erhöht, was darauf hindeutet, dass zumindest unter diesen Bedingungen mitochondriale ROS kein relevanter Auslöser für die Stabilisierung von HIF-1α und die Entwicklung einer PH sind. Unsere Daten deuten wie andere Arbeiten auf unterschiedliche Signalwege bei akuter bzw. chronischer Hypoxie hin[90,194,207]. Die genaue Rolle mitochondrialer ROS ist dabei weiterhin unklar. Bei chronischer Hypoxie wurde eine Zunahme von mitochondrialen ROS genauso diskutiert[198] wie deren Abnahme[208] mit Auswirkung auf Proliferation von PASMC und pulmonalen Gefäßumbau[209,210]. Es gibt auch widersprüchliche Berichte über die Auswirkungen mitochondrialer ROS auf die Stabilisierung von HIF-1α, einem zentralen Treiber für die Entwicklung chronischer Hypoxie-induzierter PH[209]. Einige Autoren fanden Hinweise auf seine Stabilisierung[198,211], andere fanden keinen solchen Effekt[212]. Die Tatsache, jedoch, dass AOX weder die chronische Hypoxie-induzierte PH hemmt, noch die Hypoxie-induzierte Stabilisierung von HIF-1α beeinträchtigt, könnte dazu beitragen, diese widersprüchlichen Befunde aufzulösen und die akuten und chronischen Auswirkungen von Hypoxie in der Lunge als zwei grundlegend unterschiedliche Prozesse zu erkennen. Die Diskrepanz zu anderen Studien könnte natürlich auch auf zelltypspezifische Mechanismen der Stabilisierung von HIF-1α oder zeit- und sauerstoffkonzentrationsabhängige Unterschiede hinweisen. Zum Beispiel könnten nicht-mitochondriale ROS-Quellen, wie NADPH-Oxidasen, in der pulmonalen Vaskulatur unter chronisch hypoxischen Bedingungen von größerer Bedeutung sein. Obwohl AOX unter chronischer Hypoxie keinen Einfluss auf allgemeine physiologische Parameter hatte, konnten wir bei PASMC, die AOX exprimieren, eine geringere Proliferationsfähigkeit feststellen. Dies könnte jedoch ein Zellkultur-Effekt sein, der durch eine partielle Aktivierung von AOX unter hohen glykolytischen Bedingungen entsteht. Außerdem ist nicht auszuschließen, dass *in vitro*-Effekte der mitochondrialen ROS-Freisetzung in Bezug auf HIF-1α-Stabilisierung von der *in vivo* Situation abweichen.

2.4 Bewertung des mitochondrialen Einflusses auf Zigarettenrauch-induzierte pulmonale Dysfunktion und Gewebeschäden

In diesem Teilabschnitt haben wir untersucht, inwieweit Zigarettenrauch-induzierter Lungenumbau und darauf basierende Dysfunktion des Gasaustausches auf Hemmung der mitochondrialen Atmungskette zurückzuführen ist. Resultate und Diskussion dieses Teilabschnittes entstammen in wesentlichen Teilen aus Giordano *et al.*, *Am J Resp Cell Mol.* **60**, 515–522 (2019)[150]. Unsere Ergebnisse identifizieren eine gestörte mitochondriale ETK als einen molekularen Mechanismus, der den Lungenumbau nach Zigarettenrauch-Exposition vorantreibt. Wir zeigen hier, dass ein molekularer Bypass von Teilen der Atmungskette die Zellvitalität erhöhen kann und als Konsequenz die Lungenfunktion aufrechterhält und/oder Reparaturprozesse erleichtert (**Abb. 5**). Dies ist aus einer Reihe von Gründen von Bedeutung. Insbesondere zeigt die adulte humane Lunge kaum Regenerationsfähigkeit. Daher ist jeder Mechanismus, der die Pathologie abschwächt, von großem Interesse nicht nur für Millionen von Zigarettenkonsumenten, sondern auch für Bevölkerungsgruppen, die toxischem Rauch in der Umwelt ausgesetzt ist. Dies geschieht beispielsweise durch städtische Luftverschmutzung oder im häuslichen Umfeld insbesondere in weniger entwickelten Ländern.

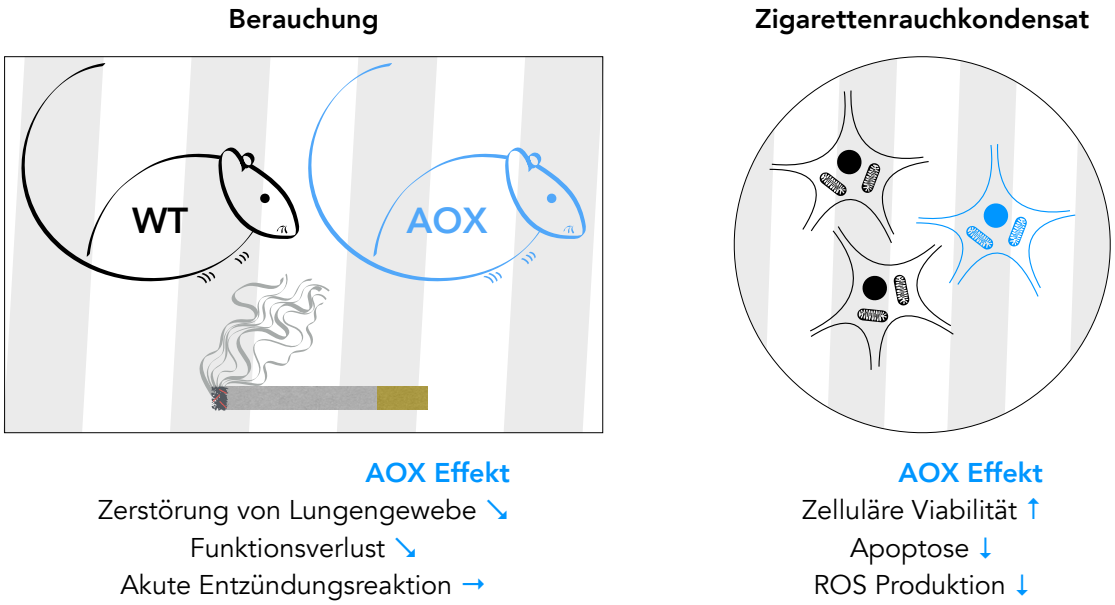

Abb. 5 *AOX^{Rosa26}-Mäuse wurden chronisch (9 Monate) oder akut (4 Tage) nach Standardprotokoll beraucht. Chronische Zigarettenrauchexposition verursachte Lungenschäden/-umbau, der durch AOX-Expression abgemildert wurde. Die akute Entzündungsreaktion (Einwandern von Makrophagen und Neutrophilen und Expression von Interleukinen) war von AOX unbeeinflusst. Fibroblasten wurden in Gegenwart von Zigarettenrauchkondensat kultiviert. AOX verbesserte die Viabilität, reduzierte die Expression von Apoptose-Markern und verhinderte eine exzessive ROS-Produktion.*

2.4.1 AOX mildert chronische Zigarettenrauch-induzierte Gewebeschäden und Lungendysfunktion

Um die Auswirkungen von Zigarettenrauch auf die Physiologie der Lunge zu messen, wurden WT- und AOX^{Rosa26}-Mäuse[136] für 9 Monate nach standardisierten Bedingungen beraucht[213,214]. Rauchexposition verursachte bei allen Mäusen einen Verlust des Körpergewichts, obwohl der

Unterschied nur bei WT-Tieren statistische Signifikanz erreichte. Um eine mögliche Verzerrung durch Unterschiede im Körpergewicht zu eliminieren, wurden deshalb alle nachfolgend gemessenen funktionellen Lungenparameter auf das jeweilige Körpergewicht normalisiert. Infolge des Zigarettenrauch-induzierten Lungenumbaus waren das Lungenvolumen und die Hysterese in WT-Mäusen signifikant erhöht. Diese Werte waren im Vergleich zu WT- in AOX-Mäusen nach Berauchung signifikant niedriger, was auf einen AOX-vermittelten Schutz hinweist. Bei anderen Parametern wie der Compliance und der forcierten Vitalkapazität erreichte der Schutz durch AOX keine statistische Signifikanz. Um den Schweregrad der Lungenschädigung durch Zigarettenrauch zu visualisieren, untersuchten wir Lungengewebe zudem mittels Stereologie und fanden eine Zunahme des Volumens der Alveolen. Auch hier waren die Umbauvorgänge in AOX^{Rosa26}-Lungen weniger ausgeprägt. Zusammengenommen zeigen diese Ergebnisse, dass AOX die Gewebezerstörung bei Zigarettenrauch-Exposition zwar nicht aufhebt aber abschwächt.

2.4.2 AOX schützt Zigarettenrauchkondensat-behandelte Zellen

Um die molekularen Mechanismen zu identifizieren, die den beobachteten Effekten von AOX bei Zigarettenrauch-Exposition zugrunde liegen, haben wir ein Zellkulturmodell etabliert. Da die stärksten Effekte Parameter betrafen, die die Elastizität der Lunge widerspiegeln (z. B. die Hysterese), wählten wir immortalisierte embryonale Mausfibroblasten (iMEFs) als Zelltyp zur Untersuchung. iMEFs wurden zunächst in Glukose-haltigem Medium kultiviert und mit Zigarettenrauchkondensat behandelt[215], ein Surrogat für Zigarettenrauch unter Zellkulturbedingungen. Die Anzahl der lebensfähigen Zellen wurde nach 2 oder 3 Tagen mit einem Zytotoxizitäts-Assay (Sulforhodamine B-Assay) bestimmt[216,217]. Zigarettenrauchkondensat senkte die zelluläre Vitalität Dosis-abhängig in WT- und AOX-iMEFs. Allerdings verlieh AOX-iMEFs einen robusten Schutz gegen die Toxizität von Zigarettenrauchkondensat. Um zu testen, ob die Ursache der Toxizität eine dysfunktionale ETK ist, die durch AOX wiederhergestellt wird, haben wir iMEFs in Galaktose-haltigem Medium kultiviert. Dieser Versuch geht auf eine Beobachtung zurück, wonach ETK-defiziente Fibroblasten in Glukose- aber nicht Galaktose-haltigem Medium überleben[218]. Ursächlich verantwortlich ist der relativ langsame Stoffwechsel von Galaktose zu Glukose-l-Phosphat und die dadurch verminderte Generierung von ATP durch Glykolyse, wenn OXPHOS gestört ist[219]. Wir konnten zeigen, dass Zigarettenrauchkondensat in Galaktose-haltigem Medium toxischer wirkt, wobei AOX erneut einen teilweisen Schutz vermittelte. Um zu testen, ob sich WT- und AOX-iMEFs in ähnlicher Weise vom Stress durch Zigarettenrauchkondensat erholen, haben wir Zigarettenrauchkondensat-haltiges Galaktose-Medium nach 48 h durch Toxin-freies Medium ersetzt. Tatsächlich konnten sich AOX-exprimierende, aber nicht WT-iMEFs von der Zigarettenrauchkondensat-Exposition erholen. Um den Mechanismus des Zelltods besser zu verstehen, haben wir mittels Western Blot-Analyse die Expression verschiedener Proteine untersucht und fanden mehr gespaltene Caspase-3 in WT- als in AOX-iMEFs nach Exposition mit Zigarettenrauchkondensat, während die Gesamt-Caspase-3 unbeeinflusst blieb. Dies lässt den Schluss zu, dass Zigarettenrauchkondensat den geordneten Zelltod, Apoptose, infolge einer gehemmten ETK aktiviert und dass AOX diesem Prozess entgegenwirkt.

2.4.3 AOX unterstützt die mitochondriale Atmung und verringert die Superoxid-Produktion in Zigarettenrauchkondensat-behandelten iMEFs

Wir nutzten Respirometrie, um die Auswirkungen von Zigarettenrauchkondensat auf die mitochondriale Atmung zu analysieren. Dabei untersuchten wir eventuelle Schäden an der ETK nach Kultivierung von iMEFs mit Zigarettenrauchkondensat und mögliche akut-toxische Effekte von Zigarettenrauchkondensat bei Exposition von iMEFs in der Sauerstoffmesskammer. In für 48 h mit Galaktose-haltigem Medium-kultivierten und mit Zigarettenrauchkondensat behandelten iMEFs konnten wir einen dosisabhängigen Abfall der Atmung nachweisen. AOX verlieh teilweisen Schutz bei niedriger Zigarettenrauchkondensat-Konzentration. Um den Ort des Schadens innerhalb der ETK zu lokalisieren, permeabilisierten wir die mit Zigarettenrauchkondensat kultivierten iMEFs mit Digitonin. Unter Verwendung von spezifischen Atmungskettensubstraten und -inhibitoren fanden wir heraus, dass Zigarettenrauchkondensat zu einer dosisabhängigen Abnahme Komplex I-abhängigen Atmung führt, was durch AOX nicht kompensiert werden konnte. Im Gegensatz dazu war AOX selbst bei hohen Dosen von Zigarettenrauchkondensat in der Lage, Komplex II-abhängige Atmung aufrechtzuerhalten. Eine beobachtete Abnahme der Komplex IV-abhängigen Atmung konnte AOX ebenfalls nicht verhindern. Eine Western Blot-Analyse ergab, dass die Behandlung mit Zigarettenrauchkondensat keinen offensichtlichen Effekt auf die Expression von Atmungskettenuntereinheiten hatte. Deshalb ist anzunehmen, dass die beobachteten Effekte auf posttranslationale Modifikationen, niedermolekulare Effektoren oder Schäden an prosthetischen Gruppen zurückzuführen sind. Wir nahmen an, dass diese möglicherweise durch mitochondrial produzierte ROS verursacht wurden und haben deshalb mithilfe von zwei unabhängigen Methoden, MitoSOX Red-Färbung und ESR-Spektroskopie, die mitochondriale Superoxid-Akkumulation in mit Glukose kultivierten iMEFs gemessen. Beide Methoden gaben einen Hinweis darauf, dass die Superoxid-Produktion in iMEFs 3 h nach Behandlung mit Zigarettenrauchkondensat dramatisch ansteigt und dass AOX diesen Anstieg begrenzt oder verhindert. Nachfolgend haben wir akute Effekte von Zigarettenrauchkondensat auf die mitochondriale Atmung untersucht. Bei intakten (nicht-permeabilisierten) Zellen waren die messbaren Einschränkungen gering. Nach Entkopplung der Atmungskette haben wir jedoch eine dosisabhängige Abnahme der Atmungskapazität gefunden, die durch AOX teilweise aufgehoben wurde. In permeabilisierten Zellen hemmte akute Behandlung mit Zigarettenrauchkondensat die Komplex I- und II-abhängige Atmung, wobei AOX erneut die Abnahme der Komplex II-abhängigen Atmung begrenzte. Komplex IV-abhängige Atmung wurde akut nicht beeinflusst. Unsere Daten belegen, dass Zigarettenrauchkondensat die einzelnen ETK-Komplexe unterschiedlich beeinflusst. Während Komplex I sowohl direkt als auch indirekt bei akuter und chronischer (48 h) Exposition gehemmt wird, zeigen die Komplexe II und IV nur eine geringe Reaktion auf die akute Behandlung mit Zigarettenrauchkondensat. Trotzdem könnten die Komplexe II und IV eine wichtige Rolle in der Pathogenese der Zigarettenrauch-vermittelten COPD spielen. Aktivierung der Komplex II-vermittelten Atmung[137] und Hemmung der Komplexe III[187] oder IV[39] führen bekanntermaßen zu einer Reduktion des CoQ-Pools und können in diesem Zusammenhang RET und ROS induzieren[40,137]. Eine beobachtete leichte Aktivierung der Komplexe II und IV erklärt sich möglicherweise durch AOX-vermitteltes Abmildern mitochondrialer ROS-Exzesse[58,136,137,149] und damit das Verhindern unspezifischer Schäden an mitochondrialen und zellulären Komponenten. Eine verminderte Aktivität von ETK-Komplexen von Zellen nach Behandlung mit Zigarettenrauchkondensat[215] und Zelltod durch Nekrose

und/oder Apoptose[220,221] wurde schon früher beschrieben. Neben ROS-vermittelten Schäden könnten Komponenten des Zigarettenrauchs alternativ auch die Fluidität mitochondrialer Membranen beeinflussen[222], was ebenfalls die beobachteten Beeinträchtigungen und Rettung durch AOX erklären würde.

2.4.4 AOX hat keinen Einfluss auf Zigarettenrauch-induzierte Entzündungsreaktionen

Da AOX schützende Effekte auf das Ergebnis der chronischen Zigarettenrauchkondensat-Exposition *in vivo* hatte und den Zigarettenrauchkondensat-induzierten Zelltod begrenzte, schlussfolgerten wir, dass es ebenfalls ein Zigarettenrauch-induziertes Einwandern von Makrophagen und neutrophilen Zellen verhindern könnte. Dieser Prozess wird allgemein als frühester Schritt in der COPD-Entwicklung angesehen. Um diese Annahme zu testen, verwendeten wir ein zuvor validiertes Modell der akuten Entzündungsreaktion auf kurzzeitige Zigarettenrauchexposition[214]. Überraschenderweise stellten wir fest, dass sowohl Makrophagen als auch neutrophile Zellen in der sogenannten bronchoalveolären Lavage (BAL) von WT- und AOX^{Rosa26}-Mäusen in gleichem Maße vermehrt waren. Da wir in einer anderen Arbeit zeigen konnten, dass AOX eine pro-inflammatorische Aktivierung von Makrophagen in einem Endotoxämie-Modell der Maus verhindert[58], wollten wir testen, ob durch den gleichen Mechanismus auch die nachteilige Zigarettenrauch-induzierte entzündliche Signalantwort in der BAL-Flüssigkeit unterbunden wird. Konkret quantifizierten wir das Vorhandensein von KC, einem mausspezifischen funktionellen Homolog des humanen IL-8, das typischerweise mit dem Schweregrad der COPD korreliert[223]; MIP2, das zusammen mit KC zur Klasse der CXC-Chemokine gehört, von denen bekannt ist, dass sie die neutrophile Chemotaxis induzieren[224,225]; IL-6, ein klassischer Entzündungsmarker, der bei COPD häufig erhöht ist; und MMP-9, das durch Acrolein[226] oder neutrophile Elastase[227] aktiviert wird und dafür bekannt ist, bei COPD-Patienten während der Exazerbation der Krankheit zum Gewebeumbau beizutragen[228]. Alle Marker waren in WT- und AOX^{Rosa26}-Mäusen gleichermaßen und signifikant erhöht, was darauf hindeutet, dass AOX keinen akuten Schutz vor Zellinfiltration und inflammatorischen Aktivierung verleiht und dass die Gewebereaktion in dieser akuten Phase nicht auf einer Beeinträchtigung der mitochondrialen ETK beruht. Dieses Ergebnis war überraschend, da in einer kürzlich durchgeführten Studie behauptet wurde, dass Makrophagen von COPD Patienten mehr Enzyme exprimieren, die den Gewebeumbau fördern, als gesunde Kontrollen. Zudem sollen Makrophagen von COPD Patienten eine höhere Expression von M2-verwandten Genen zeigen, während M1-entzündliche und immunregulierende Proteine unterdrückt werden[229]. Unsere Ergebnisse deuten darauf hin, dass eine ETK-Hemmung nicht der primäre Auslöser für die unmittelbare Gewebereaktion ist, obwohl sie eindeutig am langfristigen pathogenen Prozess beteiligt ist. Dies stellt einen Gegensatz zu früheren Befunden dar, wonach die Infiltration und Aktivierung von Makrophagen und neutrophilen Zellen mit einem ungünstigen Ergebnis korreliert[230]. Da im AOX^{Rosa26}-Modell AOX ubiquitär exprimiert wird[136], ist es nicht möglich zu unterscheiden, ob das kritische Zielgewebe, in dem die mitochondriale Atmungshemmung zu Indikatoren des Emphysems führt, das Lungenepithel selbst ist, Makrophagen oder andere Zellen des Immunsystems[231]. Diese Frage kann nur durch die Generierung von alternativen Modellen geklärt werden, in denen die AOX-Expression auf bestimmte Gewebe oder Zelltypen beschränkt ist.

Eine Studie wie hier beschrieben hat intrinsische Einschränkungen, die die Übersetzung der Ergebnisse erschweren. Zum Beispiel ist bekannt, dass die Lunge der Maus im Gegensatz zur humanen Lunge als Reaktion auf Zigarettenrauch gut regeneriert. Wir haben Mäuse mit einem C57BL/6 genetischen Hintergrund verwendet. Der Vorteil der Verwendung von C57BL/6 liegt eindeutig in der Vergleichbarkeit der Daten, da es sich um einen weit verbreiteten Stamm handelt. Leider sind C57BL/6-Mäuse jedoch außergewöhnlich resistent gegen Schäden durch Zigarettenrauch[232]. Unsere Ergebnisse könnten also im Umkehrschluss die schützende Wirkung von AOX sogar unterschätzen. In der Tat sind die Veränderungen, die auf die Entwicklung eines Emphysems hinweisen, gering, wenn auch vergleichbar mit früheren Studien mit ähnlichem experimentellem Aufbau[213,233]. Dennoch sollten Stämme mit größerer Sensitivität für Zigarettenrauch in zukünftigen Studien den Vorzug bekommen[232]. Darüber hinaus ist Zigarettenrauchkondensat zwar ein gut etabliertes Surrogat für Rauchexposition und besonders geeignet, um molekulare Mechanismen in kultivierten Zellen zu studieren. Aufgrund des Isolationsverfahrens und der Beschränkungen der Zellkultur unterscheiden sich Zigarettenrauch und Zigarettenrauchkondensat jedoch signifikant in Zusammensetzung und Wirkung. Dagegen könnte man argumentieren, dass Lungenfibroblasten, -epithelzellen oder Makrophagen auch nur den Komponenten des Zigarettenrauchs ausgesetzt sind, die sich in der Flüssigkeit der Atemwege lösen. Somit könnten die Effekte von Zigarettenrauchkondensat trotz der Einschränkungen einen signifikanten Teil der *in vivo* Situation widerspiegeln. Schließlich schützt die transgene Expression von AOX zweifellos vor zellulärer Dysfunktion und maladaptivem Umbau der Lunge. Der Einsatz von AOX als Therapeutikum liegt dennoch in weiter Ferne, da hierfür umfangreiche Studien zu Verabreichung, Haltbarkeit und Sicherheit erforderlich wären.

2.5 Charakterisierung der Rolle von Signalen der mitochondrialen Atmungskette auf den adaptiven Organumbau nach kardialer Ischämie-Reperfusion (IR)

In diesem Teilabschnitt wird beschrieben, welchen Einfluss AOX auf Funktionen der mitochondrialen Atmungskette, Gen- und Proteinexpressionen, kontraktile Funktion sowie Gewebeschäden im Herzen nach Ischämie-Reperfusion (IR) hat. Resultate und Diskussion dieses Teilabschnittes stammen in wesentlichen Teilen aus Szibor *et al.*, *J Cell Mol Med.* **24**, 3534–3548 (2020)[111]. Hier zeigen wir, dass AOX, trotz guter Expression und katalytischer Aktivität im Herzen der Maus[136,171,234], d.h. trotz Wiederherstellung des Elektronenflusses durch die ETK und Verminderung mitochondrialer ROS-Produktion, im post-ischämischen Herzen nicht kardioprotektiv wirkt (**Abb. 6**). Stattdessen begünstigt AOX nach IR den maladaptiven Umbau des Herzens bis hin zur Beeinträchtigung der kardialen Kontraktilität.

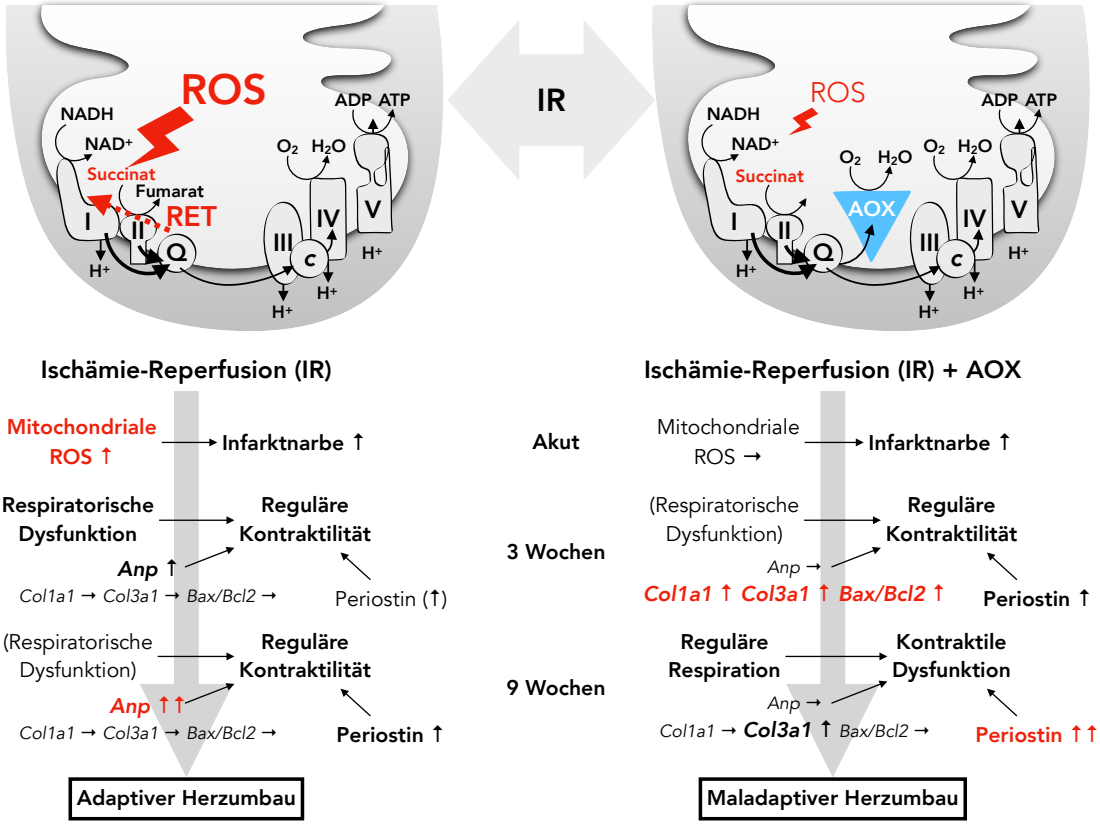

Abb. 6 *Schema für differenzielle Regenerationsantwort von Herzen nach Ischämie-Reperfusion (IR) in Abhängigkeit von AOX. AOX-Expression verschlechtert langfristig (9 Wochen nach IR) die kardiale Kontraktilität, obwohl es die Ausprägung klassischer Marker für maladaptiven Umbau wie erhöhte mitochondriale ROS-Produktion verminderte respiratorische Kapazität und Zunahme an Anp Transkripten verhindert. Besondere Unterschiede werden rot hervorgehoben. Pfeile entsprechen dem Grad der Induktion der angegebenen Marker (ein Pfeil, moderater Anstieg; zwei Pfeile, starker Anstieg).*

2.5.1 AOX kann Schäden nach kardialer Ischämie-Reperfusion nicht vermindern

Im Zuge einer kardialen Ischämie kommt es zu Akkumulation von des Krebs-Zyklus Intermediats Succinat[122], was bei Reperfusion ursächlich für RET-vermittelte ROS-Produktion und

darüber hinaus für Gewebeschäden und Funktionseinschränkungen verantwortlich gemacht wird[121]. Da wir zeigen konnten, dass AOX RET-induzierte ROS-Produktion verhindert[40,58,136,137], testeten wir zunächst, ob AOX auch das Ausmaß eines akuten IR-Schadens (Infarktgröße) in AOX^{Rosa26} vermindert. Wir nutzten dazu ein sogenanntes *in situ* IR-Modell[235], bei dem eine 30-minütige Ischämie durch Verschluss der linken anterioren absteigenden Koronararterie (*left anterior descending artery*, LAD) und anschließender 2-stündiger Reperfusion durchgeführt wurde. Die Infarktgröße wurde als prozentualer Anteil des Narbengewebes an der Risikozone ermittelt[235,236]. Überraschenderweise war die Infarktnarbe in WT- und AOX-Herzen gleich groß. Wir folgerten, dass AOX aufgrund seiner Sauerstoffabhängigkeit den Schaden im post-ischämischen Herzen möglicherweise nicht abmildern kann. Dennoch nahmen wir an, dass AOX die funktionelle Erholung der überlebenden Myozyten in der frühen post-ischämischen Phase verbessern könnte. Deshalb analysierten wir die kontraktilen Funktionen des Herzens *ex vivo* im sogenannten isolierten, perfundierten (Langendorff) Herzen. Nach 45 Minuten Ischämie zeigten WT- und AOX-Herzen nahezu identische systolische und diastolische Druck-Kurven. Darüber hinaus zeigten die entwickelten linksventrikulären Drücke (*left ventricular developed pressure*, LVDP, berechnet aus [maximalem systolischen - diastolischen Druck]) und die Herzfrequenz x Druckprodukte (*rate pressure product*, RPP, ein häufig genutzter Ersatzwert für Herzarbeit)[237] keine Unterschiede. Das isolierte, perfundierte Maus-Herz entwickelt typischerweise während einer Ischämie einen Rigor, der nach unserer Erfahrung eng mit der Infarktentwicklung korreliert. Auch dieser Rigor manifestierte sich unabhängig vom Genotyp als Druckanstieg während der ischämischen Phase, was wir als Indiz für eine fehlende AOX-vermittelte Kardioprotektion gegen Ischämie interpretierten.

2.5.2 AOX ist in post-anoxischen Herzmitochondrien katalytisch aktiv

Das Fehlen jeglicher Kardioprotektion gegen akute ischämische Insulte durch AOX ließ uns vermuten, dass die katalytische Aktivität von AOX im post-ischämischen Herzen kurz nach dem Insult möglicherweise verringert ist. Um diese Möglichkeit zu testen, isolierten wir Mitochondrien aus WT- und AOX^{Rosa26}-Herzen und maßen den Sauerstoffverbrauch und die ROS-Produktion *in vitro*. Überraschenderweise bestätigten diese Untersuchungen eine robuste Expression von AOX und Zyanid-resistente Succinat-Atmung bei gleichzeitig verminderter mitochondrialer Wasserstoffperoxid-Produktion bei Sauerstoffkonzentrationen von ≈21% absteigend bis zur vollständigen Anoxie. Um die Situation im post-ischämischen Herzen zu simulieren, wurden Herzmitochondrien in der Messkammer für 20 min einer Anoxie ausgesetzt. Post-anoxisch war der Sauerstoffverbrauch in WT-Mitochondrien bei ansteigenden Sauerstoffkonzentrationen generell etwas höher als in AOX-Mitochondrien. Die Wasserstoffperoxid-Produktion war in AOX-Mitochondrien allerdings signifikant niedriger. Zusammen mit früheren Befunden zur AOX-Aktivität im Herzen unter verschiedenen Bedingungen[136,171,234] kamen wir zu dem Schluss, dass eine funktionelle Beeinträchtigung von AOX auch im post-ischämischen Herzen unwahrscheinliche ist, und dass im Umkehrschluss eine post-ischämischen Kardioprotektion trotz katalytischer AOX-Aktivität fehlt.

2.5.3 AOX verbessert mitochondriale Funktionen 3 Wochen nach kardialer Ischämie

Wir wollten deshalb wissen, ob die Wiederherstellung des Elektronenflusses durch AOX und eine anzunehmende Reduzierung von RET-induzierten ROS im post-ischämischen Herzen

langfristig von Vorteil sein könnte, z. B. bei post-ischämischen Umbauvorgängen. Wir testeten diese Frage in WT- und AOX^{Rosa26}-Mäusen 3 Wochen nach einem transienten (45 min-dauernden) ischämischen Insult mit anschließender Wiederherstellung des Blutflusses (Reperfusion)[238]. Im Langendorff-Model *ex vivo* gemessene funktionelle Linksherzparameter (P_{syst} und LVDP) zeigten jedoch keinen signifikanten Unterschied zwischen WT- und AOX-Herzen. Im Gegensatz dazu zeigte Respirometrie mit permeabilisierten Herzfasern, dass die Komplex I-abhängige Atmung (Pyruvat, Glutamat und Malat plus ADP, phosphorylierende Atmung oder auch State 3), sowie Komplex IV-abhängige Atmung (Ascorbat/TMPD) in WT-Herzen, aber nicht in AOX-Herzen, nach IR signifikant beeinträchtigt waren. Der Befund, dass auch Komplex IV Aktivität reduziert ist, kam unerwartet, da er den ROS-produzierenden Komplexe I und III nachgeschaltet ist. Elektronenmikroskopische Aufnahmen der Herzen zeigten für eventuelle Schädigungen allerdings kein ultrastrukturelles Korrelat (wie z. B. verminderte Dichte mitochondrialer Cristae).

Typischerweise wird eine myokardiale Hypertrophie als die adaptive kardiale Antwort auf hämodynamischen oder metabolischen Stress angesehen. Diese geht einher mit einer Veränderung von Genexpressionen. Um festzustellen, ob die Wiederherstellung der Atmung durch AOX eine Verschiebung in Genexpressionen als Reaktion auf den ischämischen Insult induziert, haben wir die Expression von Markergenen gemessen. Wir untersuchten die mRNA-Expression des atrialen natriuretischen Peptids (*Anp*), das sowohl als Biomarker für die Diagnose der Herzinsuffizienz als auch als prognostischer Marker für das kardiovaskuläre Risiko gilt[239]. Die *Anp*-Expression war in WT- nicht aber in AOX-Herzen nach IR signifikant erhöht. ANP gilt als pro-fibrogener Faktor[240]. Da übermäßige kardiale Kollagensynthese und -ablagerung die kontraktile Funktion negativ beeinflusst[241], untersuchten wir die Expression der Transkripte von Kollagen 1 (*Col1a1*) und 3 (*Col3a1*). In der AOX-transgenen IR-Gruppe waren diese Transkripte signifikant erhöht. Darüber hinaus untersuchten wir mitochondriale Gene, die an der Reaktion auf oxidativen Stress beteiligt sind. Superoxid-Dismutase 2 (*Sod2*) ist beispielsweise ein mitochondriales Protein, das Superoxid durch Umwandlung in Wasserstoffperoxid und molekularen Sauerstoff entgiftet. SOD2 gilt als Teil der zelleigenen ROS-Stressreaktion[39], dessen Fehlen zu kardialen Fehlfunktionen führt[109]. *Sod2*-Transkriptlevel waren in AOX-transgenen Herzen im Vergleich zu WT-Herzen unabhängig von der Intervention niedriger. Sogenannte Entkopplungsproteine (*uncoupling proteins*, UCPs) hingegen sind mitochondriale Innenmembranproteine, die als Protonenlecks fungieren und dadurch den Protonengradienten reduzieren. Für UCP2 wurde bereits gezeigt, dass es für den Schutz vor drucküberlastungsinduzierter Rechtsherzinsuffizienz entscheidend ist[242]. Wir fanden *Ucp2*-Transkripte spezifisch in der AOX-transgenen IR-Gruppe hochreguliert. Außerdem wollten wir untersuchen, ob es Hinweise auf vermehrten Zelltod im post-ischämischen Herzen gibt (z. B. durch apoptotischen Verlust von Kardiomyozyten)[243]. Frühere Arbeiten fanden einen negativen Zusammenhang zwischen der kardialen *Bax*-Transkript-Expression (ein pro-apoptotisches Mitglied der BCL2-Proteinfamilie) und der Herzfunktion sowie positive Effekte bei erhöhter *Bcl2*-Transkript-Expression[244]. Insbesondere korreliert ein erhöhtes Verhältnis von *Bax/Bcl2* mit kardialer Fibrose[245]. Wir fanden einen signifikanten Anstieg des Verhältnisses von *Bax*- zu *Bcl2*-Transkripten speziell in den AOX-Gruppen, was auf eine zelluläre Verschiebung hin zu einem pro-apoptotischen Phänotyp hindeutet.

2.5.4 AOX beeinträchtigt die kardiale Kontraktilität 9 Wochen nach kardialer Ischämie

Das Fehlen eines positiven Einflusses auf die post-ischämische Funktion, trotz der Verhinderung der *Anp*-Transkript-Induktion, veranlasste uns, die Auswirkungen von AOX zu einem späteren Zeitpunkt zu untersuchen. 9 Wochen nach transienter Ischämie (45 min) zeigten *ex vivo* Funktionsmessungen eine signifikante Abnahme von P_{syst} und LVDP speziell in der AOX-transgenen IR-Gruppe. Respirometrie zeigte zu diesem Zeitpunkt einen geringfügigen Komplex I-Defekt in WT-IR-Herzen, während die Komplex IV-Aktivität vollständig wiederhergestellt war. Die *Anp*-Transkription war in WT-IR-Herzen noch stärker erhöht als 3 Wochen nach der Ischämie. Änderungen in den anderen beschriebenen Genen waren deutlich weniger ausgeprägt.

2.5.5 AOX fördert den Umbau der extrazellulären Matrix im post-ischämischen Herzen

Um die molekularen Mechanismen besser zu verstehen, die der post-ischämischen Funktionsverschlechterung von AOX-transgenen Herzen nach IR zugrunde liegen könnten, haben wir das kardiale Proteom unter Zuhilfenahme des GOrilla[246,247] Online-Tools analysiert (Originaldaten sind in der PRIDE-Datenbank[248–250] einsehbar, PXD014061). Wir fanden in den post-ischämischen Herzen von AOX^{Rosa26}-Mäusen eine ausgeprägte Expression von Proteinen, die an der Reorganisation der extrazellulären Matrix beteiligt sind, z. B. das Protein Periostin (POSTN). Im Vergleich zu SHAM-operierten AOX-transgenen Herzen war Periostin 3 Wochen nach Ischämie fast 5-fach und nach 9 Wochen 17-fach erhöht. In WT-Herzen war der Anstieg <2-fach bzw. 7-fach. Unklar ist bislang, wie die beobachteten Veränderungen auf Transkript- und Proteinebene gegebenenfalls zusammenhängen. Erhöhte ANP Expressionen wurde ursprünglich im versagenden Herzen unabhängig von der zugrundeliegenden Ursache gefunden[251] und als kompensatorischer Mechanismus beschrieben[252]. Diese Ansicht wurde später in Frage gestellt[253]. Trotzdem gilt ANP allgemein als diagnostischer Marker für maladaptiven kardialen Umbau[239,254–257]. In glatten Muskelzellen der Lungenarterien der Ratte hingegen soll ANP die Expression von TGFβ-induzierten extrazellulären Matrixkomponenten inhibieren[258]. Dieser Befund passt zu unseren Daten mit einer abgeschwächten reaktiven *Anp*-Expression und erhöhter Expression von *Col1a1* und *Col3a1* speziell AOX-transgener Herzen. Kollagen verringert bei erhöhter Expression zwar einerseits die Wandspannung, beeinträchtigt aber ebenfalls die kontraktile Funktion aufgrund erhöhter Wandsteifigkeit und geht mit der Entwicklung einer Herzinsuffizienz einher[241]. Der ANP-Signalweg könnte auch für die beobachtete Hochregulierung der Periostin-Expression verantwortlich sein. Tatsächlich wird Periostin eine Funktion beim progressiven Umbau der extrazellulären Matrix zugeschrieben[259]. Periostin wird außerdem mit myokardialer Fibrose bei einigen Formen der Herzinsuffizienz in Verbindung gebracht[260–262].

Insgesamt sind unsere Ergebnisse in scheinbarem Widerspruch mit anderen Studien, die mitochondriale Antioxidantien in kardialen IR-Modellen einsetzten[112,120] und eine Kardioprotektion beobachteten[263]. Dies ist insbesondere erstaunlich, weil die Akkumulation von Succinat und RET-induzierter ROS-Produktion[121,122] durch AOX nachweislich unterbunden wird[40,136,137]. Möglicherweise erklärt Mitohormese den unerwarteten Befund[126,264]. AOX könnte mitochondriale Signale, z. B. ROS, in einem Maße unterdrücken, dass den adaptiven kardialen

Umbau nach Ischämie beeinträchtigt. In der Tat wurde ein kardioprotektiver Effekt von niedrigen ROS-Spiegeln gezeigt[129]. Ein wesentlicher Unterschied zwischen Antioxidantien und AOX ist zudem, dass Antioxidantien normalerweise nicht über die akute post-ischämische Phase hinaus regeneriert werden. Auch können Antioxidantien, im Gegensatz zu AOX, während des Transports zu den Mitochondrien antioxidative Wirkungen zeigen und entgiften daher nicht ausschließlich mitochondriale ROS. Eine naheliegende Folgestudie zur Überprüfung dieser Annahme könnte eine kürzlich publizierte Maus mit induzierbarer Expression von AOX nutzen[234] oder aber AOX als Therapeutikum, z. B. in Form eines mRNA-Mimetikums, einsetzen[131]. Beide Ansätze hätten werfen jedoch andere Probleme auf wie z. B. die Zeit- und/oder Organ-unspezifische Expression relevanter Treiber, unerwünschte Nebenwirkungen derselben Treiber im Falle des genetischen Ansatzes oder Immun- und Entzündungsreaktionen im Falle des therapeutischen Einsatzes von AOX. Ein interessanter Aspekt unserer Studie ist, dass die Anwesenheit von AOX im post-ischämischen Herzen die Komplex I-getriebene Atmung wiederherstellt. Tatsächlich kann Komplex I allerdings beides sein, ein ROS-produzierender Komplex unter Bedingungen wie im post-ischämischen Herzen[121,122] oder selbst ein Ziel für ROS-Schäden[265]. In anderen Studien in Rattenherzen wurde gezeigt, dass Umgehung des nativen Komplexes I nach ischämischen Insulten durch Gabe eines Ersatzproteins (Ndi1 aus *Saccharomyces cerevisiae*) die Entwicklung IR-verursachter Infarktgrößen verringert[266,267]. Im Licht dieser Befunde kann man annehmen, dass andere Faktoren als die ROS-Produktion oder die Wiederherstellung des Elektronenflusses durch Komplex I zur kardialen Stressreaktion beitragen müssen. Unsere Ergebnisse rekapitulieren dagegen eine Studie, bei der die mitochondriale Überexpression einer Katalase eine Myopathie von Herz- und Skelettmuskeln in einem Mausmodell des Barth-Syndroms nicht verhindert[268]. Das ist auch deshalb interessant, weil Katalase und AOX unterschiedlich in die ROS-Produktion eingreifen. Während Katalase den Umsatz von Wasserstoffperoxid zu Wasser und Sauerstoff katalysiert, unterbindet AOX die Produktion von Superoxid direkt am Ort der Entstehung, der dysfunktionalen ETK.

2.6 Untersuchung der Beziehung zwischen mitochondrialen Redox-Signalen und der Entwicklung einer mitochondrialen Myopathie

In diesem Teilabschnitt wird beschrieben, welchen Einfluss AOX auf die Entwicklung einer mitochondrialen Myopathie basierend auf einem Komplex IV-Defekt hat. Wir wollten wissen, welche Mechanismen die Entwicklung der Myopathie bestimmen und welche Therapiemöglichkeiten vielversprechend wären. Resultate und Diskussion dieses Teilabschnittes stammen in wesentlichen Teilen aus Dogan *et al.*, *Cell Metab.* **28**, 764-775.e5 (2018)[39]. Wir zeigen hier, dass AOX durch Umgehung eines defekten Komplex IV im Skelettmuskel die Ausprägung einer mitochondrialen Myopathie verschlimmert. Dies geschieht durch Unterbindung der mitochondrialen ROS-Produktion und dadurch bedingte Abschwächung kompensatorischer Stressreaktionen (**Abb. 7**). Obwohl wir damit Argumente liefern, die gegen eine Nutzung von AOX als Therapeutikum sprechen, unterstreichen unsere Ergebnisse den Wert von AOX als genetisches Werkzeug, um Krankheitsmechanismen besser zu verstehen. Insbesondere der Nutzen von ROS-Signalen in der zellulären Antwort und potenzielle Gefahren einer antioxidativen Behandlung werden aufgezeigt.

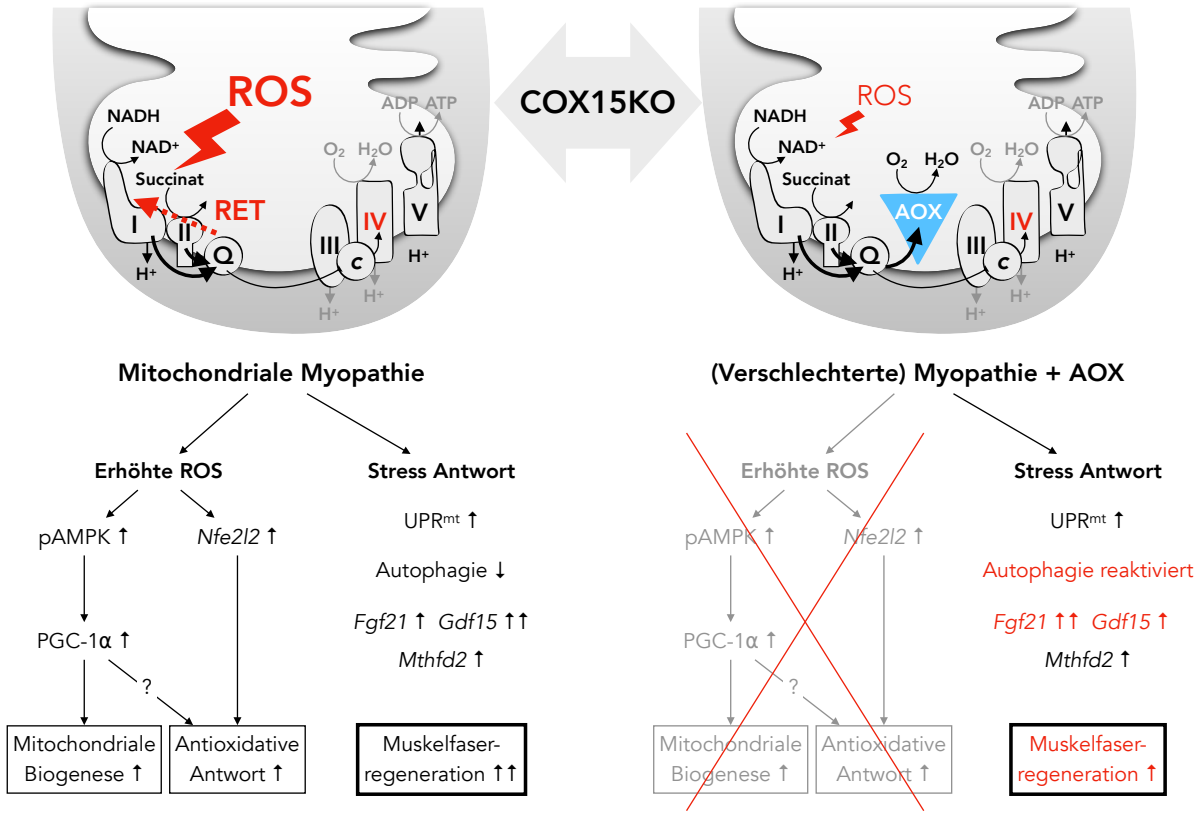

Abb. 7 *Schema für differenzielle Regenerationsantwort von Skelettmuskeln bei Skelettmuskel-spezifischem Knockout (KO) von COX15. AOX-Expression verschlimmert diese Art von mitochondrialer Myopathie. Unterschiede in Stressreaktionen werden rot hervorgehoben. Die Pfeile entsprechen dem Grad der Induktion der angegebenen Marker (ein Pfeil, moderater Anstieg; zwei Pfeile, starker Anstieg). Die Abbildung wurde adaptiert von Dogan et al., 2018[39].*

2.6.1 AOX-Expression verschlechtert den Zustand von Mäusen mit einer mitochondrialen Myopathie

Mäuse mit Skelettmuskel-spezifischer Ablation der Komplex IV-Untereinheit 15 (COX15-KO) entwickeln in Skelettmuskeln einen umfassenden Mangel an Komplex IV-Aktivität, der zu einer schweren mitochondrialen Myopathie und frühem Tod führt[269]. Um zu testen, ob AOX durch Umgehung des Komplex IV die Auswirkungen der COX15-KO-induzierten Myopathie abmildert, generierten wir Doppelmutanten (KO-AOX). Entgegen unseren Erwartungen zeigten KO-AOX-Doppelmutanten einen in allen Belangen schwereren Verlauf als COX15-KO mit früherem Beginn der Symptome wie vermindertem Körpergewicht aufgrund von vermindertem Körperfett, weniger Spontanbewegungen sowie verminderter Laufband-Leistung. Auch die Überlebenswahrscheinlichkeit der KO-AOX-Doppelmutanten war deutlich geringer mit einer medianen Lebenserwartung von ungefähr 60 Tagen im Vergleich zu 150 Tagen bei COX15-KO. Tatsächlich mussten alle KO-AOX-Mäuse bis zum Alter von 90 Tagen aufgrund des schlechten Allgemeinzustands getötet werden. Da der Komplex IV-Defekt auf Skelettmuskeln begrenzt war, nahmen wir an, dass eine Verschlechterung der Myopathie hauptsächlich für den drastischeren Phänotyp der KO-AOX-Doppelmutante verantwortlich sein muss. Wir analysierten daher die Skelettmuskulatur von 2 Monate alten Tieren der vier Genotypen (WT, AOX, COX15-KO, KO-AOX). Eine histochemische Komplex IV (COX)-/Komplex II (SDH)-Färbung bestätigte eine Zunahme Komplex IV-negativer Muskelfasern in COX15-KO-Mutanten gegenüber WT- und AOX-Tieren. Allerdings war der Defekt in KO-AOX-Doppelmutanten noch deutlicher ausgeprägt. Daneben fanden wir die Komplex II-Färbung (hier als Kontrollfärbung) bei Skelettmuskeln von COX15-KO-Mutanten erhöht, während sie bei KO-AOX-Doppelmutanten und WT-Tieren ähnlich war. Eine quantitative spektrophotometrische Bestimmung der Komplex IV-spezifischen Aktivität in Skelettmuskelhomogenaten bestätigte diese Beobachtung (IV/II: 4,2850,3556 in COX15-KO *vs* 2,460,3165 in KO-AOX; $p<0.01$). Ebenso zeigte die morphologische Analyse von Muskelfasern mittels Färbung durch Hämatoxylin und Eosin (H & E) eine signifikant verringerte Querschnittsfläche in KO-AOX *vs* COX15-KO. Nachfolgend untersuchten wir die Anzahl der zentralisierten Kerne, ein primäres Zeichen der Muskelregeneration[270]. In COX15-KO-Mutanten war, verglichen mit WT- und AOX-Mäusen, die Anzahl der zentralisierten Kerne deutlich erhöht (8.6±0.73 in COX15-KO *vs* 0.41±0.13 in WT), in KO-AOX-Doppelmutanten jedoch deutlich geringer. Dieser Befund veranlasste uns, die Differenzierung der Satellitenzellen im Skelettmuskel der verschiedenen Genotypen zu untersuchen. Die Anzahl der Zellen mit PAX7 positivem Zellkern, ein Marker für residente Myoblasten[271–273], war in Skelettmuskeln von COX15-KO gegenüber WT- und AOX-Tieren signifikant erhöht, aber in KO-AOX-Doppelmutanten auf physiologisch normalem (WT) Niveau. In ähnlicher Weise waren MYOD-positive Kerne, ein Marker der differenzierenden Satellitenzellen[271–273], in Muskeln von COX15-KO-Mutanten deutlich erhöht, in KO-AOX-Doppelmutanten jedoch auf erneut auf WT-Niveau. Während der Muskelregeneration durchlaufen Satellitenzellen, Skelettmuskelprogenitorzellen, einen Aktivierungsprozess, der gekennzeichnet ist durch Proliferation und Migration zum Ort einer Schädigung. Dort angekommen differenzieren sie zu Myozyten und fusionieren schließlich mit den vorhandenen Muskelfasern. Während dieses Prozesses werden spezifische Transkriptionsfaktoren exprimiert, darunter PAX7, MYOD und Myogenin[271–273]. Unsere Daten deuten also darauf hin, dass AOX diesen Weg beeinflusst.

Die myogene Differenzierung ist hauptsächlich aufgrund der gleichzeitigen Induktion der mitochondrialen Biogenese mit hohen ROS-Werten verbunden[274]. Gleichzeitig werden antioxidative Abwehrmechanismen aktiviert, um zelluläre Schäden zu verhindern[275]. Die verringerte Anzahl zentralisierter Kerne und reduzierte Anzahl PAX7- und MYOD-positiver Kerne in Skelettmuskeln von KO-AOX-Doppelmutanten deuten darauf hin, dass Satellitenzellen zwar vorhanden sind, sich aber nicht in Myotuben differenzieren können. Dies beeinträchtig die Fähigkeit zur Reparatur/Regeneration von Muskelfasern und dürfte eine wichtige Rolle bei der beobachteten Verschlechterung des Phänotyps in KO-AOX-Doppelmutanten spielen. Außerdem untersuchten wir, ob AOX-Expression einen Wechsel des Fasertyps induziert. Dafür färbten wir Muskelschnitte mit Antikörpern gegen die verschiedenen Myosin-Isoformen. Es wurden jedoch keine Unterschiede in der Verteilung der Fasersubtypen beobachtet. Zusammengenommen zeigen unsere Daten, dass die mitochondriale Myopathie bei KO-AOX-Doppelmutanten eine signifikant stärkere Ausprägung entwickelt, was möglicherweise mit dem Unvermögen zusammenhängt, Muskelregeneration durch Rekrutierung von Satellitenzellen zu stimulieren.

2.6.2 AOX-Expression stört die mitochondriale Biogenese in KO-AOX-Doppelmutanten

Zusätzlich zur Komplex II (SDH)-Färbung untersuchten wir die Citrat-Synthase (CS) als mitochondriales Markerenzym. Die CS-Aktivität war in COX15-KO-Mutanten im Vergleich zu Kontrollen und zu KO-AOX-Doppelmutanten erhöht. Diese Daten veranlassten uns, andere Marker im Skelettmuskel zu untersuchen, die ebenfalls mit der mitochondrialen Biogenese im Zusammenhang stehen. Die Kopien des mitochondrialen Genoms, mtDNA, und die Expression des mitochondrialen Transkriptionsfaktors A (TFAM) waren in den COX15-KO-Mutanten im Vergleich zu den WT- und AOX-Tieren erhöht, waren aber in den KO-AOX-Doppelmutanten ähnlich wie in WT-Tieren. Darüber hinaus waren mehrere Untereinheiten der Atmungskettenkomplexe in COX15-KO *vs* WT und AOX signifikant erhöht, jedoch nicht in Proben der KO-AOX-Doppelmutanten. Insgesamt deuten diese Daten darauf hin, dass AOX die in COX15-KO beobachtete Stimulation der mitochondrialen Biogenese abschwächt. Deshalb untersuchten wir, ob wichtige mitochondriale Signalwege durch AOX in Muskeln von COX15-KO-Mutanten verändert vorliegen. AMPK ist beispielsweise ein wichtiger Sensor für den zellulären Energiestatus und wird aktiviert, wenn das AMP/ATP-Verhältnis steigt[276]. Unter solchen Bedingungen wird AMPK durch Phosphorylierung von Thr172 (p-AMPK) durch die LK1-Kinase aktiviert. p-AMPK phosphoryliert wiederum eine große Anzahl von Targets wie den transkriptionellen Co-Aktivator PGC-1, einem Hauptregulator der mitochondrialen Biogenese. Wie schon in einer früheren Arbeit gezeigt[269], war p-AMPK in COX15-KO-Mutanten hochreguliert, lag aber in hier zusätzlich untersuchten KO-AOX-Doppelmutanten im normalen Bereich. Außerdem war die PGC-1-Proteinmenge in COX15-KO-Mutanten im Vergleich zu WT- und AOX-Tieren erhöht, während sie in Muskelproben von KO-AOX-Doppelmutanten normal war. Schließlich zeigte eine quantitative Transkript-Analyse in KO-AOX- im Vergleich zu COX15-KO-Tieren eine verringerte Expression verschiedener Atmungskettengene.

2.6.3 AOX beeinträchtigt ROS-Signalwege in COX15-KO-Mutanten

Das unerwartete Ergebnis in KO-AOX-Doppelmutanten könnte auf verschiedene Mechanismen hindeuten: (i) ein indirekter Effekt, der auf verringerte ROS-Signale und damit verbunden

einer Abnahme der mitochondrialen Biogenese zurückzuführen ist oder (ii) ein direktes bioenergetisches Versagen, das durch den Ausschluss der Protonenpumpaktivität der Komplexe III und IV verursacht wird. Da AOX durch Wiederherstellung des Elektronenflusses bei dysfunktionalen Atmungsketten insbesondere die ROS-Produktion verhindert, untersuchten wir zuerst, ob im KO-AOX-Modell gestörte ROS-Signalwege für die Verschlechterung des Phänotyps verantwortlich sein könnten. Wir haben dazu die ROS-Produktion in isolierten Skelettmuskel-Mitochondrien durch Messung des produzierten Wasserstoffperoxids (H_2O_2) quantifiziert. Die Succinat-getriebene H_2O_2-Produktion war in COX15-KO-Mitochondrien im Vergleich zu WT- und AOX-Mitochondrien signifikant erhöht. Demgegenüber war sie aber in KO-AOX-Doppelmutanten niedriger als in WT-Tieren. Gleichzeitig war die mitochondriale Aconitase Aktivität, die durch H_2O_2 gehemmt wird, in den COX15-KO- im Vergleich zu WT- und AOX-Mitochondrien signifikant niedriger, hatte aber normale Werte in KO-AOX-Mitochondrien. Unsere Ergebnisse stützen Studien, in denen AOX speziell unter respiratorischen Stressbedingungen katalytisch aktiv wurde[136,137]. Wie ebenfalls erwähnt, benötigt AOX für katalytische Aktivität einen stark reduzierten CoQ-Pool[142]. Wir haben deshalb die Menge an reduziertem und oxidiertem CoQ in Skelettmuskeln der Mäuse bestimmt. Die relative Menge an reduziertem CoQ war bei COX15-KO-Mutanten im Vergleich zu WT- und AOX-Mäusen erhöht, war aber bei den KO-AOX-Doppelmutanten vergleichbar mit WT-Mäusen. Diese Ergebnisse bestätigen, dass AOX den CoQ-Pool nur bis zu einem bestimmten Grad effizient oxidiert. Außerdem unterstützen die Ergebnisse die Idee, dass RET, das durch eine übermäßige Reduktion des CoQ-Pools gefördert wird[40,137], an der Erzeugung von ROS im COX15-KO-Modell beteiligt ist, und dass dies möglicherweise ebenfalls der molekulare Mechanismus ist, über den AOX seinen negativen Einfluss ausübt. Über verschiedene Signalwege können erhöhte ROS die oxidative Stressantwort auslösen, z. B. über den Keap1/NFE2L2-Signalweg. Wir fanden die Transkripte für Superoxiddismutase (*Sod2*) und Glutathionperoxidase (*Gpx1*), zwei Schlüsselenzyme der antioxidativen Antwort und NFE2L2-Targetgene, in COX15-KO- verglichen mit WT- und AOX-Mäusen signifikant erhöht, aber in KO-AOX-Doppelmutanten verglichen mit COX15-KO-Mutanten signifikant erniedrigt. Ähnliches fanden wir sowohl für Transkripte der Katalase (*Cat*) und *Sod1*, der zytosolischen Isoform der Superoxiddismutase. In COX15-KO-Mutanten, aber nicht in KO-AOX-Doppelmutanten fanden wir zudem einen signifikanten Anstieg der Transkriptlevel für *Nfe2l2*. Es gibt auch retrograde Signale aus Mitochondrien, die unter Stressbedingungen aktiviert werden und einhergehen mit ATP-Mangel, Verlust von mitochondrialem Membranpotential ($\Delta\psi$) und erhöhtem ROS[277,278]. Wir untersuchten zuerst die ATP-Produktionsrate und fanden eine starke, aber vergleichbare Beeinträchtigung der ATP-Synthese sowohl in COX15-KO- als auch in KO-AOX-Skelettmuskelmitochondrien, wobei entweder Komplex I- oder Komplex II-abhängige Substrate verwendet wurden. Darüber hinaus war der ATP-Gehalt in COX15-KO- und KO-AOX-Proben vergleichbar niedriger als in Kontrollen. Ebenso war $\Delta\psi$ sowohl in COX15-KO- als auch in KO-AOX-Muskelmitochondrien vergleichbar niedriger als in Kontrollen. Die vergleichbare Abnahme der ATP-Produktionsrate, der ATP-Werte und von $\Delta\psi$ in COX15-KO-Mutanten und KO-AOX-Doppelmutanten lässt den Schluss zu, dass die beeinträchtigte Bioenergetik nicht der Hauptgrund für den schwereren Phänotyp der KO-AOX-Doppelmutanten ist. Als Letztes wollten wir wissen, ob die in KO-AOX-Doppelmutanten gefundene verminderte ROS-Produktion dem verschlimmerten Phänotyp zugrunde liegt. Dazu ergänzten wir das Trinkwasser von COX15-KO-Mutanten nach Entwöhnung von der Mutter mit N-Acetylcystein (NAC), einer zellpermeablen Vorstufe von Glutathion[279]. Das mittlere Überleben war bei den behandelten

Tieren im Vergleich zu unbehandelten Tieren signifikant kürzer. Zusammengenommen konnten wir schlussfolgern, dass eine signifikant verminderte ROS-Produktion die mitochondriale Biogenese (und eventuell ebenfalls die Satellitenzellenrekrutierung) beeinträchtigt während wir die Möglichkeit einer gestörten ATP-Produktionsrate als Hauptursache für den beobachteten Phänotyp ausschließen konnten.

2.6.4 Autophagie ist im Skelettmuskel von KO-AOX-Doppelmutanten wiederhergestellt

Die mitochondriale Biogenese und Autophagie regulieren gemeinsam den Mitochondriengehalt[280]. Wir haben die Menge von LC3, einen Marker für Autophagosomen, und P62, einen Marker für autophagische Ladungen[281], in Skelettmuskelproben der verschiedenen Modelle gemessen. Das Verhältnis zwischen lipidiertem, Autophagosomen-assoziiertem LC3 (LC3-II) und nicht-lipidiertem, zytosolischem freiem LC3 (LC3-I) war in Skeletmuskeln von COX15-KO-Mutanten gegenüber WT- und AOX-Tieren signifikant verringert, während die Menge an P62 erhöht war, was auf eine verringerte Autophagie hindeutet. Umgekehrt zeigte Skelettmuskel von KO-AOX-Doppelmutanten ein deutlich erhöhtes LC3-II/LC3-I-Verhältnis, während die Mengen an P62 mit denen in WT-Tieren vergleichbar waren.

2.6.5 Mitochondriale Stressmarker sind bei COX15-KO-Mutanten und KO-AOX-Doppelmutanten vergleichbar erhöht

Als Reaktion auf eine mitochondriale Dysfunktion werden eine Reihe von mitochondrialen Signalwegen aktiviert. Wir haben die Expression auf Protein- und/oder mRNA-Ebene von mehreren Komponenten der sogenannten integrierten Stressantwort gemessen, darunter: (i) Schlüsselkomponenten des sogenannten UPR^{mt} (*mitochondrial unfolded protein response*)[282] wie die bZIP-Transkriptionsfaktoren CHOP (*C/EBP-homologous protein*), ATF4 und ATF5[283] und die mitochondrialen Chaperone HSP60/HSPD1 und mtHSP70/HSPA9[284]; (ii) Komponenten des Ein-Kohlenstoff-Zyklus (o.a. mitochondrialer Folatzyklus) wie beispielsweise Methylentetrahydrofolat-Dehydrogenase 2 (MTHFD2)[285,286] und Enzyme der Prolin-Biosynthese aus Glutamat wie beispielsweise Delta-1-Pyrrolin-5-Carboxylat-Synthase (ALDH18A1) und mitochondriale Pyrrolin-5-Carboxylat-Reduktase 1 (PYCR1) und (iii) die MitokineFGF21 (*fibroblast growth factor 21*) und GDF15 (*growth/differentiation factor-15*)[287]. Erhöhte Mengen dieser Marker oder ihrer Transkripte wurden sowohl in COX15-KO-Mutanten als auch in KO-AOX-Doppelmutanten nachgewiesen. Insbesondere *Fgf21*-mRNA war in Skelettmuskeln von COX15-KO-Mutanten stark exprimiert, aber überraschend noch stärker in KO-AOX-Doppelmutanten (260-fach). *Gdf15* war in COX15-KO-Tieren etwa 100-fach höher als in den Kontrollen, in KO-AOX-Doppelmutanten jedoch signifikant niedriger, wenngleich immer noch erhöht im Vergleich zu WT-Tieren. Andere Faktoren, die an der integrierten Stressreaktion beteiligt sind, einschließlich ATF3 und ATF6, die mit Zelltod- bzw. ER-Stress-Signalwegen in Verbindung stehen, veränderten sich nicht (ATF3) oder kaum (ATF6). Interessanterweise erfolgte die Aktivierung dieser stressbezogenen Wege in unserem COX15-KO-Modell über eIF2alpha und nicht über mTORC1[288]. Die Spiegel des mTORC1-Targetgens eukaryotischer Translationsinitiationsfaktor 4E (eIF4E)-bindendes Protein (4-EBP1), ein wichtiger Akteur in der Proteinsynthese[289], waren sowohl im COX15-KO- als auch im KO-AOX-Modell im Vergleich zu WT-Tieren erhöht. Das Verhältnis von phosphoryliertem zu unphosphoryliertem

4EBP1 war jedoch in COX15-KO-Mutanten und KO-AOX-Doppelmutanten im Vergleich zu WT- und AOX-Mäusen in gleichem Maße verringert. Das deutet darauf hin, dass der mTORC1-Signalweg und damit die Proteinsynthese und das Zellwachstum sowohl in Muskeln von COX15-KO- als auch in KO-AOX-Tieren reduziert waren. Im Gegensatz dazu konnten wir sowohl in COX15-KO-Mutanten als auch in KO-AOX-Doppelmutanten im Vergleich zu WT- und AOX-Tieren erhöhte Spiegel von phosphoryliertem eIF2alpha nachweisen. Diese Befunde deuten darauf hin, dass die Induktion wichtiger mitochondrialer Stressreaktionen mit der mitochondrialen Myopathie und dem Fortschreiten der Krankheit korreliert, AOX diese Wege jedoch nicht signifikant modifiziert. Allerdings verschlimmerte AOX die Myopathie, indem es die Expression relevanter endokriner Marker wie beispielsweise GDF15, beeinträchtigt. Die integrierte Stressantwort ist dagegen sowohl in COX15-KO-Mutanten als auch in KO-AOX-Doppelmutanten aktiviert. Interessanterweise wurden beide Mitokine kürzlich als Biomarker für mitochondriale Myopathien eingeführt[287], lagen hier jedoch differentiell reguliert vor. Während jedoch FGF21 in KO-AOX-Doppelmutanten deutlich höher exprimiert war als in COX15-KO-Mutanten, war GDF15 in KO-AOX-Doppelmutanten im Vergleich zu COX15-KO-Mutanten reduziert.

Zusammengenommen liefern unsere Ergebnisse einige Argumente gegen eine therapeutische Anwendung von AOX bei mitochondrialen Erkrankungen. Dieses gilt zumindest für den Skelettmuskel[128,290]. Trotzdem können die Ergebnisse potenziell für die Entwicklung wirksamer Therapien genutzt werden. Zum Beispiel könnten ROS ein wichtiges Signal sein und die lokale Proliferation von Mitochondrien induzieren, um einen funktionellen Defekt durch die Aktivierung eines mitochondriogenen Programms zu kompensieren. Die Mehrzahl der laufenden klinischen Studien für mitochondriale Erkrankungen basiert auf dem Einsatz von Antioxidantien, ausgehend von der Annahme, dass eine übermäßige ROS-Produktion oxidative Schäden an zellulären Komponenten verursacht. Allerdings ist das Ausmaß der ROS-Produktion und oxidativer Schäden bei mitochondrialen Erkrankungen *in vivo* bisher nur minimal untersucht worden und die vorliegenden Daten sind widersprüchlich. Zum Beispiel wurden in der sogenannten Mutator-Maus[291], eine Maus, die eine *proof-reading* defiziente Version der im Zellkern kodierten katalytischen Untereinheit der mtDNA-Polymerase (PolgA) exprimiert, keine Anzeichen für oxidative Schäden in postmitotischen Geweben festgestellt[292], während in kultivierten, sich vermehrende Zellen umfangreiche ROS-Schäden gezeigt wurden[293]. Unsere Daten sowohl mit AOX als auch mit NAC weisen auf ein potenzielles Risiko hin, das mit dem Einsatz von Antioxidantien verbunden ist, nämlich das Stören kompensatorischer ROS-Signalwege. Diese Annahme gilt potentiell für alle mitochondrialen Myopathien. Einschränkend muss man sagen, dass NAC und AOX durch unterschiedliche Mechanismen auf die Redox-Homöostase wirken. AOX verhindert überhöhte ROS-Produktion, während NAC lediglich bereits produzierte ROS entgiftet. Darüber hinaus unterstützen unsere Ergebnisse die Idee, dass die Induktion der mitochondrialen Biogenese, zum Beispiel durch Aktivierung der Sirt1- und/oder AMPK-abhängigen PGC-1-Achse oder anderer mitochondriogener Wege, ein potenziell effektiver Ansatz in der Therapie mitochondrialer Erkrankungen sein könnte. Interessanterweise mehren sich die Hinweise, dass AMPK direkt durch ROS reguliert wird, entweder durch Oxidation und S-Glutathionylierung der Cysteine 299 und 304 in der α-Untereinheit, was zur Aktivierung des Enzyms führt, oder durch Oxidation der Cysteine 130 und 174 in der α-Untereinheit, was zu seiner Inaktivierung führt[294]. Ein zusätzlicher

Mechanismus, der möglicherweise zur Abnahme des Mitochondriengehalts beiträgt, ist die Aufrechterhaltung des autophagischen Flusses in KO-AOX-Doppelmutanten.

Natürlich gehen nicht alle mitochondrialen Erkrankungen einher mit einer erhöhten mitochondrialen Biogenese und/oder ROS-Bildung. Auch können ROS an verschiedenen Stellen in Mitochondrien aber auch außerhalb des mitochondrialen Kompartiments gebildet werden[123] und dadurch ganz unterschiedliche Wirkungen erzielen. Kürzlich wurde gezeigt, dass ROS, die selektiv über RET produziert werden, die Lebensspanne in *Drosophila melanogaster* erhöhen[295], während ein gegenteiliger Effekt beobachtet wird, wenn RET durch eine erhöhte CoQ-Oxidation über die AOX-Expression verhindert wird[129]. Unsere Erkenntnisse aus der Verwendung von AOX als genetisches Werkzeug müssen somit im jeweiligen Erkrankungskontext kritisch hinterfragt werden.

3 Zusammenfassung

Störung des Elektronenflusses durch die mitochondriale Elektronentransportkette (ETK) beeinträchtigt die metabolische Flexibilität und wird für eine Vielzahl an Erkrankungen verantwortlich gemacht. Mehrere Mechanismen können bei ETK-Dysfunktion gleichzeitig die Funktionalität einer betroffenen Zelle oder eines Organs beeinträchtigen und so die Lebensfähigkeit eines ganzen Organismus einschränken. Zum einen ist die ETK der zentrale Baustein für die oxidative Phosphorylierung (OXPHOS). Das heißt, die mitochondriale ATP-Gewinnung ist vermindert, wenn der Elektronenfluss gestört wird. Zum anderen verursacht die Hemmung der ETK oft eine übermäßige Produktion von reaktiven Sauerstoffspezies (ROS). Diese werden für Schädigungen von mitochondrialen und zellulären Strukturen verantwortlich gemacht und können somit verstärkend auf die Entwicklung von Erkrankungen wirken. Wichtig ist aber auch, dass ein Stopp des Elektronenflusses durch die ETK zwangsläufig vor- und nachgeschaltete metabolische Prozesse hemmt, z. B. den Krebs-Zyklus. Je nach Ursache für die Störung der ETK und des betroffenen Organs ergeben sich daher sehr unterschiedliche, und zumeist sehr komplexe, Krankheitsbilder, die sich in der Klinik weitgehend den gängigen Diagnose- und Therapieverfahren entziehen.

Um Schäden im Zusammenhang mit eingeschränkter Funktion der ETK zu umgehen und die Lebensfähigkeit zu sichern, exprimieren Pflanzen und niedere Organismen (aber nicht Säuger) alternative Atmungskettenenzyme, z. B. die alternative Oxidase (AOX). In den natürlichen Wirten sichert AOX den Elektronenfluss, wenn zum Beispiel die ETK-Komplexe III und/oder IV gehemmt sind. Wir haben AOX von der Schlauchseescheide (*Ciona intestinalis*) in das Genom der Maus eingebracht und haben dieses Tiermodell verwendet, um die Rolle von mitochondrialen ETK-Dysfunktionen als Ursache von Erkrankungen zu untersuchen. Dabei konnten wir feststellen, dass selbst die globale Expression von AOX in der Maus keine Störung der normalen Physiologie verursacht. Dieser Befund kann damit begründet werden, dass AOX unter Basalbedingungen kaum aktiv ist. Bei Zuständen mit ETK-Hemmung hingegen wird AOX katalytisch aktiv und verhindert u.a. eine exzessive ROS-Bildung und Letalität bei Zyanid-Intoxikation. Wir konnten zeigen, dass AOX ganz unterschiedlichen Einfluss auf Krankheitsverläufe nimmt. AOX vermindert Zigarettenrauch-induzierte Gewebeschädigung und daraus resultierende Lungendysfunktion, hemmt akute pulmonale Sauerstoffwahrnehmung, beeinträchtigt den adaptiven Umbau nach kardialer Ischämie und verschlechtert die klinische Expression einer mitochondrialen Myopathie.

Die Ergebnisse dieser Arbeit zeigen, dass AOX ein exzellentes Werkzeug darstellt, um Krankheitsmechanismen zu entschlüsseln. Ein möglicher therapeutischer Nutzen von AOX, z. B. bei der Bekämpfung von Mitochondriopathien, muss allerdings nach derzeitigem Kenntnisstand zurückgestellt werden.

4 Summary

Disruption of electron flow through the mitochondrial electron transport chain (ETC) has been made responsible for a loss of metabolic flexibility and thus underlies a variety of diseases. Several mechanisms may simultaneously impair the functionality of a cell or an organ if the ETC is impaired, thereby limiting the viability of the entire organism. First, the ETC is the central building block for oxidative phosphorylation (OXPHOS). That means, mitochondrial ATP production is decreased when electron flow is disrupted. Second, inhibition of the ETC often causes the excessive production of reactive oxygen species (ROS). ROS can damage mitochondrial and cellular structures, and thus can have an amplifying effect on the development or progression of a disease. Importantly, however, stopping the flow of electrons through the ETC inevitably inhibits upstream and downstream metabolic processes, such as the Krebs cycle. Depending on the cause of the disruption of the ETC and the organ affected, this therefore results in very different, and usually very complex, clinical pictures of disease that largely elude standard diagnostic and therapeutic procedures.

To circumvent damage associated with impaired ETC function and to ensure viability, plants and lower organisms (but not mammals) express alternative respiratory chain enzymes, such as alternative oxidase (AOX). In its natural hosts, AOX ensures electron flow when, for example, ETC complexes III and/or IV are inhibited. We introduced AOX from the sea squirt *Ciona intestinalis* into the mouse genome and used this animal model to investigate the role of mitochondrial ETC dysfunction as a cause of disease. We found that even global expression of AOX in mice does not cause disruption of normal physiology. This finding can be explained by the fact that AOX is catalytically not engaged under basal conditions. In contrast, under conditions of ETC inhibition, AOX becomes catalytically active and prevents, among other things, excessive ROS formation and lethality following cyanide intoxication. We were able to show that AOX impacts very differently on specific disease processes. AOX reduces cigarette smoke-induced tissue injury and resulting lung dysfunction, inhibits acute pulmonary oxygen sensing, impairs adaptive remodeling after cardiac ischemia, and worsens the clinical expression of mitochondrial myopathy.

The results of this work demonstrate that AOX represents an excellent tool to unravel disease mechanisms. Any potential therapeutic benefit of AOX, *e.g.*, in combating mitochondriopathies, however, must be critically evaluated on a case-by-case basis.

5 Publikationen seit 2017

2021

1. Giordano, L., Aneja, M. K., Sommer, N., Alebrahimdehkordi, N., Seraji, A., Weissmann, N., Rudolph, C., Plank, C., Jacobs, H. T. & **Szibor, M.** Alternative oxidase encoded by sequence-optimized and chemically-modified RNA transfected into mammalian cells is catalytically active. *Gene Ther* 1-10 (2021).

2020

1. Gellerich, F. N., **Szibor, M.**, Gizatullina, Z., Lessmann, V., Schwarzer, M., Doenst, T., Vielhaber, S. & Kunz, W. S. Reply to Rutter et al.: The roles of cytosolic and intramitochondrial Ca2+ and the mitochondrial Ca2+-uniporter (MCU) in the stimulation of mammalian oxidative phosphorylation. *J Biol Chem* **295,** 10507 (2020).
2. **Szibor, M.**, Gizatullina, Z., Gainutdinov, T., Endres, T., Debska-Vielhaber, G., Kunz, M., Karavasili, N., Hallmann, K., Schreiber, F., Bamberger, A., Schwarzer, M., Doenst, T., Heinze, H.-J., Lessmann, V., Vielhaber, S., Kunz, W. S. & Gellerich, F. N. Cytosolic, but not matrix, calcium is essential for adjustment of mitochondrial pyruvate supply. *J Biol Chem* **295,** 4383–4397 (2020).
3. Sommer, N., Alebrahimdehkordi, N., Pak, O., Knoepp, F., Strielkov, I., Scheibe, S., Dufour, E., Andjelković, A., Sydykov, A., Saraji, A., Petrovic, A., Quanz, K., Hecker, M., Kumar, M., Wahl, J., Kraut, S., Seeger, W., Schermuly, R. T., Ghofrani, H. A., Ramser, K., Braun, T., Jacobs, H. T., Weissmann, N. & **Szibor, M.** Bypassing mitochondrial complex III using alternative oxidase inhibits acute pulmonary oxygen sensing. *Sci Adv* **6,** eaba0694 (2020).
4. **Szibor, M.**, Schreckenberg, R., Gizatullina, Z., Dufour, E., Wiesnet, M., Dhandapani, P. K., Debska-Vielhaber, G., Heidler, J., Wittig, I., Nyman, T. A., Gärtner, U., Hall, A. R., Pell, V., Viscomi, C., Krieg, T., Murphy, M. P., Braun, T., Gellerich, F. N., Schlüter, K.-D. & Jacobs, H. T. Respiratory chain signalling is essential for adaptive remodelling following cardiac ischaemia. *J Cell Mol Med* **24,** 3534–3548 (2020).
5. **Szibor, M.**, Gainutdinov, T., Fernández-Vizarra, E., Dufour, E., Gizatullina, Z., Debska-Vielhaber, G., Heidler, J., Wittig, I., Viscomi, C., Gellerich, F. & Moore, A. L. Bioenergetic consequences from xenotopic expression of a tunicate AOX in mouse mitochondria: Switch from RET and ROS to FET. *Biochim Biophys Acta Bioenerg* **1861,** 148137 (2020).

2019

1. Dhandapani, P. K., Begines-Moreno, I. M., Brea-Calvo, G., Gärtner, U., Graeber, T. G., Javier Sanchez, G., Morty, R. E., Schönig, K., Hoeve, J. T., Wietelmann, A., Braun, T., Jacobs, H. T. & **Szibor, M.** Hyperoxia but not AOX expression mitigates pathological cardiac remodeling in a mouse model of inflammatory cardiomyopathy. *Sci Rep* **9,** 12741 (2019).
2. Dhandapani, P. K., Lyyski, A. M., Paulin, L., Khan, N. A., Suomalainen, A., Auvinen, P., Dufour, E., **Szibor, M.** & Jacobs, H. T. Phenotypic effects of dietary stress in combination with a respiratory chain bypass in mice. *Physiol Rep* **7,** e14159 (2019).
3. Dzhuraev, G., Rodríguez-Castillo, J. A., Ruiz Camp, J., Salwig, I., **Szibor, M.**, Vadász, I., Herold, S., Braun, T., Ahlbrecht, K., Atzberger, A., Mühlfeld, C., Seeger, W. & Morty, R. E. Estimation of absolute number of alveolar epithelial type 2 cells in mouse lungs: a comparison between stereology and flow cytometry. *Journal of Microscopy* **275,** 36–50 (2019).

4. Salwig, I., Spitznagel, B., Vazquez Armendariz, A. I., Khalooghi, K., Guenther, S., Herold, S., **Szibor, M.** & Braun, T. Bronchioalveolar stem cells are a main source for regeneration of distal lung epithelia in vivo. *EMBO J* **38,** (2019).

5. Giordano, L., Farnham, A., Dhandapani, P. K., Salminen, L., Bhaskaran, J., Voswinckel, R., Rauschkolb, P., Scheibe, S., Sommer, N., Beisswenger, C., Weissmann, N., Braun, T., Jacobs, H. T., Bals, R., Herr, C. & **Szibor, M.** Alternative Oxidase Attenuates Cigarette Smoke-induced Lung Dysfunction and Tissue Damage. *American Journal of Respiratory Cell and Molecular Biology* **60,** 515–522 (2019).

6. Saari, S., Garcia, G. S., Bremer, K., Chioda, M. M., Andjelković, A., Debes, P. V., Nikinmaa, M., **Szibor, M.**, Dufour, E., Rustin, P., Oliveira, M. T. & Jacobs, H. T. Alternative respiratory chain enzymes: Therapeutic potential and possible pitfalls. *Biochim Biophys Acta Mol Basis Dis* **1865,** 854–866 (2019).

7. Rajendran, J., Purhonen, J., Tegelberg, S., Smolander, O. P., Mörgelin, M., Rozman, J., Gailus-Durner, V., Fuchs, H., Hrabé de Angelis, M., Auvinen, P., Mervaala, E., Jacobs, H. T., **Szibor, M.**, Fellman, V. & Kallijärvi, J. Alternative oxidase-mediated respiration prevents lethal mitochondrial cardiomyopathy. *EMBO Mol Med* **11,** (2019).

2018

1. Andjelković, A., Mordas, A., Bruinsma, L., Ketola, A., Cannino, G., Giordano, L., Dhandapani, P. K., **Szibor, M.**, Dufour, E. & Jacobs, H. T. Expression of the Alternative Oxidase Influences Jun N-Terminal Kinase Signaling and Cell Migration. *Mol Cell Biol* **38,** (2018).

2. Dogan, S. A., Cerutti, R., Benincá, C., Brea-Calvo, G., Jacobs, H. T., Zeviani, M., **Szibor, M.** & Viscomi, C. Perturbed Redox Signaling Exacerbates a Mitochondrial Myopathy. *Cell Metabolism* **28,** 764–775.e5 (2018).

3. Robb, E. L., Hall, A. R., Prime, T. A., Eaton, S., **Szibor, M.**, Viscomi, C., James, A. M. & Murphy, M. P. Control of mitochondrial superoxide production by reverse electron transport at complex I. *J Biol Chem* **293,** 9869–9879 (2018).

2017

1. Ntokou, A., **Szibor, M.**, Rodríguez-Castillo, J. A., Quantius, J., Herold, S., Agha, El, E., Bellusci, S., Salwig, I., Braun, T., Voswinckel, R., Seeger, W., Morty, R. E. & Ahlbrecht, K. A novel mouse Cre-driver line targeting Perilipin 2-expressing cells in the neonatal lung. *Genesis* **55,** (2017).

2. Agha, El, E., Moiseenko, A., Kheirollahi, V., De Langhe, S., Crnkovic, S., Kwapiszewska, G., **Szibor, M.**, Kosanovic, D., Schwind, F., Schermuly, R. T., Henneke, I., MacKenzie, B., Quantius, J., Herold, S., Ntokou, A., Ahlbrecht, K., Braun, T., Morty, R. E., Günther, A., Seeger, W. & Bellusci, S. Two-Way Conversion between Lipogenic and Myogenic Fibroblastic Phenotypes Marks the Progression and Resolution of Lung Fibrosis. *Cell Stem Cell* **20,** 261–273.e3 (2017).

3. **Szibor, M.**, Dhandapani, P. K., Dufour, E., Holmström, K. M., Zhuang, Y., Salwig, I., Wittig, I., Heidler, J., Gizatullina, Z., Gainutdinov, T., German Mouse Clinic Consortium, Fuchs, H., Gailus-Durner, V., de Angelis, M. H., Nandania, J., Velagapudi, V., Wietelmann, A., Rustin, P., Gellerich, F. N., Jacobs, H. T. & Braun, T. Broad AOX expression in a genetically tractable mouse model does not disturb normal physiology. *Dis Model Mech* **10,** 163–171 (2017).

6 Literaturverzeichnis

1. Martin, W. F. & Thauer, R. K. Energy in Ancient Metabolism. *Cell* **168**, 953–955 (2017).

2. Gründer, S. & Schlüter, K.-D. *Physiologie hoch2.* (Elsevier Health Sciences, 2019).

3. Galgani, J. E., Moro, C. & Ravussin, E. Metabolic flexibility and insulin resistance. *Am J Physiol-endoc M* **295**, E1009–E1017 (2008).

4. Olson, K. A., Schell, J. C. & Rutter, J. Pyruvate and Metabolic Flexibility: Illuminating a Path Toward Selective Cancer Therapies. *Trends Biochem Sci* **41**, 219–230 (2016).

5. Theurey, P. & Rieusset, J. Mitochondria-Associated Membranes Response to Nutrient Availability and Role in Metabolic Diseases. *Trends Endocrinol Metabolism* **28**, 32–45 (2017).

6. Smith, R. L., Soeters, M. R., Wüst, R. C. I. & Houtkooper, R. H. Metabolic Flexibility as an Adaptation to Energy Resources and Requirements in Health and Disease. *Endocr Rev* **39**, 489–517 (2018).

7. Saltin, B. & Gollnick, P. D. Skeletal muscle adaptability: significance for metabolism and performance. in *Handbook of Physiology* (eds. Peachy, L., Adrian, R. & Geiger, S.) 555–631 (1983).

8. Kelley, D. E., Goodpaster, B., Wing, R. R. & Simoneau, J.-A. Skeletal muscle fatty acid metabolism in association with insulin resistance, obesity, and weight loss. *Am J Physiol-endoc M* **277**, E1130–E1141 (1999).

9. Kelley, D. E. & Mandarino, L. J. Fuel selection in human skeletal muscle in insulin resistance: a reexamination. *Diabetes* **49**, 677–683 (2000).

10. Battaglia, G. M., Zheng, D., Hickner, R. C. & Houmard, J. A. Effect of exercise training on metabolic flexibility in response to a high-fat diet in obese individuals. *Am J Physiol-endoc M* **303**, E1440–E1445 (2012).

11. Speakman, J. R. Evolutionary Perspectives on the Obesity Epidemic: Adaptive, Maladaptive, and Neutral Viewpoints. *Annu Rev Nutr* **33**, 289–317 (2013).

12. López-Otín, C., Galluzzi, L., Freije, J. M. P., Madeo, F. & Kroemer, G. Metabolic Control of Longevity. *Cell* **166**, 802–821 (2016).

13. Muoio, D. M. Metabolic Inflexibility: When Mitochondrial Indecision Leads to Metabolic Gridlock. *Cell* **159**, 1253–1262 (2014).

14. Ernster, L. & Schatz, G. Mitochondria: a historical review. *J Cell Biology* **91**, 227s–255s (1981).

15. Sagan, L. On the origin of mitosing cells. *J Theor Biol* **14**, 225-IN6 (1967).

16. Spang, A. *et al.* Complex archaea that bridge the gap between prokaryotes and eukaryotes. *Nature* **521**, 173–179 (2015).

17. Shadel, G. S. & Clayton, D. A. MITOCHONDRIAL DNA MAINTENANCE IN VERTEBRATES. *Annu Rev Biochem* **66**, 409–435 (1997).

18. Jacobs, H. T., Lehtinen, S. K. & Spelbrink, J. N. No sex please, we're mitochondria: a hypothesis on the somatic unit of inheritance of mammalian mtDNA. *Bioessays* **22**, 564–572 (2000).

19. Scarpulla, R. C. Transcriptional Paradigms in Mammalian Mitochondrial Biogenesis and Function. *Physiol Rev* **88**, 611–638 (2008).

20. Anderson, S. *et al.* Sequence and organization of the human mitochondrial genome. *Nature* **290**, 457–465 (1981).

21. Race, H. L., Herrmann, R. G. & Martin, W. Why have organelles retained genomes? *Trends Genet* **15**, 364–370 (1999).

22. Chandel, N. S. Evolution of Mitochondria as Signaling Organelles. *Cell Metab* **22**, 204–206 (2015).

23. Martínez-Reyes, I. & Chandel, N. S. Mitochondrial TCA cycle metabolites control physiology and disease. *Nat Commun* **11**, 102 (2020).

24. Green, D. R. Apoptotic Pathways: Ten Minutes to Dead. *Cell* **121**, 671–674 (2005).

25. Bock, F. J. & Tait, S. W. G. Mitochondria as multifaceted regulators of cell death. *Nat Rev Mol Cell Bio* **21**, 85–100 (2020).

26. Toyama, E. Q. *et al.* AMP-activated protein kinase mediates mitochondrial fission in response to energy stress. *Science* **351**, 275–281 (2016).

27. Herzig, S. & Shaw, R. J. AMPK: guardian of metabolism and mitochondrial homeostasis. *Nat Rev Mol Cell Bio* **19**, 121–135 (2017).

28. Chandel, N. S. *et al.* Mitochondrial reactive oxygen species trigger hypoxia-induced transcription. *Proc National Acad Sci* **95**, 11715–11720 (1998).

29. Sies, H. & Jones, D. P. Reactive oxygen species (ROS) as pleiotropic physiological signalling agents. *Nat Rev Mol Cell Bio* **21**, 363–383 (2020).

30. Riley, J. S. & Tait, S. W. Mitochondria and pathogen immunity: from killer to firestarter. *Embo J* **38**, e100907 (2019).

31. Riley, J. S. & Tait, S. W. Mitochondrial DNA in inflammation and immunity. *Embo Rep* **21**, e49799 (2020).

32. Ichas, F., Jouaville, L. S. & Mazat, J.-P. Mitochondria Are Excitable Organelles Capable of Generating and Conveying Electrical and Calcium Signals. *Cell* **89**, 1145–1153 (1997).

33. Jouaville, L. S., Ichas, F. & Mazat, J.-P. Modulation of cell calcium signals by mitochondria. *Mol Cell Biochem* **184**, 371–376 (1998).

34. Wood, P. G. & Gillespie, J. I. Evidence for Mitochondrial Ca2+-Induced Ca2+Release in Permeabilised Endothelial Cells. *Biochem Bioph Res Co* **246**, 543–548 (1998).

35. Szibor, M. *et al.* Cytosolic, but not matrix, calcium is essential for adjustment of mitochondrial pyruvate supply. *J Biol Chem* **295**, 4383–4397 (2020).

36. Chance, B. & Williams, G. R. Advances in Enzymology and Related Areas of Molecular Biology. *Adv Enzym - Relat Areas Mol Biology* **17**, 65–134 (1956).

37. *Mitochondrial Bioenergetics, Methods and Protocols*. vol. 1782 (Humana Press, 2018).

38. MITCHELL, P. Coupling of Phosphorylation to Electron and Hydrogen Transfer by a Chemi-Osmotic type of Mechanism. *Nature* **191**, 144–148 (1961).

39. Dogan, S. A. *et al.* Perturbed Redox Signaling Exacerbates a Mitochondrial Myopathy. *Cell Metab* **28**, 764-775.e5 (2018).

40. Robb, E. L. *et al.* Control of mitochondrial superoxide production by reverse electron transport at complex I. *J Biol Chem* **293**, 9869–9879 (2018).

41. Krebs, H. A. & Johnson, W. A. Metabolism of ketonic acids in animal tissues. *Biochem J* **31**, 645–660 (1937).

42. Fluhrer, R. & Hampe, W. *Biochemie hoch2*. (Elsevier Health Sciences, 2019).

43. Keller, M. A., Kampjut, D., Harrison, S. A. & Ralser, M. Sulfate radicals enable a non-enzymatic Krebs cycle precursor. *Nat Ecol Evol* **1**, 0083 (2017).

44. Wächtershäuser, G. Evolution of the first metabolic cycles. *Proc National Acad Sci* **87**, 200–204 (1990).

45. Orgel, L. E. The Implausibility of Metabolic Cycles on the Prebiotic Earth. *Plos Biol* **6**, e18 (2008).

46. Sojo, V., Herschy, B., Whicher, A., Camprubí, E. & Lane, N. The Origin of Life in Alkaline Hydrothermal Vents. *Astrobiology* **16**, 181–197 (2016).

47. Chinopoulos, C. Which way does the citric acid cycle turn during hypoxia? The critical role of **α**-ketoglutarate dehydrogenase complex. *J Neurosci Res* **91**, 1030–1043 (2013).

48. Mizuarai, S., Miki, S., Araki, H., Takahashi, K. & Kotani, H. Identification of Dicarboxylate Carrier Slc25a10 as Malate Transporter in de Novo Fatty Acid Synthesis*. *J Biol Chem* **280**, 32434–32441 (2005).

49. Shi, L. & Tu, B. P. Acetyl-CoA and the regulation of metabolism: mechanisms and consequences. *Curr Opin Cell Biol* **33**, 125–131 (2015).

50. Sivanand, S., Viney, I. & Wellen, K. E. Spatiotemporal Control of Acetyl-CoA Metabolism in Chromatin Regulation. *Trends Biochem Sci* **43**, 61–74 (2018).

51. Zdzisińska, B., Żurek, A. & Kandefer-Szerszeń, M. Alpha-Ketoglutarate as a Molecule with Pleiotropic Activity: Well-Known and Novel Possibilities of Therapeutic Use. *Arch Immunol Ther Ex* **65**, 21–36 (2017).

52. Semenza, G. L. HIF-1, O2, and the 3 PHDs How Animal Cells Signal Hypoxia to the Nucleus. *Cell* **107**, 1–3 (2001).

53. Kim, J., Tchernyshyov, I., Semenza, G. L. & Dang, C. V. HIF-1-mediated expression of pyruvate dehydrogenase kinase: A metabolic switch required for cellular adaptation to hypoxia. *Cell Metab* **3**, 177–185 (2006).

54. Fukuda, R. *et al.* HIF-1 Regulates Cytochrome Oxidase Subunits to Optimize Efficiency of Respiration in Hypoxic Cells. *Cell* **129**, 111–122 (2007).

55. Zhang, H. *et al.* HIF-1 Inhibits Mitochondrial Biogenesis and Cellular Respiration in VHL-Deficient Renal Cell Carcinoma by Repression of C-MYC Activity. *Cancer Cell* **11**, 407–420 (2007).

56. Kaelin, W. G. & Ratcliffe, P. J. Oxygen Sensing by Metazoans: The Central Role of the HIF Hydroxylase Pathway. *Mol Cell* **30**, 393–402 (2008).

57. Tannahill, G. M. *et al*. Succinate is an inflammatory signal that induces IL-1β through HIF-1α. *Nature* **496**, 238–242 (2013).

58. Mills, E. L. *et al*. Succinate Dehydrogenase Supports Metabolic Repurposing of Mitochondria to Drive Inflammatory Macrophages. *Cell* **167**, 457-470.e13 (2016).

59. Baysal, B. E. *et al*. Mutations in SDHD, a Mitochondrial Complex II Gene, in Hereditary Paraganglioma. *Science* **287**, 848–851 (2000).

60. Niemann, S. & Müller, U. Mutations in SDHC cause autosomal dominant paraganglioma, type 3. *Nat Genet* **26**, 268–270 (2000).

61. Astuti, D. *et al*. Gene Mutations in the Succinate Dehydrogenase Subunit SDHB Cause Susceptibility to Familial Pheochromocytoma and to Familial Paraganglioma. *Am J Hum Genetics* **69**, 49–54 (2001).

62. Hao, H.-X. *et al*. SDH5, a Gene Required for Flavination of Succinate Dehydrogenase, Is Mutated in Paraganglioma. *Science* **325**, 1139–1142 (2009).

63. DiMauro, S. & Schon, E. A. Mitochondrial Disorders in the Nervous System. *Annu Rev Neurosci* **31**, 91–123 (2008).

64. Bertero, E. & Maack, C. Metabolic remodelling in heart failure. *Nat Rev Cardiol* **15**, 457–470 (2018).

65. Gonzalez-Franquesa, A. & Patti, M.-E. Mitochondrial Dynamics in Cardiovascular Medicine. *Adv Exp Med Biol* **982**, 465–520 (2017).

66. Liesa, M. & Shirihai, O. S. Mitochondrial Dynamics in the Regulation of Nutrient Utilization and Energy Expenditure. *Cell Metab* **17**, 491–506 (2013).

67. Sabharwal, S. S. & Schumacker, P. T. Mitochondrial ROS in cancer: initiators, amplifiers or an Achilles' heel? *Nat Rev Cancer* **14**, 709–721 (2014).

68. Pinton, P. & Kroemer, G. Altering mitochondrial properties. *Nat Chem Biol* **10**, 89–90 (2014).

69. Koppenol, W. H., Bounds, P. L. & Dang, C. V. Otto Warburg's contributions to current concepts of cancer metabolism. *Nat Rev Cancer* **11**, 325–337 (2011).

70. Lightowlers, R. N., Taylor, R. W. & Turnbull, D. M. Mutations causing mitochondrial disease: What is new and what challenges remain? *Science* **349**, 1494–1499 (2015).

71. Ng, Y. S. & Turnbull, D. M. Mitochondrial disease: genetics and management. *J Neurol* **263**, 179–191 (2016).

72. Koopman, W. J. H., Willems, P. H. G. M. & Smeitink, J. A. M. Monogenic Mitochondrial Disorders. *New Engl J Medicine* **366**, 1132–1141 (2012).

73. Nesbitt, V. *et al*. The UK MRC Mitochondrial Disease Patient Cohort Study: clinical phenotypes associated with the m.3243A>G mutation—implications for diagnosis and management. *J Neurology Neurosurg Psychiatry* **84**, 936 (2013).

74. Skladal, D., Halliday, J. & Thorburn, D. R. Minimum birth prevalence of mitochondrial respiratory chain disorders in children. *Brain* **126**, 1905–1912 (2003).

75. Gorman, G. S. *et al*. Prevalence of nuclear and mitochondrial DNA mutations related to adult mitochondrial disease. *Ann Neurol* **77**, 753–759 (2015).

76. Singer, M. The role of mitochondrial dysfunction in sepsis-induced multi-organ failure. *Virulence* **5**, 66–72 (2014).

77. Singer, M. *et al*. The Third International Consensus Definitions for Sepsis and Septic Shock (Sepsis-3). *Jama* **315**, 801–810 (2016).

78. Rica, A. S. D. L., Gilsanz, F. & Maseda, E. Epidemiologic trends of sepsis in western countries. *Ann Transl Medicine* **4**, 325–325 (2016).

79. Levy, M. M. *et al*. Outcomes of the Surviving Sepsis Campaign in intensive care units in the USA and Europe: a prospective cohort study. *Lancet Infect Dis* **12**, 919–924 (2012).

80. Landesberg, G. *et al*. Diastolic dysfunction and mortality in severe sepsis and septic shock. *Eur Heart J* **33**, 895–903 (2012).

81. Wilhelm, J. *et al*. Severity of cardiac impairment in the early stage of community-acquired sepsis determines worse prognosis. *Clin Res Cardiol* **102**, 735–744 (2013).

82. Palmieri, V. *et al*. Left Ventricular Systolic Longitudinal Function as Predictor of Outcome in Patients With Sepsis. *Circulation Cardiovasc Imaging* **8**, e003865 (2015).

83. Fink, M. Cytopathic hypoxia in sepsis. *Acta Anaesth Scand* **41**, 87–95 (1997).

84. Parker, M. M. *et al.* Profound but Reversible Myocardial Depression in Patients with Septic Shock. *Ann Intern Med* **100**, 483 (1984).

85. Singer, M. Critical illness and flat batteries. *Crit Care* **21**, 309 (2017).

86. Sylvester, J. T., Shimoda, L. A., Aaronson, P. I. & Ward, J. P. T. Hypoxic Pulmonary Vasoconstriction. *Physiol Rev* **92**, 367–520 (2012).

87. Sommer, N., Strielkov, I., Pak, O. & Weissmann, N. Oxygen sensing and signal transduction in hypoxic pulmonary vasoconstriction. *Eur Respir J* **47**, 288–303 (2016).

88. Mathew, B. & Lakshminrusimha, S. Persistent Pulmonary Hypertension in the Newborn. *Children* **4**, 63 (2017).

89. Grimminger, J. *et al.* Thin Air Resulting in High Pressure: Mountain Sickness and Hypoxia-Induced Pulmonary Hypertension. *Can Respir J* **2017**, 1–17 (2017).

90. Sommer, N. *et al.* Mitochondrial Complex IV Subunit 4 Isoform 2 Is Essential for Acute Pulmonary Oxygen Sensing. *Circ Res* **121**, 424–438 (2017).

91. Dunham-Snary, K. J. *et al.* Ndufs2, a Core Subunit of Mitochondrial Complex I, Is Essential for Acute Oxygen-Sensing and Hypoxic Pulmonary Vasoconstriction. *Circ Res* **124**, 1727–1746 (2019).

92. Waypa, G. B., Smith, K. A. & Schumacker, P. T. O2 sensing, mitochondria and ROS signaling: The fog is lifting. *Mol Aspects Med* **47**, 76–89 (2016).

93. Vestbo, J. *et al.* Global Strategy for the Diagnosis, Management, and Prevention of Chronic Obstructive Pulmonary Disease. *Am J Resp Crit Care* **187**, 347–365 (2013).

94. Chung, K. F. & Adcock, I. M. Multifaceted mechanisms in COPD: inflammation, immunity, and tissue repair and destruction. *Eur Respir J* **31**, 1334–1356 (2008).

95. PRYOR, W. A. & STONE, K. Oxidants in Cigarette Smoke Radicals, Hydrogen Peroxide, Peroxynitrate, and Peroxynitrite. *Ann Ny Acad Sci* **686**, 12–27 (1993).

96. Talhout, R. *et al.* Hazardous Compounds in Tobacco Smoke. *Int J Environ Res Pu* **8**, 613–628 (2011).

97. Bhandari, R. K. *et al.* Cyanide Toxicokinetics: The Behavior of Cyanide, Thiocyanate and 2-Amino-2-Thiazoline-4-Carboxylic Acid in Multiple Animal Models. *J Anal Toxicol* **38**, 218–225 (2014).

98. Piquereau, J. *et al.* Mitochondrial dynamics in the adult cardiomyocytes: which roles for a highly specialized cell? *Front Physiol* **4**, 102 (2013).

99. Otani, H. *et al.* In vitro study on contribution of oxidative metabolism of isolated rabbit heart mitochondria to myocardial reperfusion injury. *Circ Res* **55**, 168–175 (1984).

100. Ambrosio, G. *et al.* Evidence that mitochondrial respiration is a source of potentially toxic oxygen free radicals in intact rabbit hearts subjected to ischemia and reflow. *J Biol Chem* **268**, 18532–18541 (1993).

101. PENG, Y.-W., BULLER, C. L. & CHARPIE, J. R. Impact of N-Acetylcysteine on Neonatal Cardiomyocyte Ischemia-Reperfusion Injury. *Pediatr Res* **70**, 61–66 (2011).

102. Hao, J. *et al.* Role of Vitamin C in Cardioprotection of Ischemia/Reperfusion Injury by Activation of Mitochondrial KATP Channel. *Chem Pharm Bulletin* **64**, 548–557 (2016).

103. Nishinaka, Y., Sugiyama, S., Yokota, M., Saito, H. & Ozawa, T. The effects of a high dose of ascorbate on ischemia-reperfusion-induced mitochondrial dysfunction in canine hearts. *Heart Vessels* **7**, 18–23 (1992).

104. Mickle, D. A. G. *et al.* Myocardial salvage with trolox and ascorbic acid for an acute evolving infarction. *Ann Thorac Surg* **47**, 553–557 (1989).

105. Klein, H. H. *et al.* Combined treatment with vitamins E and C in experimental myocardial infarction in pigs. *Am Heart J* **118**, 667–673 (1989).

106. Goszcz, K. *et al.* Antioxidants in Cardiovascular Therapy: Panacea or False Hope? *Frontiers Cardiovasc Medicine* **2**, 29 (2015).

107. Bjelakovic, G., Nikolova, D., Gluud, L. L., Simonetti, R. G. & Gluud, C. Antioxidant supplements for prevention of mortality in healthy participants and patients with various diseases. *Sao Paulo Med J* **133**, 164–165 (2015).

108. Schaar, C. E. *et al.* Mitochondrial and Cytoplasmic ROS Have Opposing Effects on Lifespan. *Plos Genet* **11**, e1004972 (2015).

109. Loch, T. *et al.* Different extent of cardiac malfunction and resistance to oxidative stress in heterozygous and homozygous manganese-dependent superoxide dismutase-mutant mice. *Cardiovasc Res* **82**, 448–457 (2009).

110. Asimakis, G. K., Lick, S. & Patterson, C. Postischemic Recovery of Contractile Function is Impaired in SOD2+/− but Not SOD1+/− Mouse Hearts. *Circulation* **105**, 981–986 (2002).

111. Szibor, M. *et al.* Respiratory chain signalling is essential for adaptive remodelling following cardiac ischaemia. *J Cell Mol Med* **24**, 3534–3548 (2020).

112. Adlam, V. J. *et al.* Targeting an antioxidant to mitochondria decreases cardiac ischemia-reperfusion injury. *Faseb J* **19**, 1088–1095 (2005).

113. Dare, A. J. *et al.* The mitochondria-targeted anti-oxidant MitoQ decreases ischemia-reperfusion injury in a murine syngeneic heart transplant model. *J Hear Lung Transplant* **34**, 1471–1480 (2015).

114. Junior, R. F. R. *et al.* MitoQ improves mitochondrial dysfunction in heart failure induced by pressure overload. *Free Radical Bio Med* **117**, 18–29 (2018).

115. Szeto, H. H. Mitochondria-Targeted Cytoprotective Peptides for Ischemia-Reperfusion Injury. *Antioxid Redox Sign* **10**, 601–620 (2008).

116. Dai, D.-F. *et al.* Mitochondrial Targeted Antioxidant Peptide Ameliorates Hypertensive Cardiomyopathy. *J Am Coll Cardiol* **58**, 73–82 (2011).

117. Nickel, A. G. *et al.* Reversal of Mitochondrial Transhydrogenase Causes Oxidative Stress in Heart Failure. *Cell Metab* **22**, 472–484 (2015).

118. Rodriguez-Cuenca, S. *et al.* Consequences of long-term oral administration of the mitochondria-targeted antioxidant MitoQ to wild-type mice. *Free Radical Bio Med* **48**, 161–172 (2010).

119. Sabbah, H. N. *et al.* Chronic Therapy With Elamipretide (MTP-131), a Novel Mitochondria-Targeting Peptide, Improves Left Ventricular and Mitochondrial Function in Dogs With Advanced Heart Failure. *Circulation Hear Fail* **9**, e002206 (2016).

120. Brand, M. D. *et al.* Suppressors of Superoxide-H2O2 Production at Site IQ of Mitochondrial Complex I Protect against Stem Cell Hyperplasia and Ischemia-Reperfusion Injury. *Cell Metab* **24**, 582–592 (2016).

121. Chouchani, E. T. *et al.* A Unifying Mechanism for Mitochondrial Superoxide Production during Ischemia-Reperfusion Injury. *Cell Metab* **23**, 254–263 (2016).

122. Chouchani, E. T. *et al.* Ischaemic accumulation of succinate controls reperfusion injury through mitochondrial ROS. *Nature* **515**, 431–435 (2014).

123. Granger, D. N. & Kvietys, P. R. Reperfusion injury and reactive oxygen species: The evolution of a concept. *Redox Biol* **6**, 524–551 (2015).

124. Hegstad, A.-C., Antonsen, O. H. & Ytrehus, K. Low Concentrations of Hydrogen Peroxide Improve Post-ischaemic Metabolic and Functional Recovery in Isolated Perfused Rat Hearts. *J Mol Cell Cardiol* **29**, 2779–2787 (1997).

125. Valen, G. *et al.* Preconditioning with hydrogen peroxide (H2O2) or ischemia in H2O2-induced cardiac dysfunction. *Free Radical Res* **29**, 235–245 (1998).

126. Yun, J. & Finkel, T. Mitohormesis. *Cell Metab* **19**, 757–766 (2014).

127. Brand, M. D. Mitochondrial generation of superoxide and hydrogen peroxide as the source of mitochondrial redox signaling. *Free Radical Bio Med* **100**, 14–31 (2016).

128. Horn, A. *et al.* Mitochondrial redox signaling enables repair of injured skeletal muscle cells. *Sci Signal* **10**, eaaj1978 (2017).

129. Antonucci, S. *et al.* Selective mitochondrial superoxide generation in vivo is cardioprotective through hormesis. *Free Radical Bio Med* **134**, 678–687 (2019).

130. El-Khoury, R. *et al.* Engineering the alternative oxidase gene to better understand and counteract mitochondrial defects: state of the art and perspectives. *Brit J Pharmacol* **171**, 2243–2249 (2014).

131. Giordano, L. *et al.* Alternative oxidase encoded by sequence-optimized and chemically-modified RNA transfected into mammalian cells is catalytically active. *Gene Ther* 1–10 (2021) doi:10.1038/s41434-021-00235-z.

132. Seo, B. B. *et al.* Molecular remedy of complex I defects: Rotenone-insensitive internal NADH-quinone oxidoreductase of Saccharomyces cerevisiae mitochondria restores the NADH oxidase activity of complex I-deficient mammalian cells. *Proc National Acad Sci* **95**, 9167–9171 (1998).

133. Yagi, T. *et al.* Can a Single Subunit Yeast NADH Dehydrogenase (Ndi1) Remedy Diseases Caused by Respiratory Complex I Defects? *Rejuv Res* **9**, 191–197 (2006).

134. Perales-Clemente, E. *et al.* Restoration of electron transport without proton pumping in mammalian mitochondria. *Proc National Acad Sci* **105**, 18735–18739 (2008).

135. Saari, S. *et al.* Alternative respiratory chain enzymes: Therapeutic potential and possible pitfalls. *Biochimica Et Biophysica Acta Bba - Mol Basis Dis* **1865**, 854–866 (2019).

136. Szibor, M. *et al.* Broad AOX expression in a genetically tractable mouse model does not disturb normal physiology. *Dis Model Mech* **10**, 163–171 (2017).

137. Szibor, M. *et al.* Bioenergetic consequences from xenotopic expression of a tunicate AOX in mouse mitochondria: Switch from RET and ROS to FET. *Biochimica Et Biophysica Acta Bba - Bioenergetics* **1861**, 148137 (2020).

138. Hakkaart, G. A. J., Dassa, E. P., Jacobs, H. T. & Rustin, P. Allotopic expression of a mitochondrial alternative oxidase confers cyanide resistance to human cell respiration. *Embo Rep* **7**, 341–345 (2006).

139. Dassa, E. P., Dufour, E., Goncalves, S., Jacobs, H. T. & Rustin, P. The alternative oxidase, a tool for compensating cytochrome c oxidase deficiency in human cells. *Physiol Plantarum* **137**, 427–434 (2009).

140. Rustin, P. & Jacobs, H. T. Respiratory chain alternative enzymes as tools to better understand and counteract respiratory chain deficiencies in human cells and animals. *Physiol Plantarum* **137**, 362–370 (2009).

141. McDonald, A. E. & Vanlerberghe, G. C. Origins, evolutionary history, and taxonomic distribution of alternative oxidase and plastoquinol terminal oxidase. *Comp Biochem Physiology Part D Genom Proteom* **1**, 357–364 (2006).

142. Dry, I. B., Moore, A. L., Day, D. A. & Wiskich, J. T. Regulation of alternative pathway activity in plant mitochondria: Nonlinear relationship between electron flux and the redox poise of the quinone pool. *Arch Biochem Biophys* **273**, 148–157 (1989).

143. Dassa, E. P. *et al*. Expression of the alternative oxidase complements cytochrome c oxidase deficiency in human cells. *Embo Mol Med* **1**, 30–36 (2009).

144. Fernandez-Ayala, D. J. M. *et al.* Expression of the Ciona intestinalis Alternative Oxidase (AOX) in Drosophila Complements Defects in Mitochondrial Oxidative Phosphorylation. *Cell Metab* **9**, 449–460 (2009).

145. Humphrey, D. M. *et al.* Alternative oxidase rescues mitochondria-mediated dopaminergic cell loss in Drosophila. *Hum Mol Genet* **21**, 2698–2712 (2012).

146. Kemppainen, K. K. *et al*. Expression of alternative oxidase in Drosophila ameliorates diverse phenotypes due to cytochrome oxidase deficiency. *Hum Mol Genet* **23**, 2078–2093 (2014).

147. Vartiainen, S. *et al.* Phenotypic rescue of a Drosophila model of mitochondrial ANT1 disease. *Dis Model Mech* **7**, 635–648 (2014).

148. El-Khoury, R. *et al.* Alternative Oxidase Expression in the Mouse Enables Bypassing Cytochrome c Oxidase Blockade and Limits Mitochondrial ROS Overproduction. *Plos Genet* **9**, e1003182 (2013).

149. Sommer, N. *et al*. Bypassing mitochondrial complex III using alternative oxidase inhibits acute pulmonary oxygen sensing. *Sci Adv* **6**, eaba0694 (2020).

150. Giordano, L. *et al.* Alternative Oxidase Attenuates Cigarette Smoke–induced Lung Dysfunction and Tissue Damage. *Am J Resp Cell Mol* **60**, 515–522 (2019).

151. Capecchi, M. R. Gene targeting in mice: functional analysis of the mammalian genome for the twenty-first century. *Nat Rev Genet* **6**, 507–512 (2005).

152. Soriano, P. Generalized lacZ expression with the ROSA26 Cre reporter strain. *Nat Genet* **21**, 70–71 (1999).

153. Srinivas, S. *et al.* Cre reporter strains produced by targeted insertion of EYFP and ECFP into the ROSA26 locus. *Bmc Dev Biol* **1**, 4 (2001).

154. Friedrich, G. & Soriano, P. Promoter traps in embryonic stem cells: a genetic screen to identify and mutate developmental genes in mice. *Gene Dev* **5**, 1513–1523 (1991).

155. Zambrowicz, B. P. *et al.* Disruption of overlapping transcripts in the ROSA βgeo 26 gene trap strain leads to widespread expression of β-galactosidase in mouse embryos and hematopoietic cells. *Proc National Acad Sci* **94**, 3789–3794 (1997).

156. Hong, S. *et al*. Functional Analysis of Various Promoters in Lentiviral Vectors at Different Stages of In Vitro Differentiation of Mouse Embryonic Stem Cells. *Mol Ther* **15**, 1630–1639 (2007).

157. Alexopoulou, A. N., Couchman, J. R. & Whiteford, J. R. The CMV early enhancer/chicken β actin (CAG) promoter can be used to drive transgene expression during the differentiation of murine embryonic stem cells into vascular progenitors. *Bmc Cell Biol* **9**, 2 (2008).

158. Nyabi, O. *et al.* Efficient mouse transgenesis using Gateway-compatible ROSA26 locus targeting vectors and F1 hybrid ES cells. *Nucleic Acids Res* **37**, e55–e55 (2009).

159. Chen, C., Krohn, J., Bhattacharya, S. & Davies, B. A Comparison of Exogenous Promoter Activity at the ROSA26 Locus Using a PhiC31 Integrase Mediated Cassette Exchange Approach in Mouse ES Cells. *Plos One* **6**, e23376 (2011).

160. Koetsier, P. A., Schorr, J. & Doerfler, W. *A rapid optimized protocol for downward alkaline Southern blotting of DNA*. 260–2 (1993).

161. Rodríguez, C. I. *et al*. High-efficiency deleter mice show that FLPe is an alternative to Cre-loxP. *Nat Genet* **25**, 139–140 (2000).

162. Liu, Y., Fu, S., Niu, R., Yang, C. & Lin, J. Transcriptional activity assessment of three different promoters for mouse in utero electroporation system. *Plasmid* **74**, 52–58 (2014).

163. Ida-Hosonuma, M. *et al*. Comparison of neuropathogenicity of poliovirus in two transgenic mouse strains expressing human poliovirus receptor with different distribution patterns. *J Gen Virol* **83**, 1095–1105 (2002).

164. Kim, H. S. *et al*. In Vivo Magnetic Resonance Imaging of Transgenic Mice Expressing Human Ferritin. *Mol Imaging Biol* **15**, 48–57 (2013).

165. Banares, S. *et al*. Novel pan-neuronal Cre-transgenic line for conditional ablation of genes in the nervous system. *Genesis* **42**, 6–16 (2005).

166. Hitz, C., Wurst, W. & Kühn, R. Conditional brain-specific knockdown of MAPK using Cre/loxP regulated RNA interference. *Nucleic Acids Res* **35**, e90–e90 (2007).

167. Delaunay, D. *et al*. Genetic tracing of subpopulation neurons in the prethalamus of mice (Mus musculus). *J Comp Neurol* **512**, 74–83 (2009).

168. Klein, R. *et al*. WPRE-mediated enhancement of gene expression is promoter and cell line specific. *Gene* **372**, 153–161 (2006).

169. Yamamoto, H. & Tang, H. Antagonistic effect of melatonin against cyanide-induced seizures and acute lethality in mice. *Toxicol Lett* **87**, 19–24 (1996).

170. Zhang, D. *et al*. Protection from cyanide-induced brain injury by the Nrf2 transcriptional activator carnosic acid. *J Neurochem* **133**, 898–908 (2015).

171. Rajendran, J. *et al*. Alternative oxidase-mediated respiration prevents lethal mitochondrial cardiomyopathy. *Embo Mol Med* **11**, (2019).

172. Kermorgant, M., Bonnefoy, N. & Dujardin, G. Oxa1p, which is required for cytochrome c oxidase and ATP synthase complex formation, is embedded in the mitochondrial inner membrane. *Curr Genet* **31**, 302–307 (1997).

173. Hamel, P., Lemaire, C., Bonnefoy, N., Brivet-Chevillotte, P. & Dujardin, G. Mutations in the Membrane Anchor of Yeast Cytochrome c1 Compensate for the Absence of Oxa1p and Generate Carbonate-Extractable Forms of Cytochrome c1. *Genetics* **150**, 601–611 (1998).

174. Sakamoto, W., Spielewoy, N., Bonnard, G., Murata, M. & Wintz, H. Mitochondrial Localization of AtOXA1, an Arabidopsis Homologue of Yeast Oxa1p Involved in the Insertion and Assembly of Protein Complexes in Mitochondrial Inner Membrane. *Plant Cell Physiol* **41**, 1157–1163 (2000).

175. Wittig, I., Braun, H.-P. & Schägger, H. Blue native PAGE. *Nat Protoc* **1**, 418–428 (2006).

176. Wittig, I., Karas, M. & Schägger, H. High Resolution Clear Native Electrophoresis for In-gel Functional Assays and Fluorescence Studies of Membrane Protein Complexes*. *Mol Cell Proteomics* **6**, 1215–1225 (2007).

177. Heide, H. *et al*. Complexome Profiling Identifies TMEM126B as a Component of the Mitochondrial Complex I Assembly Complex. *Cell Metab* **16**, 538–549 (2012).

178. Vogel, F., Bornhövd, C., Neupert, W. & Reichert, A. S. Dynamic subcompartmentalization of the mitochondrial inner membrane. *J Cell Biology* **175**, 237–247 (2006).

179. Acín-Pérez, R., Fernández-Silva, P., Peleato, M. L., Pérez-Martos, A. & Enriquez, J. A. Respiratory Active Mitochondrial Supercomplexes. *Mol Cell* **32**, 529–539 (2008).

180. Chaban, Y., Boekema, E. J. & Dudkina, N. V. Structures of mitochondrial oxidative phosphorylation supercomplexes and mechanisms for their stabilisation. *Biochimica Et Biophysica Acta Bba - Bioenergetics* **1837**, 418–426 (2014).

181. Yamamoto, H. Effect of atropine on cyanide-induced acute lethality in mice. *Toxicol Lett* **80**, 29–33 (1995).

182. Schägger, H. & Pfeiffer, K. The Ratio of Oxidative Phosphorylation Complexes I–V in Bovine Heart Mitochondria and the Composition of Respiratory Chain Supercomplexes*. *J Biol Chem* **276**, 37861–37867 (2001).

183. Wittig, I., Carrozzo, R., Santorelli, F. M. & Schägger, H. Supercomplexes and subcomplexes of mitochondrial oxidative phosphorylation. *Biochimica Et Biophysica Acta Bba - Bioenergetics* **1757**, 1066–1072 (2006).

184. Moore, A. L., Bonner, W. D. & Rich, P. R. The determination of the proton-motive force during cyanide-insensitive respiration in plant mitochondria. *Arch Biochem Biophys* **186**, 298–306 (1978).

185. Fedor, J. G. & Hirst, J. Mitochondrial Supercomplexes Do Not Enhance Catalysis by Quinone Channeling. *Cell Metab* **28**, 525-531.e4 (2018).

186. Kido, Y. *et al*. Purification and kinetic characterization of recombinant alternative oxidase from Trypanosoma brucei brucei. *Biochimica Et Biophysica Acta Bba - Bioenergetics* **1797**, 443–450 (2010).

187. Affourtit, C., Krab, K. & Moore, A. L. Control of plant mitochondrial respiration. *Biochimica Et Biophysica Acta Bba - Bioenergetics* **1504**, 58–69 (2001).

188. Moore, A. L., Dry, I. B. & Wiskich, J. T. Measurement of the redox state of the ubiquinone pool in plant mitochondria. *Febs Lett* **235**, 76–80 (1988).

189. Bai, F., Fink, B. D., Yu, L. & Sivitz, W. I. Voltage-Dependent Regulation of Complex II Energized Mitochondrial Oxygen Flux. *Plos One* **11**, e0154982 (2016).

190. Sommer, N. *et al*. Mitochondrial cytochrome redox states and respiration in acute pulmonary oxygen sensing. *Eur Respir J* **36**, 1056–1066 (2010).

191. Firth, A. L. *et al*. Functional Ion Channels in Human Pulmonary Artery Smooth Muscle Cells: Voltage-Dependent Cation Channels. *Pulm Circ* **1**, 48–71 (2011).

192. Veit, F., Pak, O., Brandes, R. P. & Weissmann, N. Hypoxia-Dependent Reactive Oxygen Species Signaling in the Pulmonary Circulation: Focus on Ion Channels. *Antioxid Redox Sign* **22**, 537–552 (2015).

193. Ko, E. A. *et al*. Functional characterization of voltage-dependent Ca2+ channels in mouse pulmonary arterial smooth muscle cells: divergent effect of ROS. *Am J Physiol-cell Ph* **304**, C1042–C1052 (2013).

194. Weissmann, N. *et al*. Classical transient receptor potential channel 6 (TRPC6) is essential for hypoxic pulmonary vasoconstriction and alveolar gas exchange. *Proc National Acad Sci* **103**, 19093–19098 (2006).

195. Weir, E. K. & Olschewski, A. Role of ion channels in acute and chronic responses of the pulmonary vasculature to hypoxia. *Cardiovasc Res* **71**, 630–641 (2006).

196. Olschewski, A. *et al*. TASK-1 (KCNK3) channels in the lung: from cell biology to clinical implications. *Eur Respir J* **50**, 1700754 (2017).

197. Andjelković, A. *et al*. Diiron centre mutations in Ciona intestinalis alternative oxidase abolish enzymatic activity and prevent rescue of cytochrome oxidase deficiency in flies. *Sci Rep-uk* **5**, 18295 (2015).

198. Schumacker, P. T. Lung Cell Hypoxia: Role of Mitochondrial Reactive Oxygen Species Signaling in Triggering Responses. *Proc Am Thorac Soc* **8**, 477–484 (2011).

199. Waypa, G. B. *et al*. Superoxide Generated at Mitochondrial Complex III Triggers Acute Responses to Hypoxia in the Pulmonary Circulation. *Am J Resp Crit Care* **187**, 424–432 (2013).

200. Orr, A. L. *et al*. Suppressors of superoxide production from mitochondrial complex III. *Nat Chem Biol* **11**, 834–836 (2015).

201. Spiro, T. G. & Strekas, T. C. Resonance Raman Spectra of Hemoglobin and Cytochrome c: Inverse Polarization and Vibronic Scattering. *Proc National Acad Sci* **69**, 2622–2626 (1972).

202. Choi, S., Lee, J. J., Wei, Y. H. & Spiro, T. G. Resonance Raman and electronic spectra of heme a complexes and cytochrome oxidase. *J Am Chem Soc* **105**, 3692–3707 (1983).

203. Brazhe, N. A., Treiman, M., Faricelli, B., Vestergaard, J. H. & Sosnovtseva, O. In Situ Raman Study of Redox State Changes of Mitochondrial Cytochromes in a Perfused Rat Heart. *Plos One* **8**, e70488 (2013).

204. Erjavec, N., Pinato, G. & Ramser, K. Raman spectroscopy as a tool for detecting mitochondrial fitness. *J Raman Spectrosc* **47**, 933–939 (2016).

205. Teng, H. *et al*. Quantitative Detection of NADH Using a Novel Enzyme-Assisted Method Based on Surface-Enhanced Raman Scattering. *Sensors* **17**, 788 (2017).

206. Marshall, J. D., Bazan, I., Zhang, Y., Fares, W. H. & Lee, P. J. Mitochondrial dysfunction and pulmonary hypertension: cause, effect, or both. *Am J Physiol-lung C* **314**, L782–L796 (2018).

207. Pak, O. *et al*. Impact of the mitochondria-targeted antioxidant MitoQ on hypoxia-induced pulmonary hypertension. *Eur Respir J* **51**, 1701024 (2018).

208. Dromparis, P., Sutendra, G. & Michelakis, E. D. The role of mitochondria in pulmonary vascular remodeling. *J Mol Med* **88**, 1003–1010 (2010).

209. Ball, M. K. *et al*. Regulation of Hypoxia-induced Pulmonary Hypertension by Vascular Smooth Muscle Hypoxia-Inducible Factor-1**α**. *Am J Resp Crit Care* **189**, 314–324 (2014).

210. Adesina, S. E. *et al.* Targeting mitochondrial reactive oxygen species to modulate hypoxia-induced pulmonary hypertension. *Free Radical Bio Med* **87**, 36–47 (2015).

211. Martínez-Reyes, I. *et al.* TCA Cycle and Mitochondrial Membrane Potential Are Necessary for Diverse Biological Functions. *Mol Cell* **61**, 199–209 (2016).

212. Chua, Y. L. *et al.* Stabilization of Hypoxia-inducible Factor-1α Protein in Hypoxia Occurs Independently of Mitochondrial Reactive Oxygen Species Production*. *J Biol Chem* **285**, 31277–31284 (2010).

213. Voss, M. *et al.* Il-17A contributes to maintenance of pulmonary homeostasis in a murine model of cigarette smoke-induced emphysema. *Am J Physiol-lung C* **309**, L188–L195 (2015).

214. Wolf, L., Herr, C., Niederstraßer, J., Beisswenger, C. & Bals, R. Receptor for advanced glycation endproducts (RAGE) maintains pulmonary structure and regulates the response to cigarette smoke. *Plos One* **12**, e0180092 (2017).

215. Giordano, L. *et al.* Cigarette toxicity triggers Leber's hereditary optic neuropathy by affecting mtDNA copy number, oxidative phosphorylation and ROS detoxification pathways. *Cell Death Dis* **6**, e2021–e2021 (2015).

216. Vichai, V. & Kirtikara, K. Sulforhodamine B colorimetric assay for cytotoxicity screening. *Nat Protoc* **1**, 1112–1116 (2006).

217. Orellana, E. & Kasinski, A. Sulforhodamine B (SRB) Assay in Cell Culture to Investigate Cell Proliferation. *Bio-protocol* **6**, (2016).

218. Soderberg, K., Nissinen, E., Bakay, B. & Scheffler, I. E. The energy charge in wild-type and respiration-deficient chinese hamster cell mutants. *J Cell Physiol* **103**, 169–172 (1980).

219. Robinson, B. H., Petrova-Benedict, R., Buncic, J. R. & Wallace, D. C. Nonviability of cells with oxidative defects in galactose medium: A screening test for affected patient fibroblasts. *Biochem Med Metab B* **48**, 122–126 (1992).

220. Messner, B. *et al.* Apoptosis and necrosis: two different outcomes of cigarette smoke condensate-induced endothelial cell death. *Cell Death Dis* **3**, e424–e424 (2012).

221. Esakky, P., Hansen, D. A., Drury, A. M., Cusumano, A. & Moley, K. H. Cigarette smoke-induced cell death of a spermatocyte cell line can be prevented by inactivating the Aryl hydrocarbon receptor. *Cell Death Discov* **1**, 15050 (2015).

222. Hannan, S. E., Harris, J. O., Sheridan, N. P. & Patel, J. M. Cigarette Smoke Alters Plasma Membrane Fluidity of Rat Alveolar Macrophages. *Am Rev Respir Dis* **140**, 1668–1673 (1989).

223. Papaporfyriou, A. *et al.* Increased Levels of Osteopontin in Sputum Supernatant in Patients With COPD. *Chest* **146**, 951–958 (2014).

224. Zhang, X. W., Liu, Q., Wang, Y. & Thorlacius, H. CXC chemokines, MIP-2 and KC, induce P-selectin-dependent neutrophil rolling and extravascular migration in vivo. *Brit J Pharmacol* **133**, 413–421 (2001).

225. Thatcher, T. H. *et al.* Role of CXCR2 in cigarette smoke-induced lung inflammation. *Am J Physiol-lung C* **289**, L322–L328 (2005).

226. Deshmukh, H. S. *et al.* Acrolein-Activated Matrix Metalloproteinase 9 Contributes to Persistent Mucin Production. *Am J Resp Cell Mol* **38**, 446–454 (2008).

227. Ferry, G. *et al.* Activation of MMP-9 by neutrophil elastase in an in vivo model of acute lung injury. *Febs Lett* **402**, 111–115 (1997).

228. Mercer, P. *et al.* MMP-9, TIMP-1 and inflammatory cells in sputum from COPD patients during exacerbation. *Respir Res* **6**, 151 (2005).

229. Shaykhiev, R. *et al.* Smoking-Dependent Reprogramming of Alveolar Macrophage Polarization: Implication for Pathogenesis of Chronic Obstructive Pulmonary Disease. *J Immunol* **183**, 2867–2883 (2009).

230. Barnes, P. J. Inflammatory mechanisms in patients with chronic obstructive pulmonary disease. *J Allergy Clin Immun* **138**, 16–27 (2016).

231. Seimetz, M. *et al.* Inducible NOS Inhibition Reverses Tobacco-Smoke-Induced Emphysema and Pulmonary Hypertension in Mice. *Cell* **147**, 293–305 (2011).

232. Guerassimov, A. *et al.* The Development of Emphysema in Cigarette Smoke-exposed Mice Is Strain Dependent. *Am J Resp Crit Care* **170**, 974–980 (2004).

233. Herr, C. *et al.* Combined exposure to bacteria and cigarette smoke resembles characteristic phenotypes of human COPD in a murine disease model. *Exp Toxicol Pathol* **67**, 261–269 (2015).

234. Dhandapani, P. K. *et al.* Hyperoxia but not AOX expression mitigates pathological cardiac remodeling in a mouse model of inflammatory cardiomyopathy. *Sci Rep-uk* **9**, 12741 (2019).

235. Schmidt, K. *et al*. Cardioprotective effects of mineralocorticoid receptor antagonists at reperfusion. *Eur Heart J* **31**, 1655–1662 (2010).

236. Yeap, X.-Y., Dehn, S., Adelman, J., Lipsitz, J. & Thorp, E. B. Necrosis, Methods and Protocols. *Methods Mol Biology* **1004**, 115–133 (2013).

237. KATZ, L. N. & FEINBERG, H. The Relation of Cardiac Effort to Myocardial Oxygen Consumption and Coronary Flow. *Circ Res* **6**, 656–669 (1958).

238. Ebelt, H. *et al*. Cellular Cardiomyoplasty: Improvement of Left Ventricular Function Correlates with the Release of Cardioactive Cytokines. *Stem Cells* **25**, 236–244 (2007).

239. Pagel-Langenickel, I. Heart Failure: From Research to Clinical Practice, Volume 3. *Adv Exp Med Biol* **1067**, 109–131 (2018).

240. Polyakova, V. *et al*. Fibrosis in endstage human heart failure: Severe changes in collagen metabolism and MMP/TIMP profiles. *Int J Cardiol* **151**, 18–33 (2011).

241. Querejeta, R. *et al*. Increased Collagen Type I Synthesis in Patients With Heart Failure of Hypertensive Origin: Relation to Myocardial Fibrosis. *Circulation* **110**, 1263–1268 (2004).

242. Esfandiary, A. *et al*. Protection against pressure overload-induced right heart failure by uncoupling protein 2 silencing. *Cardiovasc Res* **115**, cvz049 (2019).

243. Olivetti, G. *et al*. Apoptosis in the Failing Human Heart. *New Engl J Medicine* **336**, 1131–1141 (1997).

244. Liu, W., Ru, L., Su, C., Qi, S. & Qi, X. Serum Levels of Inflammatory Cytokines and Expression of BCL2 and BAX mRNA in Peripheral Blood Mononuclear Cells and in Patients with Chronic Heart Failure. *Med Sci Monitor* **25**, 2633–2639 (2019).

245. Bernardo, A. F. *et al*. Overnutrition during lactation leads to impairment in insulin signaling, up-regulation of GLUT1 and increased mitochondrial carbohydrate oxidation in heart of weaned mice. *J Nutritional Biochem* **29**, 124–132 (2016).

246. Eden, E., Lipson, D., Yogev, S. & Yakhini, Z. Discovering Motifs in Ranked Lists of DNA Sequences. *Plos Comput Biol* **3**, e39 (2007).

247. Eden, E., Navon, R., Steinfeld, I., Lipson, D. & Yakhini, Z. GOrilla: a tool for discovery and visualization of enriched GO terms in ranked gene lists. *Bmc Bioinformatics* **10**, 48 (2009).

248. Perez-Riverol, Y. *et al*. PRIDE Inspector Toolsuite: Moving Toward a Universal Visualization Tool for Proteomics Data Standard Formats and Quality Assessment of ProteomeXchange Datasets*. *Mol Cell Proteomics* **15**, 305–317 (2016).

249. Deutsch, E. W. *et al*. The ProteomeXchange consortium in 2017: supporting the cultural change in proteomics public data deposition. *Nucleic Acids Res* **45**, D1100–D1106 (2017).

250. Perez-Riverol, Y. *et al*. The PRIDE database and related tools and resources in 2019: improving support for quantification data. *Nucleic Acids Res* **47**, gky1106- (2019).

251. Lowes, B. D. *et al*. Changes in gene expression in the intact human heart. Downregulation of alpha-myosin heavy chain in hypertrophied, failing ventricular myocardium. *J Clin Invest* **100**, 2315–2324 (1997).

252. Ghosh, N. & Haddad, H. Atrial natriuretic peptides in heart failure: pathophysiological significance, diagnostic and prognostic value. *Can J Physiol Pharm* **89**, 587–591 (2011).

253. Semenov, A. G. & Katrukha, A. G. Analytical Issues with Natriuretic Peptides - has this been Overly Simplified? *Ejifcc* **27**, 189–207 (2016).

254. Langenickel, T., Pagel, I., Ho□hnel, K., Dietz, R. & Willenbrock, R. Differential regulation of cardiac ANP and BNP mRNA in different stages of experimental heart failure. *Am J Physiol-heart C* **278**, H1500–H1506 (2000).

255. Wang, D. *et al*. Effects of Pressure Overload on Extracellular Matrix Expression in the Heart of the Atrial Natriuretic Peptide–Null Mouse. *Hypertension* **42**, 88–95 (2003).

256. Falcão, L. M., Pinto, F., Ravara, L. & Zwieten, P. A. van. BNP and ANP as diagnostic and predictive markers in heart failure with left ventricular systolic dysfunction. *J Renin-angio-aldo S* **5**, 121–129 (2004).

257. Moro, C. & Lafontan, M. Natriuretic peptides and cGMP signaling control of energy homeostasis. *Am J Physiol-heart C* **304**, H358–H368 (2013).

258. Li, P. *et al*. ANP signaling inhibits TGF-β-induced Smad2 and Smad3 nuclear translocation and extracellular matrix expression in rat pulmonary arterial smooth muscle cells. *J Appl Physiol* **102**, 390–398 (2007).

259. Rysä, J., Leskinen, H., Ilves, M. & Ruskoaho, H. Distinct Upregulation of Extracellular Matrix Genes in Transition From Hypertrophy to Hypertensive Heart Failure. *Hypertension* **45**, 927–933 (2005).

260. Teekakirikul, P. *et al.* Cardiac fibrosis in mice with hypertrophic cardiomyopathy is mediated by non-myocyte proliferation and requires Tgf-β. *J Clin Invest* **120**, 3520–3529 (2010).

261. Zhao, S. *et al.* Periostin expression is upregulated and associated with myocardial fibrosis in human failing hearts. *J Cardiol* **63**, 373–378 (2014).

262. Imoto, K., Okada, M. & Yamawaki, H. Periostin Mediates Right Ventricular Failure through Induction of Inducible Nitric Oxide Synthase Expression in Right Ventricular Fibroblasts from Monocrotaline-Induced Pulmonary Arterial Hypertensive Rats. *Int J Mol Sci* **20**, 62 (2018).

263. Nickel, A., Löffler, J. & Maack, C. Myocardial energetics in heart failure. *Basic Res Cardiol* **108**, 358 (2013).

264. Ristow, M. Unraveling the Truth About Antioxidants: Mitohormesis explains ROS-induced health benefits. *Nat Med* **20**, 709–711 (2014).

265. Kang, P. T. *et al.* Mitochondrial complex I in the post-ischemic heart: reperfusion-mediated oxidative injury and protein cysteine sulfonation. *J Mol Cell Cardiol* **121**, 190–204 (2018).

266. Perry, C. N. *et al.* Xenotransplantation of Mitochondrial Electron Transfer Enzyme, Ndi1, in Myocardial Reperfusion Injury. *Plos One* **6**, e16288 (2011).

267. Mentzer, R. M., Wider, J., Perry, C. N. & Gottlieb, R. A. Reduction of Infarct Size by the Therapeutic Protein TAT-Ndi1 In Vivo. *J Cardiovasc Pharm T* **19**, 315–320 (2014).

268. Johnson, J. M. *et al.* Targeted overexpression of catalase to mitochondria does not prevent cardioskeletal myopathy in Barth syndrome. *J Mol Cell Cardiol* **121**, 94–102 (2018).

269. Viscomi, C. *et al.* In Vivo Correction of COX Deficiency by Activation of the AMPK/PGC-1α Axis. *Cell Metab* **14**, 80–90 (2011).

270. Yin, H., Price, F. & Rudnicki, M. A. Satellite Cells and the Muscle Stem Cell Niche. *Physiol Rev* **93**, 23–67 (2013).

271. Olguin, H. C. & Olwin, B. B. Pax-7 up-regulation inhibits myogenesis and cell cycle progression in satellite cells: a potential mechanism for self-renewal. *Dev Biol* **275**, 375–388 (2004).

272. Zammit, P. S. *et al.* Muscle satellite cells adopt divergent fates: a mechanism for self-renewal? *J Cell Biology* **166**, 347–357 (2004).

273. Zammit, P. S. *et al.* Pax7 and myogenic progression in skeletal muscle satellite cells. *J Cell Sci* **119**, 1824–1832 (2006).

274. L'honoré, A. *et al.* Redox Regulation by Pitx2 and Pitx3 Is Critical for Fetal Myogenesis. *Dev Cell* **29**, 392–405 (2014).

275. Latella, L. & Puri, P. L. Redox or Death: Checking on Fetal Myogenesis. *Dev Cell* **29**, 373–374 (2014).

276. Lin, S.-C. & Hardie, D. G. AMPK: Sensing Glucose as well as Cellular Energy Status. *Cell Metab* **27**, 299–313 (2018).

277. Quirós, P. M., Mottis, A. & Auwerx, J. Mitonuclear communication in homeostasis and stress. *Nat Rev Mol Cell Bio* **17**, 213–226 (2016).

278. Rabinovitch, R. C. *et al.* AMPK Maintains Cellular Metabolic Homeostasis through Regulation of Mitochondrial Reactive Oxygen Species. *Cell Reports* **21**, 1–9 (2017).

279. Viscomi, C. *et al.* Combined treatment with oral metronidazole and N-acetylcysteine is effective in ethylmalonic encephalopathy. *Nat Med* **16**, 869–871 (2010).

280. Peralta, S. *et al.* Sustained AMPK activation improves muscle function in a mitochondrial myopathy mouse model by promoting muscle fiber regeneration. *Hum Mol Genet* **25**, 3178–3191 (2016).

281. Pugsley, H. R. Assessing Autophagic Flux by Measuring LC3, p62, and LAMP1 Co-localization Using Multispectral Imaging Flow Cytometry. *J Vis Exp Jove* 55637 (2017) doi:10.3791/55637.

282. Shpilka, T. & Haynes, C. M. The mitochondrial UPR: mechanisms, physiological functions and implications in ageing. *Nat Rev Mol Cell Bio* **19**, 109–120 (2017).

283. Fiorese, C. J. *et al.* The Transcription Factor ATF5 Mediates a Mammalian Mitochondrial UPR. *Curr Biol* **26**, 2037–2043 (2016).

284. Dogan, S. A. *et al.* Tissue-Specific Loss of DARS2 Activates Stress Responses Independently of Respiratory Chain Deficiency in the Heart. *Cell Metab* **19**, 458–469 (2014).

285. Kühl, I. *et al.* POLRMT regulates the switch between replication primer formation and gene expression of mammalian mtDNA. *Sci Adv* **2**, e1600963 (2016).

286. Khan, N. A. *et al.* mTORC1 Regulates Mitochondrial Integrated Stress Response and Mitochondrial Myopathy Progression. *Cell Metab* **26**, 419-428.e5 (2017).

287. Lehtonen, J. M. *et al.* FGF21 is a biomarker for mitochondrial translation and mtDNA maintenance disorders. *Neurology* **87**, 2290–2299 (2016).

288. Melber, A. & Haynes, C. M. UPRmt regulation and output: a stress response mediated by mitochondrial-nuclear communication. *Cell Res* **28**, 281–295 (2018).

289. Morita, M. *et al.* mTORC1 Controls Mitochondrial Activity and Biogenesis through 4E-BP-Dependent Translational Regulation. *Cell Metab* **18**, 698–711 (2013).

290. Reczek, C. R. & Chandel, N. S. ROS-dependent signal transduction. *Curr Opin Cell Biol* **33**, 8–13 (2015).

291. Trifunovic, A. *et al.* Premature ageing in mice expressing defective mitochondrial DNA polymerase. *Nature* **429**, 417–423 (2004).

292. Trifunovic, A. *et al.* Somatic mtDNA mutations cause aging phenotypes without affecting reactive oxygen species production. *P Natl Acad Sci Usa* **102**, 17993–17998 (2005).

293. Hämäläinen, R. H. *et al.* mtDNA Mutagenesis Disrupts Pluripotent Stem Cell Function by Altering Redox Signaling. *Cell Reports* **11**, 1614–1624 (2015).

294. Shao, D. *et al.* A Redox-Dependent Mechanism for Regulation of AMPK Activation by Thioredoxin1 during Energy Starvation. *Cell Metab* **19**, 232–245 (2014).

295. Scialò, F. *et al.* Mitochondrial ROS Produced via Reverse Electron Transport Extend Animal Lifespan. *Cell Metab* **23**, 725–734 (2016).

7 Publikationen

7.1 M. Szibor *et al.*, *Dis Model Mech*. **10**, 163–171 (2017)

© 2017. Published by The Company of Biologists Ltd | Disease Models & Mechanisms (2017) 10, 163-171 doi:10.1242/dmm.027839

RESEARCH ARTICLE

Broad AOX expression in a genetically tractable mouse model does not disturb normal physiology

Marten Szibor[1,2,3,*], Praveen K. Dhandapani[1,2,*], Eric Dufour[2], Kira M. Holmström[1,2], Yuan Zhuang[1], Isabelle Salwig[3], Ilka Wittig[4,5,6], Juliana Heidler[4], Zemfira Gizatullina[7], Timur Gainutdinov[7], German Mouse Clinic Consortium[§], Helmut Fuchs[8], Valérie Gailus-Durner[8], Martin Hrabě de Angelis[8,9,10], Jatin Nandania[11], Vidya Velagapudi[11], Astrid Wietelmann[3], Pierre Rustin[12], Frank N. Gellerich[7,13], Howard T. Jacobs[1,2,‡,¶] and Thomas Braun[3,‡]

ABSTRACT

Plants and many lower organisms, but not mammals, express alternative oxidases (AOXs) that branch the mitochondrial respiratory chain, transferring electrons directly from ubiquinol to oxygen without proton pumping. Thus, they maintain electron flow under conditions when the classical respiratory chain is impaired, limiting excess production of oxygen radicals and supporting redox and metabolic homeostasis. AOX from *Ciona intestinalis* has been used to study and mitigate mitochondrial impairments in mammalian cell lines, *Drosophila* disease models and, most recently, in the mouse, where multiple lentivector-AOX transgenes conferred substantial expression in specific tissues. Here, we describe a genetically tractable mouse model in which *Ciona* AOX has been targeted to the *Rosa26* locus for ubiquitous expression. The *AOX*^{Rosa26} mouse exhibited only subtle phenotypic effects on respiratory complex formation, oxygen consumption or the global metabolome, and showed an essentially normal physiology. AOX conferred robust resistance to inhibitors of the respiratory chain *in organello*; moreover, animals exposed to a systemically applied LD50 dose of cyanide did not succumb. The *AOX*^{Rosa26} mouse is a useful tool to investigate respiratory control mechanisms and to decipher mitochondrial disease aetiology *in vivo*.

KEY WORDS: Mitochondria, Mitochondrial disease, Respiratory chain, Alternative oxidase

[1]Institute of Biotechnology, FI-00014 University of Helsinki, Finland. [2]BioMediTech and Tampere University Hospital, FI-33014 University of Tampere, Finland. [3]Max Planck Institute for Heart and Lung Research, Cardiac Development and Remodelling (Department I), Bad Nauheim D-61231, Germany. [4]Functional Proteomics, SFB 815 Core Unit, Faculty of Medicine, Goethe-University, Frankfurt am Main D-60590, Germany. [5]German Center of Cardiovascular Research (DZHK), Partner site RheinMain, Frankfurt, Germany. [6]Cluster of Excellence "Macromolecular Complexes", Goethe-University, Frankfurt am Main D-60590, Germany. [7]Leibniz Institute for Neurobiology, Magdeburg D-39118, Germany. [8]German Mouse Clinic, Institute of Experimental Genetics, Helmholtz Zentrum München, German Research Center for Environmental Health GmbH, Ingolstaedter Landstrasse 1, Neuherberg 85764, Germany. [9]Chair of Experimental Genetics, Center of Life and Food Sciences Weihenstephan, TU Munich, Emil-Erlenmeyer-Forum 2, Freising-Weihenstephan 85350, Germany. [10]Member of German Center for Diabetes Research (DZD), Ingolstaedter Landstrasse 1, Neuherberg 85764, Germany. [11]Institute for Molecular Medicine Finland, FI-00014 University of Helsinki, Finland. [12]INSERM UMR 1141 and Université Paris 7, Hôpital Robert Debré, Paris 75019, France. [13]Department of Neurology, Otto-von-Guericke-University, Magdeburg D-39120, Germany.
*These authors contributed equally to this work.
‡These authors share senior authorship.
§A full list of consortium members appears in Supplementary information

¶Author for correspondence (howard.jacobs@helsinki.fi)

T.G., 0000-0003-1723-1780; H.T.J., 0000-0003-1895-6003

Received 14 September 2016; Accepted 30 November 2016

INTRODUCTION

The mitochondrial system for oxidative phosphorylation (OXPHOS) comprises four multisubunit complexes supporting stepwise respiratory electron flow from primary electron acceptors to oxygen, and a fifth complex (ATP synthase) that uses the proton gradient thereby generated across the inner mitochondrial membrane to synthesize ATP. In many lower organism and plants, alternative oxidases (AOXs) are expressed that branch the mitochondrial respiratory chain, thus transferring electrons directly from ubiquinol to oxygen in a non-proton-motive manner. AOXs are absent in mammals (Young et al., 2013) (Fig. 1A). Their main physiological role is to maintain electron flow under conditions when the classical respiratory chain is impaired, limiting excess production of oxygen radicals and supporting redox and metabolic homeostasis. Because AOX is also found in some invertebrate phyla (McDonald et al., 2009), we have proposed that its expression in commonly studied animal models could be used to elucidate the pathophysiology underlying mitochondrial OXPHOS disorders, providing a rational basis for its eventual implementation in therapeutic applications (Rustin and Jacobs, 2009; El-Khoury et al., 2014).

In earlier studies, AOX from the tunicate *Ciona intestinalis*, a sister group to the vertebrates, was shown to be expressible and catalytically active in human cells (Hakkaart et al., 2006). It was found to alleviate the deleterious consequences of toxic or pathological inhibition of the downstream portion of the mitochondrial respiratory chain (Hakkaart et al., 2006; Dassa et al., 2009), specifically OXPHOS complexes III (cIII) and IV (cIV), which AOX bypasses. A cDNA encoding *Ciona* AOX was subsequently shown to be ubiquitously expressible in *Drosophila*, without eliciting any harmful phenotypic effects (Fernandez-Ayala et al., 2009). In the fly, AOX expression was able to compensate a range of pathological phenotypes at the whole-organism level, including lethality caused by OXPHOS poisons such as antimycin A or cyanide (Fernandez-Ayala et al., 2009), locomotor disturbance or neurodegeneration caused by cIV knockdown (Kemppainen et al., 2014) or other causes of neurodegeneration mimicking Parkinson's (Fernandez-Ayala et al., 2009; Humphrey et al., 2012) or Alzheimer's (El-Khoury et al., 2016) diseases.

The potential for using AOX to study mitochondrial pathophysiology at the whole-organism level in mammals has been demonstrated using lentivector transduction, creating a transgenic mouse expressing *Ciona* AOX in multiple tissues (El-Khoury et al., 2013). Notably, harmful phenotypes were again not seen, despite widespread transgene expression. However, the methodological issues arising from the nature of that model have precluded its widespread use. On insertion of AOX transgenes at multiple genomic sites in the model, none of them individually conferred expression at a high level or in all tissues. Thus, the model could not be combined

Disease Models & Mechanisms (2017) 10, 163-171 doi:10.1242/dmm.027839

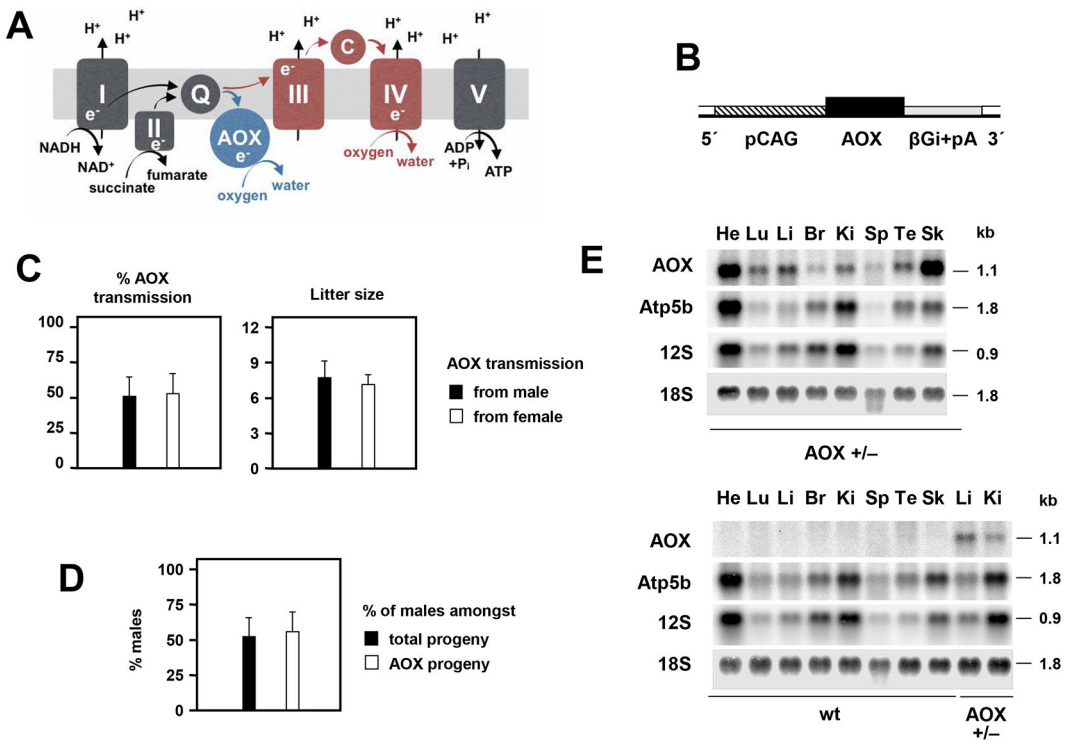

Fig. 1. Construction and characterization of *AOX*^{Rosa26} mice. (A) Schematic diagram of the mitochondrial OXPHOS system, showing the five standard OXPHOS complexes (I-V), the diffusible electron carriers ubiquinone (Q) and cytochrome c (c), and the passage of electrons and protons resulting ultimately in the synthesis of ATP from ADP and inorganic phosphate (Pi). The additional presence of AOX, whether supplied transgenically or in organisms naturally endowed with it, provides an alternative route for the reoxidation of ubiquinol by molecular oxygen, without proton pumping. (B) Schematic diagram of inserted Rosa26-AOX expression construct, following removal of additional elements (i.e. DTA negative selectable marker upon targeted integration, and neomycin resistance cassette following FRT-mediated excision *in vivo*). Remaining elements are the CAG promoter, AOX coding sequence and β-globin intron and poly(A) addition signal (βGi+pA). For full details see Fig. S1A. (C) Transmission rate of *AOX* transgenes (based on PCR) and litter sizes, according to sex of *AOX*-hemizygous parent. Transmission rates from male (n=93, 12 crosses) and from female (n=43, 6 crosses) were not significantly different from each other (Student's t-test, P>0.05, mean±s.d.) or from Mendelian expectation of 50% (chi-squared test). Litter sizes produced by *AOX*-hemizygous males and females also showed no significant difference (Student's t-test, P>0.05). (D) Sex (% of males) of transgenic and wild-type progeny of hemizygous *AOX*^{Rosa26} mice (n=136, 18 crosses), again showing no significant differences (Student's t-test, P>0.05, mean±s.d.). (E) Northern blot showing *AOX* expression in RNA (10 μg) from tissues of one-year-old, male, hemizygous *AOX*^{Rosa26} mice and wild-type (wt) littermate controls: He, heart; Lu, lung; Li, liver; Br, brain; Ki, kidney; Sp, spleen; Te, testis; Sk, skeletal muscle. The blot was reprobed for *Atp5b* mRNA as well as mitochondrial 12S and cytosolic 18S rRNAs as loading controls. RNA molecular weights were extrapolated from rRNA migration in the ethidium bromide-stained gel.

with genetic disease models or other mouse mutants, could not be practically transferred into other strain backgrounds, and its long-term maintenance was essentially impossible.

Here, we report the creation of a genetically tractable transgenic mouse that ubiquitously expresses a single copy of *Ciona* AOX at substantial levels, after targeted insertion into the *Rosa26* locus. The *Rosa26* knock-in gave rise to a functional enzyme, which conferred resistance to respiratory poisons. Surprisingly, comprehensive phenotyping revealed only minor, biologically inconsequential effects of AOX expression in the *AOX*^{Rosa26} mouse. The new model offers great promise as a tool for elucidating the mechanisms of mitochondrial pathology and charting the way towards future therapies.

RESULTS

Construction of *AOX*^{Rosa26} mice

To create a genetically tractable mouse model ubiquitously expressing *Ciona* AOX, we used gene targeting into the ubiquitously active *Rosa26* locus (Hitoshi et al., 1991) in mouse embryonic stem cells (ESC) (Soriano, 1999; Srinivas et al., 2001). Previous authors have reported no detectable pathological alterations arising from insertions at this locus (Friedrich and Soriano, 1991; Zambrowicz et al., 1997), and transgene expression seems to be stable (Zambrowicz et al., 1997). To boost expression from the *Rosa26* locus, we incorporated the synthetic CAG enhancer-promoter into the construct (Fig. 1B; Fig. S1), which enhances expression several-fold (Nyabi et al., 2009; Chen et al., 2011). After verification of the insertion in ESCs by Southern blotting (Fig. S1B,C), a chimeric line was established via blastocyst injection, with subsequent elimination of the positive-selectable (neomycin resistance) cassette (Fig. S1A,B) by Flp recombination *in vivo*, following germ-line transmission. Founders were backcrossed over more than seven generations to strain C57Bl/6J, with transgene presence checked at each step by PCR (Fig. S1D). The rate of transmission of the *AOX* transgene from heterozygous parents of either sex did not significantly deviate from 50% (Fig. 1C), nor was there any significant parent-of-origin effect on litter size (Fig. 1C). The progeny sex ratio was also unaffected by the *AOX* transgene (Fig. 1D).

AOX is ubiquitously expressed in the *AOX*^{Rosa26} mouse

Northern blotting (Fig. 1E) confirmed widespread, though somewhat uneven, expression with highest *AOX* mRNA levels in heart and skeletal muscle, but lower expression in brain, taking account of the

Disease Models & Mechanisms (2017) 10, 163-171 doi:10.1242/dmm.027839

loading controls. At the protein level, expression seemed more uniform, but was again highest in heart, skeletal muscle and pancreas, and lowest in brain (Fig. 2A; Fig. S2). Brain expression was highest in newborn mice (Fig. S2C), but declined substantially by one month of age (Fig. S2C). As expected, AOX expression was higher in homozygotes compared with heterozygous animals (Fig. S2D). The enzyme was found to be associated with the membrane fraction of isolated mitochondria after carbonate extraction (Fig. S2E), albeit less tightly bound than some integral membrane proteins of the OXPHOS complexes, such as subunit 1 of cIV (Mtco1).

In each tissue tested, the expression of representative subunits of the five OXPHOS complexes was essentially unaffected by AOX expression (Fig. 2A; Fig. S2A). Moreover, the overall structure of the respiratory membrane, specifically its organization into supercomplexes, was similarly unaltered, based on blue-native electrophoresis (BNE) followed by in-gel histochemistry of heart mitochondria (Fig. 2B), and on BNE combined with western blots for OXPHOS subunits, for eight different tissues (Fig. S2F). In BNE gels, AOX itself migrated mainly at the size of a dimer and as multimers thereof (Fig. S2F,G), rather than associating specifically with any other respiratory complex. In each tissue tested, the mobility of the respiratory chain complexes detected by BNE was identical to that in controls (Fig. S2F). Principal component analysis of metabolite levels in skeletal muscle (Fig. 2C) and heart (Fig. S2H) showed no consistent effect of AOX expression, nor did any of 100 individual metabolites analyzed show any significant difference (Tables S1, S2).

AOX is functional in *AOX*^{Rosa26} mice

We conducted respirometry to determine whether AOX is enzymatically functional in the *AOX*^{Rosa26} knock-in mice. Mitochondria from six tissues (Fig. 3) were tested in a standard protocol for oxygen consumption in the presence of complex I-, II- and IV-linked substrates, successively using inhibitors of cI (rotenone), cIII (antimycin A), AOX (n-propyl gallate) and cIV (cyanide or azide). There were no significant differences when oxygen consumption was compared with that from mitochondria of wild-type littermates, except for substrate oxidation in the presence of antimycin A (i.e. mediated by AOX), which was significant for all tissues tested except brain, where expression was low. Mitochondria from tissues of *AOX*^{Rosa26} mice other than brain showed antimycin A-resistant (AOX-dependent) oxygen consumption between 30% and 70% of the uninhibited level driven by succinate (Fig. 3A), similar also to preliminary measurements in the founder mouse (Fig. S3A). In heart mitochondria from AOX-expressing compared with control mice, antimycin A- and azide-resistant substrate oxidation was evident across a wide range of drug concentrations (Fig. S3B). Compared with littermate controls, mitochondrial ROS production driven by succinate was greatly decreased (Fig. 3B). Interestingly, this was only significant in the absence of rotenone, implicating AOX in providing

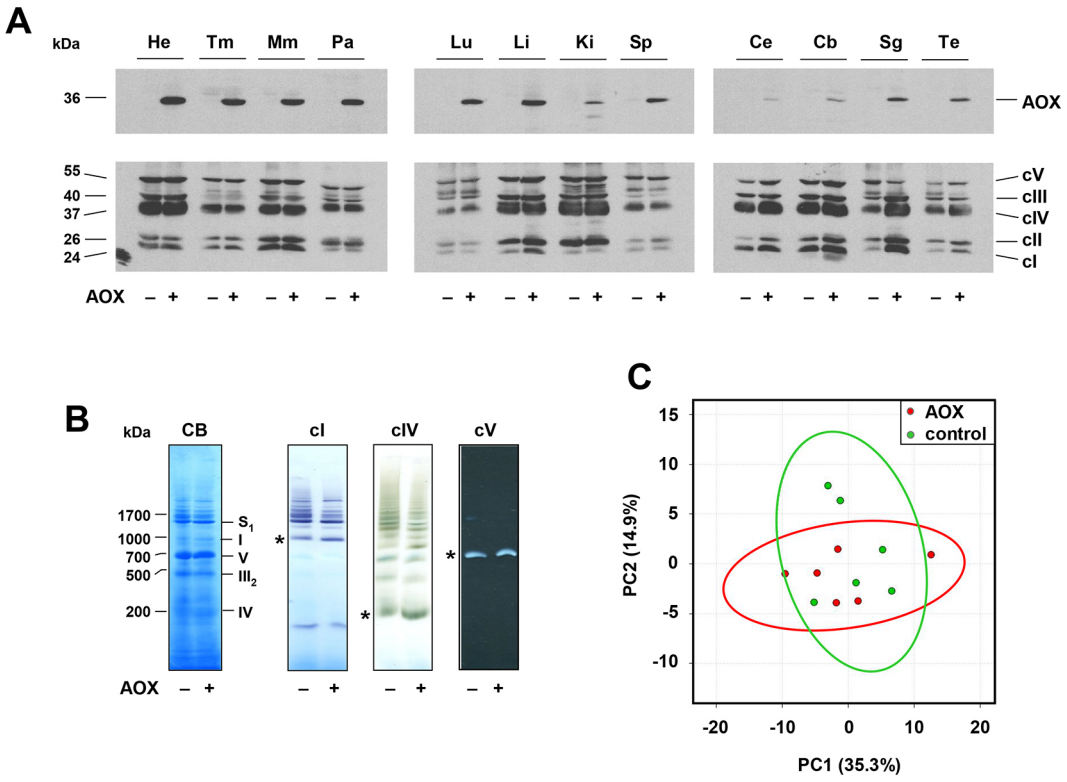

Fig. 2. *AOX*^{Rosa26} mice show broad AOX expression and normal metabolism. (A) Western blots of 20 µg total protein extracts from the indicated tissues (He, heart; Tm, thigh muscle; Mm, masseter muscle; Pa, pancreas; Lu, lung; Li, liver; Ki, kidney; Sp, spleen; Ce, cerebrum; Cb, cerebellum; Sg, salivary gland; Te, testis) of 54-week-old male hemizygous *AOX*^{Rosa26} (+) and wild-type littermate control (–) mice, probed for AOX and for representative subunits of the five OXPHOS complexes (see Materials and Methods, protein molecular weights extrapolated from markers). For Ponceau S staining of the membranes see Fig. S2B. See also Fig. S2A,C,D. (B) BNE gels of mitochondrial membrane proteins from hemizygous *AOX*^{Rosa26} (+) and wild-type littermate control (–) mice, stained with Coomassie Blue (CB) or probed by in-gel histochemistry for the indicated OXPHOS complexes. * denotes the migration of the respective monomeric complexes. Assignment of mitochondrial complexes (I, cI; III_2, dimeric cIII; IV, cIV; V, cV; S_1, respiratory supercomplexes containing cI, dimeric cIII and one copy of cIV) is based on protein molecular weights extrapolated from the migration of the complexes from bovine heart mitochondria, whose subunit composition is known. (C) Principal component analysis of metabolome data from skeletal muscle of hemizygous *AOX*^{Rosa26} (red circles) and wild-type littermate control mice (green circles). The two sets of analysed data overlap, apart from two minor outliers from the control group. See also Fig. S2H.

Disease Models & Mechanisms (2017) 10, 163-171 doi:10.1242/dmm.027839

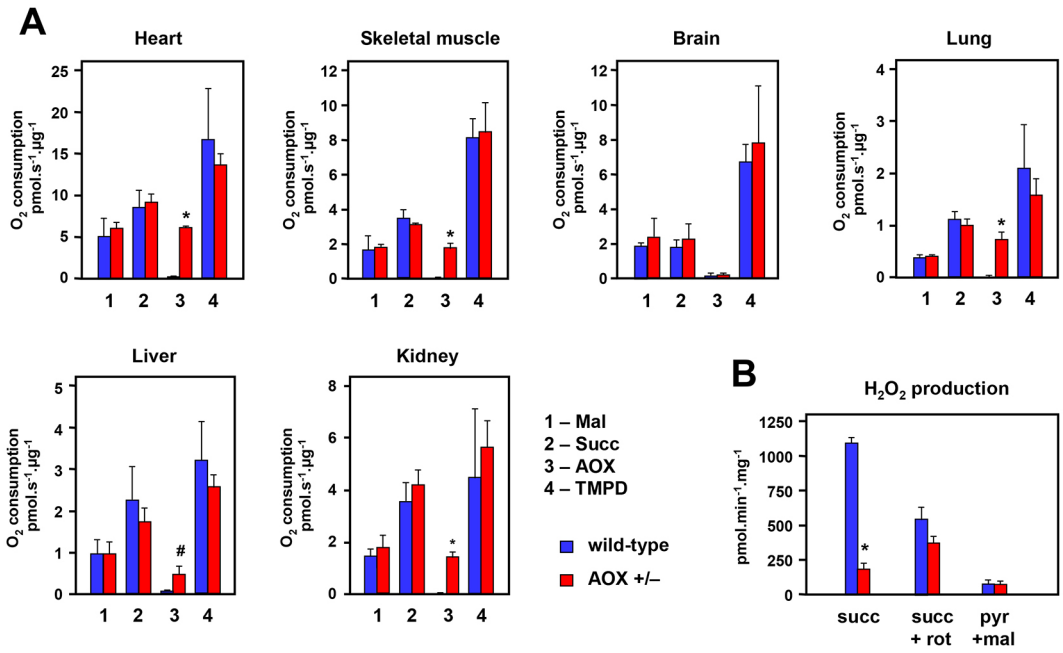

Fig. 3. AOX is enzymatically functional in mitochondria from *AOX*^{Rosa26} mice. (A) Respirometry (oxygen consumption in the indicated units) from isolated mitochondria prepared from the indicated tissues of hemizygous *AOX*^{Rosa26} mice and wild-type littermate controls, as shown; means±s.d. of three biological replicates in each case. Note the different scales. 1 (Mal) – rotenone-sensitive oxidation of malate in the presence of glutamate, pyruvate and ADP; 2 (Succ) – antimycin A- plus n-propyl gallate-sensitive succinate oxidation; 3 (AOX) – rate of n-propyl gallate-sensitive, antimycin A-insensitive succinate oxidation; 4 (TMPD) – rate of ascorbate-reduced TMPD oxidation. For further details see Materials and Methods. See Fig. S3C for respiratory control ratio in these samples. (B) ROS production, measured as H_2O_2 output, from heart mitochondria of *AOX*^{Rosa26} mice and wild-type littermates, as indicated, driven by the indicated substrates or inhibitors (succ, succinate; rot, rotenone; pyr, pyruvate; mal, malate). $^{\#}P<0.05$ or $^{*}P<0.001$ between given pairs of control and *AOX*^{Rosa26} values, Student's *t*-test, means±s.d. Note that it is not possible to verify that this effect depends on the enzymatic activity of AOX, because the AOX inhibitor, n-propyl gallate, is itself a potent antioxidant.

an alternative pathway for succinate oxidation other than reverse electron transport through cI.

AOX^{Rosa26} mice exhibit normal physiology

The high level of AOX expression, capable of replacing a large fraction of electron flow when cIII/IV is inhibited, raised the question of potentially deleterious consequences under normal physiological conditions. Surprisingly, *AOX*^{Rosa26} mice of both sexes were similar in size to littermate controls and gained weight normally during development (Fig. 4A). Muscle and heart functions showed no significant differences from littermate controls, based on standard assays of grip strength (Fig. 4B), treadmill performance (Fig. 4B), cardiac ejection fraction (Fig. 4C) and left ventricular mass (LVM; Fig. 4C), conducted on mice of different ages. To complement these data we implemented a comprehensive phenotyping, using the resources of the German Mouse Clinic (https://www.mouseclinic.de, search 'phenomap'; hereafter referred to as 'GMC Phenomap'). This analysis covered metabolic, behavioural, morphological, immunological, cardiac and neurological parameters, amongst others. None of the parameters tested showed substantial or systematic deviations from littermate controls.

AOX confers protection against an LD50 dose of systemically delivered cyanide

Despite the absence of any meaningful phenotype under standard (non-stressful) physiological conditions, we reasoned that the ubiquitous expression (Fig. 2) of functional AOX (Fig. 3) should confer whole-organism resistance to a respiratory poison targeting cIII or cIV. Sample cohorts of female mice were thus tested for their response to systemically administered potassium cyanide at ∼LD50 (Yamamoto, 1995), with evaluation of survival after 1, 24 and 48 h. All five *AOX*^{Rosa26} transgenic mice tested survived the treatment, whereas three of six littermate controls succumbed as expected (Fig. 5). Although the sample sizes are small, hence indicative rather than definitive, the result is consistent with protection against cyanide at the whole-organism level.

DISCUSSION

In this study we successfully engineered mice for stable, ubiquitous expression of *Ciona* AOX, via a single-copy insertion into the *Rosa26* locus, controlled by the synthetic CAG promoter. AOX protein was widely expressed and enzymatically functional when tested in the presence of antimycin A *in organello*. AOX expression produced negligible phenotypic effects under standard physiological conditions, but seemed able to protect mice from the lethal effects of injected cyanide. The *AOX*^{Rosa26} mouse provides a genetically tractable tool for analyzing the pathophysiology of a wide spectrum of diseases proposed to be linked to mitochondrial respiratory dysfunction.

The *AOX*^{Rosa26} mouse is a genetically tractable model

The 'MitAOX' transgenic mice, previously generated by lentivector transduction (El-Khoury et al., 2013), provided a preliminary indication that widespread *Ciona* AOX expression in the mouse is not harmful. However, owing to the multi-copy nature of the inserted transgene at different genomic sites, as well as varying expression levels, MitAOX mice were not suitable for studies using genetic disease models. To avoid these problems, we created a revised model containing a single insertion of *AOX* cDNA at the *Rosa26* locus on chromosome 6. We demonstrated (Fig. 1) that the

Disease Models & Mechanisms (2017) 10, 163-171 doi:10.1242/dmm.027839

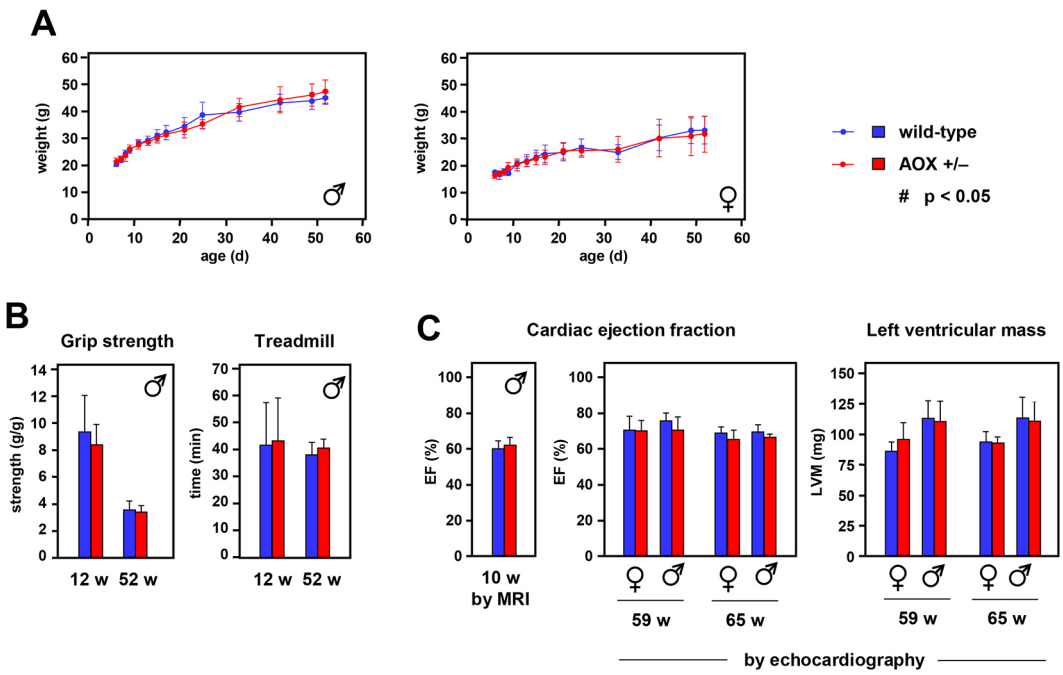

Fig. 4. *AOX*^{Rosa26} mice exhibit normal physiology. (A) Mean weight±s.d. of hemizygous *AOX*^{Rosa26} and wild-type littermate control mice of the sexes indicated, during post-natal development, $n \geq 8$ for each sex and genotype analysed. (B) Muscle parameters of male hemizygous *AOX*^{Rosa26} and wild-type littermate control mice of the ages indicated; means±s.d. For each group analysed $n \geq 4$ (grip strength) or $n \geq 6$ (treadmill). (C) Cardiac parameters, as indicated, of hemizygous *AOX*^{Rosa26} and wild-type littermate control mice of the sex and ages indicated; means±s.d., $n \geq 4$ for each group analysed. All data obtained by echocardiography except ejection fraction at 10 w of age, which used MRI, $n \geq 5$. There were no significant differences between *AOX*^{Rosa26} and wild-type values for any parameter measured (Student's *t*-test, $P > 0.05$).

introduced AOX gene is stably transmitted in a Mendelian manner, remains active beyond at least seven generations of backcrossing to strain C57Bl/6J, shows no parent-of-origin or sex-specific lethality, and is widely expressed. The AOX transgene can, in principle, be transferred to any desired strain background suitable for combination with a given genetic model of disease, although our current analysis was confined to the C57Bl/6J genetic background. We expect that the *AOX*^{Rosa26} mouse will become a versatile model for studying the nature of mitochondrial involvement in disease-like phenotypes.

AOX seems inert under standard physiological conditions

Although AOX was enzymatically functional in the presence of antimycin A *in organello*, our data indicate that the metazoan enzyme is functionally inert under standard physiological conditions, as suggested previously (Hakkaart et al., 2006; Fernandez-Ayala et al., 2009; El-Khoury et al., 2013). Several lines of evidence support this conclusion: (1) any substantial contribution by the non-proton-motive AOX to respiratory electron flow should manifest in a significantly decreased respiratory control ratio in respirometric measurements *in organello*. However, we did not observe any significant alteration in our tissue survey at least for cI-linked substrates and within the detection limits of the method applied (Fig. S3C). (2) Inefficient mobilization of nutritional resources by AOX-expressing mice should alter metabolic parameters *in vivo*. However, there were no differences in whole body weight (Fig. 4A), fat or lean body mass determined by nuclear magnetic resonance (NMR) (see GMC Phenomap), or physiological parameters determined by indirect calorimetry, including food intake, body temperature, oxygen/CO_2 exchange or activity (see GMC Phenomap). (3) No significant differences in heart performance were detected by electro- or echocardiography, or MRI (Fig. 4C; GMC Phenomap), although the heart is the most energy-demanding tissue and showed the highest AOX expression.

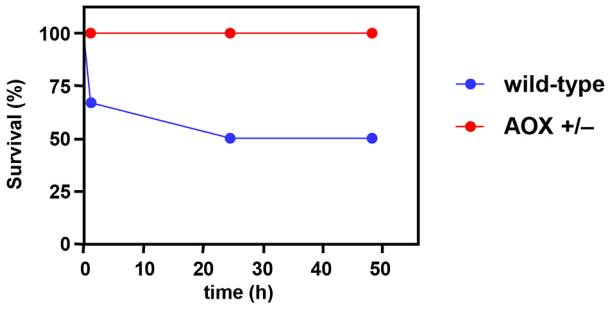

Fig. 5. Sampled *AOX*^{Rosa26} mice are protected against cyanide toxicity *in vivo*. Survival curves of samples of hemizygous female *AOX*^{Rosa26} mice (n=5) and wild-type controls (n=6) treated systemically with KCN as described in Materials and Methods. Note that the experiment would need to be conducted on a much greater scale to generate fully reliable statistics, but is precluded by ethical considerations.

Low AOX expression in brain

The relatively low expression of the *AOX* transgene in adult brain (Fig. 1E, Fig. 2A, Fig. S2A,D) is somewhat puzzling, given previous reports. The CAG promoter has previously been used to drive transgene expression at a high level in the mouse brain during development (Liu et al., 2014) as well as in the adult (Ida-Hosonuma et al., 2002; Kim et al., 2013), and the *Rosa26* locus efficiently drives expression in the brain (Banares et al., 2005; Hitz et al., 2007; Delaunay et al., 2009). Moreover, we also achieved substantial expression in the brains of MitAOX transgenic mice (El-Khoury et al., 2013), using the same CAG promoter.

Disease Models & Mechanisms (2017) 10, 163-171 doi:10.1242/dmm.027839

Intriguingly, neonatal *AOX*^{Rosa26} brains expressed substantially more AOX at the protein level than adults (Fig. S2C), indicating that the transgene can be active, but apparently regulated, in neural cells. At present we do not have a convincing explanation for these anomalies. However, the relatively low expression of AOX in the adult brain seemed sufficient to protect against the lethality of systemically delivered cyanide (Fig. 5), which can cross the blood-brain barrier and has major toxic effects in the central nervous system (Yamamoto and Tang, 1996; Reiter et al., 2010; Zhang et al., 2015). It will be interesting to explore in greater depth the specific physiological effects of this dose of cyanide and how these effects are modified by AOX expression.

Lack of metabolic disturbance resulting from AOX expression

The lack of any discernible, deleterious phenotype at the whole-organism level arising from AOX expression (Fig. 4; supplementary Data), mirrors the lack of biochemical disturbance in the *AOX*^{Rosa26} mouse. This was the case even in heart (Fig. 2A,B) and skeletal muscle (Fig. 2A) tissues showing high levels of AOX expression. The highly proteinaceous inner mitochondrial membrane is organized into different subcompartments with distinct structures, protein composition and biochemical functions (Vogel et al., 2006). In particular, the supramolecular organization of the OXPHOS system in supercomplexes is generally considered to maximize the efficiency of electron flow (Acín-Pérez et al., 2008; Chaban et al., 2014). We observed no structural (Fig. 2B) or functional (Fig. 3A) disturbance of the endogenous respiratory membrane upon AOX expression, which might reflect natural properties of *Ciona* AOX, enabling it to reside in the mitochondria of its parent species. Transgenic AOX seems to form homomeric complexes, rather than associating with (and potentially disrupting) other OXPHOS complexes. The electrophoretic mobility of the standard OXPHOS complexes was indistinguishable from that in controls, in all tissues tested (Fig. 2B; Fig. S2F,G). Our findings imply that these multimers are themselves benign, although it remains unknown whether AOX is structurally arrayed in a similar manner in its natural context in *Ciona*. We reason that, by remaining uncomplexed with other respiratory chain components, the enzyme would be functionally adapted to act as a sink for electrons transferred from diffusible quinols in the inner mitochondrial membrane. Quinone reduction might arise from the operation of diverse dehydrogenases, including, for example, cII, electron transferring flavoprotein dehydrogenase, the mitochondrial isoform of glycerol-3-phosphate dehydrogenase and dihydroorotate dehydrogenase. Under normal physiological conditions, diffusible quinols would be efficiently mopped up by (dimeric) cIII, whether alone or attached to cIV as a supercomplex. As in plants (Hoefnagel and Wiskich, 1998; Castro-Guerrero et al., 2004), AOX would only become active at high quinol concentrations, reflecting its lower affinity for quinols than cIII. Thus, AOX would be brought into play only when quinols accumulate as a result of inhibition or overload of the standard respiratory pathway, as inferred previously in human cells (Dassa et al., 2009). This hypothesis is also consistent with our observation that AOX expression drastically decreases mitochondrial ROS production by heart mitochondria in the presence of high levels of succinate (Fig. 3B), which promotes reverse electron flow through cI (Chouchani et al., 2014). Our observations suggest that AOX might have dramatic consequences under stress, especially in heart and other tissues where it is highly expressed. Tests of this hypothesis will also reveal whether AOX could have beneficial roles in future therapies (El-Khoury et al., 2014). A first demonstration of the utility of *AOX*^{Rosa26} mice has recently been published (Mills et al., 2016), in which AOX was shown to confer resistance against lethality in models of bacterial sepsis. Further trials, combining *AOX*^{Rosa26} with specific genetic disease models, should reveal the extent to which AOX can alleviate the pathophysiology of respiratory chain dysfunction. The *AOX*^{Rosa26} mouse model should have wide applications and is available for the research community, upon request.

MATERIALS AND METHODS

Construction of targeting vector

Standard cloning and recombineering procedures (Liu et al., 2003; Warming et al., 2005) were used to assemble the pRosa26-Aox targeting vector. Briefly, PL451 was adapted to serve as AOX entry vector, by integrating homology arms for the mouse *Rosa26* locus (PL451-Rosa26) upstream and downstream of the neomycin selection cassette. *Ciona* AOX (Hakkaart et al., 2006) was integrated upstream of the selection cassette, and used to co-transform recombineering-competent *Escherichia coli* (EL250) with a *Rosa26*-targeting plasmid (pRosa26-DTA). Positive clones were selected by kanamycin resistance (pRosa26-Aox), verified by PCR and sequencing, and electroporated into v6.5 ESCs following linearization with *Sal*I. After negative (DTA, Diptheria toxin A) and positive (G418) selection, homologous integration was verified by Southern blotting (Koetsier et al., 1993) using gene-specific restriction enzymes and probes to distinguish the wild-type and manipulated alleles (see supplementary Materials and Methods and Fig. S1B,C for further details).

Creation of transgenic mice

ESC clones positive for integration were injected into blastocysts and transferred to pseudopregnant mice. Chimeric males were then backcrossed onto the C57Bl/6J strain background to generate heterozygous animals, and subsequently bred with mice ubiquitously expressing FLP recombinase (Rodríguez et al., 2000), in order to delete the neomycin selection cassette. Mice were backcrossed (>7 generations) to C57Bl/6J females to obtain a clean genetic background for all subsequent studies.

PCR genotyping of *AOX*^{Rosa26} mice

Crude DNA for genotyping was extracted from ear punches or tail cuts by standard methods (proteinase K treatment, isopropanol precipitation and overnight resuspension in TE at 56°C). Multiplex PCR genotyping was carried out using primers Aox 317 s: 5′-GCGATGCAAGATGGAGGGTA-3′ plus Aox 317 as: 5′-TGAATCCAACCGTGGTCTCG-3′ for *AOX*, and Rosa26_wt s: 5′-GACCTCCATCGCGCACTCCG-3′ plus Rosa26_wt as: 5′-CTCCGAGGCGGATCACAAGC-3′ for the wild-type *Rosa26* locus, giving respective products of 317 and 523 bp. PCR reactions of 20 µl contained 4 pmol of each primer, DMSO at 2% and 0.2 µl DyNazyme II (Thermo Fisher Scientific), with cycle parameters of initial denaturation at 95°C for 5 min, then 39 cycles of denaturation at 95°C for 20 s, annealing at 56°C for 30 s and extension at 72°C for 60 s, with final extension step at 72°C for 10 min, followed by 1.5% agarose gel electrophoresis. See Fig. S1D for example gel.

RNA analysis

RNA was prepared from dissected mouse tissues by bead homogenization in 700 µl (>10 volumes) of Trizol reagent (Sigma). After incubation for 5 min at room temperature, samples were gently extracted with 0.2 volumes of chloroform and centrifuged at 12,000 $\boldsymbol{g}_{max}$ for 15 min at 4°C. The upper (aqueous) phase was decanted and RNA recovered by isopropanol precipitation and centrifugation. Using standard procedures (Sambrook et al., 1989), air-dried RNA pellets were resuspended in 20 µl RNase-free water, fractionated on formaldehyde-agarose gels, blotted to Hybond-N+ membrane (GE Healthcare) in 10×SSC and hybridized to end-labelled DNA oligonucleotide probes for *AOX*, mitochondrial 12S and cytosolic 18S rRNA, and *Atp5b* mRNA, respectively 5′-CTTGACCCACTGTTTCTCA-TCTAGCCG-3′, 5′-CATGGGCTACACCTTGACCT-3′, 5′-TCGAACCC-TGATTCCCCGTCACCC-3′ and 5′-GGTGAATATGACCATCTCCCAG-AACAAGC-3′.

Disease Models & Mechanisms (2017) 10, 163-171 doi:10.1242/dmm.027839

Protein analysis

For protein extraction, small pieces of fresh or frozen tissue from dissected organs were placed in 500 µl of lysis buffer (50 mM Tris/HCl, 150 mM NaCl, 1 mM EDTA, 1% Triton X-100, pH 7.4), containing a dissolved protease inhibitor cocktail tablet (Pierce), in a 5 ml tube on ice. After homogenization using a POLYTRON PT 1200 E Manual Disperser (Ecoline), samples were incubated on ice for 30 min followed by centrifugation at 14,000 g_{max} for 5 min at 4°C. Supernatants were saved and protein concentration was measured using Bradford reagent (Bio-Rad) before dilution into SDS-PAGE sample buffer for electrophoresis on SDS 12% polyacrylamide gels. After semi-dry transfer to PROTRAN nitrocellulose membranes (PerkinElmer), western blots were probed using primary antibodies for AOX [customized rabbit antibody, 21st Century Biochemicals (Fernandez-Ayala et al., 2009), 1:40,000 in Tris-buffered saline (TBST) containing 5% BSA] with secondary antibody peroxidase-conjugated AffiniPure goat anti-rabbit IgG (Jackson ImmunoResearch, 111-035-144, 1:20,000). After stripping by two 20 min washes with 100 mM β-mercaptoethanol, 2% SDS, 62.5 mM Tris-HCl (pH 6.7), each followed by blocking with TBST containing 5% milk for 30 min, blots were reprobed for representative subunits of the OXPHOS complexes, using Total OXPHOS Cocktail antibody [Abcam, ab110413, 1:250; visualizing Sdhb (cII), Uqcrc2 (cIII), Mtco1 (cIV) and Atp5a (cV)], plus an antibody against complex 1 subunit Ndufs3 (Mitosciences, ab14711, 1:4000), both detected with peroxidase-conjugated AffiniPure goat anti-mouse IgG (Jackson ImmunoResearch, 115-035-146, 1:1000) as secondary antibody. Chemiluminescent detection used 20× LumiGLO Reagent and 20× Peroxide from Cell Signaling Technology, according to manufacturer's recommendations. Enrichment of mitochondrial membranes, solubilisation of mitochondrial complexes and BNE were carried out as described (Wittig et al., 2006; Heidler et al., 2013). Mitochondrial complexes were stained with Coomassie Blue (Wittig et al., 2006) and specific in-gel histochemical staining for cI, cIV, and cV was performed as described previously (Wittig et al., 2007). For immunodetection, BNE-gels were blotted onto PVDF membranes and probed with antibodies against AOX (1:50,000) or mitochondrial complexes (MitoProfile Total OXPHOS Rodent WB Antibody Cocktail, Mitosciences, ab110413, 1:250) and cIV (1:1000; Heidler et al., 2013).

Metabolomics

Metabolite analysis was conducted as described previously (Nikkanen et al., 2016), using skeletal muscle from six hemizygous AOX^{Rosa26} and six wild-type littermate control mice (8-week-old males, all culled at a single time in the morning). Briefly, targeted metabolomics was implemented by ultra-performance liquid chromatography tandem mass-spectrometry using a Waters XEVO-TQ-S mass spectrometer. Metabolites extracted with acetonitrile were separated by hydrophilic liquid-interaction chromatography, then analysed spectrometrically by multiple reaction monitoring. Raw data were collected and analysed with TargetLynx software (Waters), and metabolites quantified using internal standards and calibration curves. For full details, see supplementary Materials and Methods.

Bioenergetic experiments

For respirometry of mitochondria from different tissues, mice were euthanised by cervical dislocation and organs were dissected and collected into ice-cold PBS. Soft tissues were fine chopped (1 mm^3) in ice-cold PBS and hand-homogenized in 3 ml re-suspension buffer [225 mM sucrose, 75 mM D-mannitol, 10 mM Tris/HCl, 1 mM EGTA, 1 mg/ml bovine serum albumin (BSA), pH 7.4], using a glass-teflon homogenizer (tight-fitting pestle). Hard tissues (heart, skeletal muscle and kidney), chopped to a similar size, were pre-treated with 3 ml (~10 volumes) ice-cold trypsin-EDTA [500 µg/ml trypsin (Difco), 0.5 mM EDTA, 10 µg/ml phenol red, pH 7.4] for 10 min, followed by blocking with 300 µl foetal bovine serum (Gibco/Life Technologies) and recovery by low-speed centrifugation (40 g_{max}, 1 min, 4°C) before homogenization. Homogenates were centrifuged at 1300 g_{max} for 5 min at 4°C, after which supernatants were collected and re-centrifuged at 17,000 g_{max} for 15 min at 4°C. The mitochondrial pellet was resuspended, according to its size, in 75-250 µl ice-cold MiR05 buffer [0.5 mM EGTA, 3 mM $MgCl_2$, 60 mM lactobionic acid (Aldrich, buffered to pH 7.0 with 5 M KOH), 20 mM taurine (Sigma), 10 mM KH_2PO_4, 20 mM HEPES/KOH, 110 mM sucrose and 1 g/l fatty-acid free BSA (Sigma), pH 7.2 at room temperature] and stored on ice until respirometry. Mitochondrial protein content was assayed using Bradford reagent (Bio-Rad). Respirometry, using an O2K oxygraph (Oroboros), was conducted in MiR05 buffer in a 2 ml chamber, to which was added 50 or 100 µg of mitochondria according to the tissue. Substrates and inhibitors were added in the following order: (1) 5 mM sodium pyruvate+5 mM sodium glutamate+5 mM sodium malate, (2) 4 mM ADP, (3) 150 nM rotenone (Sigma), (4) 17 mM sodium succinate, (5) 22.5 ng/ml antimycin A (Sigma), (6) 200 µM n-propyl gallate (nPG, Sigma), (7) 0.5 mM N,N,N′,N′-tetramethyl-p-phenylenediamine (TMPD, Sigma) +2 mM sodium L-ascorbate, (8) 100 mM NaN_3 or 1 mM KCN. The flux values [pmol/(s×ml)] obtained from the trace were normalized to the amount of mitochondrial protein. For measurements of ROS production, mouse heart mitochondria were isolated essentially as described (Mela and Seitz, 1979), with minor modifications: tissue was minced in 225 mM mannitol, 20 mM MOPS, 75 mM sucrose, 1 mM EGTA, 0.5 mM dithiothretol, pH 7.4 and hand-homogenized in 10 ml/g tissue of the same buffer containing 0.05% Nagarse (Sigma). After addition of 30 ml of the original buffer, the homogenate was centrifuged at 2000 g_{max} for 4 min at 4°C. The supernatant was passed through cheesecloth and re-centrifuged at 12,000 g_{max} for 10 min. The resulting pellet was resuspended in 225 mM mannitol, 20 mM MOPS, 75 mM sucrose, 0.1 mM EGTA, 75 mM KCl, pH 7.4. Mitochondrial protein content was determined using the bicinchoninic acid assay (Wiechelman et al., 1988), with BSA as standard. ROS production under conditions used for respirometry was measured fluorimetrically using 5 µM Amplex Red (Hydrogen Peroxide Assay Kit, Thermo Fisher Scientific) and 3 units/ml horseradish peroxidase at 30°C, using a Carry Eclipse fluorimeter (Varian) with excitation at 560 nm and detection at 590 nm (Zhou et al., 1997).

Mouse phenotyping

Mouse body weight was measured using a small electronic balance suitable for rodents. Grip strength was measured using the BIO-GS3 apparatus (Bioseb). Mice were placed on the platform until all four limbs were engaged on the grid, and then pulled to measure the force generated. The mean of three measurements was normalised to body weight (g/g) for each animal tested. All animals were trained for three successive days before the actual experiment. Endurance running was measured as previously (Yatsuga and Suomalainen, 2012), as the run time on a standard running belt (Exer-6M Treadmill, Columbus Instruments), set to reach a speed of 6.5 m/min in steps of 0.5 m/min every 3 min. A stay of more than 5 s on the electrified motivation grid (0.5 mA current) was considered as the end point of each test. Cardiac parameters (ejection fraction, left ventricular mass) were determined by echocardiography (Vevo 2100 system, FujiFilm VisualSonics Inc.) or, where indicated in figure legends, by magnetic resonance imaging (MRI), performed essentially as described elsewhere (Ziebart et al., 2008). MRI data were analysed using OsiriX Imaging Software (http://www.osirix-viewer.com/index.html). Comprehensive phenotyping by the German Mouse Clinic (GMC) was conducted using the protocols described and referenced at https://www.mouseclinic.de (search 'phenomap'). In all tests, mouse genotypes were blinded to the experimenter and verified subsequently.

Systemic administration of cyanide

The procedure was implemented under contract by Luria Scientific Industries, Herzliya, Israel (responsible scientist Dr Iris Maimon). Mice, whose genotypes were blinded to the experimenter, were anesthetized with 3% isoflurane in an induction chamber, after which anaesthesia was maintained by 2% isoflurane using a nose cone. Core temperature was kept at 36.5°C using a heating pad. KCN was dissolved in distilled water at 10 mg/ml and delivered by IP injection to the mice at 8.5 mg/kg. Animals were observed for 48 h for the onset of death, defined as apnea without further respiratory effort or movement or palpable cardiac pulsation.

Ethical permits

All mouse breeding and experiments were approved by the national ethical committee in Finland, under permits ESAVI/8766/04.10.07/2015 and ESAVI/

2954/04.10.07/2015. Mouse experiments conducted under contract by Luria Scientific Industries were approved by IACUC under assurance 7433J45, 07/22/2015. Maintenance of mice in Magdeburg was in accord with procedures specified by the Animal Health and Care Committees of the Otto-von-Guericke University, Magdeburg, and of the State of Sachsen-Anhalt, Germany.

Image processing

Images were optimized for brightness and contrast and cropped for clarity. No other manipulations such as gamma corrections were made, nor was any relevant information excluded by cropping. Full, original gel images are available on request.

Acknowledgements

We thank Maarit Myöhänen, Sonja Krüger, Susanne Kreutzer, Birgit Spitznagel and Jana Meisterknecht for excellent technical assistance, Christopher Carroll, Giuseppe Cannino, Luca Giordano, Riikka Kivelä and Uwe Richter for technical advice and help, Anu Suomalainen and Brendan Battersby, for useful discussions, and Troy Faithfull for critical reading of the manuscript.

Competing interests

The authors declare no competing or financial interests.

Author contributions

H.T.J., T.B., P.R. and M.S. jointly conceived the project and developed the strategy to create the *AOX*^{Rosa26} mouse. M.S. supervised and coordinated the laboratory work, which was conducted by M.S., P.K.D., E.D., K.M.H., Y.Z., I.S., I.W., J.H., Z.G., T.G., J.N., V.V., A.W. and F.N.G. H.F., V.G.-D. and M.H.d.A. implemented comprehensive phenotyping in collaboration with their colleagues from the German Mouse Clinic. H.T.J. compiled the manuscript and figures with assistance from all authors.

Funding

This work was supported by funding from the European Research Council (Advanced Grant 232738 to H.T.J.), Academy of Finland (Suomen Akatemia) Terveyden Tutkimuksen Toimikunta (grant 272376); Tampere University (Tampereen Yliopisto) Hospital Medical Research Fund; the Sigrid Juselius Foundation (Sigrid Juséliuksen Säätiö), Max-Planck-Gesellschaft, Deutsche Forschungsgemeinschaft (DFG SFB 815 project Z1 to I.W. and DFG SFB 1213 project A2 to T.B.), the Cluster of Excellence "Macromolecular Complexes", Goethe-Universität Frankfurt am Main, Germany (to I.W.), the Cluster of Excellence "Cardiopulmonary System" (to T.B.), the German Center for Lung Research (DLZ), and the Universities of Helsinki and Tampere (Helsingin Yliopisto and Tampereen Yliopisto). This work has also been funded by the German Federal Ministry of Education and Research (Bundesministerium für Bildung und Forschung) to the German Mouse Clinic (Infrafrontier grant 01KX1012).

Data availability

Comprehensive phenotyping by the German Mouse Clinic (GMC) was conducted using the protocols described and referenced at https://www.mouseclinic.de (search 'phenomap').

Supplementary information

Supplementary information available online at
http://dmm.biologists.org/lookup/doi/10.1242/dmm.027839.supplemental

References

Acín-Pérez, R., Fernández-Silva, P., Peleato, M. L., Pérez-Martos, A. and Enriquez, J. A. (2008). Respiratory active mitochondrial supercomplexes. *Mol. Cell* **32**, 529-539.

Banares, S., Zeh, K., Krajewska, M., Kermer, P., Baribault, H., Reed, J. C. and Krajewski, S. (2005). Novel pan-neuronal Cre-transgenic line for conditional ablation of genes in the nervous system. *Genesis* **42**, 6-16.

Castro-Guerrero, N. A., Krab, K. and Moreno-Sánchez, R. (2004). The alternative respiratory pathway of euglena mitochondria. *J. Bioenerg. Biomembr.* **36**, 459-469.

Chaban, Y., Boekema, E. J. and Dudkina, N. V. (2014). Structures of mitochondrial oxidative phosphorylation supercomplexes and mechanisms for their stabilisation. *Biochim. Biophys. Acta* **1837**, 418-426.

Chen, C. M., Krohn, J., Bhattacharya, S. and Davies, B. (2011). A comparison of exogenous promoter activity at the ROSA26 locus using a PhiC31 integrase mediated cassette exchange approach in mouse ESCs. *PLoS ONE* **6**, e23376.

Chouchani, E. T., Pell, V. R., Gaude, E., Aksentijević, D., Sundier, S. Y., Robb, E. L., Logan, A., Nadtochiy, S. M., Ord, E. N. J., Smith, A. C. et al. (2014). Ischaemic accumulation of succinate controls reperfusion injury through mitochondrial ROS. *Nature* **515**, 431-435.

Dassa, E. P., Dufour, E., Gonçalves, S., Paupe, V., Hakkaart, G. A. J., Jacobs, H. T. and Rustin, P. (2009). Expression of the alternative oxidase complements cytochrome c oxidase deficiency in human cells. *EMBO Mol. Med.* **1**, 30-36.

Delaunay, D., Heydon, K., Miguez, A., Schwab, M., Nave, K.-A., Thomas, J. L., Spassky, N., Martinez, S. and Zalc, B. (2009). Genetic tracing of subpopulation neurons in the prethalamus of mice (Mus musculus). *J. Comp. Neurol.* **512**, 74-83.

El-Khoury, R., Dufour, E., Rak, M., Ramanantsoa, N., Grandchamp, N., Csaba, Z., Duvillié, B., Bénit, P., Gallego, J., Gressens, P. et al. (2013). Alternative oxidase expression in the mouse enables bypassing cytochrome c oxidase blockade and limits mitochondrial ROS overproduction. *PLoS Genet.* **9**, e1003182.

El-Khoury, R., Kemppainen, K. K., Dufour, E., Szibor, M., Jacobs, H. T. and Rustin, P. (2014). Engineering the alternative oxidase gene to better understand and counteract mitochondrial defects: state of the art and perspectives. *Br. J. Pharmacol.* **171**, 2243-2249.

El-Khoury, R., Kaulio, E., Lassila, K. A., Crowther, D. C., Jacobs, H. T. and Rustin, P. (2016). Expression of the alternative oxidase mitigates beta-amyloid production and toxicity in model systems. *Free Radic. Biol. Med.* **96**, 57-66.

Fernandez-Ayala, D. J. M., Sanz, A., Vartiainen, S., Kemppainen, K. K., Babusiak, M., Mustalahti, E., Costa, R., Tuomela, T., Zeviani, M., Chung, J. et al. (2009). Expression of the Ciona intestinalis alternative oxidase (AOX) in Drosophila complements defects in mitochondrial oxidative phosphorylation. *Cell Metab.* **9**, 449-460.

Friedrich, G. and Soriano, P. (1991). Promoter traps in embryonic stem cells: a genetic screen to identify and mutate developmental genes in mice. *Genes Dev.* **5**, 1513-1523.

Hakkaart, G. A. J., Dassa, E. P., Jacobs, H. T. and Rustin, P. (2006). Allotopic expression of a mitochondrial alternative oxidase confers cyanide resistance to human cell respiration. *EMBO Rep.* **7**, 341-345.

Heidler, J., Strecker, V., Csintalan, F., Bleier, L. and Wittig, I. (2013). Quantification of protein complexes by blue native electrophoresis. *Methods Mol. Biol.* **1033**, 363-379.

Hitoshi, N., Ken-ichi, Y. and Jun-ichi, M. (1991). Efficient selection for high-expression transfectants with a novel eukaryotic vector. *Gene* **108**, 193-199.

Hitz, C., Wurst, W. and Kühn, R. (2007). Conditional brain-specific knockdown of MAPK using Cre/loxP regulated RNA interference. *Nucleic Acids Res.* **35**, e90.

Hoefnagel, M. H. N. and Wiskich, J. T. (1998). Activation of the plant alternative oxidase by high reduction levels of the Q-pool and pyruvate. *Arch. Biochem. Biophys.* **355**, 262-270.

Humphrey, D. M., Parsons, R. B., Ludlow, Z. N., Riemensperger, T., Esposito, G., Verstreken, P., Jacobs, H. T., Birman, S. and Hirth, F. (2012). Alternative oxidase rescues mitochondria-mediated dopaminergic cell loss in Drosophila. *Hum. Mol. Genet.* **21**, 2698-2712.

Ida-Hosonuma, M., Iwasaki, T., Taya, C., Sato, Y., Li, J., Nagata, N., Yonekawa, H. and Koike, S. (2002). Comparison of neuropathogenicity of poliovirus in two transgenic mouse strains expressing human poliovirus receptor with different distribution patterns. *J. Gen. Virol.* **83**, 1095-1105.

Kemppainen, K. K., Rinne, J., Sriram, A., Lakanmaa, M., Zeb, A., Tuomela, T., Popplestone, A., Singh, S., Sanz, A., Rustin, P. et al. (2014). Expression of alternative oxidase in Drosophila ameliorates diverse phenotypes due to cytochrome oxidase deficiency. *Hum. Mol. Genet.* **23**, 2078-2093.

Kim, H. S., Joo, H. J., Woo, J. S., Choi, Y. S., Choi, S. H., Kim, H. and Moon, W. K. (2013). In vivo magnetic resonance imaging of transgenic mice expressing human ferritin. *Mol. Imaging Biol.* **15**, 48-57.

Koetsier, P. A., Schorr, J. and Doerfler, W. (1993). A rapid optimized protocol for downward alkaline Southern blotting of DNA. *Biotechniques* **15**, 260-262.

Liu, P., Jenkins, N. A. and Copeland, N. G. (2003). A highly efficient recombineering-based method for generating conditional knockout mutations. *Genome Res.* **13**, 476-484.

Liu, Y., Fu, S., Niu, R., Yang, C. and Lin, J. (2014). Transcriptional activity assessment of three different promoters for mouse *in utero* electroporation system. *Plasmid* **74**, 52-58.

McDonald, A. E., Vanlerberghe, G. C. and Staples, J. F. (2009). Alternative oxidase in animals: unique characteristics and taxonomic distribution. *J. Exp. Biol.* **212**, 2627-2634.

Mela, L. and Seitz, S. (1979). Isolation of mitochondria with emphasis on heart mitochondria from small amounts of tissue. *Methods Enzymol.* **55**, 39-46.

Mills, E. L., Kelly, B., Logan, A., Costa, A. S. H., Varma, M., Bryant, C. E., Tourlomousis, P., Däbritz, J. H. M., Gottlieb, E. , Latorre I. et al. (2016). Succinate dehydrogenase supports metabolic repurposing of mitochondria to drive inflammatory macrophages. *Cell* **167**, 457-470.

Nikkanen, J., Forsström, S., Euro, L., Paetau, I., Kohnz, R. A., Wang, L., Chilov, D., Viinamäki, J., Roivainen, A., Marjamäki, P. et al. (2016). Mitochondrial DNA replication defects disturb cellular dNTP pools and remodel one-carbon metabolism. *Cell Metab.* **23**, 635-648.

Nyabi, O., Naessens, M., Haigh, K., Gembarska, A., Goossens, S., Maetens, M., De Clercq, S., Drogat, B., Haenebalcke, L., Bartunkova, S. et al. (2009). Efficient mouse transgenesis using Gateway-compatible ROSA26 locus targeting vectors and F1 hybrid ESCs. *Nucleic Acids Res.* **37**, e55.

Reiter, R. J., Manchester, L. C. and Tan, D. X. (2010). Neurotoxins: free radical mechanisms and melatonin protection. *Curr. Neuropharmacol.* **8**, 194-210.
Rodríguez, C. I., Buchholz, F., Galloway, J., Sequerra, R., Kasper, J., Ayala, R., Stewart, A. F. and Dymecki, S. M. (2000). High-efficiency deleter mice show that FLPe is an alternative to Cre-loxP. *Nat. Genet.* **25**, 139-140.
Rustin, P. and Jacobs, H. T. (2009). Respiratory chain alternative enzymes as tools to better understand and counteract respiratory chain deficiencies in human cells and animals. *Physiol. Plant.* **137**, 362-370.
Sambrook, J., Fritsch, E. F. and Maniatis, T. (1989). *Molecular Cloning: A Laboratory Manual*. New York, USA: Cold Spring Harbor Laboratory Press.
Soriano, P. (1999). Generalized lacZ expression with the ROSA26 Cre reporter strain. *Nat. Genet.* **21**, 70-71.
Srinivas, S., Watanabe, T., Lin, C.-S., William, C. M., Tanabe, Y., Jessell, T. M. and Costantini, F. (2001). Cre reporter strains produced by targeted insertion of EYFP and ECFP into the ROSA26 locus. *BMC Dev. Biol.* **1**, 4.
Vogel, F., Bornhövd, C., Neupert, W. and Reichert, A. S. (2006). Dynamic subcompartmentalization of the mitochondrial inner membrane. *J. Cell. Biol.* **175**, 237-247.
Warming, S., Costantino, N., Court, D. L., Jenkins, N. A. and Copeland, N. G. (2005). Simple and highly efficient BAC recombineering using galK selection. *Nucleic Acids Res.* **33**, e36.
Wiechelman, K. J., Braun, R. D. and Fitzpatrick, J. D. (1988). Investigation of the bicinchoninic acid protein assay: identification of the groups responsible for color formation. *Anal. Biochem.* **175**, 231-237.
Wittig, I., Braun, H.-P. and Schägger, H. (2006). Blue native PAGE. *Nat. Protoc.* **1**, 418-428.
Wittig, I., Karas, M. and Schägger, H. (2007). High resolution clear native electrophoresis for in-gel functional assays and fluorescence studies of membrane protein complexes. *Mol. Cell. Proteomics* **6**, 1215-1225.
Yamamoto, H. (1995). Effect of atropine on cyanide-induced acute lethality in mice. *Toxicol. Lett.* **80**, 29-33.
Yamamoto, H. and Tang, H. W. (1996). Antagonistic effect of melatonin against cyanide-induced seizures and acute lethality in mice. *Toxicol Lett.* **87**, 19-24.
Yatsuga, S. and Suomalainen, A. (2012). Effect of bezafibrate treatment on late-onset mitochondrial myopathy in mice. *Hum. Mol. Genet.* **21**, 526-535.
Young, L., Shiba, T., Harada, S., Kita, K., Albury, M. S. and Moore, A. L. (2013). The alternative oxidases: simple oxidoreductase proteins with complex functions. *Biochem. Soc. Trans.* **41**, 1305-1311.
Zambrowicz, B. P., Imamoto, A., Fiering, S., Herzenberg, L. A., Kerr, W. G. and Soriano, P. (1997). Disruption of overlapping transcripts in the ROSA beta geo 26 gene trap strain leads to widespread expression of beta-galactosidase in mouse embryos and hematopoietic cells. *Proc. Natl. Acad. Sci. USA* **94**, 3789-3794.
Zhang, D., Lee, B., Nutter, A., Song, P., Dolatabadi, N., Parker, J., Sanz-Blasco, S., Newmeyer, T., Ambasudhan, R., McKercher, S. R. et al. (2015). Protection from cyanide-induced brain injury by the Nrf2 transcriptional activator carnosic acid. *J. Neurochem.* **133**, 898-908.
Zhou, M., Diwu, Z., Panchuk-Voloshina, N. and Haugland, R. P. (1997). A stable nonfluorescent derivative of resorufin for the fluorometric determination of trace hydrogen peroxide: applications in detecting the activity of phagocyte NADPH oxidase and other oxidases. *Anal. Biochem.* **253**, 162-168.
Ziebart, T., Yoon, C.-H., Trepels, T., Wietelmann, A., Braun, T., Kiessling, F., Stein, S., Grez, M., Ihling, C., Muhly-Reinholz, M.et al. (2008). Sustained persistence of transplanted proangiogenic cells contributes to neovascularization and cardiac function after ischemia. *Circ. Res.* **103**, 1327-1334.

7.2 M. Szibor *et al.*, *Biochimica Et Biophysica Acta - Bioenergetics*. **1861**, 148137 (2020)

BBA - Bioenergetics 1861 (2020) 148137

Contents lists available at ScienceDirect

BBA - Bioenergetics

journal homepage: www.elsevier.com/locate/bbabio

Bioenergetic consequences from xenotopic expression of a tunicate AOX in mouse mitochondria: Switch from RET and ROS to FET

Marten Szibor[a,b,*], Timur Gainutdinov[c,e,1], Erika Fernandez-Vizarra[d,1], Eric Dufour[a], Zemfira Gizatullina[c], Grazyna Debska-Vielhaber[c], Juliana Heidler[f], Ilka Wittig[f,g], Carlo Viscomi[d], Frank Gellerich[c,2], Anthony L. Moore[h,2]

[a] Faculty of Medicine and Health Technology, Tampere University, FI-33520 Tampere, Finland
[b] Department of Cardiothoracic Surgery, Jena University Hospital, D-07747 Jena, Germany
[c] Department of Neurology, Otto-von-Guericke-University, D-39120 Magdeburg, Germany
[d] MRC Mitochondrial Biology Unit, University of Cambridge, Cambridge CB2 0XY, UK
[e] Research Institute for Problems of Ecology and Mineral Wealth Use, Tatarstan Academy of Sciences, Kazan 420087, Russian Federation
[f] Functional Proteomics, Faculty of Medicine, Goethe University, D-60590 Frankfurt am Main, Germany
[g] German Center for Cardiovascular Research (DZHK), Partner site RheinMain, D-60590 Frankfurt am Main, Germany
[h] Biochemistry & Biomedicine, School of Life Sciences, University of Sussex, Falmer BN19QG, Brighton, UK

ARTICLE INFO

Keywords:
Mitochondria
OXPHOS
Quinone pool
ROS
Xenotopic expression
Alternative oxidase (AOX)

ABSTRACT

Electron transfer from all respiratory chain dehydrogenases of the electron transport chain (ETC) converges at the level of the quinone (Q) pool. The Q redox state is thus a function of electron input (reduction) and output (oxidation) and closely reflects the mitochondrial respiratory state. Disruption of electron flux at the level of the cytochrome bc_1 complex (cIII) or cytochrome *c* oxidase (cIV) shifts the Q redox poise to a more reduced state which is generally sensed as respiratory stress. To cope with respiratory stress, many species, but not insects and vertebrates, express alternative oxidase (AOX) which acts as an electron sink for reduced Q and by-passes cIII and cIV. Here, we used *Ciona intestinalis* AOX xenotopically expressed in mouse mitochondria to study how respiratory states impact the Q poise and how AOX may be used to restore respiration. Particularly interesting is our finding that electron input through succinate dehydrogenase (cII), but not NADH:ubiquinone oxidoreductase (cI), reduces the Q pool almost entirely (> 90%) irrespective of the respiratory state. AOX enhances the forward electron transport (FET) from cII thereby decreasing reverse electron transport (RET) and ROS specifically when non-phosphorylating. AOX is not engaged with cI substrates, however, unless a respiratory inhibitor is added. This sheds new light on Q poise signaling, the biological role of cII which enigmatically is the only ETC complex absent from respiratory supercomplexes but yet participates in the tricarboxylic acid (TCA) cycle. Finally, we delineate potential risks and benefits arising from therapeutic AOX transfer.

1. Introduction

Mitochondria are cellular organelles with vital functions that range from ATP production and redox homeostasis to cellular signaling. Consequently, mitochondrial dysfunction is present in a number of the most threatening human pathologies including neurodegenerative [1] and cardiovascular diseases [2,3], obesity, diabetes mellitus [4,5], malignant cell transformation [6–8] and septic organ failure [9].

A key component for mitochondrial functions is the electron transport chain (ETC) which consists of four multi-subunit protein complexes and their redox partners. *i.e.* the quinone (Q) pool and cytochrome *c*. NADH:ubiquinone oxidoreductase (cI) and succinate dehydrogenase (cII) facilitate substrate oxidation and Q pool reduction (quinone-reducing complexes) whilst cytochrome bc_1 complex (cIII), cytochrome *c* and cytochrome *c* oxidase (cIV or COX) are the quinol-oxidizing components of the *ETC*. Notably, substrate oxidation and transfer of reducing equivalents through the ETC is coupled to tricarboxylic acid (TCA) cycle activity *via* cII and, in addition, to the generation of a proton-electrochemical gradient by the respiratory complexes cI, cIII and cIV. The mitochondrial membrane potential ($\Delta\Psi$)

* Corresponding author at: Department of Cardiothoracic Surgery, Jena University Hospital, D-07747 Jena, Germany.
E-mail addresses: Marten.Szibor@tuni.fi, Marten.Szibor@med.uni-jena.de (M. Szibor).
[1] T.G. and E.F.-V. contributed equally to this work.
[2] F.N.G. and A.L.M. share senior authorship.

https://doi.org/10.1016/j.bbabio.2019.148137
Received 28 August 2019; Received in revised form 1 December 2019; Accepted 5 December 2019
Available online 09 December 2019

is the major component of the proton-electrochemical gradient which itself is indispensable for ATP generation and mitochondrial redox homeostasis. Therefore, electron transfer from all respiratory chain dehydrogenases converges at the level of the Q pool and controlled electron flux through the ETC is the basis for metabolic homeostasis. Conversely, any blockade of cIII and cIV results in the Q pool becoming highly reduced thereby disturbing metabolic homeostasis and decreasing cellular viability [10,11]. Consequently, controlling the Q reduction state affects $\Delta\Psi$ and ATP production and is of vital importance and decisive for health or disease. To cope with respiratory impairment, many species, but not insects and vertebrates, express alternative oxidase (AOX), a di-iron carboxylate protein which oxidizes the Q-pool in a non-protonmotive fashion [12] thereby acting as an electron sink for reduced Q and by-passing cIII and cIV. Such a by-pass of impaired ETC complexes by xenotopic expression of AOX has been suggested to alleviate diseases, if not offer a cure [13–15].

In previous studies, the presence of AOX in models in which ETC complexes have been disrupted has proved beneficial in restoring respiratory activity and correcting metabolism in cultured mammalian cells [16–18], fruit flies [19–22] and mice [23]. Furthermore, AOX conferred resistance to cyanide toxicity [24,25] and decreased lethality from sepsis [26]. Confusingly, AOX expression, however, had detrimental consequences in a mouse model of mitochondrial myopathy [11]. We thus sought to revisit mechanisms of ETC control in an attempt to determine how AOX expression interferes with mammalian bioenergetics. Using isolated heart mitochondria from mice xenotopically expressing *Ciona intestinalis* AOX [25], we show that respiratory activity of cII, but not cI, causes a rapid reduction of Q (Qr > 90%) of total Q (Qt). Importantly, a high Qr/Qt state is a condition favoring reverse electron transport (RET) [10,57], a signaling event of pathophysiologic relevance, but has only a marginal impact on forward electron transport (FET). In different species, a high Qr/Qt state has also been identified as a pre-requisite for the engagement of AOX activity [27,28].

Here, the use of AOX revealed the extent to which the interplay of the dehydrogenases and oxidases defines the direction of electron flow (*i.e.* RET or FET). Our results also raise the question as to the legitimacy of the dual function of cII acting both, as an ETC complex and a member of the TCA cycle. Finally, the results presented in this study underline the potential benefits and risks that AOX expression may have as a diagnostic tool and/or treatment option.

2. Materials and methods

2.1. Mouse model

Ciona intestinalis alternative oxidase (AOX) coding sequence was knocked into the genomic mouse *Rosa26* locus. AOX expression was controlled by a ubiquitous and strong CAG promoter [25]. Part of the animal experiments were conducted under the 1986 UK Animals (Scientific Procedures) Act and approved by Home Office licenses (PPL: 7538 and P6C97520A) and local ethical review. All mice were kept on a C57Bl6, and WT littermates were used as controls. Animals were maintained in a temperature- and humidity-controlled facility, with a 12-h light/dark cycle and free access to water and food.

2.2. Isolation of heart mitochondria

Heart mitochondria from 12 to 18-week-old mice were isolated as described [29]. Briefly, hearts were rapidly removed and transferred to ice-cold MMSE-A buffer (225 mM D-mannitol (Sigma-Aldrich, M4125), 20 mM MOPS (Sigma, M1254), 75 mM sucrose (Sigma, S7903), 1 mM ethylene glycol-bis(2-aminoethylether)-*N,N,N′,N′*-tetraacetic acid (EGTA, Sigma-Aldrich, E4378), 0.5 mM DL-dithiothreitol (DTT, Sigma, 43819), pH 7.4). All further steps were performed on ice. Heart tissues were minced using scissors and manually pottered in a glass-on-Teflon homogenizer until homogenous in MMSE-B buffer (MMSE-A buffer plus 0.05% nagarse, Sigma, P8038). Nagarse activity was stopped by 1:30 dilution of the homogenate in MMSE-A buffer. The homogenate was centrifuged at 2000 $\times g$ for 4 min at 4 °C and the supernatant passed through cheesecloth. The flow-through was centrifuged at 12,000 $\times g$ for 10 min at 4 °C and the pellet resuspended in ice-cold MMSE-C buffer (225 mM D-mannitol, 20 mM MOPS, 75 mM sucrose, 0.1 mM EGTA, 75 mM KCl, pH 7.4). Mitochondrial protein content was estimated using bicinchoninic acid assay (Pierce BCA Protein Assay Kit, Thermo Scientific, 23225) with bovine serum albumin used as standard.

2.3. Blue-native (BN) gel electrophoresis

Blue-native (BN) and BN/BN gel electrophoresis, complex I in-gel activity staining and sample preparations were performed as previously described [30,31] using ~3% digitonin (Serva, 19551) and 0.02% n-dodecyl β-maltoside (GLYCON Biochemicals, D97002-C) as detergents.

2.4. Western blot analysis

Blue-native (BN)/BN gels were blotted onto polyvinylidene difluoride (PVDF) membranes as described [30] and probed with custom-made AOX anti-serum (1:10,000; 21st Century Biochemicals) [17]. Goat anti-rabbit IgG (whole molecule)-Peroxidase antibody (Sigma, A0545) served as secondary antibody. Enhanced chemiluminescence (ECL) was used and the signal detected in a ChemiDoc XRS (Bio-Rad).

2.5. Complexome profiling

A first dimensional BN electrophoresis gel was stained with Coomassie Brilliant Blue G 250 (Serva, 17524) and the appropriate lane was cut into 96 fractions. Proteins in the gel fractions were digested using trypsin (Promega, V5111) and analyzed by mass spectrometry (MS) essentially as described [32]. MS data were analyzed by MaxQuant (v1.5.2.8) [33]. Proteins were identified using a mouse reference proteome database UniProtKB released in 6/2015 supplemented with *Ciona intestinalis* AOX. Enzyme specificity was set to trypsin. Acetylation (+42.01) at N-terminus, oxidation of methionine (+15.99), deamidation of asparagine and glutamine were selected as variable modifications and carbamidomethylation (+57.02) as fixed modification on cysteines. The false discovery rate (FDR) for the identification of proteins and peptides was 1%. Intensity-based absolute quantification (IBAQ) values were recorded. Protein abundance within native lanes were normalized to maximum appearance. Slice numbers of the maximum appearance of mitochondrial complex III dimer (483 kDa), complex IV (213 kDa), complex V (538 kDa) and respiratory supercomplex containing complex I, III dimer and one copy of complex IV (1676 kDa) were used for native mass calibration. The mass spectrometry proteomics data have been deposited to the ProteomeXchange [34] Consortium *via* the PRIDE [35] partner repository with the dataset identifier PXD014016.

2.6. Respirometry and mitochondrial ROS measurements

Mitochondrial oxygen consumption was measured using high-resolution respirometry (O2k oxygraph, Oroboros Instruments, Innsbruck, Austria) at 30 °C [36] in air-saturated medium (200 nmol O_2/ml at 95 kPa). Weight-specific oxygen consumption was calculated from the time derivative of the oxygen concentration (DatLab 7 software, Oroboros Instruments, Innsbruck, Austria). Respiration of isolated heart mitochondria (0.03 mg protein per ml) was measured in MMMP-K buffer (120 mM D-mannitol, 20 mM MOPS, 5 mM KH_2PO_4, 60 mM KCl, 5 mM $MgCl_2$, pH 7.4) in the presence and absence of substrates and inhibitors as described [37]. Briefly, we used complex I substrates 10 mM pyruvate (P, Pyr, Sigma, P5280), 10 mM glutamate (G, Glu, Aldrich, 49621), 2 mM malate (M, Mal, Sigma, M1000);

complex II substrate 10 mM succinate (Succ, Sigma-Aldrich, S2378) in presence or absence of 1.5 μM rotenone (ROT, Sigma-Aldrich, R8875); adenosine 5′-diphosphate (ADP, Sigma, A2754) as indicated; 5 μM carboxyatractyloside (CAT, Calbiochem, 21-620), antimycin A (AA, Sigma, A8674) as indicated; azide (Az, Sigma-Aldrich, S2002) as indicated; 1 μM carbonyl cyanide 4-(trifluoromethoxy)phenylhydrazone (FCCP, Sigma, C2920); 2.5 μM oligomycin (Sigma, O4876); 100 μM n-propyl gallate (n-PG, Sigma, P3130).

Mitochondrial ROS production was measured in parallel to oxygen consumption by attaching a fluorometer module to the respirometer and using a probe specific for the detection of H_2O_2 production [38]. Briefly, 10 μM of Amplex UltraRed Reagent (Invitrogen, A36006), 1 U/ml of peroxidase from horseradish (Sigma, P8250) and 5 U/ml of superoxide dismutase (SOD, Sigma, S8409) were added to the chamber before starting the measurement. The raw fluorescence signal was calibrated to H_2O_2 concentrations of a standard H_2O_2 solution in the presence of isolated heart mitochondria.

2.7. Qr/Qt measurements

Mitochondrial respiration and the level of Q-pool reduction were simultaneously measured voltametrically in a custom-made chamber using an oxygen electrode and a glassy carbon electrode and a platinum electrode connected to an Ag/AgCl electrode for reference essentially as previously described [39].

2.8. Measuring mitochondrial membrane potential (ΔΨ)

ΔΨ was monitored fluorimetrically using 2 μM of the ΔΨ-sensitive probe Safranin O (Sigma-Aldrich, S2255) as described [40]. The fluorescence signal was detected as arbitrary units (a.u.) and the signal after uncoupling with 1 μM FCCP served as zero value. ΔΨ is shown as positive value reciprocal to the fluorescence signal.

2.9. Statistical analyses

Statistical analyses were performed using GraphPad Prism (GraphPad Software, version 7.0d). 2way ANOVA was used for comparisons of at least $n = 3$ independent experiments and a P value < 0.05 was considered being statistically significant. All data are shown as mean. Error bars represent standard deviations (SD).

3. Results

3.1. AOX forms homo-oligomers but does not affect the assembly or stoichiometry of other ETC complexes

We first sought to determine if AOX activity requires the recognition of specific interaction partners or if its presence affects the composition or stoichiometries of the native mouse ETC complexes. We studied this using digitonin-solubilized heart mitochondria separated by blue-native (BN) polyacrylamide gel electrophoresis [41,42]. Two mutually complementary strategies were followed. First, we digested individual gel slices by trypsin and performed mass spectrometry analysis to compose a mitochondrial complexome migration profile (Fig. 1A) [32]. In parallel, we incubated BN first dimensions with the more stringent detergent n-dodecyl β-maltoside (DDM) to in-gel dissociate high-molecular weight assemblies [30] and separated DDM-treated lanes in a second dimension (BN/BN) (Fig. 1B,C). Together, both approaches failed to identify AOX interaction partners apart from the previously described homomeric high-molecular AOX assemblies (circles in Fig. 1B,C) [25]. Importantly, AOX did not cluster with any mitochondrial protein or ETC complex with similar migration pattern (Fig. 1A), and ETC complexes showed regular migration patterns, protein composition and supercomplex stoichiometries (Supplementary Table S1; PRIDE dataset PXD014016). Taken together, our data confirm a xenotopically expressed tunicate AOX in the mouse as a freely diffusible redox partner.

3.2. AOX maintains phosphorylating respiration with cI substrates

A freely diffusible redox partner may pose a metabolic threat if it allows an uncontrolled ETC by-pass since electron flux through the AOX is non-protonmotive [43]. Recent experiments in which trypanosomal AOX allowed maximal NADH oxidation in submitochondrial particles from bovine heart seemingly support this notion [44]. Earlier, we observed that global AOX expression exerts no deleterious effects on the general mouse physiology whilst conferring resistance to systemic cyanide application [25], which may be accounted for by the inability of AOX to effectively compete with cIII for respiratory flux [45]. We tested this assumption in isolated intact mitochondria and found that there was little to no engagement of AOX during cI activity as reflected by the respiratory control index (RCI) of 6.9 ± 1.7 (mean ± SD, $n = 8$) in wild-type (WT) and 4.9 ± 1.5 ($n = 7$) in AOX mitochondria (Fig. 2A,B) when energized with pyruvate, glutamate and malate (PGM). Such respiration was not sensitive to n-propyl gallate (n-PG), a potent AOX inhibitor. The observed decrease in AOX RCI is based on a slightly higher rate of non-phosphorylating respiration (state 4), *i.e.* respiration upon ADP turnover or upon inhibition of the adenine nucleotide translocase (ANT) by carboxyatractyloside (CAT) (Fig. 2B). This indicates that in the absence of respiratory inhibition only approx. 7% (or 14 nmol O_2/mg/min, blue trace in Fig. 2B) of the total electron flow is diverted to AOX. Another bioenergetic parameter for estimating the efficiency of oxidative phosphorylation is the ADP/oxygen ratio, or P/O value. It refers to the number of moles of ADP phosphorylated to ATP per two electrons flowing through the ETC to oxygen. P/O values for isolated WT and AOX heart mitochondria for different substrate combinations (Supplementary Fig. S1F) are largely in agreement with literature values. Note, inhibition of two proton pumps, *i.e.* cIII and cIV by the addition of cIV inhibitor azide (Az), decreases the P/O value for AOX respiration driven by cI substrates PGM to one coupling site. It should be emphasized, however, that such measurements are notoriously inaccurate as they assume state 4 respiration (the proton leak) ceases during phosphorylating conditions which is obviously not the case when AOX is engaged (Supplementary Fig. S1B). Under these conditions P/O ratios *via* an oxygen electrode are unreliable as the so-called state 4 respiration is too high (~200 nmol O_2/mg/min) to distinguish any measurable change in rate upon addition of ADP.

We reasoned that the inability of AOX to be engaged as a terminal oxidase, despite seemingly optimal conditions, may be due to its high K_M for Qr [28]. Therefore, we determined Qr/Qt ratios (in %) in parallel to respiratory rates in WT and AOX heart mitochondria energized by PGM using a Q-electrode [39]. Surprisingly, Qr/Qt values remained low (~13% Qr/Qt; Fig. 2C) and did not differ despite changing respiratory states. The failure to reach a critical threshold of Qr/Qt (blue horizontal bar in Fig. 2C) [27,28] in principle impedes an AOX engagement. In contrast, under conditions of known Q-pool reduction [28] such as upon cIII (antimycin A, AA) or cIV (azide, Az) inhibition, AOX expression allows respiratory rates in excess of 200 nmol O_2/mg/min (blue traces in Fig. 2E,F; Supplementary Fig. S1A,B). Moreover, inhibitor titrations in AOX-expressing mitochondria resulted in a non-linear dependency of the respiratory rate as the levels of Qr increase [28] under non-phosphorylating conditions (Fig. 2F; Supplementary Fig. S1B). The fact that AA and Az evoked similar responses make unspecific toxic inhibitor effects unlikely and Qr release due to a loss of supercomplex integrity was ruled out by measuring cI activity on a BN gel (Supplementary Fig. S1C). Importantly, despite being non-protonmotive [43], AOX indirectly maintained ΔΨ in PGM energized mitochondria in the presence of AA (Fig. 2D) [46]. Such a finding is substantiated by the result that subsequent addition of cI inhibitor rotenone (ROT) collapses ΔΨ (Fig. 2D). This demonstrates that AOX can act as an effective electron sink *in vivo* allowing phosphorylating (state

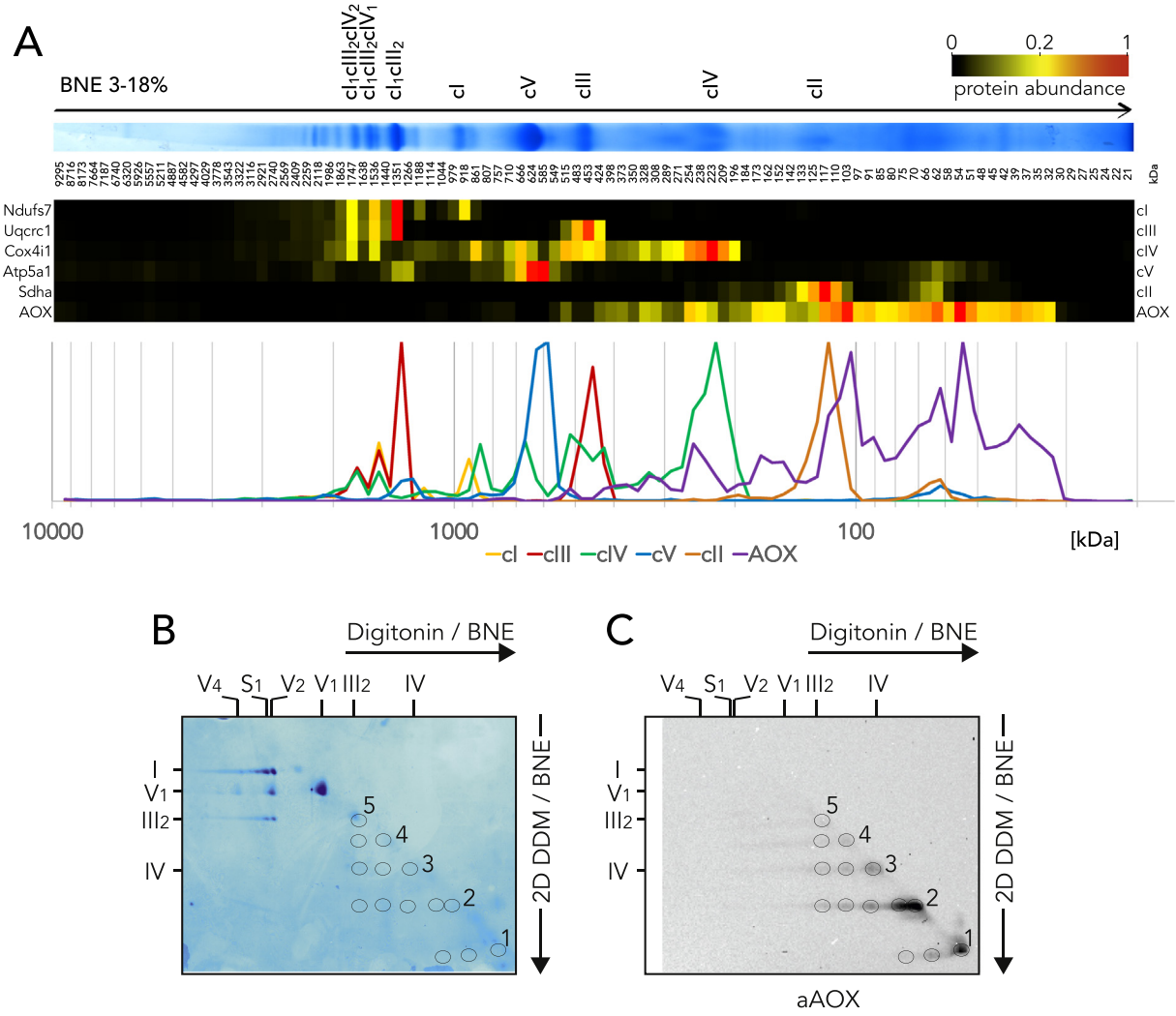

Fig. 1. AOX acts as a freely diffusible Qr redox partner. (**A**) Digitonin-solubilized AOX heart mitochondria separated by 1D blue-native (BN) polyacrylamide gel electrophoresis, analyzed by mass spectrometry. Heat maps of selected protein subunits representing individual respiratory complexes with red color representing a high and black color representing a low expression. cI, Ndufs7; cIII, Uqcrc1; cIV, Cox4i1; cV, Atp5a1; cII, Sdha. Line-chart to illustrate the migration pattern of classical respiratory complexes and AOX assemblies. Note, estimated molecular masses support the notion that AOX expressed in the mouse assembles into homo-oligomers mainly consisting of multimers of dimers. (**B**) Coomassie stain of digitonin-solubilized AOX heart mitochondria separated by tandem BN/BN using n-dodecyl β-maltoside (DDM) treatment before second dimensional run. (**C**) AOX protein detected by western blot analysis. Of note, the regular pattern of AOX assemblies marked by circles again indicates that AOX does not form erratic aggregates but rather assembles into multimers of different stoichiometries. Circles from the western blot analysis have been superposed onto the Coomassie stained gel to visualize the AOX multimer migration pattern in comparison to other mitochondrial complexes.

3) respiration on cI substrates when electron flux through the ETC downstream of Q is blocked.

3.3. AOX facilitates succinate-dependent FET under high protonmotive force

Similar to AOX, cII is also non-protonmotive and succinate oxidation has previously been shown to rapidly increase Qr/Qt levels to approx. 90% [28]. Since succinate is a TCA substrate, it is plausible that cII and AOX together may form a futile respiratory cycle with detrimental consequences on cell viability. Our previous results suggest that an activation of such futile cycle does not happen in the AOX mouse under non-stressed conditions [25]. To understand the mechanistic basis for this paradox, we energized isolated heart mitochondria with succinate and measured respiratory rates in the presence of ROT (Fig. 3A). Our data reveal that succinate rapidly reduces the Q-pool above a critical threshold (blue horizontal bar in Fig. 3B) without generating relevant amount of mitochondrial reactive oxygen species (ROS) under any respiratory state (Fig. 3C) and that the presence of AOX does indeed enhance mitochondrial respiratory rates both under phosphorylating (presence of ADP, state 3) and non-phosphorylating (absence of ADP, state 4) conditions (Fig. 3A). Diversion of electron flux through AOX is also reflected by a decrease in RCI from 3.2 ± 0.5 (mean ± SD, $n = 5$) in WT to 1.3 ± 0.1 ($n = 7$) in AOX mitochondria (Supplementary Fig. S1D,E). Interestingly, the respiratory rate has little, if any, effect on the Qr/Qt ratios (Fig. 3B). Similar to cI substrates, $\Delta\Psi$ is still maintained during succinate-driven respiration (Fig. 3D), suggesting that even in the presence of AOX, a significant proportion of the electron flux is mediated *via* the proton-pumping activities of cIII and cIV (representative traces shown in Fig. 3E,F). P/O values were also calculated for succinate-dependent respiration in WT heart mitochondria (Supplementary Fig. S1F). As indicated previously, AOX activity is a complicating factor during succinate-dependent respiration (both in the presence and absence of ADP, respectively). This prevents any accurate calculation of P/O values with AOX respiring mitochondria. In support of such a notion, it is apparent from the original respiratory traces (Supplementary Fig. S1D,E) that the P/O ratio of isolated AOX

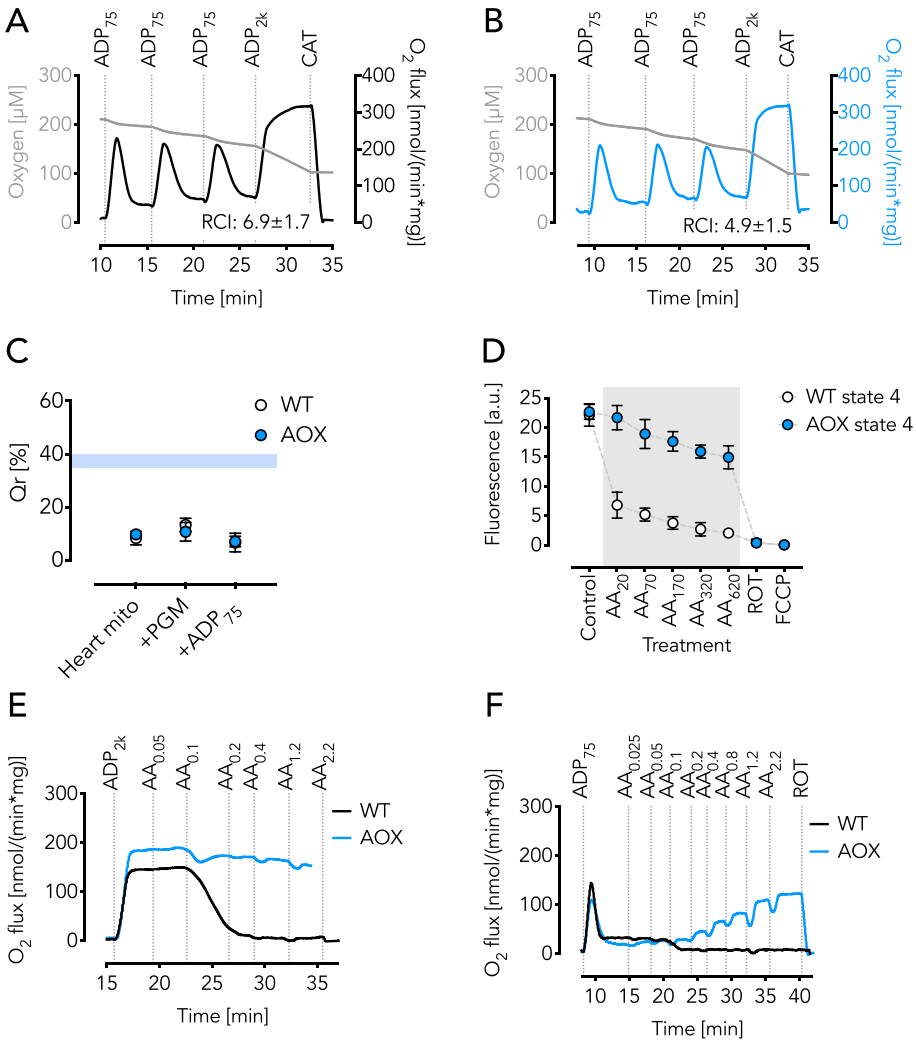

Fig. 2. AOX is engaged on cI substrates only in the presence of respiratory inhibitors. Representative respirometry traces of isolated WT (**A**) and AOX (**B**) heart mitochondria respiring on cI substrates pyruvate, glutamate and malate (PGM) with adenosine diphosphate (ADP in µM) and carboxyatractyloside (CAT) additions as indicated. Respiratory control indices (RCI) shown as mean ± SD, WT $n = 8$, AOX $n = 7$. (**C**) Qr/Qt ratios (%) shown as mean ± SD, $n = 3$. Blue horizontal bar represents putative threshold for AOX engagement. (**D**) Mitochondrial membrane potential ($\Delta\Psi$) shown as arbitrary units (a.u.) as mean ± SD, n = 3. AA, antimycin A. Grey area indicates significant difference between WT and AOX ($P < 0.05$) analyzed by 2way ANOVA with post-hoc Sidak's multiple comparisons test. Representative respiratory rate traces of isolated WT and AOX heart mitochondria in non-phosphorylating (absence of ADP, state 4) (**E**) and phosphorylating (presence of ADP, state 3) (**F**) conditions with PGM as substrates. ADP (in µM) and AA (in µM) additions as indicated. (For interpretation of the references to color in this figure legend, the reader is referred to the web version of this article.)

heart mitochondria must be significantly lower than in WT even if an accurate number cannot be reliably determined because of the high basal respiratory rate.

3.4. AOX prevents RET under non-phosphorylating conditions

Succinate accumulation along with high $\Delta\Psi$ and Qr/Qt has been described as mechanism for RET [10] in ischemia-reperfusion injury and inflammatory diseases [26,47,48]. For the latter, AOX was demonstrated to have beneficial effects [26]. The bioenergetic rationale for such beneficial effects was believed to depend upon the ability of AOX to maintain the Q-pool in a more oxidized state in comparison to WT mitochondria thereby reducing RET-mediated ROS production [10,25]. We sought to test if this was the case by determining how AOX exerts its effects on mitochondrial respiration on succinate in the absence of ROT and thus in the presence of a fully functional cI. Again, isolated heart mitochondria expressing AOX were used and we discovered enhanced succinate-driven respiration under non-phosphorylating conditions (Fig. 4A; Supplementary Fig. S1G). Although the addition of small amounts of ADP increased respiration in WT mitochondria, the presence of AOX had no additive effect (Fig. 4A; Supplementary Fig. S1G). The addition of saturating amounts of ADP failed to induce sustained phosphorylating respiration (Fig. 4A; Supplementary Fig. S1G) both in WT and AOX heart mitochondria. This was previously attributed to a loss of $\Delta\Psi$ and the generation of the potent cII inhibitor oxaloacetate [49]. As demonstrated here (Fig. 4D), such a notion is not supported by $\Delta\Psi$ measurements (original traces shown in Fig. 4E,F). Although addition of ADP severely diminished the magnitude of $\Delta\Psi$, the fact that it is restored upon ANT inhibition by CAT (Fig. 4D), suggests that the observed depolarization is due to ATP/ADP exchange and not due to a proposed inhibition of cII activity [49]. In support of this notion, respiratory uncoupling by carbonyl cyanide 4-(trifluoromethoxy)phenylhydrazone (FCCP) following CAT fully depolarizes $\Delta\Psi$ (Fig. 4D–F). Furthermore, measurements of the steady-state redox poise of the Q-pool in the absence of ROT showed that the pool is highly reduced irrespective of the respiratory state and presence or absence of ADP and/or AOX (Fig. 4B). Although the subsequent addition of PGM and/or ROT in the presence of succinate dramatically increased respiratory rates (Fig. 4A; Supplementary Fig. S1G) addition of ROT caused negligible Q oxidation (Fig. 4B). Of particular importance is the observation that the presence of AOX, in the absence of ROT, substantially reduces ROS production in comparison to WT mitochondria (Fig. 4C; Supplementary Fig. S1H) both in the presence of succinate alone or under non-phosphorylating conditions. Such results indicate that under pathologic conditions, AOX can shift the electron flux through the ETC from RET (and ROS) towards FET.

4. Discussion

In the present study, we confirm that AOX from the tunicate *Ciona intestinalis* functions as a freely diffusible mitochondrial oxidase potentially without mobility restrictions when xenotopically expressed in the mouse (Fig. 1A). This may seem surprising considering the formation of high-molecular weight assemblies which have previously been

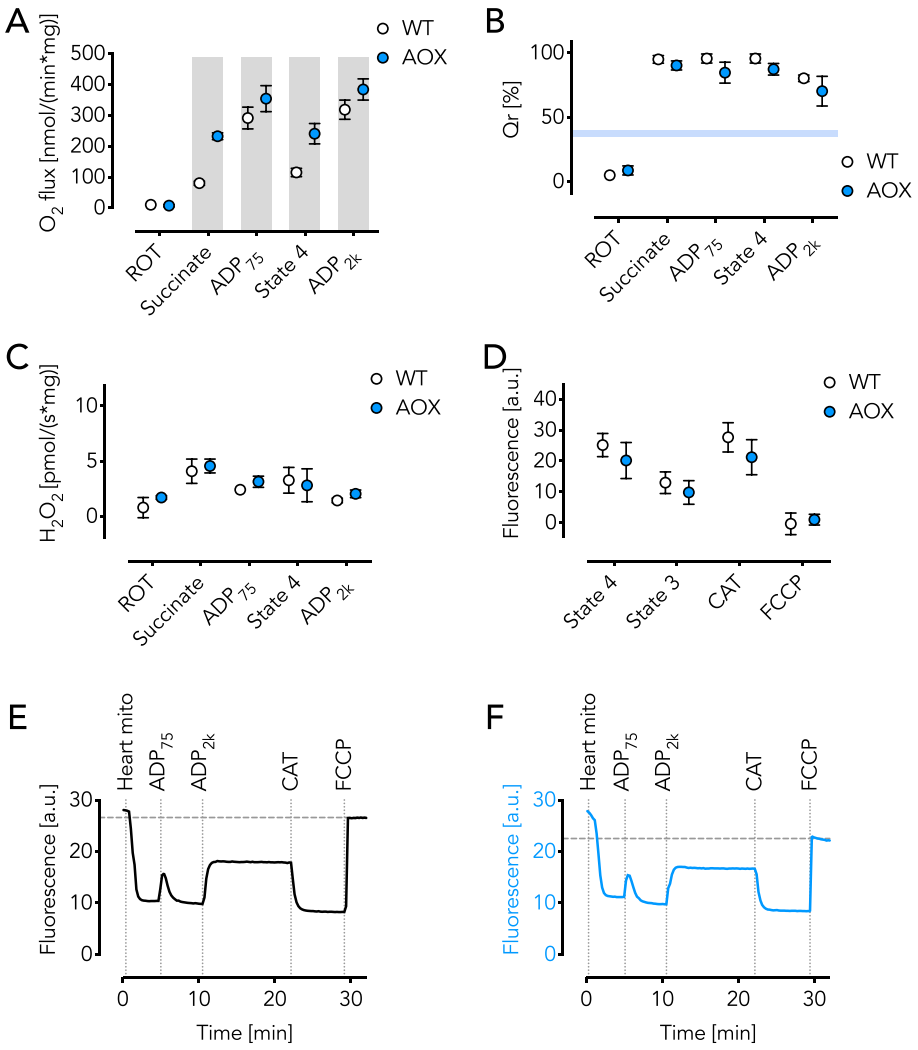

Fig. 3. AOX engages on cII substrate succinate when cI is inhibited. (**A**) Respiratory rates of isolated heart mitochondria shown as mean ± SD, n = 3. ROT, rotenone; ADP in μM. Grey areas indicate significant difference between WT and AOX ($P < 0.05$) analyzed by 2way ANOVA with post-hoc Sidak's multiple comparisons test. (**B**) Qr/Qt ratios (%) shown as mean ± SD, n = 3. Blue horizontal bar represents putative threshold for AOX engagement. (**C**) Hydrogen peroxide production shown as mean ± SD, n = 3. (**D**) Mitochondrial membrane potential ($\Delta\Psi$) using safranin O shown as mean ± SD, n = 3. (**E**) Representative trace showing $\Delta\Psi$ under conditions as indicated in WT mitochondria. (**F**) Representative trace showing $\Delta\Psi$ under conditions as indicated in AOX mitochondria. (For interpretation of the references to color in this figure legend, the reader is referred to the web version of this article.)

described as mainly homo-oligomers of dimers [25]. Indeed, it is unclear thus far, which assembly stoichiometry may constitute the most active AOX form in the mouse *in vivo*. Interestingly, the expression of AOX as dimer was first described for plants and its reduction state was related to its catalytic activity [50]. Later it was proposed that AOX dimerization is common to all AOXs and that such assemblies may be of mechanistic or structural importance [12,51,52]. Respiratory stress may result in the buildup of reducing equivalents within the mitochondrial matrix thereby facilitating the reduction of regulatory residues, *e.g.* cysteines forming disulfide bonds [50]. It is unlikely, however, that this mechanism controls AOX activity in its host *Ciona intestinalis* since this tunicate AOX does not contain the conserved cysteine residues necessary for activation as is the case in plants. How homo-oligomerization of xenotopically expressed tunicate AOX in the mouse affects its catalytic engagement cannot be concluded with absolute certainty to date, however, it is obvious from this and previous studies that a xenotopically expressed tunicate AOX is highly active. Furthermore, apart from the formation of homo-oligomers, AOX association with supercomplexes has never been demonstrated although it is conceivable, albeit unlikely, that the inclusion of digitonin may have removed AOX from high-molecular structures. Altogether, this supports the notion that xenotopically expressed AOX acts as a freely diffusible redox partner. Indeed, when trypansomal AOX was added to submitochondrial particles (SMPs) in the presence of cyanide, respiratory activity was restored [44] from which it was concluded that Q channeling in mitochondrial supercomplexes does not exist. We found, however, that in isolated mouse heart mitochondria respiring on cI substrates in the absence of respiratory inhibitors AOX only marginally affected the RCI suggesting that under these conditions AOX was barely engaged (Fig. 2B). Such a lack of engagement was substantiated by the discovery that in the absence of respiratory inhibitors the Q-pool is insufficiently reduced by cI to maintain AOX activity (Fig. 2C). Addition of respiratory inhibitors, however, engages AOX both under phosphorylating (state 3) [25] and non-phosphorylating (state 4) conditions (Fig. 2E,F; Supplementary Fig. S1A,B) whilst maintaining $\Delta\Psi$ (Fig. 2D). Of course, the measured global Qr/Qt ratio cannot exclude different local Qr/Qt conditions, for instance in a putative compartment within respirasomes between cI and cIII [53]. The fact that AOX and Q are freely diffusible, yet cI substrates do not support high AOX respiration, however, indicate that such high Qr/Qt ratios are not achieved or immediately decreased through oxidation by cIII. Titration of cI activity with AA or Az, however, resulted in an exponential increase in the presence of AOX (Fig. 2F; Supplementary Fig. S1B) suggesting that the pool is accessible to AOX under all Qr/Qt ratios. This is of importance for the biological function of AOX, *e.g.* during stress response. It has recently been shown in its natural host, *Ciona intestinalis*, that AOX transcript levels are upregulated upon exposure to hypoxia and by sulfide, a potent cIV inhibitor, whilst being unresponsive to other environmental stressors such as physiologically stressful temperature or heavy-metal exposure [54]. Here, due to the genetic design, AOX transcript level cannot directly correlate with its catalytic function. In fact, our results explain the lack of a detrimental phenotype when AOX

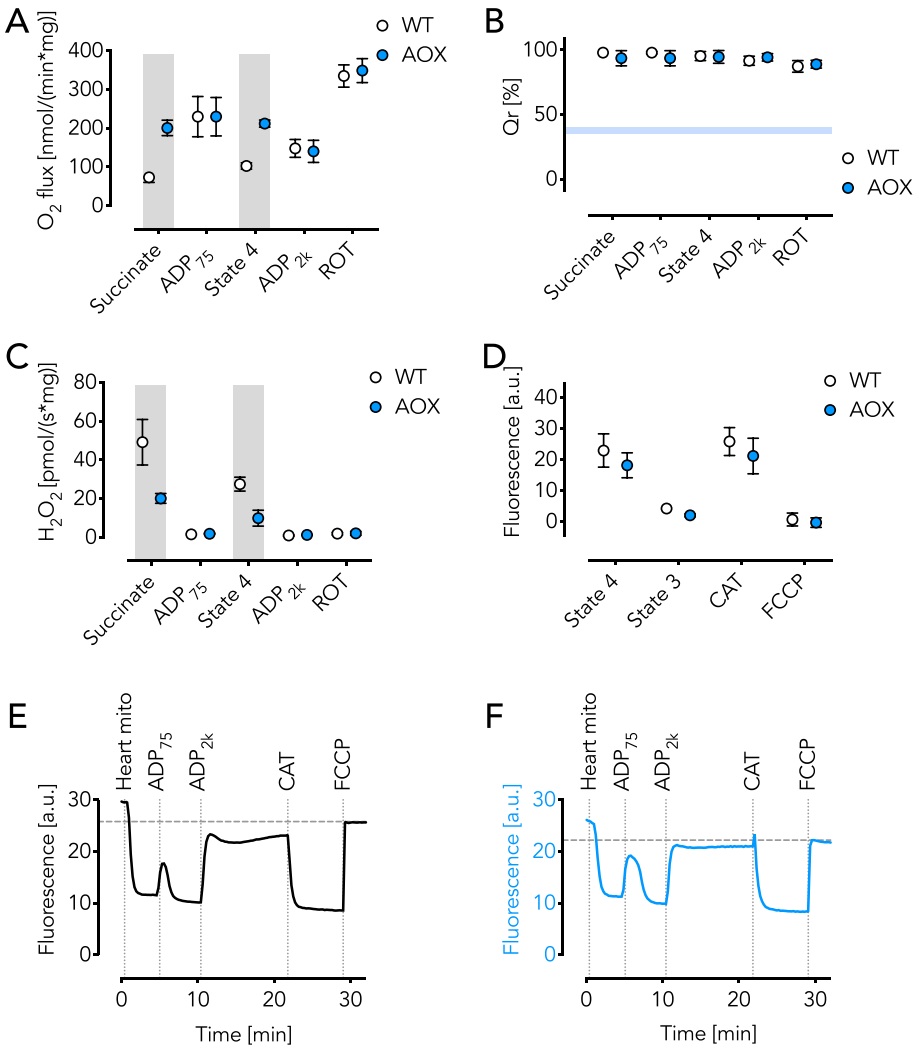

Fig. 4. AOX engages on cII substrate succinate only under non-phosphorylating conditions. (**A**) Respiratory rates of isolated heart mitochondria shown as mean ± SD, n = 3. ADP in μM; ROT, rotenone. Grey areas indicate significant difference between WT and AOX ($P < 0.05$) analyzed by 2way ANOVA with post-hoc Sidak's multiple comparisons test. (**B**) Qr/Qt ratios (%) shown as mean ± SD, n = 3. Blue horizontal bar represents putative threshold for AOX engagement. (**C**) Hydrogen peroxide production shown as mean ± SD, n = 3. Grey areas indicate significant difference between WT and AOX ($P < 0.05$) analyzed by 2way ANOVA with post-hoc Sidak's multiple comparisons test. Note the inverse relation of hydrogen peroxide production and respiratory rate. (**D**) Mitochondrial membrane potential ($\Delta\Psi$) using safranin O shown as mean ± SD, n = 3. Note the lack of membrane potential restoration in state 3. (**E**) Representative trace showing $\Delta\Psi$ under conditions as indicated in WT mitochondria. (**F**) Representative trace showing $\Delta\Psi$ under conditions as indicated in AOX mitochondria. (For interpretation of the references to color in this figure legend, the reader is referred to the web version of this article.)

protein is ubiquitously expressed in the mouse despite its ability to resist cyanide intoxication [24,25].

Although, AOX confers resistance to cyanide, the failure to rescue a COX15 knock-out in mouse skeletal muscle at first appeared somewhat mysterious. However, it may be explained by the fact that under disease and respiratory stress conditions, the metabolic situation is different. One major difference between the acute application of cyanide and the permanent ablation of COX15 is that the long-term disruption of signaling cascades required for mitochondrial biogenesis and muscle repair may outweigh potential benefits such as a decreased ROS load. In contrast, succinate accumulation and RET induction has been described for the post-ischemic heart and sepsis [26,47] and for the latter AOX expression showed beneficial effects [26]. Of note, all aforementioned examples concentrate on a putative effect of AOX on pathophysiologic conditions whilst seemingly ignoring physiological signals originating from the respiratory chain. In fact, some stress responses related to mitochondrial dysfunction viewed as detrimental thus far, such as ROS emitted from COX15 deficient mitochondria [11], are now recognized as essential for adaptive remodeling, mitochondrial biosynthesis and survival. In other words, mitochondrial ROS may be of vital importance for adaptation and thus having physiological relevance. This is specifically true for oxygen sensing in the pulmonary vasculature [55] and glomus cells of the carotid body [56]. In both cases, signals from the respiratory chain are required, and an increase of the Qr/Qt ratio can safely be assumed or has been demonstrated. It is tempting to speculate how AOX would interfere with oxygen sensing in the two cell types considering their specific physiological function and what role succinate may play under such conditions. In an attempt to replicate the above-described metabolic situations, we tested AOX heart mitochondria in the presence of succinate plus ROT (to prevent RET) and observed high respiratory activity even in the absence of ADP which, importantly, was associated with a dramatic decrease in the RCI (also seen as high state 4 respiration in Fig. 3A) suggesting that AOX was engaged. Since cII is generally not present in supercomplex assemblies, the observed respiration is likely based on random collision of the three independent freely diffusible redox partners, *i.e.* cII, the Q pool and AOX. Qr/Qt measurements revealed that in the presence of cII substrate succinate, irrespective of the presence or absence of ROT, another criterion for AOX engagement is fulfilled, namely the presence of high Qr/Qt ratios (Figs. 3B; 4B). In plants, engagement of the alternative respiratory pathway occurs only when Qr/Qt ratios reach critical thresholds of 35–40% (blue horizontal bars in Figs. 2C; 3B; 4B) [27,28]. Previously, *Ciona intestinalis* AOX expressed in mouse skeletal muscle has revealed strikingly similar Qr/Qt values for catalytic engagement [11]. Surprisingly, we found AOX to be regularly engaged during cII respiration under non-phosphorylating (state 4) but not phosphorylating (state 3) conditions although never achieving maximal respiratory rates (Figs. 3A; 4A) suggesting there is some restriction of electron flow. Importantly, our findings demonstrate that any observed restriction of electron flow is not necessarily due to a lack of Q-pool reduction as Qr levels remain high (Figs. 3B; 4B). It may be due to a loss of $\Delta\Psi$ [49] although addition of ADP depolarizes $\Delta\Psi$ which is CAT-

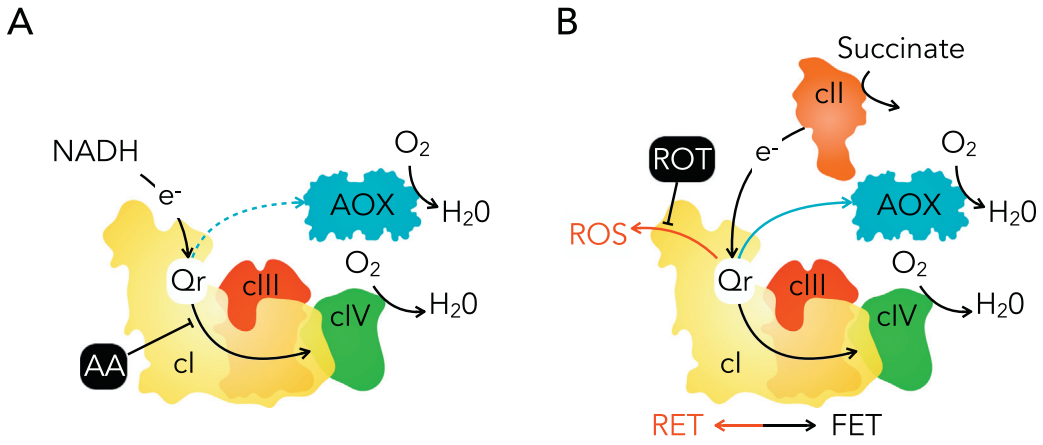

Fig. 5. Graphical overview on AOX engagement. (**A**) cI substrates do not allow AOX respiration unless cIII and/or cIV are inhibited. AA, antimycin A. (**B**) cII substrate succinate readily engages AOX when cI is inhibited (ROT, rotenone) or in the absence of ADP. Note, ROT acts upstream of Q thus being indicative for a cI control mechanism on AOX engagement independent from the Qr/Qt ratio.

insensitive and thus not due to phosphorylation (Figs. 3D–F; 4D–F). Obviously, some electron flux continues to be mediated by cIII as $\Delta\Psi$ is still maintained even with AOX. The finding that electron flux through AOX, in the absence of ROT, is very low may suggest that the regulated element may be cII itself, possibly as a result of oxaloacetate accumulation [49]. If AOX is engaged, however, it supports respiration and abolishes mitochondrial ROS production by RET in a similar manner to ADP addition (Fig. 4A,C). Altogether, our data support the notion that *in vivo* succinate is unlikely to be a major respiratory substrate since a non-phosphorylating respiratory shunt (cII-Q-AOX), would inevitably lead to a severe, non-viable, phenotype which is obviously not the case [25].

Interestingly, the Qr/Qt ratios appear unaffected by any changes of the respiratory state (Figs. 2C; 3B; 4B). Thus, although Qr is fully reduced and potentially accessible to AOX, respiration is low under phosphorylating (state 3) yet high under non-phosphorylating (state 4) conditions (Fig. 4A; Supplementary Fig. S1G). A high electron flux through cII in the presence of oxaloacetate is not likely and contrary to expectations a decrease in the Qr/Qt ratio was not observed. More importantly, when cI substrates were added to the mitochondria we observed an increase in phosphorylating, oligomycin-sensitive, respiration and a decrease in ROS production (Supplementary Fig. S1G,H). Such stimulation, however, is not solely dependent on an increase in $\Delta\Psi$ or electron flow through cI since ROT addition showed the same result (Fig. 4A,C). This finding raises questions regarding the true function of cII *in vivo* in health and disease. We propose that under disease conditions, cII-induced RET may be a pivotal signal for adaptation. Under all other conditions, regular succinate levels in the presence of ADP, RET and FET seem to be restricted by a number of possible factors, including cI presence and, may be, its catalytic activity. The fact that a minimum of 84% of cI is complexed in respiratory supercomplexes [42] suggests that some sort of Q flux control or Q compartmentalization may be potentially a reason for the development of supercomplexes.

In conclusion, xenotopically expressed tunicate AOX is a freely diffusible redox partner in mouse mitochondria which is catalytically active when the Q pool is highly reduced (summarized in Fig. 5). However, respiratory engagement is favored under non-phosphorylating (state 4) conditions generally described as respiratory stress. AOX thus is an invaluable tool to investigate respiratory control mechanisms and may become a treatment option for mitochondriopathies based on respiratory disruption.

Transparency document

The Transparency document associated with this article can be found, in online version.

Acknowledgements

The authors thank Howard T. Jacobs, Pierre Rustin and Massimo Zeviani for valuable discussions and support, and Jana Meisterknecht for excellent technical assistance. This work was supported by: the ERC Advanced Grants 232738 and 322424 to Howard T. Jacobs and Massimo Zeviani, respectively, and Academy of Finland grants 272376 and 256615 to Howard T. Jacobs; the Deutsche Forschungsgemeinschaft (SFB 815/Z1) and the BMBF mitoNET-German Network for Mitochondrial Disorders (01GM1906D) to I.W.; BBSRC (BB/N010051/1) to A.L.M.; and a core grant of the MRC (MC_UU_00015/5) to the Mitochondrial Biology Unit.

Author contributions

M.S. designed and supervised research; M.S., Z.G., E.F.-V., E.D. G.D.-V., T.G., J.H., I.W., C.V., F.N.G., and A.L.M. performed research; M.S., E.F.-V., I.W., E.D., C.V., F.N.G., and A.L.M. compiled and analyzed data; M.S., C.V., F.N.G., and A.L.M. drafted the manuscript with support from all authors.

Declaration of competing interest

M.S. declares himself as a shareholder in a start-up company to develop therapeutics based on alternative oxidase. All other authors declare no competing interests.

Appendix A. Supplementary data

Supplementary data to this article can be found online at https://doi.org/10.1016/j.bbabio.2019.148137.

References

[1] S. DiMauro, E.A. Schon, Mitochondrial disorders in the nervous system, Annu. Rev. Neurosci. 31 (2008) 91–123, https://doi.org/10.1146/annurev.neuro.30.051606.094302.
[2] E. Bertero, C. Maack, Metabolic remodelling in heart failure, Nat. Rev. Cardiol. 15 (2018) 457–470, https://doi.org/10.1038/s41569-018-0044-6.
[3] E. Murphy, H. Ardehali, R.S. Balaban, F. DiLisa, G.W. Dorn, R.N. Kitsis, et al., Mitochondrial function, biology, and role in disease: a scientific statement from the American Heart Association, Circ Res. 118 (2016) 1960–1991, https://doi.org/10.1161/RES.0000000000000104.
[4] A. Gonzalez-Franquesa, M.-E. Patti, Insulin resistance and mitochondrial dysfunction, Adv. Exp. Med. Biol. 982 (2017) 465–520, https://doi.org/10.1007/978-3-319-55330-6_25.
[5] M. Liesa, O.S. Shirihai, Mitochondrial dynamics in the regulation of nutrient utilization and energy expenditure, Cell Metab. 17 (2013) 491–506, https://doi.org/10.1016/j.cmet.2013.03.002.
[6] S.S. Sabharwal, P.T. Schumacker, Mitochondrial ROS in cancer: initiators, amplifiers or an Achilles' heel? Nat. Rev. Cancer 14 (2014) 709–721, https://doi.org/10.1038/nrc3803.
[7] P. Pinton, G. Kroemer, Cancer therapy: altering mitochondrial properties, Nat.

Chem. Biol. 10 (2014) 89–90, https://doi.org/10.1038/nchembio.1440.
[8] W.H. Koppenol, P.L. Bounds, C.V. Dang, Otto Warburg's contributions to current concepts of cancer metabolism, Nat. Rev. Cancer 11 (2011) 325–337, https://doi.org/10.1038/nrc3038.
[9] M. Singer, The role of mitochondrial dysfunction in sepsis-induced multi-organ failure, Virulence. 5 (2014) 66–72, https://doi.org/10.4161/viru.26907.
[10] E.L. Robb, A.R. Hall, T.A. Prime, S. Eaton, M. Szibor, C. Viscomi, et al., Control of mitochondrial superoxide production by reverse electron transport at complex I, J. Biol. Chem. 293 (2018) 9869–9879, https://doi.org/10.1074/jbc.RA118.003647.
[11] S.A. Dogan, R. Cerutti, C. Benincá, G. Brea-Calvo, H.T. Jacobs, M. Zeviani, et al., Perturbed redox signaling exacerbates a mitochondrial myopathy, Cell Metabolism 28 (2018) 764–775.e5, https://doi.org/10.1016/j.cmet.2018.07.012.
[12] A.L. Moore, T. Shiba, L. Young, S. Harada, K. Kita, K. Ito, Unraveling the heater: new insights into the structure of the alternative oxidase, Annu. Rev. Plant Biol. 64 (2013) 637–663, https://doi.org/10.1146/annurev-arplant-042811-105432.
[13] S. DiMauro, M. Hirano, E.A. Schon, Approaches to the treatment of mitochondrial diseases, Muscle Nerve 34 (2006) 265–283, https://doi.org/10.1002/mus.20598.
[14] R. El-Khoury, K.K. Kemppainen, E. Dufour, M. Szibor, H.T. Jacobs, P. Rustin, Engineering the alternative oxidase gene to better understand and counteract mitochondrial defects: state of the art and perspectives, Br. J. Pharmacol. 171 (2014) 2243–2249, https://doi.org/10.1111/bph.12570.
[15] P. Rustin, H.T. Jacobs, Respiratory chain alternative enzymes as tools to better understand and counteract respiratory chain deficiencies in human cells and animals, Physiol. Plant. 137 (2009) 362–370, https://doi.org/10.1111/j.1399-3054.2009.01249.x.
[16] G.A.J. Hakkaart, E.P. Dassa, H.T. Jacobs, P. Rustin, Allotopic expression of a mitochondrial alternative oxidase confers cyanide resistance to human cell respiration, EMBO Rep. 7 (2006) 341–345, https://doi.org/10.1038/sj.embor.7400601.
[17] E.P. Dassa, E. Dufour, S. Goncalves, V. Paupe, G.A.J. Hakkaart, H.T. Jacobs, et al., Expression of the alternative oxidase complements cytochrome c oxidase deficiency in human cells, EMBO Mol. Med. 1 (2009) 30–36, https://doi.org/10.1002/emmm.200900001.
[18] E.P. Dassa, E. Dufour, S. Goncalves, H.T. Jacobs, P. Rustin, The alternative oxidase, a tool for compensating cytochrome c oxidase deficiency in human cells, Physiol. Plant. 137 (2009) 427–434, https://doi.org/10.1111/j.1399-3054.2009.01248.x.
[19] D.J.M. Fernández-Ayala, A. Sanz, S. Vartiainen, K.K. Kemppainen, M. Babusiak, E. Mustalahti, et al., Expression of the Ciona intestinalis alternative oxidase (AOX) in Drosophila complements defects in mitochondrial oxidative phosphorylation, Cell Metab. 9 (2009) 449–460, https://doi.org/10.1016/j.cmet.2009.03.004.
[20] D.M. Humphrey, R.B. Parsons, Z.N. Ludlow, T. Riemensperger, G. Esposito, P. Verstreken, et al., Alternative oxidase rescues mitochondria-mediated dopaminergic cell loss in Drosophila, Hum. Mol. Genet. 21 (2012) 2698–2712, https://doi.org/10.1093/hmg/dds096.
[21] K.K. Kemppainen, J. Rinne, A. Sriram, M. Lakanmaa, A. Zeb, T. Tuomela, et al., Expression of alternative oxidase in Drosophila ameliorates diverse phenotypes due to cytochrome oxidase deficiency, Hum. Mol. Genet. 23 (2014) 2078–2093, https://doi.org/10.1093/hmg/ddt601.
[22] S. Vartiainen, S. Chen, J. George, T. Tuomela, K.R. Luoto, K.M.C. O'Dell, et al., Phenotypic rescue of a Drosophila model of mitochondrial ANT1 disease, Dis. Model. Mech. 7 (2014) 635–648, https://doi.org/10.1242/dmm.016527.
[23] R. El-Khoury, E. Kaulio, K.A. Lassila, D.C. Crowther, H.T. Jacobs, P. Rustin, Expression of the alternative oxidase mitigates beta-amyloid production and toxicity in model systems, Free Radic. Biol. Med. 96 (2016) 57–66, https://doi.org/10.1016/j.freeradbiomed.2016.04.006.
[24] R. El-Khoury, E. Dufour, M. Rak, N. Ramanantsoa, N. Grandchamp, Z. Csaba, et al., Alternative oxidase expression in the mouse enables bypassing cytochrome c oxidase blockade and limits mitochondrial ROS overproduction, PLoS Genet. 9 (2013) e1003182, , https://doi.org/10.1371/journal.pgen.1003182.
[25] M. Szibor, P.K. Dhandapani, E. Dufour, K.M. Holmström, Y. Zhuang, I. Salwig, et al., Broad AOX expression in a genetically tractable mouse model does not disturb normal physiology, Dis. Model. Mech. 10 (2017) 163–171, https://doi.org/10.1242/dmm.027839.
[26] E.L. Mills, B. Kelly, A. Logan, A.S.H. Costa, M. Varma, C.E. Bryant, et al., Succinate dehydrogenase supports metabolic repurposing of mitochondria to drive inflammatory macrophages, Cell 167 (2016) 457–470.e13, https://doi.org/10.1016/j.cell.2016.08.064.
[27] I.B. Dry, A.L. Moore, D.A. Day, J.T. Wiskich, Regulation of alternative pathway activity in plant mitochondria: nonlinear relationship between electron flux and the redox poise of the quinone pool, Arch. Biochem. Biophys. 273 (1989) 148–157.
[28] C. Affourtit, K. Krab, A.L. Moore, Control of plant mitochondrial respiration, Biochim. Biophys. Acta 1504 (2001) 58–69.
[29] M. Fontana-Ayoub, G. Krumschnabel, Laboratory protocol: isolation of mouse heart mitochondria, Mitochondrial Physiology Network. 20.06(01), 2015, pp. 1–2.
[30] I. Wittig, H.-P. Braun, H. Schägger, Blue native PAGE, Nat. Protoc. 1 (2006) 418–428, https://doi.org/10.1038/nprot.2006.62.
[31] I. Wittig, M. Karas, H. Schägger, High resolution clear native electrophoresis for in-gel functional assays and fluorescence studies of membrane protein complexes, Mol. Cell. Proteomics 6 (2007) 1215–1225, https://doi.org/10.1074/mcp.M700076-MCP200.
[32] H. Heide, L. Bleier, M. Steger, J. Ackermann, S. Dröse, B. Schwamb, et al., Complexome profiling identifies TMEM126B as a component of the mitochondrial complex I assembly complex, Cell Metab. 16 (2012) 538–549, https://doi.org/10.1016/j.cmet.2012.08.009.
[33] J. Cox, M. Mann, MaxQuant enables high peptide identification rates, individualized p.p.b.-range mass accuracies and proteome-wide protein quantification, Nat. Biotechnol. 26 (2008) 1367–1372, https://doi.org/10.1038/nbt.1511.
[34] E.W. Deutsch, A. Csordás, Z. Sun, A. Jarnuczak, Y. Perez-Riverol, T. Ternent, et al., The ProteomeXchange consortium in 2017: supporting the cultural change in proteomics public data deposition, Nucleic Acids Res. 45 (2017) D1100–D1106, https://doi.org/10.1093/nar/gkw936.
[35] Y. Perez-Riverol, A. Csordás, J. Bai, M. Bernal-Llinares, S. Hewapathirana, D.J. Kundu, et al., The PRIDE database and related tools and resources in 2019: improving support for quantification data, Nucleic Acids Res. 47 (2019) D442–D450, https://doi.org/10.1093/nar/gky1106.
[36] E. Gnaiger, Bioenergetics at low oxygen: dependence of respiration and phosphorylation on oxygen and adenosine diphosphate supply, Respir. Physiol. 128 (2001) 277–297.
[37] Z.Z. Gizatullina, T.M. Gaynutdinov, H. Svoboda, D. Jerzembek, A. Knabe, S. Vielhaber, et al., Effects of cyclosporine A and its immunosuppressive or non-immunosuppressive derivatives [D-Ser]8-CsA and Cs9 on mitochondria from different brain regions, Mitochondrion. 11 (2011) 421–429, https://doi.org/10.1016/j.mito.2010.12.012.
[38] G. Krumschnabel, M. Fontana-Ayoub, Z. Sumbalova, J. Heidler, K. Gauper, M. Fasching, et al., Simultaneous high-resolution measurement of mitochondrial respiration and hydrogen peroxide production, Methods Mol. Biol. 1264 (2015) 245–261, https://doi.org/10.1007/978-1-4939-2257-4_22.
[39] A.L. Moore, I.B. Dry, J.T. Wiskich, Measurement of the redox state of the ubiquinone pool in plant mitochondria, FEBS Lett. 235 (1988) 76–80, https://doi.org/10.1016/0014-5793(88)81237-7.
[40] F.N. Gellerich, Z. Gizatullina, S. Trumbekaite, B. Korzeniewski, T. Gaynutdinov, E. Seppet, et al., Cytosolic Ca2+ regulates the energization of isolated brain mitochondria by formation of pyruvate through the malate-aspartate shuttle, Biochem J. (2012) 747–755, https://doi.org/10.1042/BJ20110765.
[41] I. Wittig, R. Carrozzo, F.M. Santorelli, H. Schägger, Supercomplexes and subcomplexes of mitochondrial oxidative phosphorylation, Biochim. Biophys. Acta 1757 (2006) 1066–1072, https://doi.org/10.1016/j.bbabio.2006.05.006.
[42] H. Schägger, K. Pfeiffer, The ratio of oxidative phosphorylation complexes I-V in bovine heart mitochondria and the composition of respiratory chain supercomplexes, J. Biol. Chem. 276 (2001) 37861–37867, https://doi.org/10.1074/jbc.M106474200.
[43] A.L. Moore, W.D. Bonner, P.R. Rich, The determination of the proton-motive force during cyanide-insensitive respiration in plant mitochondria, Arch. Biochem. Biophys. 186 (1978) 298–306.
[44] J.G. Fedor, J. Hirst, Mitochondrial supercomplexes do not enhance catalysis by quinone channeling, Cell Metabolism. 28 (2018) 525–531.e4, https://doi.org/10.1016/j.cmet.2018.05.024.
[45] Y. Kido, K. Sakamoto, K. Nakamura, M. Harada, T. Suzuki, Y. Yabu, et al., Purification and kinetic characterization of recombinant alternative oxidase from Trypanosoma brucei brucei, Biochim. Biophys. Acta 1797 (2010) 443–450, https://doi.org/10.1016/j.bbabio.2009.12.021.
[46] A.L. Moore, W.D. Bonner, Measurements of membrane potentials in plant mitochondria with the safranine method, Plant Physiol. 70 (1982) 1271–1276.
[47] E.T. Chouchani, V.R. Pell, E. Gaude, D. Aksentijević, S.Y. Sundier, E.L. Robb, et al., Ischaemic accumulation of succinate controls reperfusion injury through mitochondrial ROS, Nature. 515 (2014) 431–435, https://doi.org/10.1038/nature13909.
[48] F. Scialò, A. Sriram, D. Fernández-Ayala, N. Gubina, M. Lõhmus, G. Nelson, et al., Mitochondrial ROS produced via reverse electron transport extend animal lifespan, Cell Metab. 23 (2016) 725–734, https://doi.org/10.1016/j.cmet.2016.03.009.
[49] F. Bai, B.D. Fink, L. Yu, W.I. Sivitz, Voltage-dependent regulation of complex II energized mitochondrial oxygen flux, PLoS One 11 (2016) e0154982, , https://doi.org/10.1371/journal.pone.0154982.
[50] A.L. Umbach, J.N. Siedow, Covalent and noncovalent dimers of the cyanide-resistant alternative oxidase protein in higher plant mitochondria and their relationship to enzyme activity, Plant Physiol. 103 (1993) 845–854, https://doi.org/10.1104/pp.103.3.845.
[51] T. Shiba, Y. Kido, K. Sakamoto, D.K. Inaoka, C. Tsuge, R. Tatsumi, et al., Structure of the trypanosome cyanide-insensitive alternative oxidase, Proc Natl Acad Sci USA 110 (2013) 4580–4585, https://doi.org/10.1073/pnas.1218386110.
[52] B. May, L. Young, A.L. Moore, Structural insights into the alternative oxidases: are all oxidases made equal? Biochem. Soc. Trans. 45 (2017) 731–740, https://doi.org/10.1042/BST20160178.
[53] G. Benard, B. Faustin, A. Galinier, C. Rocher, N. Bellance, K. Smolkova, et al., Functional dynamic compartmentalization of respiratory chain intermediate substrates: implications for the control of energy production and mitochondrial diseases, Int. J. Biochem. Cell Biol. 40 (2008) 1543–1554, https://doi.org/10.1016/j.biocel.2007.11.023.
[54] S. Saari, G.S. Garcia, K. Bremer, M.M. Chioda, A. Andjelković, P.V. Debes, et al., Alternative respiratory chain enzymes: therapeutic potential and possible pitfalls, Biochim Biophys Acta Mol Basis Dis. (1865) 854–866, https://doi.org/10.1016/j.bbadis.2018.10.012 (2019).
[55] N. Sommer, M. Hüttemann, O. Pak, S. Scheibe, F. Knoepp, C. Sinkler, et al., Mitochondrial complex IV subunit 4 isoform 2 is essential for acute pulmonary oxygen sensing, Circ. Res. 121 (2017) 424–438, https://doi.org/10.1161/CIRCRESAHA.116.310482.
[56] I. Arias-Mayenco, P. González-Rodríguez, H. Torres-Torrelo, L. Gao, M.C. Fernández-Agüera, V. Bonilla-Henao, et al., Acute O2 sensing: role of coenzyme QH2/Q ratio and mitochondrial ROS compartmentalization, Cell Metabolism 28 (2018) 145–158.e4, https://doi.org/10.1016/j.cmet.2018.05.009.
[57] A. Guarás, E. Perales-Clemente, E. Calvo, et al., The CoQH2/CoQ Ratio Serves as a Sensor of Respiratory Chain Efficiency, Cell Rep 15 (2016) 197–209.

7.3 N. Sommer *et al.*, *Sci Adv*. **6**, eaba0694 (2020)

HEALTH AND MEDICINE

Bypassing mitochondrial complex III using alternative oxidase inhibits acute pulmonary oxygen sensing

Natascha Sommer[1], Nasim Alebrahimdehkordi[1], Oleg Pak[1], Fenja Knoepp[1], Ievgen Strielkov[1], Susan Scheibe[1], Eric Dufour[2], Ana Andjelković[2], Akylbek Sydykov[1], Alireza Saraji[1], Aleksandar Petrovic[1], Karin Quanz[1], Matthias Hecker[1], Manish Kumar[1], Joel Wahl[3], Simone Kraut[1], Werner Seeger[1], Ralph T. Schermuly[1], Hossein A. Ghofrani[1,4], Kerstin Ramser[3], Thomas Braun[5], Howard T. Jacobs[2], Norbert Weissmann[1]*, Marten Szibor[2]*†

Mitochondria play an important role in sensing both acute and chronic hypoxia in the pulmonary vasculature, but their primary oxygen-sensing mechanism and contribution to stabilization of the hypoxia-inducible factor (HIF) remains elusive. Alteration of the mitochondrial electron flux and increased superoxide release from complex III has been proposed as an essential trigger for hypoxic pulmonary vasoconstriction (HPV). We used mice expressing a tunicate alternative oxidase, AOX, which maintains electron flux when respiratory complexes III and/or IV are inhibited. Respiratory restoration by AOX prevented acute HPV and hypoxic responses of pulmonary arterial smooth muscle cells (PASMC), acute hypoxia-induced redox changes of NADH and cytochrome c, and superoxide production. In contrast, AOX did not affect the development of chronic hypoxia-induced pulmonary hypertension and HIF-1α stabilization. These results indicate that distal inhibition of the mitochondrial electron transport chain in PASMC is an essential initial step for acute but not chronic oxygen sensing.

INTRODUCTION

Hypoxic pulmonary vasoconstriction (HPV) is a vital response mechanism that diverts pulmonary blood flow away from poorly ventilated to well-ventilated lung alveoli, thereby optimizing arterial oxygenation under conditions of local alveolar hypoxia (*1*, *2*). Disturbed or inappropriate HPV may cause life-threatening oxygen deprivation, for instance during anesthesia, pneumonia, adult respiratory distress syndrome, septic events, or liver failure. It also contributes to the development of high-altitude pulmonary edema. Under global alveolar hypoxia, HPV can also cause an increase in pulmonary vascular pressure. This occurs naturally in the hypoxic lungs of the unborn fetus, and inappropriate continuation of HPV after birth causes persistent pulmonary hypertension (PH) of the newborn, which is associated with significant mortality and morbidity (*3*). HPV also contributes to the development of PH caused by chronic hypoxia-induced pulmonary vascular remodeling, which can eventually lead to right heart failure (*4*).

Recently, we provided evidence that acute HPV may be regulated by a central oxygen sensor within the mitochondrial respiratory chain, which depends on the presence of the mitochondrial complex IV [cIV; cytochrome c (Cyt c) oxidase] subunit 4 isoform 2 (Cox4i2) (*5*). We were able to demonstrate that acute hypoxia induces Cox4i2-dependent mitochondrial hyperpolarization, leading to increased mitochondrial superoxide release from the respiratory complex III (cIII; ubiquinol:Cyt c oxidoreductase) and/or complex I [cI; reduced form of nicotinamide adenine dinucleotide (NADH):ubiquinone oxidoreductase] with subsequent inhibition of cellular potassium channels (K_V), cellular membrane depolarization, and activation of voltage-gated calcium channels, resulting in intracellular calcium increase and HPV. Similarly, we found that chronic hypoxia results in mitochondrial membrane hyperpolarization (*6*) and K_V channel inhibition (*7*), leading to a proliferative and antiapoptotic phenotype of pulmonary arterial smooth muscle cells (PASMC). However, the underlying mechanism for these alterations remains elusive. In particular, it remains unclear whether inhibition of mitochondrial respiration by oxygen deprivation at cIV could act as the actual trigger for HPV under acute hypoxia, as HPV is caused already by mild hypoxia at oxygen levels at which cIV oxygen affinity should overcome inhibitory consequences. Moreover, the downstream signaling consequences are still under debate and decreased reactive oxygen species (ROS) release from cI (*8*) during acute hypoxia contrasts to the concept of increased ROS from cIII being the major cause (*9*). Conversely, there is broad consensus that chronic hypoxia inhibits mitochondrial respiration regulated by hypoxia-inducible factor 1α (HIF-1α)–dependent gene expression. HIF-1α stabilization, in turn, has been suggested to depend on mitochondrial ROS release. We, thus, investigated (i) whether HPV and chronic hypoxia-induced PH and HIF-1α stabilization are prompted by hypoxia-induced inhibition of mitochondrial respiration, (ii) the mechanisms of downstream signaling of the mitochondrial respiratory chain, and (iii) whether partial restoration of mitochondrial respiration by expression of alternative oxidase (AOX) could prevent HPV and hypoxia-induced PH.

To this end, we made use of a mouse model ubiquitously expressing *Ciona intestinalis* AOX (*10*), hereafter referred to as AOX mouse. Many organisms, including plants and some metazoans, but not insects and mammals, have AOX, which branches the mitochondrial respiratory chain when electron flux through cIII and cIV is impaired and the quinone pool is highly reduced (*11*, *12*). Under such conditions, AOX accepts electrons from ubiquinol and directly reduces

[1]Excellence Cluster Cardio-Pulmonary Institute (CPI), University of Giessen and Marburg Lung Center (UGMLC), Member of the German Center for Lung Research (DZL), Justus-Liebig-University, Giessen, D-35392 Giessen, Germany. [2]Faculty of Medicine and Health Technology, Tampere University, FI-33014 Tampere, Finland. [3]Department of Engineering Sciences and Mathematics, Luleå University of Technology, SE-97187 Luleå, Sweden. [4]Department of Medicine, Imperial College London, Du Cane Road, Hammersmith Campus, London W12 0NN, UK. [5]Department I, Cardiac Development and Remodelling, Max Planck Institute for Heart and Lung Research, D-61231 Bad Nauheim, Germany.
*Corresponding author. Email: marten.szibor@tuni.fi (M.S.); norbert.weissmann@innere.med.uni-giessen.de (N.W.)
†Present address: Department of Cardiothoracic Surgery, Jena University Hospital, D-07747 Jena, Germany.

oxygen to water in a thermogenic reaction. AOX thus prevents overreduction of the mitochondrial quinone pool and the resulting excess ROS production and maintains the activity of the Krebs cycle. Despite its enzymatic function, AOX expression alone does not disturb normal mouse physiology (*10*, *13*). However, it is able to correct pathological states associated with respiratory inhibition, notably those affecting cIII and/or cIV (*10*, *13*–*16*). This makes AOX a valuable tool to study the involvement of mitochondria and their hierarchy in physiological and pathophysiological processes affecting health and disease (*17*–*19*).

RESULTS

AOX is expressed in the pulmonary vasculature and inhibits HPV under acute hypoxia

We first verified widespread AOX expression in the lung, including the vasculature and airways (Fig. 1A), and then tested the effects of AOX on cyanide- (fig. S1) and hypoxia-induced vasoconstriction (Fig. 1B). Vasoconstriction was quantified as the increase in pulmonary arterial pressure (ΔPAP) in isolated, ventilated lungs perfused with buffer at constant flow. In wild-type (WT) lungs, ΔPAP reached a maximum value after 10 min of hypoxic ventilation (acute HPV), transiently decreasing before rising again under prolonged hypoxia of up to 3 hours (sustained HPV) (Fig. 1B). AOX-expressing lungs showed inhibition of HPV under acute hypoxia (Fig. 1B) and a diminished PAP response in the presence of cyanide (fig. S1). HPV inhibition by AOX was confirmed using the AOX-specific inhibitor n-propyl gallate (nPG). The presence of nPG during 10 min of hypoxic ventilation abrogated the AOX effect and restored HPV (Fig. 1C). To verify that the effect of AOX was not due to nonspecific lung damage and/or impaired calcium signaling, we stimulated isolated lungs with the hypoxia-independent vasoconstrictor U46619, a thromboxane mimetic. WT and AOX lungs responded similarly to U46619 (Fig. 1D), with an increase in PAP indicating intact pulmonary vasculature physiology, showing the AOX effect to be specific to HPV and, thus, oxygen-dependent vasoconstriction.

Moreover, there was no difference between isolated WT and AOX-overexpressing lungs with regard to postischemic endothelial damage during ischemia-reperfusion, measured as the increase in capillary filtration rate (Kfc; Fig. 1E) and gain of lung weight (Fig. 1F). These results support the conclusion that AOX expression in murine lungs specifically inhibited the response of the pulmonary vasculature to acute and sustained hypoxia and, notably, implicate different underlying mechanisms in ischemia-reperfusion injury.

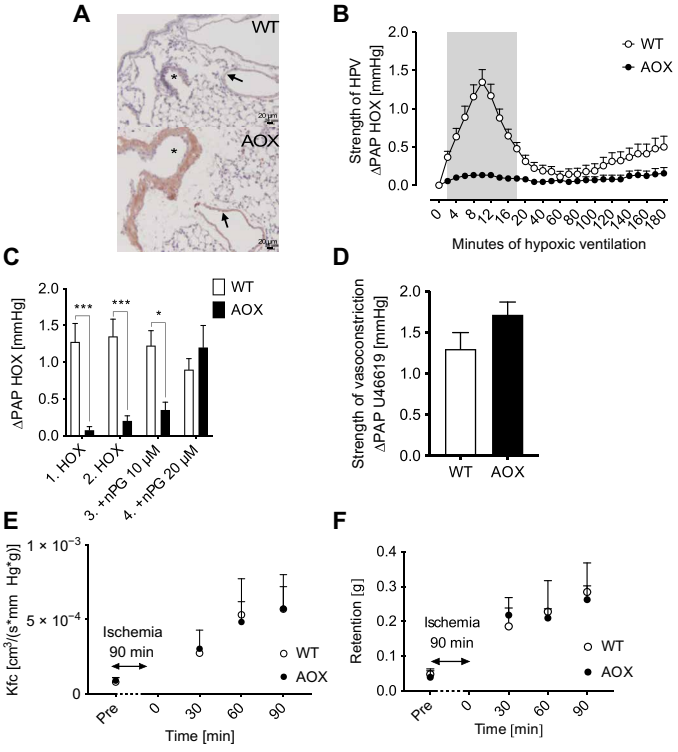

Fig. 1. Acute HPV is absent in AOX-expressing isolated murine lungs. (**A**) AOX protein expression detected as brownish color in bronchial walls (*) and pulmonary arteries (arrows). (**B**) PAP response of isolated, buffer-perfused WT and AOX murine lungs ventilated with 1% O_2 for time as indicated. Data are shown as means ± SEM of $n = 9$ experiments. Gray area indicates significant difference with $P < 0.05$ tested by multiple t tests. (**C**) PAP response to hypoxic (HOX; 1% O_2) challenge with and without AOX inhibitor nPG applied 5 min before sequential HOX. Data are shown as means ± SEM of $n = 4$ experiments. *$P < 0.05$, ***$P < 0.001$ for comparison as indicated, analyzed by two-way analysis of variance (ANOVA) and Sidak's multiple comparisons test. (**D**) PAP response to pulmonary artery infusion of the thromboxane mimetic U46619. Data are shown as means ± SEM of $n = 6$ experiments. (**E**) Kfc after 90 min of ischemia. Data are shown as means ± SEM of $n = 3$ experiments. (**F**) Lung weight gain (retention) during reperfusion after 90 min of ischemia. Data are shown as means ± SEM of $n = 3$ experiments.

AOX decreases hypoxia-induced cellular membrane depolarization in PASMC

We next investigated the hypoxia response in isolated PASMC. Since cellular membrane depolarization is an essential step in HPV signaling, upstream of cytoplasmic calcium increase but downstream of superoxide release, we measured cellular membrane potential by patch clamp analysis. In WT PASMC, cellular membrane potential was increased upon exposure to hypoxia (Fig. 2, A and C). By contrast, the hypoxic response in AOX PASMC was blunted (Fig. 2, B and D), with the membrane potential reaching a lower plateau level than in WT (Fig. 2E). AOX inhibition by nPG renormalized membrane depolarization (Fig. 2, B, D, and E), while the basal membrane potential did not differ between WT and AOX PASMC (Fig. 2, C and D). Again, this indicates that AOX, by accepting electrons from ubiquinol, specifically interferes with the hypoxic signal originating from mitochondria, leaving general cellular physiology unaffected.

To test this assumption in a more physiological context, we measured hypoxia-induced vasoconstriction of pulmonary arterial vessels, which was again prevented by AOX (Fig. 2F). However, vasoconstriction was restored in isolated vessels expressing AOX when perfused with potassium chloride (Fig. 2, F and G). Moreover, we observed that addition of potassium chloride to the perfusate in isolated AOX lungs also restored HPV (Fig. 2H). This indicates that mitochondria, and specifically the electron flux through the respiratory chain, lie upstream of potassium channel inhibition in the hierarchy of acute HPV signaling, and reveals that other minor hypoxia-dependent processes must contribute to reaching the threshold of depolarization necessary to trigger HPV.

AOX inhibits hypoxia-induced mitochondrial superoxide release and membrane hyperpolarization in PASMC

Since a hallmark of impaired electron flux through the respiratory chain is the production of ROS and reactive nitrogen species (RNS),

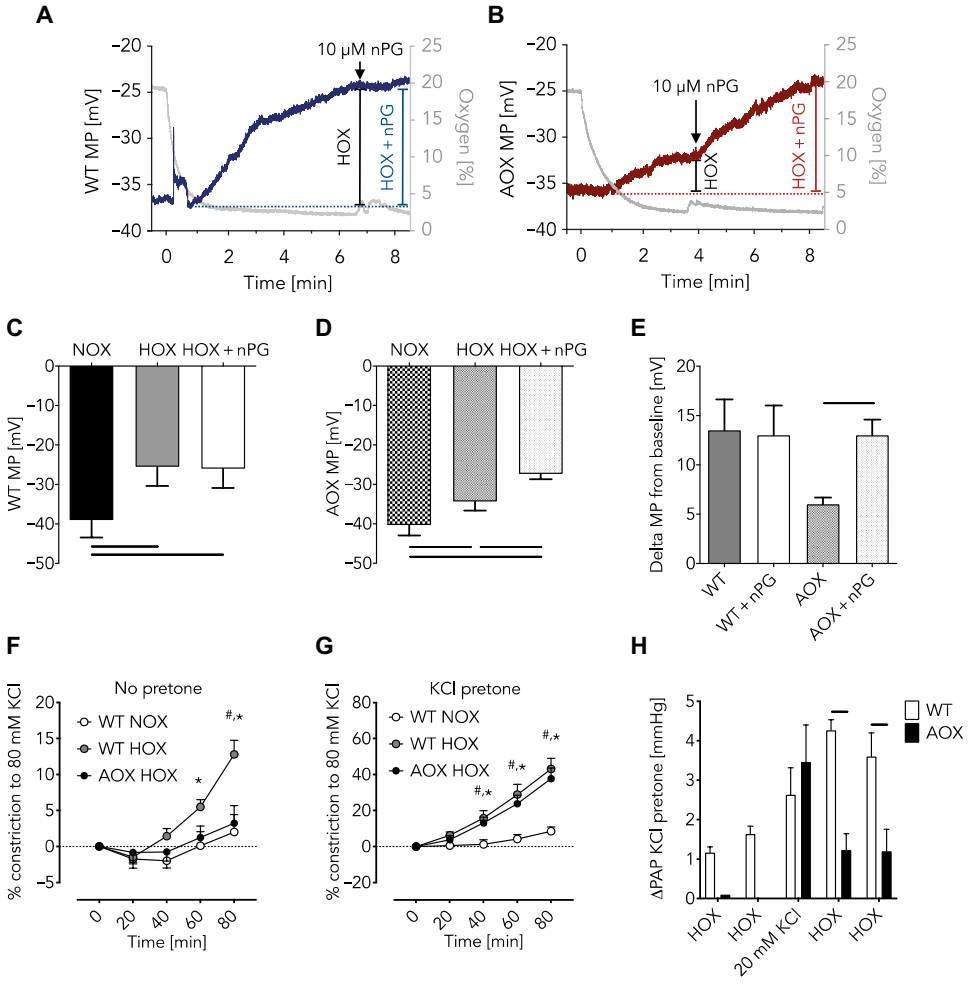

Fig. 2. Hypoxia-induced cellular membrane depolarization is decreased in AOX-expressing PASMC. (**A** and **B**) Representative traces of patch clamp measurements to determine cellular membrane potential (MP) during acute HOX (1% O_2) in mouse WT (A) and AOX (B) PASMC. Gray traces depict oxygen concentration in %; blue (WT) and red (AOX) traces indicate MP in millivolts. Addition of AOX inhibitor nPG as indicated. Cellular MP in mouse WT (**C**) and AOX (**D**) PASMC during normoxia (NOX) and acute HOX or acute HOX plus nPG. (**E**) Change of cellular MP compared with NOX in the absence and presence of nPG as indicated. Data of (C) to (E) shown as means ± SEM of $n = 6$ experiments. Horizontal bars indicate significant difference with $P < 0.05$ analyzed by repeated-measures one-way ANOVA and Tukey's multiple comparisons test. (**F**) Vasoconstriction of isolated pulmonary arteries during superfusion with hypoxic (1% O_2) or normoxic KCl-free buffer shown as % of response to 80 mM KCl. Data are shown as means ± SEM of $n = 8$ experiments. *$P < 0.05$ WT NOX versus WT HOX; #$P < 0.05$ WT HOX versus AOX HOX analyzed by two-way ANOVA and Tukey's multiple comparisons test. (**G**) Vasoconstriction as in (F) but in the presence of ~20 mM KCl. Data are shown as means ± SEM of $n = 8$ experiments. *$P < 0.05$ WT NOX versus WT HOX; #$P < 0.05$ WT NOX versus AOX HOX analyzed by two-way ANOVA and Tukey's multiple comparisons test. (**H**) PAP response of isolated WT and AOX lungs during HOX (10% O_2) ventilation before and after infusion of 20 mM KCl. Data are shown as means ± SEM of $n = 3$ experiments. Horizontal bars indicated significant difference with $P < 0.05$ analyzed by two-way ANOVA and Sidak's multiple comparisons test.

we tested whether ROS/RNS are the mitochondrial signals that trigger HPV. We measured ROS/RNS release in hypoxia-exposed snap-frozen mouse PASMC using the spin probe CMH (1-hydroxy-3-methoxycarbonyl-2,2,5,5-tetramethylpyrrolidine) with electron spin resonance (ESR) spectroscopy (Fig. 3A). To determine the proportion of superoxide within the total ROS/RNS load, we incubated parallel samples with polyethylene glycol–conjugated superoxide dismutase (pSOD) (Fig. 3, A and B). Superoxide levels increased under hypoxic conditions in WT but not in AOX PASMC. To validate this finding, we expressed either native AOX or a catalytically inactive mutant AOX (*20*) in WT mouse PASMC. Only the inactive mutant AOX showed a hypoxia-dependent increase in superoxide (Fig. 3C). To investigate the mechanism behind increased superoxide production, we measured the mitochondrial membrane potential ($\Delta\psi$), which was increased in WT but not in AOX PASMC during superfusion with hypoxic medium (Fig. 3, D and E). We also assayed the oxygen dependence of mitochondrial respiration, in this case using transfected rat PASMC (rPASMC) to obtain sufficient material. rPASMC transfected with an AOX expression plasmid or with empty vector both showed decreased respiration under oxygen deprivation. However, at low oxygen concentrations, AOX-expressing rPASMC had slightly, but significantly, higher oxygen consumption than the control (Fig. 3F). These data confirm that AOX is catalytically engaged during acute hypoxic inhibition of the respiratory chain,

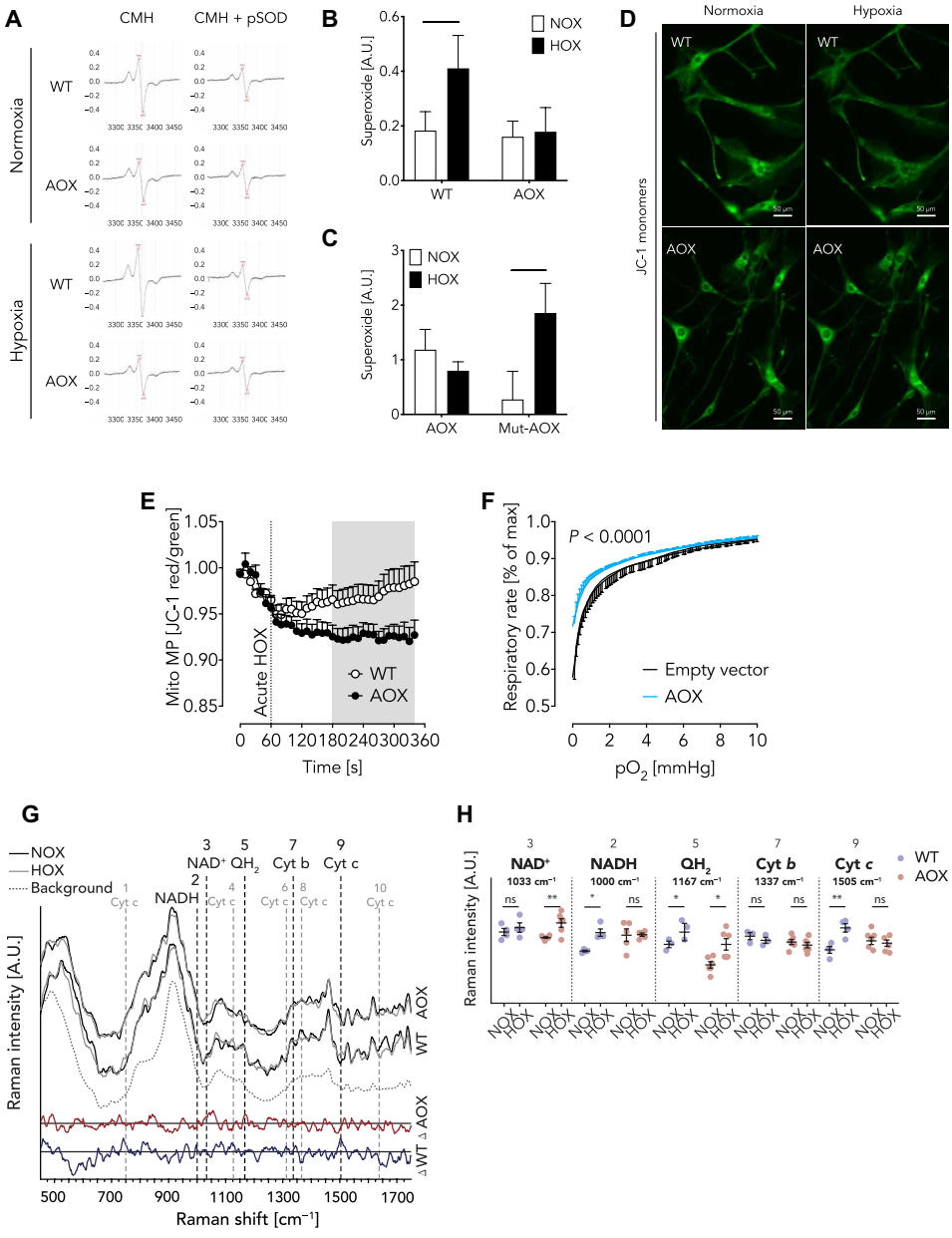

Fig. 3. AOX inhibits hypoxia-induced superoxide release and mitochondrial membrane hyperpolarization in PASMC and affects the redox state of mitochondrial biomarkers. (**A**) Representative ESR spectra from mouse WT and AOX PASMC using the probe CMH and pSOD for control. (**B**) Superoxide production in mouse WT and AOX PASMC during exposure to normoxia (NOX) and hypoxia (HOX, 1% O_2) for 5 min. A.U., arbitrary units. Data are shown as means ± SEM of $n = 4$ experiments. The horizontal bar indicates significant difference with $P < 0.05$ analyzed by two-way ANOVA and Sidak's multiple comparisons test. (**C**) Superoxide production in WT mouse PASMC transfected with plasmids encoding native Ciona AOX or a catalytically inactive mutant AOX exposed to NOX and HOX. Data are shown as means ± SEM of $n = 12$ experiments. The horizontal bar indicates significant difference with $P < 0.05$ analyzed by two-way ANOVA and Sidak's multiple comparisons test. No significant differences were detected between the genotypes. Data in (B) and (C) are depicted as the portion of CMH signal inhibited by pSOD. (**D**) Representative mouse WT and AOX PASMC stained with JC-1 under normoxia and hypoxia (1% O_2) as indicated. (**E**) Mitochondrial MP (Mito MP) determined as JC-1 red/green ratio under acute HOX as indicated. Data are shown as means ± SEM of $n = 10$ (WT) and $n = 12$ (AOX) experiments. Gray area depicts significant difference with $P < 0.05$ analyzed by two-way ANOVA and uncorrected Fisher's least significant difference (LSD). (**F**) Oxygen-dependent respiratory rate of 100,000 to 300,000 intact rPASMC per experiment transfected with an empty vector or AOX encoding plasmid. Data are shown as means ± SEM in % of rate at normoxia (max) with $P < 0.0001$ indicating significant difference between WT and AOX analyzed by paired t test. (**G**) Normalized fluorescence-corrected Savitzky-Golay reconstructed Raman spectra taken from WT ($n = 4$) and AOX ($n = 6$) PASMC before (black line = NOX) and after (gray line) exposure to acute hypoxia (HOX, 5% O_2). Background spectrum from microfluidic system and buffer solution is shown as dashed line ($n = 25$). Differences between NOX and HOX are highlighted with a difference spectrum for each corresponding sample type (WT, blue; AOX, red). Peak locations for mitochondrial biomarkers NAD^+ (3: 1033 cm^{-1}), NADH (2: 1000 cm^{-1}), ubiquinol (QH_2; 5: 1167 cm^{-1}), and cytochrome b (Cyt b; 7: 1337 cm^{-1}) as well as peaks associated with reduced (1: 750 cm^{-1}; 4: 1127 cm^{-1}; 6: 1313 cm^{-1}; 9: 1505 cm^{-1}) and oxidized forms of Cyt c (8: 1369 cm^{-1}; 10: 1638 cm^{-1}) are shown as vertical dashed lines. (**H**) Raman intensity for individual biomarkers are shown as means ± SEM of $n \geq 3$ experiments. ns, not significant. *$P < 0.05$; **$P < 0.01$; ***$P < 0.001$ analyzed by two-way ANOVA and uncorrected Fisher's LSD.

thereby affecting, besides ROS production, the mitochondrial redox state and accumulation of Krebs cycle intermediates.

AOX affects the mitochondrial redox state

In respiring mitochondria, the redox state of the individual chain complexes is highly dynamic and depends particularly on oxygen supply. Accordingly, hypoxic inhibition at cIV should impair electron flux in WT PASMC, thereby reducing the individual mitochondrial complexes and ultimately resulting in an increased cellular NADH/NAD^+ ratio. Since AOX branches the mitochondrial chain when electron flux through cIII and cIV is impaired (*14*), we hypothesized that both the redox state of mitochondrial complexes downstream of AOX and the NADH/NAD^+ ratio would be unaffected by hypoxic challenge in AOX PASMC. To test this hypothesis, we performed Raman spectroscopy, which allows the redox state of individual mitochondrial complexes and NADH/NAD^+ ratios to be simultaneously studied in single living PASMC (*21*–*25*). As expected, acute hypoxia shifted NADH, ubiquinol (QH_2), and Cyt c in WT PASMC toward a more reduced state (Fig. 3, G and H, and fig. S2, A and B). The redox state of cytochrome b (Cyt b) was unaltered, which is indicative for an electron leak at cIII. In accordance with our hypothesis, no change in redox state at cIII (Cyt b) and cIV (Cyt c) was observed in AOX PASMC (Fig. 3H and fig. S2B), consistent with a bypass of electrons from reduced ubiquinol to AOX. Furthermore, NAD^+, but not NADH levels, increased upon hypoxia (Fig. 3H). These findings further support the concept of AOX being catalytically engaged in acute hypoxic inhibition and suggest that NADH is the respective electron donor for mitochondrial respiration through AOX.

AOX does not affect adaptation processes upon chronic hypoxia

Notably, mitochondrial impairment has also been identified as an underlying mechanism for chronic hypoxia-induced PH (*26*), a life-threatening disease occurring, for example, at high altitude. To test whether AOX expression can also prevent the adverse effects of generalized chronic hypoxia, we exposed WT and AOX mice to 4 weeks of hypoxia (10% O_2). In contrast to expectations, both WT and AOX mice developed PH to a similar degree, with similar alterations in right ventricular systolic pressure (Fig. 4A), right ventricular hypertrophy (Fulton index; Fig. 4B), cardiac output (Fig. 4C), and

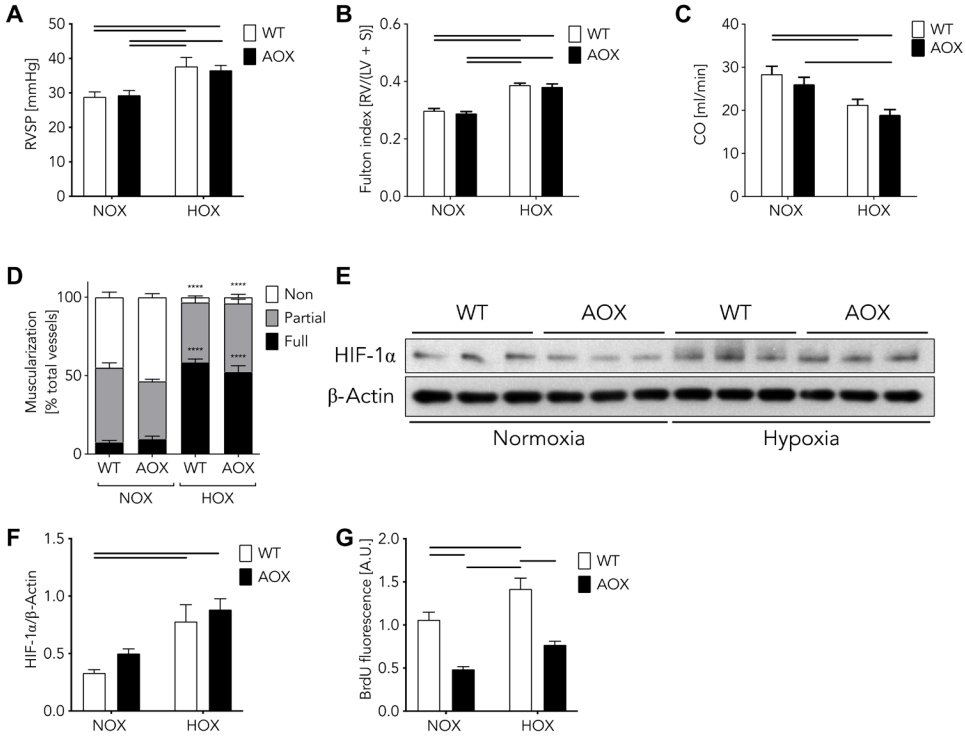

Fig. 4. Adaptation processes upon chronic hypoxia in WT and AOX transgenic mice. (**A**) Right ventricular systolic pressure (RVSP) after normoxia (NOX) or hypoxia (HOX, 10% O_2) for 28 days. Data are shown as means ± SEM of $n \geq 9$ experiments. Horizontal bars indicate significant difference with $P < 0.05$ analyzed by two-way ANOVA and Tukey's multiple comparisons test. (**B**) Ratios of right ventricle (RV) and left ventricle (LV) plus septum (S) (Fulton index). Data are shown as means ± SEM of $n = 10$ experiments. Horizontal bars indicate significant difference with $P < 0.05$ analyzed by two-way ANOVA and Tukey's multiple comparisons test. (**C**) Cardiac output (CO) measured by echocardiography. Data are shown as means ± SEM of $n = 10$ experiments. Horizontal bars indicate significant difference with $P < 0.05$ analyzed by two-way ANOVA and Tukey's multiple comparisons test. (**D**) Vascular remodeling quantified as degree of muscularization of small (20- to 70-μm diameter) pulmonary arterial vessels. Vessel muscularization categorized as non, partial, or full after immunostaining against α-smooth muscle actin as marker for PASMC and von Willebrand factor to discard endothelium. Data are shown as means ± SEM of $n \geq 4$ experiments. ****$P < 0.0001$ NOX versus HOX analyzed by two-way ANOVA and Tukey's multiple comparisons test. Note, no difference observed between WT versus AOX. (**E**) Western blots showing HIF-1α and β-actin expression in WT and AOX transgenic PASMC under normoxia and hypoxia. (**F**) Quantification of protein expression shown in (E). Data are shown as means ± SEM of $n = 3$ experiments. Horizontal bars indicate significant difference with $P < 0.05$ analyzed by two-way ANOVA and Sidak's multiple comparisons test. (**G**) Proliferation assay of WT and AOX PASMC cultured under normoxia (NOX) or hypoxia (HOX, 1% O_2) for 48 hours. Data are shown as means ± SEM of $n = 9$ experiments. Horizontal bars indicate significant difference with $P < 0.05$ analyzed by two-way ANOVA and Tukey's multiple comparisons test. BrdU, bromodeoxyuridine.

pulmonary vascular muscularization (Fig. 4D). Also, we failed to find an advantage of expressing AOX in other cardiac and/or systemic parameters characterizing the response to hypoxia (figs. S3 and S4). HIF-1α expression was similarly increased in PASMC of both strains after 3 days of hypoxia (1% O_2; Fig. 4, E and F), indicating that, at least under these conditions, mitochondrial ROS are not a relevant trigger for HIF-1α stabilization. By contrast, PASMC proliferation was induced by hypoxia in both strains, but its level was generally lower in the presence of AOX (Fig. 4G).

DISCUSSION

Our data substantiate the concept that an increase in superoxide production at cIII is an essential trigger for the HPV signaling cascade, as bypassing cIII during acute hypoxia by AOX inhibits HPV and hypoxia-induced responses in PASMC (summarized in Fig. 5). Going beyond, we demonstrate that inhibition of the electron flux distal from the quinone pool and, most likely, at the level of cIV results in electron accumulation at the electron transport chain, which may promote superoxide release from cIII. Restoration of even a small amount of electron flux by bypassing cIII and cIV with AOX is sufficient to prevent HPV. These findings indicate that the mitochondrial respiratory chain can be the primary step in acute hypoxia signaling in the lung, resulting in HPV. Moreover, bypassing the Cox4i2 isoform of cIV as the oxygen-sensitive mitochondrial component at the head of the pathway, which we previously showed to be essential for hypoxia-induced ROS release and mitochondrial hyperpolarization (*5*), may inhibit hypoxic signaling. Last, our data show that distinct mechanisms underlie acute and chronic oxygen sensing and signaling in the pulmonary vasculature.

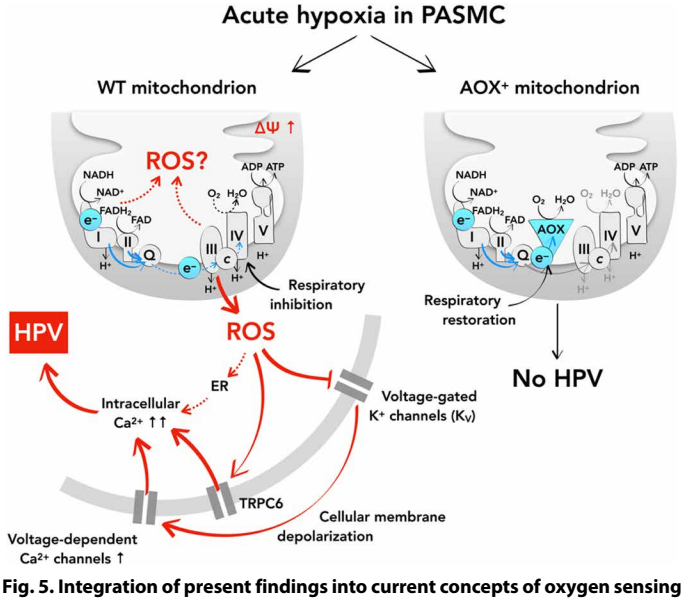

Fig. 5. Integration of present findings into current concepts of oxygen sensing and HPV in the murine lung. Acute HPV depends on a central oxygen sensor within the mitochondrial respiratory chain. Hypoxia induces mitochondrial membrane hyperpolarization, an increase in mitochondrial superoxide release, and subsequent inhibition of cellular potassium channels (K_V), which leads to cellular membrane depolarization and activation of voltage-gated calcium channels. This sequence of events results in intracellular calcium increase and HPV. AOX prevents HPV in mouse PASMC by preventing mitochondrial ROS production and release. This places mitochondria and electron flux through the mitochondrial respiratory chain at the top level in the hierarchy of oxygen sensing and signaling controlling HPV. ADP, adenosine diphosphate; FAD, flavin adenine dinucleotide.

It has been suggested that ROS release from cIII into the intermembrane space could be the essential step in HPV (*27*, *28*). Our previous findings implicating a cIV subunit in hypoxia signaling and cellular membrane depolarization (*5*) were consistent with this hypothesis, but the initial triggering mechanism of acute hypoxia remained unclear. In the present study, we found that AOX, which is catalytically engaged only when the quinone pool is sufficiently reduced (*11*), can prevent mitochondrial membrane hyperpolarization, increased superoxide production, and consequent hypoxic signaling. Thus, distal mitochondrial respiratory inhibition and electron flux stalling may act as the initial step in HPV, resulting either in electron accumulation at the quinone pool or the Krebs cycle. As AOX supports electron flux in PASMC under low-oxygen conditions that are sufficient to trigger HPV, accumulation of electrons (and thus the hypoxic signaling) is inhibited. A limitation of the current approach using AOX is that one cannot conclude from its effect alone whether the exact source of the excess ROS is cI, cIII, or both. However, we are not aware of any study proposing an increase in ROS formation from cI as a trigger of HPV. Moreover, we cannot exclude that a hypoxia-induced increase or decrease in Krebs cycle intermediates also contributes to the inhibition of hypoxic signaling by AOX. Furthermore, Cox4i2-dependent mitochondrial hyperpolarization may be inhibited as a result of bypassing cIII/cIV. Although the underlying mechanism is not fully elucidated, mitochondrial hyperpolarization may be downstream of ROS, or more distant mechanisms such as glycolytic adenosine triphosphate (ATP) production may contribute to hyperpolarization. Consistent with our study, AOX has previously been shown to decrease mitochondrial ROS production in mouse tissues and cells under various conditions (*10*, *13*, *15*, *16*). Despite the possibility of multiple trigger mechanisms, the prominent role of hypoxia-induced superoxide release from cIII has been demonstrated previously using the specific cIII inhibitor S3QEL2 (*29*), which was shown to prevent HPV (*5*). This finding is now substantiated by our investigation, using AOX. Moreover, knockdown of subunits of cIII was demonstrated to inhibit acute hypoxia-induced responses of the pulmonary vasculature (*27*).

Hypoxia-dependent PASMC membrane depolarization was only partially prevented by AOX, and hypoxia-induced vasoconstriction could be restored by experimentally shifting the cellular membrane potential to higher levels. These findings suggest that multiple sensing mechanisms may contribute to reaching a threshold of cellular membrane depolarization necessary for the final execution of HPV (*30*). Cellular membrane depolarization might be achieved by a change in cellular redox state or activation of ROS-dependent signaling pathways that influence cell membrane ion channels (*1*), such as the hydrogen peroxide–mediated inhibition of K_V channels (*5*). Accordingly, K_V channel inhibition causes cell membrane depolarization and subsequent activation of L- and T-type calcium channels, increasing intracellular calcium levels and triggering HPV (*31*, *32*). The threshold for activation of voltage-dependent calcium channels has been shown to be at a membrane potential between −30 and − 20 mV in mouse PASMC (*33*). Thus, while WT PASMC can reach this threshold in hypoxia, the presence of AOX prevents membrane depolarization from reaching the critical threshold. The mechanism behind the partial depolarization remains to be identified. A plethora of additional oxygen-sensitive components in PASMC have been suggested (*1*), including hypoxia-sensitive potassium channels (*34*, *35*). Substituting

the hypoxic mitochondrial signal by shifting the cellular membrane potential to a critical threshold, as in our experiments by the addition of potassium chloride, may therefore bypass the mitochondrial signaling and thus restore hypoxia-induced cellular membrane depolarization to a level that can trigger calcium increase and HPV. This indicates that mitochondria must be acting far upstream in the signaling hierarchy, and thus, our results demonstrate the essential role of the mitochondrial respiratory chain in acute oxygen sensing and, in addition, provide an explanation for previous, seemingly contradictory, findings with regard to oxygen-sensitive components in PASMC.

The acute and chronic responses of the pulmonary vasculature to hypoxia have hitherto been assumed to involve similar primary mechanisms and to share regulatory components. However, our data point toward different signaling pathways operating in the two conditions and thus support previous studies that demonstrated a different mechanism of acute HPV and chronic hypoxia-induced PH (*5*, *30*, *36*). Confusingly, previous studies have implicated directionally opposite changes in mitochondrial ROS in chronic hypoxia showing both an increase (*28*) and a decrease in mitochondrial ROS (*37*) affecting PASMC proliferation and pulmonary vascular remodeling (*38*, *39*). There are also contradictory reports on the effects of mitochondrial ROS on HIF-1α, which is a major driver for the development of chronic hypoxia-induced PH (*39*), with some authors finding evidence of its stabilization by ROS (*28*, *40*), while others found no such effect (*41*). Recently, we found evidence for a decrease in PASMC ROS levels in chronic as opposed to acute hypoxia (*36*). The fact that AOX did not inhibit chronic hypoxia-induced PH, nor interfere with hypoxia-induced stabilization of HIF-1α, may help resolve these discordant findings, recasting the acute and chronic effects of hypoxia in lungs as two fundamentally different processes. The discrepancy to other studies may be due to cell type–specific mechanisms of HIF-1α stabilization, or time- and oxygen concentration–dependent differences. For example, nonmitochondrial ROS sources, such as NADPH (reduced form of nicotinamide adenine dinucleotide phosphate) oxidases, may be of greater importance in the pulmonary vasculature under chronic hypoxic conditions. Although under chronic hypoxia AOX did not influence general physiological parameters, we did record a lower proliferation capacity in PASMC expressing AOX. However, this may be a cell culture effect arising from partial activation of AOX under high glycolytic conditions. It should be emphasized, however, that in vitro effects of mitochondrial superoxide release with regard to HIF-1α stabilization and PASMC proliferation may differ from the in vivo situation.

In summary, our data indicate that respiratory inhibition is an upstream event in HPV signaling, substantiate that mitochondrial superoxide derived from cIII is essential for acute HPV, and provide evidence for the multifactorial nature of HPV with several hypoxia-sensitive components contributing to hypoxia-induced cellular membrane depolarization in PASMC (Fig. 5). Conversely, oxygen sensing under chronic hypoxia in pulmonary cells operates by distinct mechanisms. The differential effect of AOX on acute and chronic hypoxia in the lung illustrates its value as a tool to study disease etiologies, and eventually opens the possibility of a novel therapeutic approach.

MATERIALS AND METHODS

Reagents and resources

A list of reagents and resources is given in Table 1.

Animal housing and experiments

All animals were maintained and treated according to the regulations of the animal welfare agencies, and all of the experimental protocols were approved by the local "Animal Investigation Care and Use Committee" and the "Regierungspräsidium Darmstadt" (B2/292). Mice and rats were housed in a humidity- and temperature-regulated animal facility with food and water provided ad libitum. A general description and characterization of the AOX-expressing strain have been published elsewhere (*10*). C57BL/6J mice and Sprague-Dawley rats were obtained from Charles River (Sulzfeld, Germany) (Table 1). A list of reagents and resources is given in Table 1 (see below).

Immunohistochemistry

Formalin-fixed paraffin-embedded mouse lung tissue was used for staining with AOX antiserum (1:2000; custom raised in rabbit; 21st Century Biochemicals, Marlborough, MA, USA) (*42*), visualized using the ZytoChem Plus (HRP) Polymer Bulk Kit (Zytomed Systems GmbH, Berlin, Germany) and VECTOR NovaRED Peroxidase (HRP) Substrate Kit (Vector Laboratories, Burlingame, USA).

Hemodynamic measurements in isolated, perfused, and ventilated mouse lungs

Lungs of WT or AOX littermates were isolated, perfused, and ventilated as described elsewhere (*30*, *43*). The AOX inhibitor nPG (Sigma-Aldrich) was titrated to confirm AOX dependence (10 to 20 μM). The thromboxane analog U46619 (Enzo Life Sciences, Exeter, UK) was used to test the intactness of vasoconstriction (1 ml of bolus with a concentration of 66 ng/ml).

Intrapulmonary artery isolation and tension measurements

Mouse intrapulmonary arteries were isolated and mounted in wire myograph chambers (Danish Myo Technology A/S, Aarhus, Denmark) as described (*44*). Each experiment was started by 3 × 3–min exposures to 80 mM KCl containing physiological saline solution. To induce hypoxia upon reaching a stable vascular tone, the N_2-balanced gassing was switched from 21% O_2, 5% CO_2 (Praxair, Danbury, CT, USA) to 1% O_2, 5% CO_2 (Praxair). The partial pressure of O_2 during the hypoxic challenge was 15 to 22 mmHg tested by a FireStingO_2 oxygen meter (PyroScience, Aachen, Germany). Changes in isometric tension from the baseline values were expressed as percentages of the maximum constriction induced by the final exposure to 80 mM KCl. In some experiments, 15 to 20 mM KCl was applied before a hypoxic challenge to achieve preconstriction that was ~20% of the maximal constriction induced by 80 mM KCl.

Isolation of mouse and rPASMC and mouse pulmonary arterial vessels

PASMC and pulmonary arterial vessels were isolated as described previously (*30*, *45*).

Estimation of the cellular membrane potential

The cellular membrane potential was measured using the patch clamp technique. Mouse PASMC (passage 0), grown on culture dishes (Greiner Bio-One, Frickenhausen, Germany), were continuously perfused with extracellular analogous bath solution [126.7 mM NaCl (Sigma-Aldrich), 5.4 mM KCl (Carl Roth, Karlsruhe, Germany), 1.8 mM $CaCl_2$ (Carl Roth), 1.05 mM $MgCl_2$ (Carl Roth), 0.42 mM NaH_2PO_4 (Merck Millipore, Darmstadt, Germany), 22 mM $NaHCO_3$ (Carl Roth), 10 mM glucose (Carl Roth), pH7.4]. Bath solution was

Table 1. List of reagents and resources.

Reagents	Source	Identifier
Antibodies		
AOX antiserum (custom raised in rabbit)	21st Century Biochemicals, Marlborough, MA, USA	(*42*)
HIF-1α (C-Term) polyclonal antibody	Cayman Chemical	10006421
Anti-beta actin antibody [mAbcam 8226]—loading control (HRP)	Abcam	ab20272
Anti-rabbit IgG (H + L), HRP conjugate	Promega	W4011
Anti-mouse IgG (H + L), HRP conjugate	Promega	W4021
Lentiviral particles		
Lentiviral *Ciona intestinalis* AOX	This paper	N/A
Lentiviral catalytic inactive (mutant) AOX	This paper	(*20*)
Chemicals		
n-Propyl gallate (nPG, AOX inhibitor)	Sigma-Aldrich	P3130
U46619 (prostaglandin H2/thromboxane A2 receptor agonist)	Enzo Life Sciences, Exeter, UK	PG-023
Sodium chloride (NaCl)	Sigma-Aldrich	31434
Potassium chloride (KCl)	Carl Roth, Karlsruhe, Germany	5346.1
Calcium chloride ($CaCl_2$)	Carl Roth	CN93.1
Magnesium chloride ($MgCl_2$)	Carl Roth	KK36.1
Sodium dihydrogen phosphate dihydrate ($NaH_2PO_4{\cdot}2H_2O$)	Merck Millipore, Darmstadt, Germany	1063421000
Sodium hydrogen carbonate ($NaHCO_3$)	Carl Roth	8551
D(+)-Glucose	Carl Roth	X997.1
L-Aspartic acid potassium salt (L-aspartate)	Sigma-Aldrich	A6558
Adenosine 5′-triphosphate magnesium salt, ATP	Sigma-Aldrich	A9187
Ethylene glycol-bis(2-aminoethylether)-N,N,N′,N′-tetraacetic acid (EGTA)	Sigma-Aldrich	03777
Hepes (PUFFERAN®)	Carl Roth	9105.3
Potassium hydroxide (KOH)	Carl Roth	6751
1-Hydroxy-3-methoxycarbonyl −2,2,5,5-tetramethylpyrrolidine (CMH spin probe)	Noxygen, Elzach, Germany	NOX-02.2
Superoxide dismutase–polyethylene glycol (pSOD, PEG-SOD)	Sigma-Aldrich	S9549
5,5′,6,6′-Tetrachloro-1,1′,3,3′-tetraethyl-imidacarbocyanine iodide (JC-1)	ThermoFisher Scientific	T3168
Penicillin-streptomycin	Gibco, ThermoFisher Scientific	1507–063
Normocin—antimicrobial reagent	InvivoGen, San Diego, USA	ant-nr-1
Assays		
ZytoChem Plus (HRP) Polymer Bulk Kit	Zytomed Systems GmbH, Berlin, Germany	POLHRP-100
VECTOR NovaRED Peroxidase (HRP) Substrate Kit	Vector Laboratories, Burlingame, USA	SK-4800
Enhanced chemiluminescence ECL Prime Western Blotting System	GE Healthcare	RPN2232
Cell Proliferation ELISA, BrdU (colorimetric) assay	Sigma-Aldrich	11647229001
Primary cells		
Mouse PASMC from precapillary pulmonary arterial vessels	(*30*)	N/A
Rat PASMC from precapillary pulmonary arterial vessels	(*45*)	N/A

continued to next page

Reagents	Source	Identifier
Rodent models		
Mouse: Rosa26-Aox (aka Aox^{Rosa26})	*(10)*	N/A
Mouse: C57BL/6J	Charles River, Sulzfeld, Germany	Strain Code 632
Rat: Sprague-Dawley (Crl:SD)	Charles River	Strain Code 400
Plasmid and vectors		
pWPXL (constitutive lentiviral plasmid)	Addgene, Boston, MA, USA	Plasmid #12257
pMD2.G (envelope vector)	Addgene	Plasmid #12259
psPAX2 (packing vector)	Addgene	Plasmid #12260
Software and algorithms		
Patchmaster software	HEKA, Lambrecht, Germany	v2x90
IGOR Pro software	Wavemetrics, Lake Oswego, OR, USA	version 6.37
DatLab software	Oroboros Instruments, Innsbruck, Austria	DatLab 5
Prism software	GraphPad Software; San Diego, CA, USA	version 8.2.0
Other		
Multi Wire Myograph System	Danish Myo Technology A/S, Aarhus, Denmark	620 M
N_2-balanced gas (21% O_2, 5% CO_2)	Praxair, Danbury, CT, USA	592091 (custom made)
N_2-balanced gas (1% O_2, 5% CO_2)	Praxair	650329 (custom made)
Optical Oxygen Meter (FireStingO2)	Pyro Science, Aachen, Germany	FSO2–2
Culture dishes	Greiner Bio-One, Frickenhausen, Germany	627860
Multi-line in-line solution heater	Warner Instruments, Hamden, CT, USA	SHM-8
Borosilicate glass capillary tubes	Sutter Instrument, Novato, CA, USA	BF150–86-10HP
DMZ universal electrode puller	Zeitz, Martinsried, Germany	N/A
EPC 10 USB patch clamp amplifier	HEKA	895000
EMXmicro ESR spectrometer	Bruker Biospin GmbH, Rheinstetten, Germany	N/A
OROBOROS-2k oxygraph	Oroboros Instruments	N/A
Media 199—Mammalian Cell Culture	Gibco, ThermoFisher Scientific	31150–022
Vevo2100 high-resolution imaging system equipped with a 40-MHz transducer	VisualSonics, Toronto, Canada	N/A
Raman spectrometer Shamrock 303i	Andor, Technology, Belfast, UK	SR-303i-A
Laser	Altechna, Vilnius, Lithuania	DPSS 532
Raman filter cube with dichroic mirror	Semrock, Rochester, NY, USA	zt532/640rpc
532-nm EdgeBasic best-value long-pass edge filter	Semrock	BLP01-532R-25
×40 magnification objective	Olympus, Tokyo, Japan	LUCPLFLN

gassed—normoxic (21% O_2, 5.3% CO_2, rest N_2) or hypoxic (1% O_2, 5.3% CO_2, rest N_2)—and preheated to 37°C via an in-line solution heater (Warner Instruments, Hamden, CT, USA). Acute hypoxia was applied by switching from a normoxic to a hypoxic bath solution, and the pO_2 near the cell was recorded by an optical needle-type FireStingO_2 oxygen meter (PyroScience, Aachen, Germany).

Fire-polished patch pipettes with a tip resistance of 3 to 5 megohms were pulled from borosilicate glass capillary tubes (Sutter Instrument, Novato, CA, USA) using a DMZ universal electrode puller (Zeitz, Martinsried, Germany) and filled with intracellular analogous solution containing 105 mM L-aspartate (Sigma-Aldrich), 25 mM KCl (Carl Roth), 4 mM NaCl (Sigma-Aldrich), 1 mM $MgCl_2$ (Carl Roth), 4 mM ATP (Sigma-Aldrich), 10 mM EGTA (Sigma-Aldrich), and 10 mM Hepes (Carl Roth), pH 7.2 adjusted with 1 M KOH (Carl Roth). Experimentally determined liquid junction potential (+12.3 mV) was corrected electronically. Cells used for experiments were either relaxed or partially contracted and exhibited spindle-shaped morphology (round and fully contracted cells were discarded). The membrane potential was recorded under current clamp mode ($I = 0$) in whole-cell configuration using an EPC 10 USB patch clamp amplifier (HEKA, Lambrecht, Germany). nPG (Sigma-Aldrich) was added to confirm AOX dependence (10 μM). Data were filtered at 2.9 kHz and sampled at 50 Hz using Patchmaster software (HEKA). Data were analyzed using IGOR Pro software (Wavemetrics, Lake Oswego, OR, USA).

Quantification of superoxide levels by ESR spectroscopy

Intracellular and extracellular ROS concentration was measured using an EMXmicro ESR spectrometer (Bruker Biospin GmbH, Rheinstetten, Germany) using 0.5 mM of the spin probe CMH (Noxygen, Elzach, Germany). The superoxide portion of ROS was determined by

subtracting the ESR signal of the sample with pSOD (Sigma-Aldrich) from the sample incubated for 90 min without pSOD (45 U/ml) in ESR-Krebs Hepes buffer (*46*, *47*). Hypoxia was applied by incubating the cells in a hypoxic chamber (1% O_2 for 5 min).

Lentivirus production and mouse PASMC transduction

Native or mutated AOX were subcloned into the pWPXL plasmid and packed in a second-generation lentivirus transduction system with pMD2.G as the envelope and psPAX2 as a packing vector (all lentiviral plasmids from Addgene, Boston, MA, USA). Lentiviral transduction was performed with a titer of at least 1×10^7 particles according to established protocols (see http://tronolab.epfl.ch/ for more details). After 3 days of transduction, PASMC were used for further experiments.

Measuring mitochondrial membrane potential

The mitochondrial membrane potential was studied by fluorescence microscopy using 5,5′,6,6′-tetrachloro-1,1′,3,3′-tetraethylimidacarbocyanine iodide (JC-1) as recommended by the manufacturer (Thermo Fisher Scientific, Waltham, MA, USA). Acute hypoxia was induced by switching from a normoxic perfusion buffer to a hypoxic buffer (1% O_2).

High-resolution respirometry

Oxygen consumption was determined at 37°C using an OROBOROS-2 k oxygraph (Oroboros Instruments, Innsbruck, Austria) as described previously (*5*). Briefly, primary rPASMC were trypsinized, washed two times, and resuspended in M199 medium (Gibco, Thermo Fisher Scientific, Hampton, NH, USA) containing 1% penicillin-streptomycin (Gibco, Thermo Fisher Scientific) and 10% Hepes (Carl Roth). PASMC transfected with an empty or AOX-containing vector were measured in parallel. Oxygen consumption was recorded continuously until the oxygen was depleted. DatLab software (Oroboros Instruments) was used to calculate oxygen consumption as the time derivative of the oxygen content, standardized to cell number.

Raman spectroscopy on PASMC

Raman spectra of mouse WT and AOX PASMC were measured using a home-built microscope equipped with a ×40 magnification microscope objective (Olympus, Tokyo, Japan), a Raman spectrometer (Andor Technology, Belfast, UK), and a laser with an excitation wavelength of 532 nm (Altechna, Vilnius, Lithuania). The Raman signal was filtered out from the laser light using a filter cube containing a dichroic mirror (Semrock, Rochester, NY, USA) and a 532-nm edge filter (Semrock). An in-house–designed gas-tight microfluidic system was used to register Raman spectra on the cultured PASMC at different oxidation states, i.e., normoxic and hypoxic conditions (*48*). The sample was illuminated with a laser output power of 3.1 mW with an integration time of 60 s. Acquired Raman data were processed in two steps. First, Cosmic rays were removed using the 2D second difference (*49*). Second, an optimal reconstruction was done using a Savitzky-Golay filter (*50*). To confirm the Raman signal from the single live cells, background spectra of the microfluidic system and the buffer were taken.

Right ventricular hemodynamics and morphometry and vascular remodeling

Mice were exposed to normobaric hypoxia (10% O_2) for 4 weeks. Quantification of PH was performed as described (*30*). Measurement of transthoracic echocardiography was performed in the mice before measurement of invasive hemodynamics using a Vevo2100 high-resolution imaging system equipped with a 40-MHz transducer (VisualSonics, Toronto, Canada) as described previously (*5*, *36*).

Western blot analysis

Hypoxic exposure of PASMC, protein extraction, and Western blot analysis were performed as described (*5*). Primary antibodies used were anti–HIF-1α (1:1000 dilution; Cayman Chemical) and anti–β-actin (1:50,000 dilution; Abcam). Specific immune-reactive signals were detected using enhanced chemiluminescence ECL Prime Western Blotting System (GE Healthcare) using a proprietary secondary antibody coupled to horseradish peroxidase (1:5000 dilution; Promega).

Bromodeoxyuridine proliferation assay

For assessment of proliferation, mouse PASMC (5000 cells per well) from passage 1 were seeded in 24-well plates in smooth muscle cell basal medium containing 1% normocin (InvivoGen, San Diego, USA). After 24 hours of starvation, cells were exposed to normoxia (21% O_2, 5% CO_2) or hypoxia (1% O_2, 5% CO_2) at 37°C in water-saturated incubators for 72 hours. Bromodeoxyuridine (BrdU) labeling reagent was added 18 hours before the end of the incubation period. The proliferation assay was performed according to the manufacturer's instructions [Cell Proliferation ELISA, BrdU (colorimetric), Sigma-Aldrich]. The absorbance of the substrate reaction was measured after 15 min of incubation at 370 nm (reference wavelength, 492 nm).

Statistical analysis

All data depicted are shown as means ± SEM. The exact group size is stated in each figure legend. If not stated otherwise, statistical analysis was done using Prism (GraphPad Software). Differences were considered statistically significant at a P value <0.05.

SUPPLEMENTARY MATERIALS

Supplementary material for this article is available at http://advances.sciencemag.org/cgi/content/full/6/16/eaba0694/DC1

View/request a protocol for this paper from *Bio-protocol*.

REFERENCES AND NOTES

1. N. Sommer, I. Strielkov, O. Pak, N. Weissmann, Oxygen sensing and signal transduction in hypoxic pulmonary vasoconstriction. *Eur. Respir. J.* **47**, 288–303 (2016).
2. J. T. Sylvester, L. A. Shimoda, P. I. Aaronson, J. P. T. Ward, Hypoxic pulmonary vasoconstriction. *Physiol. Rev.* **92**, 367–520 (2012).
3. B. Mathew, S. Lakshminrusimha, Persistent pulmonary hypertension in the newborn. *Children* **4**, 63 (2017).
4. J. Grimminger, M. Richter, K. Tello, N. Sommer, H. Gall, H. A. Ghofrani, Thin air resulting in high pressure: Mountain sickness and hypoxia-induced pulmonary hypertension. *Can. Respir. J.* **2017**, 8381653 (2017).
5. N. Sommer, M. Hüttemann, O. Pak, S. Scheibe, F. Knoepp, C. Sinkler, M. Malczyk, M. Gierhardt, A. Esfandiary, S. Kraut, F. Jonas, C. Veith, S. Aras, A. Sydykov, N. Alebrahimdehkordi, K. Giehl, M. Hecker, R. P. Brandes, W. Seeger, F. Grimminger, H. A. Ghofrani, R. T. Schermuly, L. I. Grossman, N. Weissmann, Mitochondrial complex IV subunit 4 isoform 2 is essential for acute pulmonary oxygen sensing. *Circ. Res.* **121**, 424–438 (2017).
6. O. Pak, N. Sommer, T. Hoeres, A. Bakr, S. Waisbrod, A. Sydykov, D. Haag, A. Esfandiary, B. Kojonazarov, F. Veit, B. Fuchs, F. C. Weisel, M. Hecker, R. T. Schermuly, F. Grimminger, H. A. Ghofrani, W. Seeger, N. Weissmann, Mitochondrial hyperpolarization in pulmonary vascular remodeling. Mitochondrial uncoupling protein deficiency as disease model. *Am. J. Respir. Cell Mol. Biol.* **49**, 358–367 (2013).
7. M. Mittal, X. Q. Gu, O. Pak, M. E. Pamenter, D. Haag, D. B. Fuchs, R. T. Schermuly, H. A. Ghofrani, R. P. Brandes, W. Seeger, F. Grimminger, G. G. Haddad, N. Weissmann, Hypoxia induces Kv channel current inhibition by increased NADPH oxidase-derived reactive oxygen species. *Free Radic. Biol. Med.* **52**, 1033–1042 (2012).

8. K. J. Dunham-Snary, D. Wu, F. Potus, E. A. Sykes, J. D. Mewburn, R. L. Charles, P. Eaton, R. A. Sultanian, S. L. Archer, Ndufs2, a core subunit of mitochondrial complex I, is essential for acute oxygen-sensing and hypoxic pulmonary vasoconstriction. *Circ. Res.* **124**, 1727–1746 (2019).
9. G. B. Waypa, K. A. Smith, P. T. Schumacker, O2 sensing, mitochondria and ROS signaling: The fog is lifting. *Mol. Aspects Med.* **47-48**, 76–89 (2016).
10. M. Szibor, P. K. Dhandapani, E. Dufour, K. M. Holmström, Y. Zhuang, I. Salwig, I. Wittig, J. Heidler, Z. Gizatullina, T. Gainutdinov; German Mouse Clinic Consortium, H. Fuchs, V. Gailus-Durner, M. H. de Angelis, J. Nandania, V. Velagapudi, A. Wietelmann, P. Rustin, F. N. Gellerich, H. T. Jacobs, T. Braun, Broad AOX expression in a genetically tractable mouse model does not disturb normal physiology. *Dis. Model. Mech.* **10**, 163–171 (2017).
11. I. B. Dry, A. L. Moore, D. A. Day, J. T. Wiskich, Regulation of alternative pathway activity in plant mitochondria: Nonlinear relationship between electron flux and the redox poise of the quinone pool. *Arch. Biochem. Biophys.* **273**, 148–157 (1989).
12. E. L. Robb, A. R. Hall, T. A. Prime, S. Eaton, M. Szibor, C. Viscomi, A. M. James, M. P. Murphy, Control of mitochondrial superoxide production by reverse electron transport at complex I. *J. Biol. Chem.* **293**, 9869–9879 (2018).
13. R. El-Khoury, E. Dufour, M. Rak, N. Ramanantsoa, N. Grandchamp, Z. Csaba, B. Duvillié, P. Bénit, J. Gallego, P. Gressens, C. Sarkis, H. T. Jacobs, P. Rustin, Alternative oxidase expression in the mouse enables bypassing cytochrome *c* oxidase blockade and limits mitochondrial ROS overproduction. *PLOS Genet.* **9**, e1003182 (2013).
14. M. Szibor, T. Gainutdinov, E. Fernández-Vizarra, E. Dufour, Z. Gizatullina, G. Debska-Vielhaber, J. Heidler, I. Wittig, C. Viscomi, F. Gellerich, A. L. Moore, Bioenergetic consequences from xenotopic expression of a tunicate AOX in mouse mitochondria: Switch from RET and ROS to FET. *Biochim. Biophys. Acta Bioenerg.* **1861**, 148137 (2019).
15. E. L. Mills, B. Kelly, A. Logan, A. S. H. Costa, M. Varma, C. E. Bryant, P. Tourlomousis, J. H. M. Däbritz, E. Gottlieb, I. Latorre, S. C. Corr, G. McManus, D. Ryan, H. T. Jacobs, M. Szibor, R. J. Xavier, T. Braun, C. Frezza, M. P. Murphy, L. A. O'Neill, Succinate dehydrogenase supports metabolic repurposing of mitochondria to drive inflammatory macrophages. *Cell* **167**, 457–470.e13 (2016).
16. L. Giordano, A. Farnham, P. K. Dhandapani, L. Salminen, J. Bhaskaran, R. Voswinckel, P. Rauschkolb, S. Scheibe, N. Sommer, C. Beisswenger, N. Weissmann, T. Braun, H. T. Jacobs, R. Bals, C. Herr, M. Szibor, Alternative oxidase attenuates cigarette smoke-induced lung dysfunction and tissue damage. *Am. J. Respir. Cell Mol. Biol.* **60**, 515–522 (2019).
17. R. El-Khoury, K. K. Kemppainen, E. Dufour, M. Szibor, H. T. Jacobs, P. Rustin, Engineering the alternative oxidase gene to better understand and counteract mitochondrial defects: State of the art and perspectives. *Br. J. Pharmacol.* **171**, 2243–2249 (2014).
18. E. P. Dassa, E. Dufour, S. Goncalves, H. T. Jacobs, P. Rustin, The alternative oxidase, a tool for compensating cytochrome *c* oxidase deficiency in human cells. *Physiol. Plant.* **137**, 427–434 (2009).
19. P. Rustin, H. T. Jacobs, Respiratory chain alternative enzymes as tools to better understand and counteract respiratory chain deficiencies in human cells and animals. *Physiol. Plant.* **137**, 362–370 (2009).
20. A. Andjelković, M. T. Oliveira, G. Cannino, C. Yalgin, P. K. Dhandapani, E. Dufour, P. Rustin, M. Szibor, H. T. Jacobs, Diiron centre mutations in ciona intestinalis alternative oxidase abolish enzymatic activity and prevent rescue of cytochrome oxidase deficiency in flies. *Sci. Rep.* **5**, 18295 (2015).
21. N. A. Brazhe, M. Treiman, B. Faricelli, J. H. Vestergaard, O. Sosnovtseva, In situ Raman study of redox state changes of mitochondrial cytochromes in a perfused rat heart. *PLOS ONE* **8**, e70488 (2013).
22. H. Teng, M. Lv, L. Liu, X. Zhang, Y. Zhao, Z. Wu, H. Xu, Quantitative detection of NADH using a novel enzyme-assisted method based on surface-enhanced raman scattering. *Sensors* **17**, E788 (2017).
23. T. G. Spiro, T. C. Strekas, Resonance Raman spectra of hemoglobin and cytochrome *c*: Inverse polarization and vibronic scattering. *Proc. Natl. Acad. Sci. U.S.A.* **69**, 2622–2626 (1972).
24. N. Erjavec, G. Pinato, K. Ramser, Raman spectroscopy as a tool for detecting mitochondrial fitness. *J. Raman Spectrosc.* **47**, 933–939 (2016).
25. S. Choi, J. J. Lee, Y. H. Wei, T. G. Spiro, Resonance Raman and electronic spectra of heme a complexes and cytochrome oxidase. *J. Am. Chem. Soc.* **105**, 3692–3707 (1983).
26. J. D. Marshall, I. Bazan, Y. Zhang, W. H. Fares, P. J. Lee, Mitochondrial dysfunction and pulmonary hypertension: Cause, effect, or both. *Am. J. Physiol. Lung Cell. Mol. Physiol.* **314**, L782–L796 (2018).
27. G. B. Waypa, J. D. Marks, R. D. Guzy, P. T. Mungai, J. M. Schriewer, D. Dokic, M. K. Ball, P. T. Schumacker, Superoxide generated at mitochondrial complex III triggers acute responses to hypoxia in the pulmonary circulation. *Am. J. Respir. Crit. Care Med.* **187**, 424–432 (2013).
28. P. T. Schumacker, Lung cell hypoxia: Role of mitochondrial reactive oxygen species signaling in triggering responses. *Proc. Am. Thorac. Soc.* **8**, 477–484 (2011).
29. A. L. Orr, L. Vargas, C. N. Turk, J. E. Baaten, J. T. Matzen, V. J. Dardov, S. J. Attle, J. Li, D. C. Quackenbush, R. L. S. Goncalves, I. V. Perevoshchikova, H. M. Petrassi, S. L. Meeusen, E. K. Ainscow, M. D. Brand, Suppressors of superoxide production from mitochondrial complex III. *Nat. Chem. Biol.* **11**, 834–836 (2015).
30. N. Weissmann, A. Dietrich, B. Fuchs, H. Kalwa, M. Ay, R. Dumitrascu, A. Olschewski, U. Storch, M. Mederos y Schnitzler, H. A. Ghofrani, R. T. Schermuly, O. Pinkenburg, W. Seeger, F. Grimminger, T. Gudermann, Classical transient receptor potential channel 6 (TRPC6) is essential for hypoxic pulmonary vasoconstriction and alveolar gas exchange. *Proc. Natl. Acad. Sci. U.S.A.* **103**, 19093–19098 (2006).
31. F. Veit, O. Pak, R. P. Brandes, N. Weissmann, Hypoxia-dependent reactive oxygen species signaling in the pulmonary circulation: Focus on ion channels. *Antioxid. Redox Signal.* **22**, 537–552 (2015).
32. A. L. Firth, C. V. Remillard, O. Platoshyn, I. Fantozzi, E. A. Ko, J. X.-J. Yuan, Functional ion channels in human pulmonary artery smooth muscle cells: Voltage-dependent cation channels. *Pulm. Circ.* **1**, 48–71 (2011).
33. E. A. Ko, J. Wan, A. Yamamura, A. M. Zimnicka, H. Yamamura, H. Y. Yoo, H. Tang, K. A. Smith, P. C. Sundivakkam, A. Zeifman, R. J. Ayon, A. Makino, J. X.-J. Yuan, Functional characterization of voltage-dependent Ca^{2+} channels in mouse pulmonary arterial smooth muscle cells: Divergent effect of ROS. *Am. J. Physiol. Cell Physiol.* **304**, C1042–C1052 (2013).
34. A. Olschewski, E. L. Veale, B. M. Nagy, C. Nagaraj, G. Kwapiszewska, F. Antigny, M. Lambert, M. Humbert, G. Czirják, P. Enyedi, A. Mathie, TASK-1 (KCNK3) channels in the lung: From cell biology to clinical implications. *Eur. Respir. J.* **50**, 1700754 (2017).
35. E. K. Weir, A. Olschewski, Role of ion channels in acute and chronic responses of the pulmonary vasculature to hypoxia. *Cardiovasc. Res.* **71**, 630–641 (2006).
36. O. Pak, S. Scheibe, A. Esfandiary, M. Gierhardt, A. Sydykov, A. Logan, A. Fysikopoulos, F. Veit, M. Hecker, F. Kroschel, K. Quanz, A. Erb, K. Schäfer, M. Fassbinder, N. Alebrahimdehkordi, H. A. Ghofrani, R. T. Schermuly, R. P. Brandes, W. Seeger, M. P. Murphy, N. Weissmann, N. Sommer, Impact of the mitochondria-targeted antioxidant MitoQ on hypoxia-induced pulmonary hypertension. *Eur. Respir. J.* **51**, 1701024 (2018).
37. P. Dromparis, G. Sutendra, E. D. Michelakis, The role of mitochondria in pulmonary vascular remodeling. *J. Mol. Med.* **88**, 1003–1010 (2010).
38. S. E. Adesina, B.-Y. Kang, K. M. Bijli, J. Ma, J. Cheng, T. C. Murphy, C. Michael Hart, R. L. Sutliff, Targeting mitochondrial reactive oxygen species to modulate hypoxia-induced pulmonary hypertension. *Free Radic. Biol. Med.* **87**, 36–47 (2015).
39. M. K. Ball, G. B. Waypa, P. T. Mungai, J. M. Nielsen, L. Czech, V. J. Dudley, L. Beussink, R. W. Dettman, S. K. Berkelhamer, R. H. Steinhorn, S. J. Shah, P. T. Schumacker, Regulation of hypoxia-induced pulmonary hypertension by vascular smooth muscle hypoxia-inducible factor-1α. *Am. J. Respir. Crit. Care Med.* **189**, 314–324 (2014).
40. I. Martínez-Reyes, L. P. Diebold, H. Kong, M. Schieber, H. Huang, C. T. Hensley, M. M. Mehta, T. Wang, J. H. Santos, R. Woychik, E. Dufour, J. N. Spelbrink, S. E. Weinberg, Y. Zhao, R. J. DeBerardinis, N. S. Chandel, TCA cycle and mitochondrial membrane potential are necessary for diverse biological functions. *Mol. Cell* **61**, 199–209 (2016).
41. Y. L. Chua, E. Dufour, E. P. Dassa, P. Rustin, H. T. Jacobs, C. T. Taylor, T. Hagen, Stabilization of hypoxia-inducible factor-1α protein in hypoxia occurs independently of mitochondrial reactive oxygen species production. *J. Biol. Chem.* **285**, 31277–31284 (2010).
42. E. P. Dassa, E. Dufour, S. Gonçalves, V. Paupe, G. A. J. Hakkaart, H. T. Jacobs, P. Rustin, Expression of the alternative oxidase complements cytochrome *c* oxidase deficiency in human cells. *EMBO Mol. Med.* **1**, 30–36 (2009).
43. N. Weissmann, A. Sydykov, H. Kalwa, U. Storch, B. Fuchs, M. Mederos y Schnitzler, R. P. Brandes, F. Grimminger, M. Meissner, M. Freichel, S. Offermanns, F. Veit, O. Pak, K.-H. Krause, R. T. Schermuly, A. C. Brewer, H. H. H. W. Schmidt, W. Seeger, A. M. Shah, T. Gudermann, H. A. Ghofrani, A. Dietrich, Activation of TRPC6 channels is essential for lung ischaemia-reperfusion induced oedema in mice. *Nat. Commun.* **3**, 649 (2012).
44. I. Strielkov, N. C. Krause, N. Sommer, R. T. Schermuly, H. A. Ghofrani, F. Grimminger, T. Gudermann, A. Dietrich, N. Weissmann, Hypoxic pulmonary vasoconstriction in isolated mouse pulmonary arterial vessels. *Exp. Physiol.* **103**, 1185–1191 (2018).
45. F. Veit, O. Pak, B. Egemnazarov, M. Roth, D. Kosanovic, M. Seimetz, N. Sommer, H. A. Ghofrani, W. Seeger, F. Grimminger, R. P. Brandes, R. T. Schermuly, N. Weissmann, Function of NADPH oxidase 1 in pulmonary arterial smooth muscle cells after monocrotaline-induced pulmonary vascular remodeling. *Antioxid. Redox Signal.* **19**, 2213–2231 (2013).
46. N. Weissmann, N. Kuzkaya, B. Fuchs, V. Tiyerili, R. U. Schäfer, H. Schütte, H. A. Ghofrani, R. T. Schermuly, C. Schudt, A. Sydykov, B. Egemnazarow, W. Seeger, F. Grimminger, Detection of reactive oxygen species in isolated, perfused lungs by electron spin resonance spectroscopy. *Respir. Res.* **6**, 86 (2005).
47. S. I. Dikalov, W. Li, P. Mehranpour, S. S. Wang, A. M. Zafari, Production of extracellular superoxide by human lymphoblast cell lines: Comparison of electron spin resonance techniques and cytochrome C reduction assay. *Biochem. Pharmacol.* **73**, 972–980 (2007).
48. F. Knoepp, J. Wahl, A. Andersson, J. Borg, N. Weissmann, K. Ramser, Development of a gas-tight microfluidic system for Raman sensing of single pulmonary arterial smooth muscle cells under Normoxic/Hypoxic conditions. *Sensors* **18**, E3238 (2018).
49. H. G. Schulze, R. F. B. Turner, A two-dimensionally coincident second difference cosmic ray spike removal method for the fully automated processing of Raman spectra. *Appl. Spectrosc.* **68**, 185–191 (2014).

50. A. Savitzky, M. J. E. Golay, Smoothing and differentiation of data by simplified least squares procedures. *Anal. Chem.* **36**, 1627–1639 (1964).

Acknowledgments: We thank K. Homberger, E. Kappes, I. Breitenborn-Mueller, and M. Partanen for technical assistance. **Funding:** This work was supported by the European Research Council (Advanced Grant 232738), Academy of Finland (Centre of Excellence grant 272376 and Academy Professorship grant 256615), Tampere University Hospital Medical Research Fund and Sigrid Juselius Foundation (to H.T.J.), the Swedish Research Council (grant 2016-04220 to K.R.), and the Deutsche Forschungsgemeinschaft (DFG, German Research Foundation, project no. 268555672, SFB 1213, A06 to N.W. and N.S.). **Author contributions:** All authors performed research or compiled and analyzed data. N.S., N.W., H.T.J., and M.S. designed and supervised the research and drafted the manuscript, which was then finalized by all authors. **Competing interests:** H.T.J. is an inventor on a PATENT related to this work filed by Inst Nat Sante Rech Med (no. 7572616, published 10/09/2008). M.S. declares himself a shareholder in a startup company to develop AOX therapeutics. All other authors declare that they have no competing interests. **Data and materials availability:** All data needed to evaluate the conclusions in the paper are present in the paper and/or the Supplementary Materials. The mice xenotopically expressing Ciona intestinalis alternative oxidase (AOX) can be provided by the Faculty of Medicine and Health Technology, Tampere University, FI-33520 Tampere, Finland, pending scientific review and a completed material transfer agreement. Requests for the mice should be submitted to Prof. Howard T. Jacobs (howard.jacobs@tuni.fi).

Submitted 1 November 2019
Accepted 22 January 2020
Published 15 April 2020
10.1126/sciadv.aba0694

Citation: N. Sommer, N. Alebrahimdehkordi, O. Pak, F. Knoepp, I. Strielkov, S. Scheibe, E. Dufour, A. Andjelković, A. Sydykov, A. Saraji, A. Petrovic, K. Quanz, M. Hecker, M. Kumar, J. Wahl, S. Kraut, W. Seeger, R. T. Schermuly, H. A. Ghofrani, K. Ramser, T. Braun, H. T. Jacobs, N. Weissmann, M. Szibor, Bypassing mitochondrial complex III using alternative oxidase inhibits acute pulmonary oxygen sensing. *Sci. Adv.* **6**, eaba0694 (2020).

7.4 L. Giordano *et al.*, *Am J Resp Cell Mol*. **60**, 515–522 (2019)

ORIGINAL RESEARCH

Alternative Oxidase Attenuates Cigarette Smoke–induced Lung Dysfunction and Tissue Damage

Luca Giordano[1,2,3,4], Antoine Farnham[1,2], Praveen K. Dhandapani[1,2], Laura Salminen[1,2], Jahnavi Bhaskaran[1,2], Robert Voswinckel[5], Peter Rauschkolb[3,4], Susan Scheibe[3,4], Natascha Sommer[3,4], Christoph Beisswenger[6], Norbert Weissmann[3,4], Thomas Braun[7], Howard T. Jacobs[1,2], Robert Bals[6], Christian Herr[6]*, and Marten Szibor[1,2,7]*

[1]Faculty of Medicine and Life Sciences, University of Tampere, Tampere, Finland; [2]Institute of Biotechnology, University of Helsinki, Helsinki, Finland; [3]Excellence Cluster Cardio-Pulmonary System, University of Giessen, Giessen, Germany; [4]Marburg Lung Center, Member of the German Center for Lung Research, Justus Liebig University, Giessen, Germany; [5]Bürgerhospital Friedberg, Klinik für Innere Medizin, Friedberg, Germany; [6]Department of Internal Medicine V–Pulmonology, Allergology, Intensive Care Medicine, Saarland University, Homburg/Saar, Germany; and [7]Department I Cardiac Development and Remodeling, Max Planck Institute for Heart and Lung Research, Bad Nauheim, Germany

ORCID IDs: 0000-0001-6315-7361 (L.G.); 0000-0001-9422-6569 (C.H.); 0000-0003-4029-160X (M.S.).

Abstract

Cigarette smoke (CS) exposure is the predominant risk factor for the development of chronic obstructive pulmonary disease (COPD) and the third leading cause of death worldwide. We aimed to elucidate whether mitochondrial respiratory inhibition and oxidative stress are triggers in its etiology. In different models of CS exposure, we investigated the effect on lung remodeling and cell signaling of restoring mitochondrial respiratory electron flow using alternative oxidase (AOX), which bypasses the cytochrome segment of the respiratory chain. AOX attenuated CS-induced lung tissue destruction and loss of function in mice exposed chronically to CS for 9 months. It preserved the cell viability of isolated mouse embryonic fibroblasts treated with CS condensate, limited the induction of apoptosis, and decreased the production of reactive oxygen species (ROS). In contrast, the early-phase inflammatory response induced by acute CS exposure of mouse lung, i.e., infiltration by macrophages and neutrophils and adverse signaling, was unaffected. The use of AOX allowed us to obtain novel pathomechanistic insights into CS-induced cell damage, mitochondrial ROS production, and lung remodeling. Our findings implicate mitochondrial respiratory inhibition as a key pathogenic mechanism of CS toxicity in the lung. We propose AOX as a novel tool to study CS-related lung remodeling and potentially to counteract CS-induced ROS production and cell damage.

Keywords: cigarette smoke; COPD; mitochondria; alternative oxidase

Clinical Relevance

Cigarette smoke exposure triggers mitochondrial respiratory inhibition and oxidative stress. The use of an alternative respiratory enzyme relieves mitochondrial stress and attenuates lung dysfunction and tissue damage.

Chronic obstructive pulmonary disease (COPD), which is largely caused by exposure to cigarette smoke (CS), represents a rapidly growing global health burden in terms of suffering and mortality. It is estimated that it will soon become the third most common cause of death worldwide (1). The clinical hallmarks of COPD are airflow limitations and lung tissue destruction. The poor regeneration capacity of the adult human lung and the lack of therapeutic interventions to arrest or reverse tissue

(Received in original form August 12, 2018; accepted in final form October 18, 2018)

*These authors contributed equally to this work.

Supported by the European Research Council Advanced Grant 232738 (H.T.J.), the Academy of Finland (Centre of Excellence grant 272376 and Academy Professorship grant 256615) (H.T.J.), the Tampere University Medical Research Fund (H.T.J.), and the Deutsche Forschungsgemeinschaft (SFB1213, project A07; N.W. and T.B.). L.G. was supported by a fellowship from the European Respiratory Society (STRTF-201710-00228).

Author Contributions: L.G., R.V., C.H., and M.S. conceived and designed the study, and supervised the work. L.G., A.F., P.K.D., L.S., J.B., P.R., S.S., N.S., C.H., and M.S. generated and analyzed data. L.G., R.V., C.B., N.W., T.B., H.T.J., R.B., C.H., and M.S. collected data and drafted the manuscript.

Correspondence and requests for reprints should be addressed to Marten Szibor, M.D., University of Tampere, Arvo Ylpön katu 34, 33520 Tampere, Finland. E-mail: marten.szibor@uta.fi.

This article has a data supplement, which is accessible from this issue's table of contents at www.atsjournals.org.

Am J Respir Cell Mol Biol Vol 60, Iss 5, pp 515–522, May 2019

Originally Published in Press as DOI: 10.1165/rcmb.2018-0261OC on October 19, 2018
Internet address: www.atsjournals.org

destruction make COPD a terminal condition. Different possible mechanisms driving the pathology of this disease are currently the subject of intense debate and experimentation. It has been proposed, for instance, that local inflammation and production of reactive oxygen species (ROS) induced upon CS exposure initiate adverse lung remodeling (2). The prooxidant nature of CS is well documented and supports this hypothesis (3). However, its complex composition, which includes more than 5,000 compounds (4), many of which are known toxins or carcinogens, complicates efforts to elucidate the underlying mechanism. Two prominent CS compounds are known as potent inhibitors of mitochondrial respiratory complex IV (cIV), i.e., carbon monoxide and hydrogen cyanide. Exposure to either toxin disrupts electron transport, inducing cellular redox imbalance and excessive ROS production. Because cyanide has a systemic half-life of up to 25 hours (5), mitochondrial impairment cannot be considered as an inert bystander in the development of COPD. Instead, excess ROS produced as a result of respiratory chain inhibition may be the actual trigger for adverse signaling that initiates and accelerates the pathology.

Plants and many lower organisms, including the sea-squirt *Ciona intestinalis*, but not mammals, express alternative oxidase (AOX), which is able to maintain mitochondrial respiration under conditions in which the cytochrome segment of the electron transport chain is blocked. Specifically, AOX accepts electrons from ubiquinol to reduce oxygen to water. Notably, because AOX is a single-subunit oxidase and nonproton pumping, it does not add to the proton motive force across the inner mitochondrial membrane and thus does not directly support mitochondrial ATP production. Recently, we engineered and characterized mouse models that ubiquitously expressed AOX (6, 7). Even globally expressed AOX caused no deviation from normal physiology, including body temperature and regular mitochondrial oxygen consumption, while conferring resistance to respiratory chain inhibitors such as antimycin A and cyanide (6, 7). This seemingly counterintuitive outcome can be explained by the biochemical properties of AOX, which requires respiratory disruption and sufficient Q-pool reduction for proper functioning (8). This makes AOX an ideal tool for studying mitochondrial involvement in pathogenesis in the mouse (9, 10). For example, the use of AOX mice in a disease model for sepsis revealed that mitochondria are responsible for the detrimental proinflammatory phenotype shift of macrophages, and, more importantly, that transgenic expression of AOX decreases lethality by restoring mitochondrial respiration and blunting the production of mitochondrial ROS in bone marrow–derived macrophages (11). Our previous data indicate that AOX is sufficiently active in immune cells, which are also responsible for the local inflammation and excess ROS production seen in the course of COPD (11). Thus, we sought to test whether CS-induced respiratory inhibition could be revoked by AOX and whether this would decrease ROS production, alleviating cell damage and limiting immune cell migration to the lung and adverse organ remodeling *in vivo*.

Here, we show in AOX mice chronically exposed to CS that detrimental lung remodeling is attenuated while functional lung parameters (lung mechanics) are preserved. At the cellular level, AOX protects against the toxicity of CS condensate (CSC), decreasing mitochondrial superoxide production and preserving cell viability. In contrast, the acute response to short-term CS exposure, i.e., the infiltration of neutrophils and macrophages, is not prevented by AOX, suggesting that the relationship between the early inflammatory response and long-term lung remodeling is not straightforward. We infer that the early- and late-phase responses must differ, with mitochondrial signaling being sufficient to account only for the latter. Nevertheless, the use of AOX provides novel insights into disease etiologies and may form the basis for novel approaches to counteract the development of chronic lung remodeling, such as that seen in COPD.

Methods

Animal Experiments

A mouse strain ubiquitously expressing AOX was recently described (6). All animal experiments were approved by the Landesamt für Soziales, Gesundheit und Verbraucherschutz, of the State of Saarland following the national guidelines for animal treatment (18/2011), and were performed according to the Declaration of Helsinki conventions for the use and care of animals.

CS Exposure

Female heterozygous AOX transgenic mice and wild-type (WT) littermates were exposed to CS (3R4F cigarettes, College of Agriculture, Reference Cigarette Program, University of Kentucky) in a TE-10 smoking machine (Teague Enterprises) starting at 8 weeks of age (12, 13).

Lung Function Measurements

Respiratory system mechanics were analyzed using the flexiVent system (SCIREQ) as previously described (12, 14).

Stereological Lung-Tissue Analysis

Lungs were fixed by instillation of PBS-buffered 4% formaldehyde in PBS under constant hydrostatic pressure, prepared by systematic uniform random sampling, and analyzed as previously described (12, 13).

BAL

Animals were anesthetized as described above and tracheotomized. BAL was performed as previously described (12, 13). A minimum of 200 cells were counted and differentiated based on morphology.

Quantification of Inflammatory Mediators

Concentrations of IL-6 (DY406), KC (keratinocyte derived cytokine, CXCL1) (DY453), MIP2 (macrophage inflammatory protein) (DY452), and MMP9 (matrix metalloprotease 9) (DY6718) were measured by ELISA (DuoSet; R&D Systems) according to the manufacturer's instructions. Signals were quantified using a FLUOstar Omega ELISA reader and MARS data analysis software V3.10.R6 (both from BMG Labtech).

Isolating Primary Mouse Embryonic Fibroblasts

Primary mouse embryonic fibroblasts (MEFs) from embryos at embryonic day 13.5 (E13.5)–E15.5 were isolated and immortalized (generating iMEFs) as described elsewhere (15, 16).

Generation of CSC

CSC was obtained from Vectis s.r.l. Cava dei Tirreni as the solid fraction derived from tobacco smoke and thus devoid of volatile components such as carbon monoxide (17).

Sulforhodamine B Viability Assay

Toxicity screening was conducted using the sulforhodamine B (SRB) assay (S1402; Sigma-Aldrich), which is based on measurement of cellular protein content (18).

Respirometry

Mitochondrial respiration of permeabilized cells was assayed using a respirometer (OROBOROS) as previously described (19).

ROS Measurements

The amount of ROS in iMEFs was measured using MitoSOX Red (M36008; Thermo-Fisher Scientific) and the electron-spin-resonance method as described in detail elsewhere (20, 21).

Statistics

The sample size for each experiment is stated in the figures, with all data shown as mean ± SEM or box-and-whiskers plots (SRB viability assay). Statistical analysis was performed with GraphPad Prism software (GraphPad Software Inc.). Differences were considered statistically significant at a P value of <0.05.

Results

AOX Attenuates Chronic CS-induced Lung Dysfunction and Tissue Damage

To test whether mitochondrial respiratory inhibition could be the trigger for lung damage and remodeling driven by chronic CS exposure, we subjected WT and AOX mice to chronic CS for 9 months. CS stress caused a loss of body weight in all of the exposed mice, although significance was reached only in WT animals (Figure 1A). To eliminate a possible bias by differences in body weight, all measured functional lung parameters were normalized to the actual body weight. Respiratory-system mechanics related to CS-induced lung remodeling showed a significant deterioration in WT mice (Figures 1B–1E; Figure E1A in the data supplement). In AOX mice, the loss of lung function was generally less severe or absent (Figures 1B–1E). Compared with WT controls, AOX mice were significantly protected from the effects of CS exposure as determined by volume (Figure 1B) and hysteresis (Figure 1D), whereas other parameters only showed a trend toward protection (Figures 1C and 1E). Parameters typically altered in restrictive airway diseases were unaffected by both CS exposure and AOX expression (Figures E1B–E1E).

To visualize the severity of lung damage upon chronic exposure to CS, we quantified the mean chord length by stereology (Figure 2). Again, we found an increase in CS-exposed mice, corresponding to the observed changes in alveoli volume (Figure 2B), which were less pronounced in the CS-exposed AOX group. Taken together, these results show that AOX attenuates tissue destruction upon CS exposure.

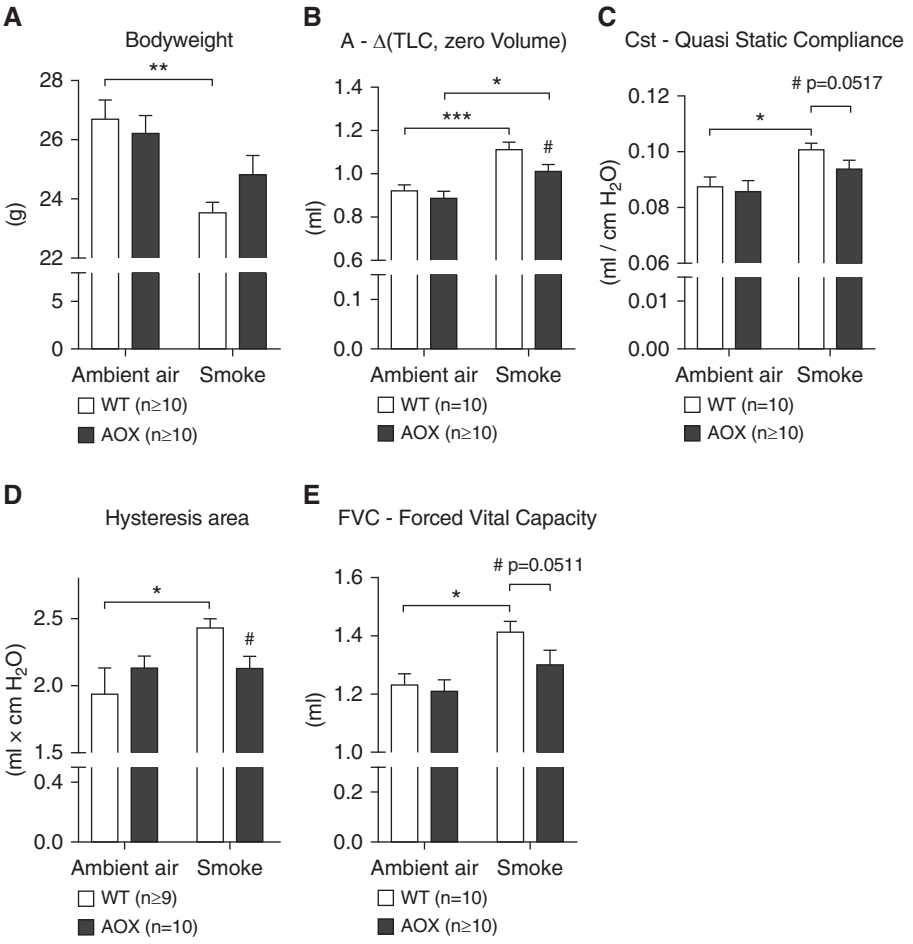

Figure 1. Effect of chronic cigarette smoke (CS) exposure on lung function in wild-type (WT) and alternative oxidase (AOX) mice. (*A*) Body weight of WT and AOX mice after smoke exposure. (*B–E*) Respiratory system mechanics measured using the SCIREQ FlexiVent system. All data are shown as mean ± SEM; $^{*}P < 0.05$, $^{**}P < 0.005$, and $^{***}P < 0.0005$ by two-way ANOVA; if not stated otherwise, $^{\#}P < 0.05$ by paired t test on CS-exposed groups.

AOX Improves Cell Viability upon CSC Exposure

To identify molecular mechanisms underlying the observed effects of AOX upon CS exposure, we used a cell-culture model. Because the strongest effects seen *in vivo* affected parameters reflecting the lung's ability to stretch and expand, such as hysteresis, we chose fibroblasts (iMEFs) as the most suitable cell type to study. Growing cells were treated with CSC and the number of viable cells after 2 or 3 days was determined using the SRB assay (Figure 3). CSC decreased SRB staining in both WT and AOX iMEFs in a dose-dependent manner (Figures 3A and 3B). AOX conferred robust protection against CSC toxicity to cells grown in glucose (Figures 3A and 3B) or in galactose (Figures 3C and 3D), which enforces the use of mitochondrial oxidative phosphorylation (22), and where CSC had a more dramatic effect. When CSC-containing galactose medium was replaced with toxin-free medium after 48 hours, AOX-expressing, but not WT, iMEFs were able to recover (Figure 3C). Cleaved caspase-3 (Figures 3D and 3E) was significantly increased in WT, but not AOX, iMEFs after CSC exposure, whereas total caspase-3 was unaffected (Figure E2). This is consistent with the idea that CSC activates apoptosis as a result of mitochondrial respiratory inhibition, against which AOX affords protection.

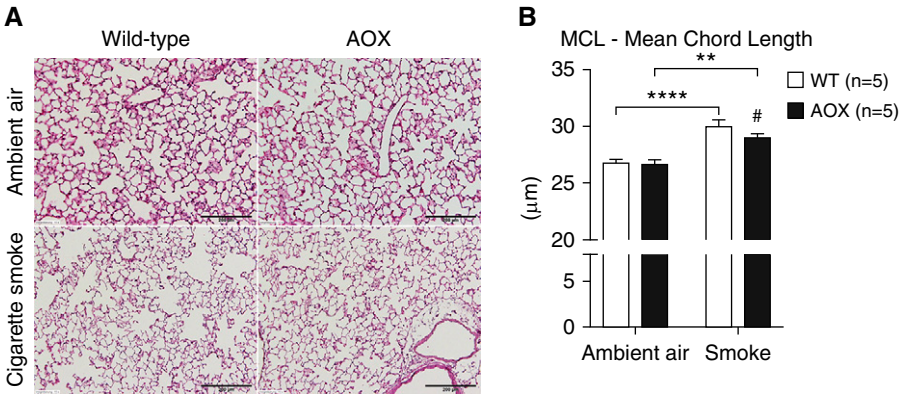

Figure 2. Stereological analysis of lung tissue. (*A*) Representative tissue slices (hematoxylin and eosin stained). (*B*) Statistical analysis of mean chord length (MCL). All data are shown as mean ± SEM; $^{**}P < 0.005$ and $^{****}P < 0.0001$ by two-way ANOVA; $^{\#}P < 0.05$ by paired *t* test on smoke-exposed groups. Scale bars: 200 μm.

AOX Supports Mitochondrial Respiration and Decreases Superoxide Production in iMEFs Exposed to CSC

We used respirometry to analyze the effects of CSC on mitochondrial respiration, and how this is modified by AOX expression. Two different assays were implemented to analyze damage-associated effects of CSC on respiration and to profile any acute toxic effects of CSC on respiration. Intact iMEFs cultured in galactose medium in the presence of CSC for 48 hours showed a dose-dependent drop in respiration with partial protection by AOX at low CSC concentration (Figure E3A). To identify the specific sites of CSC-induced damage and its mitigation by AOX, we used digitonin-permeabilized cells supplied with specific substrate mixes and inhibitors. Culturing of cells in CSC resulted in a dose-dependent decrease in respiration driven by a complex I (cI)-linked substrate mix (Figure 4A), which was not compensated for by AOX expression. In contrast, AOX was able to maintain or increase respiration driven by the complex II (cII) substrate succinate, even at high doses of CSC (Figure 4B). AOX was unable to prevent the large decrease in complex IV (cIV)-driven respiration produced by a high dose of CSC, although it stimulated cIV-driven respiration at a lower (noninhibitory) dose (Figure 4C). These effects were not reflected by altered levels of representative protein subunits of the respiratory chain complexes (Figure 4D), and therefore were likely due to post-translational modifications, small-molecule effectors, or damage to prosthetic groups, e.g., brought about by ROS.

Because enhanced ROS production is a well-characterized effect of respiratory chain inhibition, specifically at the levels of cIII and cIV, we measured mitochondrial superoxide accumulation using two different methods in glucose-cultured iMEFs: MitoSOX Red staining and electron spin resonance (Figures 4E, 4F, E3B, and E3C). With either method, superoxide levels increased dramatically in iMEFs exposed to CSC for 3 hours, whereas AOX limited or prevented this induction.

Intact cell respiration was unaffected by acute exposure to CSC (Figure E4A) unless the cells were first treated with an uncoupling agent such as FCCP (carbonyl cyanide 4-[trifluoromethoxy] phenylhydrazone), revealing a dose-dependent decrease in respiratory capacity that was again mitigated by AOX (Figure E4B). In permeabilized cells, CSC inhibited respiration driven by cI- or cII-linked substrates (Figures E4C and E4D), but AOX was able to limit only the latter. cIV-driven respiration was unaffected by AOX or by CSC (Figure E4E).

AOX Has No Effect on Acute CS-induced Inflammation

Because AOX had protective effects on the outcome of chronic CS exposure *in vivo* and limited CSC-induced cell death, we reasoned that it may also prevent what is considered to be the earliest step in COPD development, i.e., CS-induced pulmonary inflammation. To test this assumption, we used a previously validated model of the acute inflammatory response to short-term CS exposure (12). This model is mainly based on neutrophilic inflammation, mimicking conditions seen in patients. Surprisingly, we found that both macrophages and neutrophils were increased to the same degree in the BAL of WT and AOX mice (Figures 5A–5C).

Because we have shown previously that AOX expression prevents proinflammatory activation in a mouse sepsis model (11), we tested whether AOX would also prevent the adverse CS-induced inflammatory signaling response in the BAL fluid. Specifically, we quantified the presence of KC, a mouse-specific functional homolog of human IL-8, which typically correlates with the severity of COPD (23); MIP2, which together with KC belongs to the class of CXC chemokines known to induce neutrophil chemotaxis (24, 25); IL-6, which is a typical inflammatory marker that is often elevated during COPD; and MMP-9, which is activated by acrolein (26) or neutrophil elastase (27) and is known to contribute to tissue remodeling in patients with COPD during disease exacerbation (28). All of the markers were significantly and comparably upregulated in WT and AOX mice (Figures 5D–5G), indicating that AOX does not confer any protection, and suggesting that the acute-phase tissue response is not based on mitochondrial respiratory impairment.

Discussion

Our results identify impaired mitochondrial respiration as a molecular mechanism that drives lung remodeling upon CS exposure. Here, we show that a respiratory bypass can increase cell viability and, as a consequence, maintain lung function and/or facilitate repair processes. This is of significance for a number of reasons. Notably, the adult human lung lacks proper regeneration capacity. Therefore, any mechanism that attenuates the pathology is of great interest not only for millions of cigarette abusers but also for the even larger population that is exposed to toxic smoke in the environment due to urban air pollution or in a domestic setting.

By using AOX, we were able to demonstrate the involvement of mitochondria in the pathogenesis of COPD resulting from smoke exposure, and reveal relevant mechanisms underlying the effects of CS on mitochondrial respiration. For instance, we showed that CSC affects individual respiratory complexes differently.

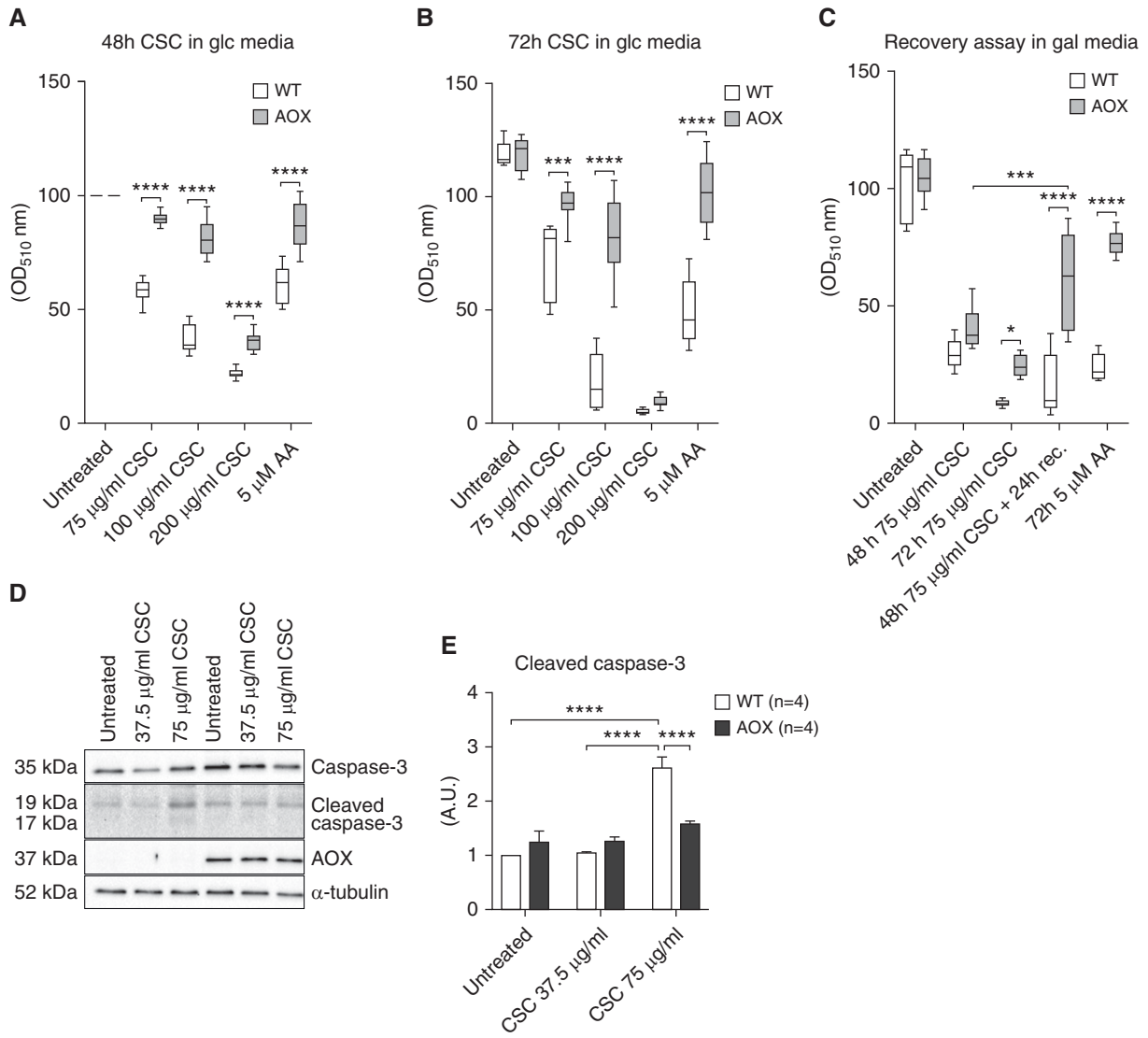

Figure 3. Analysis of CS condensate (CSC) toxicity in cultured immortalized mouse embryonic fibroblasts (iMEFs). (*A–C*) WT and AOX-expressing iMEFs cultured in glucose (glc, 10 mM) or galactose (gal, 10 mM) media and treated with CSC as indicated. Numbers of viable cells were estimated using the sulforhodamine B assay (absorbance at OD_{510}) and normalized against the value at 48 hours for untreated cells on the given medium (shown in %). In *C*, cells recovered for 24 hours in gal (10 mM) without CSC as indicated after CSC (75 μg/ml) exposure. Horizontal bands inside the boxes represent the median (second quartile), the bottom and top of the box are the first and third quartiles, respectively, and the ends of the whiskers represent the minimum and maximum values of the data set. (*D*) Western blot of caspase-3, cleaved caspase-3, and AOX, with α-tubulin as the loading control. For entire blots, including molecular-weight markers for cropped Western blot bands, please refer to Figure E5. (*E*) Relative densitometric analysis ($n \geq 3$) on proteins extracted from WT and AOX iMEFs exposed to CSC as indicated in gal media. Bar graph represents mean ± SEM; $^{*}P < 0.05$, $^{***}P < 0.0005$, and $^{****}P < 0.0001$ by two-way ANOVA. AA = antimycin A; OD = optical density.

Although cI was inhibited both directly and indirectly upon acute and chronic (48 h) exposure, cII and cIV showed only a mild response to acute CSC exposure (Figures 4, E3, and E4). Of note, due to its mode of action, AOX cannot rescue a cI impairment, as the Q-pool will likely remain oxidized, whereas inhibition of cIII or cIV causes a Q-pool reduction. Moreover, the cII substrate succinate is known to highly reduce the Q-pool, thereby inducing reverse electron transport and thus mitochondrial ROS production when no cI inhibitor is added. Yet, the mechanisms underlying the observed activation of respiratory complexes remain to be elucidated. Although cII-driven respiration in the presence of AOX can overcome inhibition of cIII and/or cIV, the reason for the observed cII and cIV activation (Figures 4B and 4C) is unclear. One plausible explanation is that AOX prevents excessive ROS production (6, 11), as shown directly in the case of CSC exposure (Figures 4E, 4F, E3B, and E3C), and thus may prevent unspecific damage to mitochondrial and cellular components. In support of our findings, it has previously been shown that CSC inhibits the activity of respiratory complexes (17) and causes cell

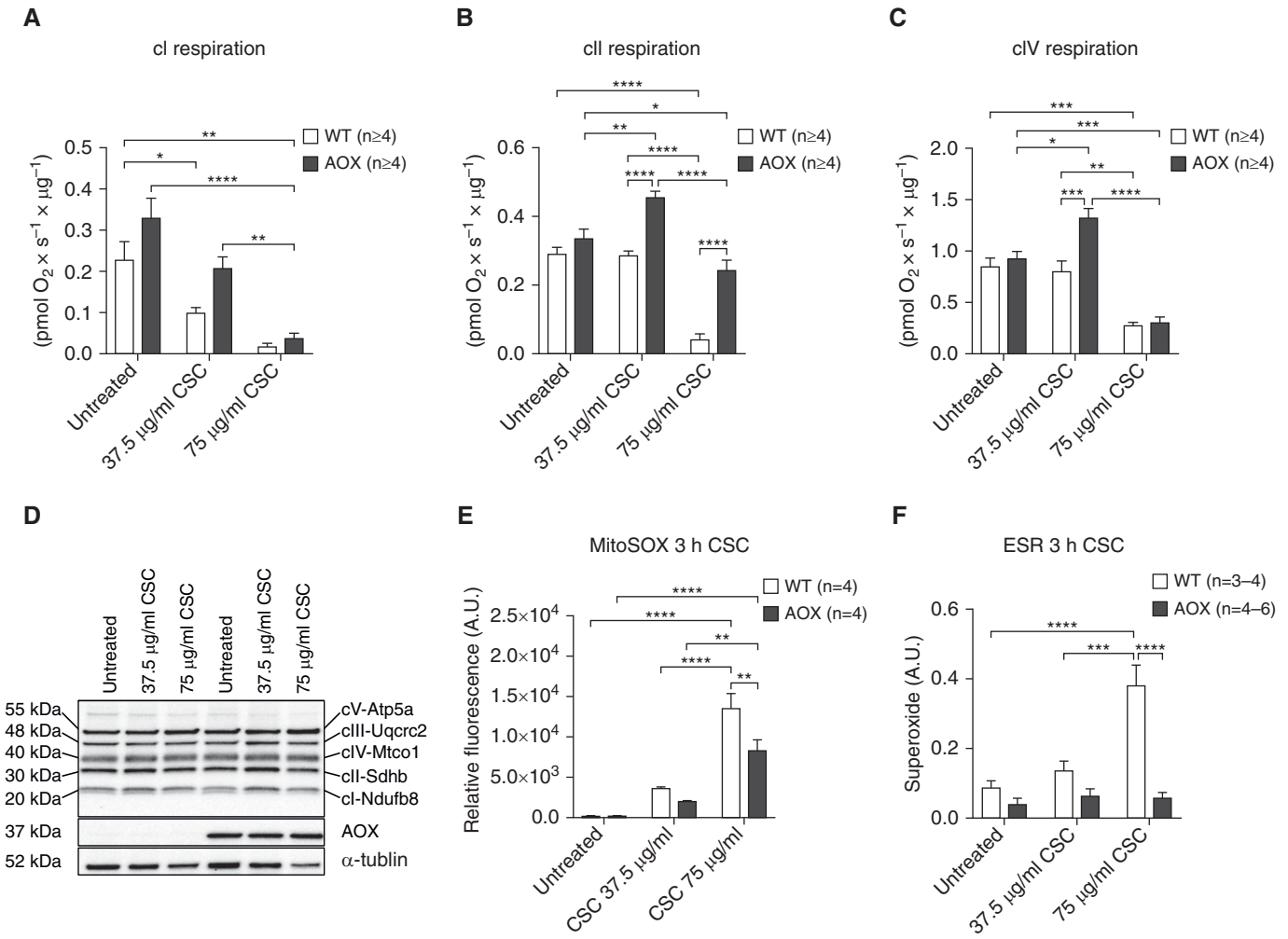

Figure 4. CSC toxicity effect on mitochondrial respiration and reactive oxygen species production in cultured iMEFs. (*A*) Oxygen consumption of permeabilized iMEFs in respiration buffer after culturing in gal media for 48 hours conditioned with CSC as indicated. Rotenone-sensitive oxygen consumption in the presence of complex I (cI) substrates pyruvate, glutamate, and malate plus ADP. (*B*) Antimycin A- plus n-propyl gallate–sensitive oxygen consumption in the presence of succinate (complex II [cII]) plus rotenone. (*C*) Sodium azide–sensitive oxygen consumption in the presence of ascorbate/TMPD (complex IV [cIV]). (*D*) Representative Western blot ($n \geq 3$) probed for subunits of the complexes of the mitochondrial OXPHOS system as indicated, with AOX and α-tubulin as the loading control. For entire blots, including molecular-weight markers for cropped Western blot bands, please refer to Figure E6. (*E*) Mitochondrial superoxide production measured using MitoSOX Red in iMEFs grown in glucose media (10 mM) after 3 hours of CSC exposure as indicated. (*F*) Determination of superoxide production using the spin probe CMH (1-hydroxy3-methoxycarbonyl-2,2,5,5-tetramethylpyrrolidine) and subtraction of pSOD (superoxide dismutase)-sensitive signal from total signal [CMH − (CMH + pSOD)] in iMEFs grown in glucose media (10 mM) after 3 hours of CSC exposure as indicated. All data are shown as mean ± SEM; $^{*}P < 0.05$, $^{**}P < 0.005$, $^{***}P < 0.0005$, and $^{****}P < 0.0001$ by two-way ANOVA. ESR = electronic spin resonance.

death by necrosis and/or apoptosis (29, 30). It is also of interest that the contents of CS affect membrane fluidity (31, 32). This alone may explain the observed respiratory impairment. More experiments will be needed to elucidate the exact pathomechanism, but the use of AOX provides a powerful route to this end.

A study of this type has intrinsic limitations that complicate translation of the results. For instance, it is well known that the murine lung regenerates much more efficiently than the adult human lung in response to CS. Here, we used mice on a C57BL/6 genetic background. The advantage of using such mice lies clearly in the comparability of data, as this strain is widely used. Unfortunately, however, C57BL/6 mice are exceptionally well protected against CS (33). Our results may therefore underestimate the protective effect of AOX. Indeed, the changes indicative of the development of emphysema are small, albeit significant, and compatible with previous results obtained using the same smoke machine and strain (13, 14). Nevertheless, other strains, such as AKR/J, are more susceptible to CS (33) and should be used in follow-up studies. Furthermore, CSC is a well-established surrogate for smoke exposure in cultured cells, but due to the isolation procedure and the constraints of cell culture, smoke and CSC differ significantly in composition. On the other hand, lung fibroblasts, epithelial cells, and macrophages also detect only those CS components that are dissolved in the fluid

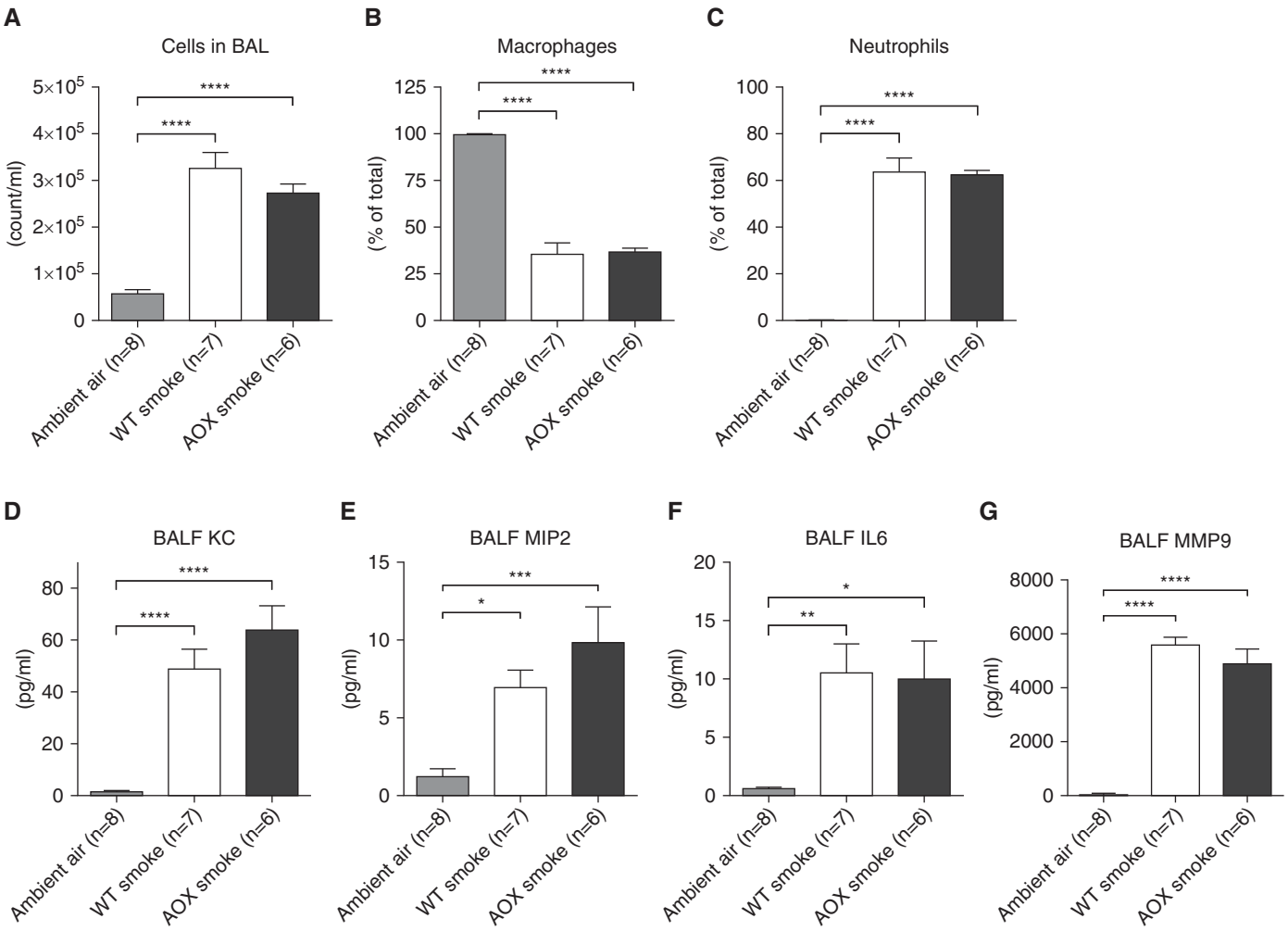

Figure 5. Testing the effect of acute CS exposure and AOX on inflammatory cell infiltration. (*A*) Total number of cells in BAL of WT and AOX mice upon short-term smoke exposure. (*B* and *C*) Macrophages and neutrophils as a percentage of total cells in BAL. (*D–G*) Selected inflammatory signals in BAL fluid (BALF). Note that owing to identical behavior and phenotype, the control group in ambient air is composed of WT and AOX mice. All data are shown as mean ± SEM; $^{*}P < 0.05$, $^{**}P < 0.005$, $^{***}P < 0.0005$, and $^{****}P < 0.0001$ by one-way ANOVA. KC = keratinocyte-derived cytokine, CXCL1; MIP2 = macrophage inflammatory protein 2; MMP9 = matrix metalloprotease 9.

lining the airways. Thus, the effects of CSC may actually truly reflect the *in vivo* situation. Finally, although the transgenic expression of AOX undoubtedly protects against cellular and lung maladaptation, deploying AOX in a therapeutic context remains a distant prospect. This will require extensive studies on its delivery, durability, and safety.

The most surprising finding of the current study is that the inflammatory response to acute CS exposure for 3 days was unaffected by AOX. A recent study claimed that macrophages from patients with COPD expressed more enzymes that promote tissue remodeling than healthy control subjects, and macrophages from patients with COPD showed higher expression of M2-related genes while suppressing M1 inflammatory and immune-regulatory proteins (34). Our findings indicate that mitochondrial respiratory inhibition is not the trigger for the immediate tissue response, even though it is clearly involved in the long-term pathogenic process. This appears to contrast with previous findings that infiltration and activation of macrophages and especially neutrophils correlate with an adverse outcome (35). Importantly, in our model, AOX is expressed ubiquitously (6). Thus, it is not possible to distinguish whether the critical target tissue in which mitochondrial respiratory inhibition leads to indicators of emphysema is the lung epithelium itself, macrophages, or other cells of the immune system (36), or some other tissue entirely. This can only be addressed by the creation of models in which AOX expression is limited to specific tissues or cell types, which will clearly be the subject of future studies.

In conclusion, expression of AOX attenuates CS-induced lung remodeling and protects cultured fibroblasts from CSC-induced cell death. This is associated with maintenance of respiration and decreased ROS production. Thus, AOX represents an innovative tool to study CS-induced lung diseases and may serve as the basis for lung protection. ■

Author disclosures are available with the text of this article at www.atsjournals.org.

Acknowledgment: The authors thank Maarit Partanen, Nils Schupp, Anja Honecker, and Andreas Kamyschnikov for technical assistance, and Troy Faithfull for a critical reading of the manuscript. In thankful memory we are grateful for the contribution of Luís Esteves.

References

1. Vestbo J, Hurd SS, Agustí AG, Jones PW, Vogelmeier C, Anzueto A, *et al*. Global strategy for the diagnosis, management, and prevention of chronic obstructive pulmonary disease: GOLD executive summary. *Am J Respir Crit Care Med* 2013;187:347–365.
2. Chung KF, Adcock IM. Multifaceted mechanisms in COPD: inflammation, immunity, and tissue repair and destruction. *Eur Respir J* 2008;31: 1334–1356.
3. Pryor WA, Stone K. Oxidants in cigarette smoke. Radicals, hydrogen peroxide, peroxynitrate, and peroxynitrite. *Ann N Y Acad Sci* 1993; 686:12–27; discussion 27–28.
4. Talhout R, Schulz T, Florek E, van Benthem J, Wester P, Opperhuizen A. Hazardous compounds in tobacco smoke. *Int J Environ Res Public Health* 2011;8:613–628.
5. Bhandari RK, Oda RP, Petrikovics I, Thompson DE, Brenner M, Mahon SB, *et al*. Cyanide toxicokinetics: the behavior of cyanide, thiocyanate and 2-amino-2-thiazoline-4-carboxylic acid in multiple animal models. *J Anal Toxicol* 2014;38:218–225.
6. Szibor M, Dhandapani PK, Dufour E, Holmström KM, Zhuang Y, Salwig I, *et al*.; German Mouse Clinic Consortium. Broad AOX expression in a genetically tractable mouse model does not disturb normal physiology. *Dis Model Mech* 2017;10:163–171.
7. El-Khoury R, Dufour E, Rak M, Ramanantsoa N, Grandchamp N, Csaba Z, *et al*. Alternative oxidase expression in the mouse enables bypassing cytochrome c oxidase blockade and limits mitochondrial ROS overproduction. *PLoS Genet* 2013;9:e1003182.
8. Dry IB, Moore AL, Day DA, Wiskich JT. Regulation of alternative pathway activity in plant mitochondria: nonlinear relationship between electron flux and the redox poise of the quinone pool. *Arch Biochem Biophys* 1989;273:148–157.
9. El-Khoury R, Kemppainen KK, Dufour E, Szibor M, Jacobs HT, Rustin P. Engineering the alternative oxidase gene to better understand and counteract mitochondrial defects: state of the art and perspectives. *Br J Pharmacol* 2014;171:2243–2249.
10. Dassa EP, Dufour E, Goncalves S, Jacobs HT, Rustin P. The alternative oxidase, a tool for compensating cytochrome c oxidase deficiency in human cells. *Physiol Plant* 2009;137:427–434.
11. Mills EL, Kelly B, Logan A, Costa ASH, Varma M, Bryant CE, *et al*. Succinate dehydrogenase supports metabolic repurposing of mitochondria to drive inflammatory macrophages. *Cell* 2016;167: 457–470.e13.
12. Wolf L, Herr C, Niederstraßer J, Beisswenger C, Bals R. Receptor for advanced glycation endproducts (RAGE) maintains pulmonary structure and regulates the response to cigarette smoke. *PLoS One* 2017;12:e0180092.
13. Voss M, Wolf L, Kamyschnikow A, Wonnenberg B, Honecker A, Herr C, *et al*. Il-17A contributes to maintenance of pulmonary homeostasis in a murine model of cigarette smoke-induced emphysema. *Am J Physiol Lung Cell Mol Physiol* 2015;309:L188–L195.
14. Herr C, Han G, Li D, Tschernig T, Dinh QT, Beißwenger C, *et al*. Combined exposure to bacteria and cigarette smoke resembles characteristic phenotypes of human COPD in a murine disease model. *Exp Toxicol Pathol* 2015;67:261–269.
15. Abbondanzo SJ, Gadi I, Stewart CL. Derivation of embryonic stem cell lines. *Methods Enzymol* 1993;225:803–823.
16. Lochmüller H, Johns T, Shoubridge EA. Expression of the E6 and E7 genes of human papillomavirus (HPV16) extends the life span of human myoblasts. *Exp Cell Res* 1999;248:186–193.
17. Giordano L, Deceglie S, d'Adamo P, Valentino ML, La Morgia C, Fracasso F, *et al*. Cigarette toxicity triggers Leber's hereditary optic neuropathy by affecting mtDNA copy number, oxidative phosphorylation and ROS detoxification pathways. *Cell Death Dis* 2015;6:e2021.
18. Vichai V, Kirtikara K. Sulforhodamine B colorimetric assay for cytotoxicity screening. *Nat Protoc* 2006;1:1112–1116.
19. Kuznetsov AV, Veksler V, Gellerich FN, Saks V, Margreiter R, Kunz WS. Analysis of mitochondrial function in situ in permeabilized muscle fibers, tissues and cells. *Nat Protoc* 2008;3:965–976.
20. Wojtala A, Bonora M, Malinska D, Pinton P, Duszyński J, Wieckowski MR. Methods to monitor ROS production by fluorescence microscopy and fluorometry. *Methods Enzymol* 2014;542:243–262.
21. Sommer N, Hüttemann M, Pak O, Scheibe S, Knoepp F, Sinkler C, *et al*. Mitochondrial complex IV subunit 4 isoform 2 is essential for acute pulmonary oxygen sensing. *Circ Res* 2017;121:424–438.
22. Robinson BH, Petrova-Benedict R, Buncic JR, Wallace DC. Nonviability of cells with oxidative defects in galactose medium: a screening test for affected patient fibroblasts. *Biochem Med Metab Biol* 1992;48: 122–126.
23. Papaporfyriou A, Loukides S, Kostikas K, Simoes DCM, Papatheodorou G, Konstantellou E, *et al*. Increased levels of osteopontin in sputum supernatant in patients with COPD. *Chest* 2014;146: 951–958.
24. Thatcher TH, McHugh NA, Egan RW, Chapman RW, Hey JA, Turner CK, *et al*. Role of CXCR2 in cigarette smoke-induced lung inflammation. *Am J Physiol Lung Cell Mol Physiol* 2005;289: L322–L328.
25. Zhang XW, Liu Q, Wang Y, Thorlacius H. CXC chemokines, MIP-2 and KC, induce P-selectin-dependent neutrophil rolling and extravascular migration in vivo. *Br J Pharmacol* 2001;133:413–421.
26. Deshmukh HS, Shaver C, Case LM, Dietsch M, Wesselkamper SC, Hardie WD, *et al*. Acrolein-activated matrix metalloproteinase 9 contributes to persistent mucin production. *Am J Respir Cell Mol Biol* 2008;38:446–454.
27. Ferry G, Lonchampt M, Pennel L, de Nanteuil G, Canet E, Tucker GC. Activation of MMP-9 by neutrophil elastase in an in vivo model of acute lung injury. *FEBS Lett* 1997;402:111–115.
28. Mercer PF, Shute JK, Bhowmik A, Donaldson GC, Wedzicha JA, Warner JA. MMP-9, TIMP-1 and inflammatory cells in sputum from COPD patients during exacerbation. *Respir Res* 2005;6:151.
29. Esakky P, Hansen DA, Drury AM, Cusumano A, Moley KH. Cigarette smoke-induced cell death of a spermatocyte cell line can be prevented by inactivating the Aryl hydrocarbon receptor. *Cell Death Discov* 2015;1:15050.
30. Messner B, Frotschnig S, Steinacher-Nigisch A, Winter B, Eichmair E, Gebetsberger J, *et al*. Apoptosis and necrosis: two different outcomes of cigarette smoke condensate-induced endothelial cell death. *Cell Death Dis* 2012;3:e424.
31. Hannan SE, Harris JO, Sheridan NP, Patel JM. Cigarette smoke alters plasma membrane fluidity of rat alveolar macrophages. *Am Rev Respir Dis* 1989;140:1668–1673.
32. Collin A, Hardonnière K, Chevanne M, Vuillemin J, Podechard N, Burel A, *et al*. Cooperative interaction of benzo[a]pyrene and ethanol on plasma membrane remodeling is responsible for enhanced oxidative stress and cell death in primary rat hepatocytes. *Free Radic Biol Med* 2014;72:11–22.
33. Guerassimov A, Hoshino Y, Takubo Y, Turcotte A, Yamamoto M, Ghezzo H, *et al*. The development of emphysema in cigarette smoke-exposed mice is strain dependent. *Am J Respir Crit Care Med* 2004; 170:974–980.
34. Shaykhiev R, Krause A, Salit J, Strulovici-Barel Y, Harvey B-G, O'Connor TP, *et al*. Smoking-dependent reprogramming of alveolar macrophage polarization: implication for pathogenesis of chronic obstructive pulmonary disease. *J Immunol* 2009;183:2867–2883.
35. Barnes PJ. Inflammatory mechanisms in patients with chronic obstructive pulmonary disease. *J Allergy Clin Immunol* 2016;138: 16–27.
36. Seimetz M, Parajuli N, Pichl A, Veit F, Kwapiszewska G, Weisel FC, *et al*. Inducible NOS inhibition reverses tobacco-smoke-induced emphysema and pulmonary hypertension in mice. *Cell* 2011;147: 293–305.

7.5 M. Szibor *et al.*, *J Cell Mol Med*. **24**, 3534–3548 (2020)

Received: 1 December 2019 | Revised: 19 January 2020 | Accepted: 21 January 2020

DOI: 10.1111/jcmm.15043

WILEY

ORIGINAL ARTICLE

Respiratory chain signalling is essential for adaptive remodelling following cardiac ischaemia

Marten Szibor[1,2,3] | Rolf Schreckenberg[4] | Zemfira Gizatullina[5] | Eric Dufour[1] | Marion Wiesnet[6] | Praveen K. Dhandapani[1,2] | Grazyna Debska-Vielhaber[5] | Juliana Heidler[7] | Ilka Wittig[7] | Tuula A. Nyman[8] | Ulrich Gärtner[9] | Andrew R. Hall[10] | Victoria Pell[11] | Carlo Viscomi[10,12] | Thomas Krieg[11] | Michael P. Murphy[10] | Thomas Braun[6] | Frank N. Gellerich[5] | Klaus-Dieter Schlüter[4] | Howard T. Jacobs[1,2]

[1]Faculty of Medicine and Health Technology, Tampere University, Tampere, Finland

[2]Institute of Biotechnology, University of Helsinki, Helsinki, Finland

[3]Department of Cardiothoracic Surgery, Jena University Hospital, Jena, Germany

[4]Department of Physiology, Justus-Liebig University Giessen, Giessen, Germany

[5]Department of Neurology, Otto-von-Guericke-University, Magdeburg, Germany

[6]Department Cardiac Development and Remodelling, Max Planck Institute for Heart and Lung Research, Bad Nauheim, Germany

[7]Functional Proteomics, Faculty of Medicine, Goethe University, Frankfurt am Main, Germany

[8]Department of Immunology, Institute of Clinical Medicine, Oslo University Hospital, University of Oslo, Oslo, Norway

[9]Institute of Anatomy and Cell Biology, Justus-Liebig-University Giessen, Giessen, Germany

[10]Medical Research Council Mitochondrial Biology Unit, University of Cambridge, Cambridge, UK

[11]Department of Medicine, University of Cambridge, Cambridge, UK

[12]Department of Biomedical Sciences, University of Padova, Padova, Italy

Correspondence
Marten Szibor, Faculty of Medicine and Health Technology, Tampere University, Arvo Ylpön katu 34, FI-33520 Tampere, Finland.
Email: Marten.Szibor@tuni.fi

Funding information
BMBF mitoNET-German Network for Mitochondrial Disorders, Grant/Award Number: 01GM1906D ; Academy of Finland grants, Grant/Award Number: 256615 and 272376 ; ERC Advanced Grant, Grant/Award Number: 232738 ; Wellcome Trust Investigator award, Grant/Award Number: 110159/Z/15/Z; Deutsche Forschungsgemeinschaft, Grant/Award Number: SFB 815/Z1 and SFB1213 ;

Abstract

Cardiac ischaemia-reperfusion (I/R) injury has been attributed to stress signals arising from an impaired mitochondrial electron transport chain (ETC), which include redox imbalance, metabolic stalling and excessive production of reactive oxygen species (ROS). The alternative oxidase (AOX) is a respiratory enzyme, absent in mammals, that accepts electrons from a reduced quinone pool to reduce oxygen to water, thereby restoring electron flux when impaired and, in the process, blunting ROS production. Hence, AOX represents a natural rescue mechanism from respiratory stress. This study aimed to determine how respiratory restoration through xenotopically expressed AOX affects the re-perfused post-ischaemic mouse heart. As expected, AOX supports ETC function and attenuates the ROS load in post-anoxic heart mitochondria.

Schreckenberg and Gizatullina are contributed equally.

Schlüter and Jacobs are both senior authors.

Medical Research Council (MRC), Grant/Award Number: MC_U105663142 and MC_UU_00015/5

However, post-ischaemic cardiac remodelling over 3 and 9 weeks was not improved. AOX blunted transcript levels of factors known to be up-regulated upon I/R such as the *atrial natriuretic peptide* (*Anp*) whilst expression of pro-fibrotic and pro-apoptotic transcripts were increased. Ex vivo analysis revealed contractile failure at nine but not 3 weeks after ischaemia whilst label-free quantitative proteomics identified an increase in proteins promoting adverse extracellular matrix remodelling. Together, this indicates an essential role for ETC-derived signals during cardiac adaptive remodelling and identified ROS as a possible effector.

KEYWORDS

adaptive cardiac remodelling, alternative oxidase, cardiac ischaemia-reperfusion, electron transport chain, mouse, reactive oxygen species

1 | INTRODUCTION

The high susceptibility of cardiomyocytes to oxygen deprivation has been originally attributed to their almost exclusive dependence on oxidative metabolism for ATP production.[1] Indeed, approximately 30% of the cardiomyocyte's intracellular volume is occupied by mitochondria which harbour the electron transport chain (ETC) in their inner membrane. The ETC is composed of four oxidoreductase complexes (cI-cIV) that facilitate substrate oxidation and electron transfer with oxygen being the final acceptor. Importantly, electron transfer is coupled to the generation of a proton-electrochemical potential gradient across the inner mitochondrial membrane, which itself is the driving force for ATP production, a process described as oxidative phosphorylation (OXPHOS). Although the ETC thus couples ATP production to oxygen consumption, pioneering work in isolated rabbit heart mitochondria[2] as well as in intact rabbit hearts[3] revealed that cardiac ATP depletion alone is insufficient to account for all post-ischaemic tissue damage.[2] Instead, electron flow through the ETC upon reperfusion was described as a source of potentially detrimental reactive oxygen species (ROS), proposed to trigger ischaemia-reperfusion (I/R) injuries.[2] Conversely, the therapeutic use of untargeted antioxidants such as vitamin C for post-ischaemic cardioprotection has given contradictory results,[4-9] and itself produced detrimental side effects when therapeutically used.[10] These seemingly contradictory results were thought to be due to biphasic effects of ROS with high ROS concentrations leading to damage and lower concentrations eliciting adaptive responses.[11,12] The term 'mitohormesis' was proposed[13] to describe this phenomenon. Indeed, a recent study demonstrated that increased ROS levels specifically in the mitochondrial compartment have a cardioprotective effect upon I/R.[14] Of course, it could equally be possible that untargeted antioxidants cannot reach sufficient levels in the mitochondrial compartment to be effective, and therefore fail to detoxify mitochondrial ROS at the site of its production. Furthermore, ROS may generate positive or negative effects in a time-dependent manner.

To test this assumption, a number of mitochondrial-targeted antioxidants have been designed. MitoQ, one prominent example, consists of ubiquinol (reduced quinone) targeted specifically to mitochondria by a covalently fused lipophilic triphenyl phosphonium (TPP) cation.[15] Importantly, in rats that underwent cardiac I/R, MitoQ, but not the untargeted antioxidant or TPP alone, significantly decreased contractile dysfunction, cell death and mitochondrial damage.[15] Positive effects of MitoQ were also seen in other studies addressing post-transplantation injury[16] and pressure overload-induced heart failure.[17] Following a similar rationale, Szeto-Schiller (SS) peptides[18] were used, which accumulate in mitochondria in a membrane potential-independent manner. The use of SS peptides caused phenotypic improvements in a model of angiotensin II-induced mitochondrial ROS production and myocardial contractile failure[19] as well as upon transverse-aortic constriction.[20] Both, MitoQ and SS peptides appeared biologically safe and beneficial when long-term administered[21,22] arguing that intramitochondrial ROS are rather detrimental than physiologically relevant. Finally, using high-throughput chemical screening, small molecules that suppress superoxide and/or hydrogen peroxide production at the I_Q site of cI were identified, S1QELs,[23] that act through a mechanism that does not affect regular OXPHOS. Most importantly, ROS generated at I_Q was discussed to be instrumental for cellular stress signalling. Indeed, application of S1QELs protected the perfused mouse heart from I/R injuries.[23] A unifying mechanism by which the different mitochondrially targeted antioxidants may fulfil their beneficial effects was recently put forward.[24] According to this, succinate, an intermediate metabolite of the tricarboxylic acid cycle, accumulates during cardiac ischaemia.[25] Reperfusion evokes rapid succinate oxidation through reverse electron transport (RET) from ubiquinol to cI concomitant with a burst of mitochondrial ROS. Scavenging RET-induced ROS may therefore be the mechanism by which cellular and organ damage is prevented although other sources of ROS, that are intrinsically linked, may play a signalling role as well.[26]

Plants and many other organisms, but not insects or vertebrates, harbour a by-pass mechanism to protect from ETC-mediated respiratory stress conditions, the alternative oxidase (AOX).[27] AOX is a non-protonmotive single di-iron carboxylate redox transfer protein.[28] Where expressed, AOX oxidizes ubiquinol and by-passes cIII and cIV, directly transferring electrons to oxygen. In previous studies, we were

able to show that a xenotopically expressed AOX from the tunicate *Ciona intestinalis* (hereafter called AOX) is catalytically active under various experimental conditions. In human cells, AOX conferred resistance against the ETC inhibitor cyanide[29] and corrected genetic defects which caused ETC dysfunction.[30] In fruit flies, AOX complemented ETC defects in vivo and restored viability.[31] Global expression in the mouse protected against cyanide toxicity[32,33] decreased lethality from endotoxemia[34] and alleviated cigarette smoke-induced lung remodelling and cell death.[35] AOX was demonstrated to effectively decrease RET-induced ROS[36,37] driven by succinate. Most importantly, however, expression of AOX prevented the development of a lethal cardiomyopathy in a cIII mouse mutant strain[38] indicating sufficient expression for full respiratory restoration in the stressed heart. Interestingly, in a mouse model of inflammatory cardiomyopathy,[39] AOX expression in cardiomyocytes conferred detrimental effects.[40] This suggests a role for the mitochondrial respiratory chain in both, energy homeostasis and stress signalling.

Here, we tested how maintaining electron flow impacts on remodelling in the post-ischaemic mouse heart. We show that AOX expression supports ETC function and decreases mitochondrial ROS levels, yet impairs adaptive cardiac remodelling. This indicates an essential role for ETC-derived stress signals in post-ischaemic cardiac adaptation.

2 | MATERIALS AND METHODS

2.1 | Animal models

Mice with ubiquitous expression of *Ciona intestinalis* AOX[33] were maintained on a C57BL/6J background in temperature- and humidity-controlled facilities at 12 hours of light-to-dark cycles with access to water and food ad libitum. Open-chest in situ I/R procedures were conducted at the University of Cambridge, Cambridge, UK upon approval by Home Office license 70/8238. In vivo I/R procedures were conducted at the Max Planck Institute for Heart and Lung Research in Bad Nauheim, Germany upon approval by the Regierungspräsidium Darmstadt (V54-19c20/15-B2/1014).

2.2 | Open-chest in situ I/R mouse model and estimation of infarct size and zone at risk

Details of the procedure have been published elsewhere.[14,41] Briefly, WT and AOX transgenic littermates were anesthetized and ventilated with ambient air supplemented with oxygen (peak inspiratory pressure of 10 mbar and positive end-expiratory pressure of 3 mbar) throughout the experiment. The ventilation settings were adjusted to a frequency of 110 hubs per minutes and a tidal volume of 200-250 μL. Left anterolateral thoracotomy was performed to visualize the mouse heart and lay open the left anterior descending artery (LAD). The LAD was then surrounded by a 7-0 nylon suture to form a snare. After a 15 minutes period of stabilization, the I/R procedure was started with 30 minutes of ischaemia followed by 2 hour reperfusion. After the I/R procedure, the LAD was re-occluded and Evans blue was injected retrogradely through the aortic root. Evans blue staining was used to demarcate the zone of ischaemia hereafter referred to as the region at risk zone. After staining, hearts were excised, perfused with 0.9% saline solution, frozen and transversely cut into 1 mm slices. The slices were incubated in 1% triphenyltetrazolium chloride (TTC) in sodium phosphate buffer (pH 7.4) and incubated at 38°C for 20 minutes. TTC stains the viable (non-infarcted myocardium) brick-red based on catalytic dehydrogenase activity. Finally, the slices were immersed in 10% formalin and areas of infarct and risk zone determined slice by slice using planimetry.

2.3 | In vivo I/R mouse model

Male WT and AOX littermates received 0.1 mg/kg bodyweight buprenorphine *s.c.* prior to anaesthesia to minimize postoperative pain. For anaesthesia induction, mice were exposed to 4.5 Vol% isoflurane in ambient air for approximately 3 minutes in an air-tight box. Anaesthesia was maintained after intra-tracheal intubation and ventilation using 1.5 Vol% isoflurane using the rodent MiniVent ventilator (Harvard Apparatus, HSE) adjusted to 225 hubs per minutes with a tidal volume of 250 μL. During the procedure, animals were kept in a supine position on a heat-controlled plate at 37°C. A left anterolateral thoracotomy was performed between the second and third rib to visualize the mouse heart and lay open the LAD. The LAD was ligated in a proximal position using a 7-0 prolene suture. Pale discoloration of ventricular tissue demarcated the region of ischaemia. After ligation, animals received 5 IU of Heparin-Natrium s.c. and the open wound was covered using cheese cloth soaked with 0.9% NaCl solution. After 45 minutes of ischaemia, the ligation was opened and cardiac reperfusion confirmed by visual control. The wound was closed using absorbable, synthetic 5-0 vicryl (polyglactin 910) sutures. Weaning from ventilation took several minutes and was ended when spontaneous respiration became evident.

2.4 | Langendorff perfusion experiments

Hearts were isolated from mice, and procedures to measure cardiac functions were performed as previously described.[42] Briefly, after deep anaesthesia with isoflurane (5%), hearts were excised from the chest cavity, transferred rapidly to ice-cold saline and immediately mounted on the cannula of Langendorff perfusion system. Heart perfusion and all next steps were done at 37°C. Perfusion of hearts was performed with perfusate (in mmol/L: NaCl 118, KCl 4.7, KH_2PO_4 1.2, KCl 2.5, $MgSO_4$ 0.8, $NaHCO_3$ 25, glucose 5, $C_3H_3NaO_3$ 1.9, $CaCl_2$ 2.5). Perfusate flow was adjusted to a perfusion pressure of 70 mm Hg. To determine left ventricular pressure, a balloon was inserted into the left ventricle and inflated at 10 mm Hg. Ischaemia was initiated by flow stop.

2.5 | Respirometry and ROS production using isolated mitochondria

Mitochondria were isolated from cardiac tissue as described previously.[43] Mitochondrial oxygen consumption and ROS production were measured using an Oroboros O2k oxygraph (Oroboros Instruments) at 37°C. Standard experimental set-up was 200 μg of mitochondrial protein per mL of mitochondrial respiration buffer (120 mmol/L KCl, 1 mmol/L EGTA, 10 mmol/L HEPES, 5 mmol/L KH_2PO_4, pH 7.2; Sigma, P5405, E3889, H3375, P5655) along with 30 μL of 1 mg/mL superoxide dismutase (Sigma, S5395), 30 μL of 1 mg/mL horseradish peroxidase (Sigma, 77332), 30 μL of 10 mg/mL fatty acid-free-BSA (Sigma, A6003) and 5 μL of Amplex Red Reagent (ThermoFisher, A12222) for hydrogen peroxide detection. Mitochondrial respiration was initiated by the addition of 10 mmol/L succinate (Sigma, S3674). To confirm AOX activity, 1 mmol/L cyanide (KCN, Sigma, 60178) was added to both WT and AOX mitochondria, prior to AOX inhibition by 100 μM *n*-propyl gallate (Sigma, P3130). To assess hydrogen peroxide production as the consequence of RET, mitochondrial respiration was stimulated by the addition of succinate and respiration allowed to diminish all oxygen present within the chamber. Once anoxic, mitochondria were left for 20 or 30 minutes to simulate ischaemia, after which oxygen was allowed back into the chamber and oxygen consumption and ROS production measured. To assess sole AOX activity, cyanide was added at the start of the experiment.

2.6 | Western blot analysis

Western blots were performed essentially as described elsewhere.[44] Rabbit serum raised against two AOX peptides (anti-AOX, 1:20 000, 21st Century Biochemicals)[30] and mouse monoclonal antibody against the voltage-dependent anion channel (anti-VDAC1, 1:1000, Abcam ab14734) were used and protein bands were visualized using a LI-COR Odyssey flatbed scanner with anti-mouse and anti-rabbit secondary antibodies conjugated to IRDye 680RD and IRDye 800CW, respectively.

2.7 | Respirometry using skinned heart fibres and heart tissue homogenate

Mitochondrial respiratory activity upon in vivo I/R was measured using skinned fibre isolation (3-weeks I/R) as described in detail elsewhere[45,46] or after homogenization of heart tissue using a POLYTRON PT 1200 E Manual Disperser (Ecoline; 9-weeks I/R). For skinned fibre isolation, left-ventricular heart tissue was dissected on ice in a plastic cell-culture dish using extra sharp forceps to extract thin muscle fibres. These fibres were permeabilized for 30 minutes using saponin (50 μg/mL) as previously described.[45,46] Upon washing, fibres were dried on Whatman paper and weighted before transfer to the oxygraph chamber. For heart tissue homogenization, left-ventricular heart tissue was weighted and then minced on ice using scissors and a POLYTRON homogenizer before transfer to the oxygraph chamber. Using either technique, mitochondria were found to be accessible for substrates and inhibitors, and exhibited coupled respiration albeit at different activity levels per mg of the respective sample. Oxygen consumption was measured using Oroboros O2k oxygraphs (Oroboros Instruments, Innsbruck, Austria)[47] at 30°C calculated from the time derivative of the oxygen concentration using DatLab 7 software (Oroboros Instruments, Innsbruck, Austria). 1-2 mg of fibre/tissue homogenate was added per chamber to respiration buffer containing 120 mmol/L D-mannitol (Sigma-Aldrich, M4125), 20 mmol/L MOPS (Sigma, M1254), 5 mmol/L KH_2PO_4 (Sigma, P5655), 60 mmol/L KCl, 5 mmol/L $MgCl_2$, pH7.4. Substrates used for cI-driven respiration (PGM plus ADP): 10 mmol/L pyruvate (P, Sigma, P5280), 10 mmol/L glutamate (G, Aldrich, 49621), 2 mmol/L malate (M, Sigma, M1000) and adenosine 5′-diphosphate (ADP, Sigma, A2754). Substrates used for cIV measurements: 2 mmol/L (+)-sodium L-ascorbate (Asc, Sigma, A7631) and 0.5 mmol/L *N*,*N*,*N*′,*N*′-tetramethyl-*p*-phenylenediamine (TMPD, Sigma, T7394). Respiratory inhibitors used for control: 1.5 μmol/L rotenone (Sigma-Aldrich, R8875), 5 mmol/L sodium azide (Sigma-Aldrich, S2002), 1 mmol/L cyanide (Sigma, 60178) and 100 μmol/L *n*-propyl gallate (Sigma, P3130).

2.8 | RNA extraction, reverse transcription (RT) and qPCR

Total RNA was extracted from left ventricles by RNeasy Micro Kit (Qiagen). The extracted RNA was reverse-transcribed (RT) to cDNA using iScript cDNA Synthesis Kit (Bio-Rad). qPCR was done using iTaq SYBR Green Supermix with ROX (Bio-Rad) and Mx3000P qPCR System (Agilent Technologies). All measurements were carried out in duplicate. Melting curves confirmed desired products formation. The calculation of ΔCt values was done by subtracting the Ct values of the target gene from the endogenous control [ΔCt = Ct (endogenous control) − Ct (target)]. Transcript expression levels as fold change were calculated from $2^{-\Delta\Delta Ct}$. *B2m* (*β_2 microglobulin*) served as a reference housekeeping gene.

Gene	Forward primer	Reverse primer
B2m	GCTATCCAGAAAACCCCTCAA	CATGTCTCGATCCCAGTAGACGGT
Anp	GGCTCCTCCCTCGTCTTGG	GCTTCCTCAGTCTGCTCAC
Col1a1	TTCTCCTGGAAAGATGGTGC	GGACCAGCATCACCTTTAACA
Col3a1	CTTTCCCGGTGGGCGTGGTC	TGAGCACCAGGTGGCCCCTT
Sod2	GACTATGGCGCGCTGGAGCC	TCCCTTGGCCAGAGCCTCGT
Ucp2	GGCCTCTGGAAAGGGACTTC	GACCACATCAACAGGGGAGG
Bax	TACAGGGTTTCATCCAGG	ATTGCTATCCAGCCTATCTC
Bcl2	TCGCAGAGATGTCCAGTC	CCCACCGAACTCAAAGAAG

2.9 | Transmission electron microscopy

A small piece of tissue from the heart apex was kept in storage buffer containing 1.5% glutaraldehyde, 1.5% formaldehyde, 0.15 mol/L

HEPES/KOH (pH 7.4) at 4°C until embedding and sectioning. For epoxy resin embedding, samples were fixed in 1% osmium tetroxide, stained *en bloc* in half-saturated uranyl acetate, dehydrated in an ascending ethanol series and embedded in Agar 100 (Agar Scientific). Ultra-thin sections were cut using an ultramicrotome (Reichert Ultracut E, Leica) and examined in a transmission electron microscope (Zeiss EM 902). Digital images were captured with a slow-scan 2K CCD camera (TRS, Tröndle, Moorenweis, Germany).

2.10 | Nano LC-MS/MS and data analysis

Mouse heart samples were homogenized using a FastPrep-24 5G High Speed Homogenizer (MP Biomedicals). Tissue pieces were transferred to 2 mL tubes with Lysing matrix D, and 750 µL 8 mol/L urea (Sigma, U5378) in 50 mmol/L NH_4HCO_3 (Sigma, A6141) and protease inhibitor mix (cOmplete ULTRA Tablets, 05892970001, Roche Applied Science) were added. Homogenization was done with five cycles of 30 seconds 6 m/s pulses and had 5 minutes break on ice in between the cycles. After homogenization, the protein concentration was measured using NanoDrop, and a volume corresponding to 200 µg protein was used for further analysis. Proteins were reduced with dithiothreitol (DTT, Sigma, D9779), alkylated with iodoacetamide (Sigma, I6125) and in-solution digested with LysC (2 hours at room temperature, Wako, 125-05061) and trypsin (overnight at room temperature, Promega, V5111).

The resulting peptides were desalted and concentrated before mass spectrometry using µC18 tip (Pierce C18 Tips). The peptides were eluted with 0.1% trifluoroacetic acid (TFA, Merck, 0.08260.0101) in 60% acetonitrile (ACN, Merck, 1.00029.2500), dried and solubilized in 7 µL 0.1% formic acid (FA, Merck, 1.59013.2500) for mass spectrometry analysis. Each peptide mixture was analysed on an Easy nLC1000 nano-LC system connected to a quadrupole Orbitrap mass spectrometer (QExactive, ThermoElectron, Bremen, Germany) equipped with a nano-electrospray ion source (EasySpray, Thermo). For the liquid chromatography separation of the peptides, an EasySpray column capillary of 25 cm bed length was employed. The flow rate was 300 nL/min, and the peptides were eluted with a 2%-30% gradient of solvent B in 240 minutes. Solvent A was aqueous 0.1% FA and solvent B 0.1% FA in acetonitrile. The data-dependent acquisition automatically switched between MS and MS/MS mode. Survey full scan MS spectra were acquired from a mass-to-charge ratio (m/z) of 400 to 1200 with the resolution R = 70 000 at m/z 200 after accumulation to a target of 3 000 000 ions in the quadruple. For MS/MS, the ten most abundant multiple-charged ions were selected for fragmentation on the high-energy collision dissociation cell at a target value of 100 000 charges or maximum acquisition time of 100 ms The MS/MS scans were collected at a resolution of 17 500. Target ions already selected for MS/MS were dynamically excluded for 30 seconds.

The resulting MS raw files were submitted to the MaxQuant software (version 1.5.7.4)[48] for protein identification and quantitation using the Andromeda search engine. MaxQuant search was done against the UniProt mouse database (March 2017). Carbamidomethyl (C) was set as a fixed modification and protein N-acetylation and methionine oxidation were set as variable modifications. First search peptide tolerance of 20 ppm and main search error 4.5 ppm were used. Trypsin without proline restriction enzyme option was used, with two allowed miscleavages. The minimal unique + razor peptides number was set to 1 and the allowed false discovery rate (FDR) was 0.01 (1%) for peptide and protein identification. Label-free quantification (LFQ) was done with default settings in MaxQuant. The mass spectrometry proteomics data have been deposited to the ProteomeXchange[49] Consortium via the PRIDE[50] partner repository with the dataset identifier: PXD014061 and the project name 'Expression of *Ciona intestinalis* AOX in a mouse model of cardiac ischemia-reperfusion'.

2.11 | Statistical analyses

Statistical analyses, except for proteome, were performed using GraphPad Prism (GraphPad Software, version 7 for Mac OS X). 1way or 2way ANOVA and post hoc analyses were used as indicated for comparisons of at least n = 3 independent experiments, and a P value <.05 was considered being statistically significant. All data are shown as mean. Error bars represent standard error of the mean (SEM). Proteome analysis was done using Perseus software (version 1.6.1.3).[51] LFQ values were log2 transformed and filtered to include only proteins identified and quantified in at least three out of five replicates in at least one experimental group, and missing values were imputed with values representing background from a normal distribution with default settings in Perseus. To find statistically significant differences between the sample groups Student's t test was done with a P value of <.05 being considered statistically significant.

3 | RESULTS

3.1 | AOX does not decrease acute I/R injuries

Succinate accumulation during cardiac ischaemia[25] is one proposed trigger for RET-mediated ROS production[24] and supposedly I/R-mediated injury. AOX was previously demonstrated to blunt RET-induced ROS production under various conditions.[33,34,36,37] We therefore first tested whether the extent of acute I/R injury (infarct size) would be decreased in the post-ischaemic heart of mice with excellent cardiac AOX protein expression and catalytic AOX activity.[33] Using the open-chest in situ I/R model,[41] 30 minutes of ischaemia were applied by occluding the left anterior descending (LAD) coronary artery followed by 2 hours of reperfusion in wild-type (WT) and AOX littermates. The infarct size was estimated as a percentage scar tissue of the risk zone.[41,52] As shown in Figure 1A,B, AOX expression did not confer any benefit. We next sought to investigate whether the heart might nevertheless benefit during the early post-ischaemic phase through improved functional recovery of surviving myocytes and analysed heart contractile

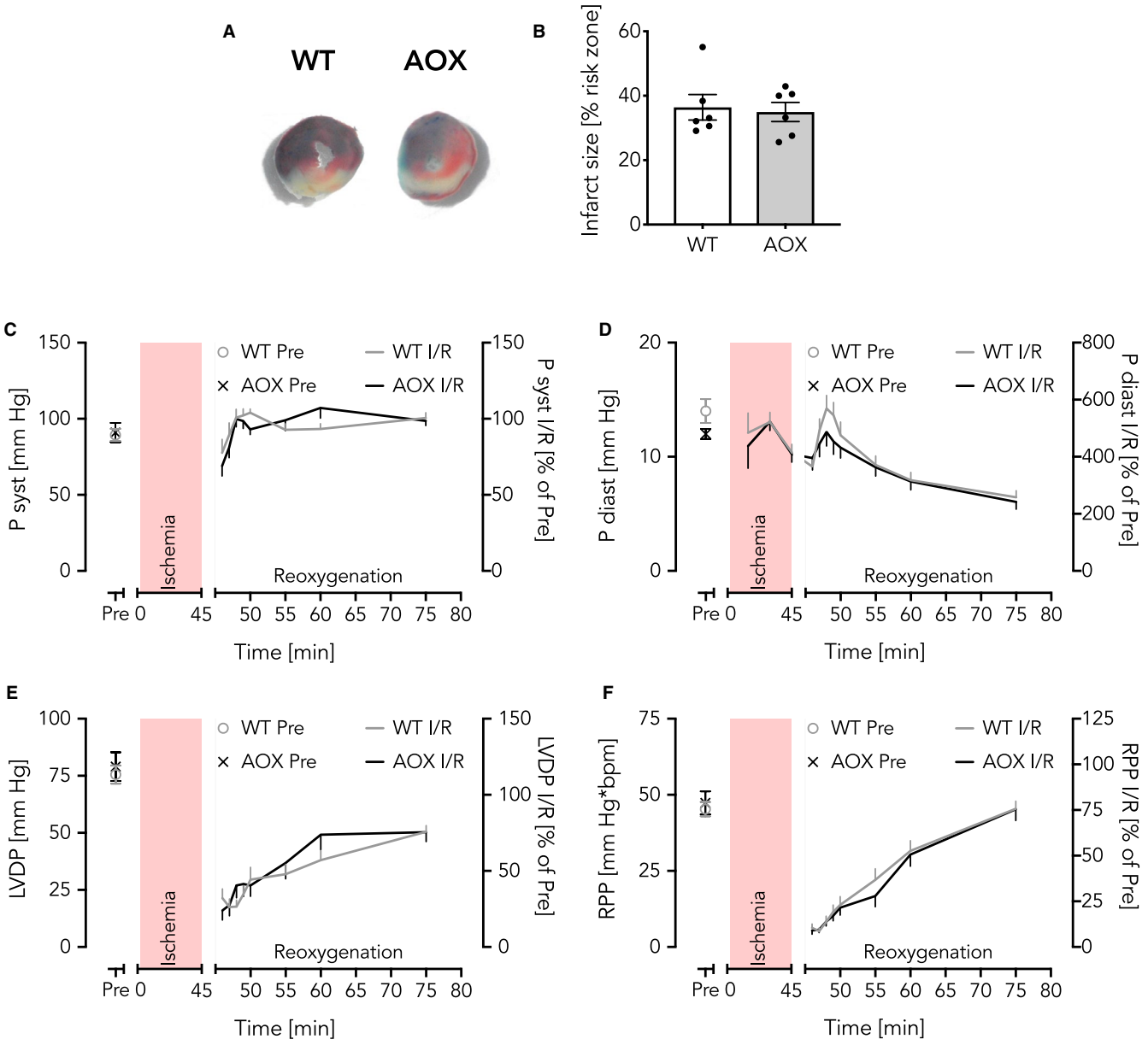

FIGURE 1 AOX does not protect the heart from I/R injury. A, B, Open-chest in situ mouse heart model with 30 min ischaemia and 2 h reperfusion. A, Representative images of infarcts from WT and AOX mice as indicated. Blue, Evans blue staining indicates perfused tissue; brick-red, TTC converted to precipitate indicates viable post-ischaemic tissue; white, indicates scar tissue; brick-red and white together form the 'region of risk' zone. B, Infarct size depicted as % of region at risk zone. Data shown as mean ± SEM of n = 6 experiments. C-F, Response curves from the ex vivo isolated perfused Langendorff heart model with 45 min ischaemia (red area) and 30 min reoxygenation. C, Systolic pressure (P syst); D, diastolic pressure (P diast); E, left ventricular developed pressure (LVDP); F, heart rate*pressure product (RPP). Pre, control values at time point 0. All Langendorff data are shown as mean ± SEM of n ≥ 8 experiments

functions ex vivo in the isolated, perfused (Langendorff) heart. Upon 45 minutes of ischaemia, WT and AOX hearts showed nearly indistinguishable systolic (P syst, Figure 1C) and diastolic (P diast, Figure 1D) pressure-response curves. Furthermore, calculated left ventricular developed pressures (LVDP [maximal systolic–diastolic pressure]) (Figure 1E) and heart rate*pressure products (RPP, a surrogate value of cardiac work)[53] (Figure 1F) revealed no difference. Of note, hearts typically develop a rigour during ischaemia. This manifests as an increase in pressure during the ischaemic insult and, in our experience, correlates closely with the infarct size. WT and AOX hearts developed the same degree of rigour during ischaemia (Figure 1D) once again being indicative for a lack AOX-mediated cardioprotection during I/R.

3.2 | AOX is catalytically active in post-anoxic heart mitochondria

One possible explanation for the observed failure of protection could be insufficient AOX expression or its catalytic impairment in the

post-ischaemic heart. To test this possibility, we isolated mitochondria from WT and AOX mouse hearts and measured oxygen consumption and ROS production in vitro, and, importantly, confirmed a robust expression of AOX by Western blot (Figure S1A). As expected, AOX supported succinate-driven respiration in a cyanide-resistant manner (Figure 2A) at ambient oxygen concentrations. AOX-driven cyanide-resistant respiration was associated with the prevention of mitochondrial hydrogen peroxide production (Figure 2B). Next, we tested whether AOX catalytic activity depends on a certain oxygen concentration. In other words, we sought to test if AOX loses its catalytic activity underneath a critical threshold of oxygen availability such as seen in the ischaemic heart. We thus measured oxygen consumption and hydrogen peroxide production under different oxygen concentrations ranging from ~21% (ambient air) to full anoxia (Figure 2C,D). We found that the oxygen consumption in AOX heart mitochondria was slightly higher than in WT across a broad range of oxygen concentrations (Figure 2C). Hydrogen peroxide production showed a linear relationship with oxygen availability in WT and was lower in AOX mitochondria (Figure 2D). To simulate the situation in the post-ischaemic heart, we challenged heart mitochondria by a 20 minutes period of anoxia (simulated ischaemia, Figure 2E,F). Using this approach, oxygen consumption in WT heart mitochondria was slightly higher than in those from AOX hearts, at all oxygen concentrations (Figure 2E). In contrast, hydrogen peroxide production, which again showed a linear relationship with oxygen availability, was significantly lower in AOX heart mitochondria (Figure 2F). To rule out the possibility that the period of anoxia was not sufficient, we replicated the experiments with an extended period of anoxia (30 minutes), which essentially gave the same results (Figure S1B-E). Together with previous findings of AOX activity in the heart under various conditions,[33,38,40] we concluded that a functional

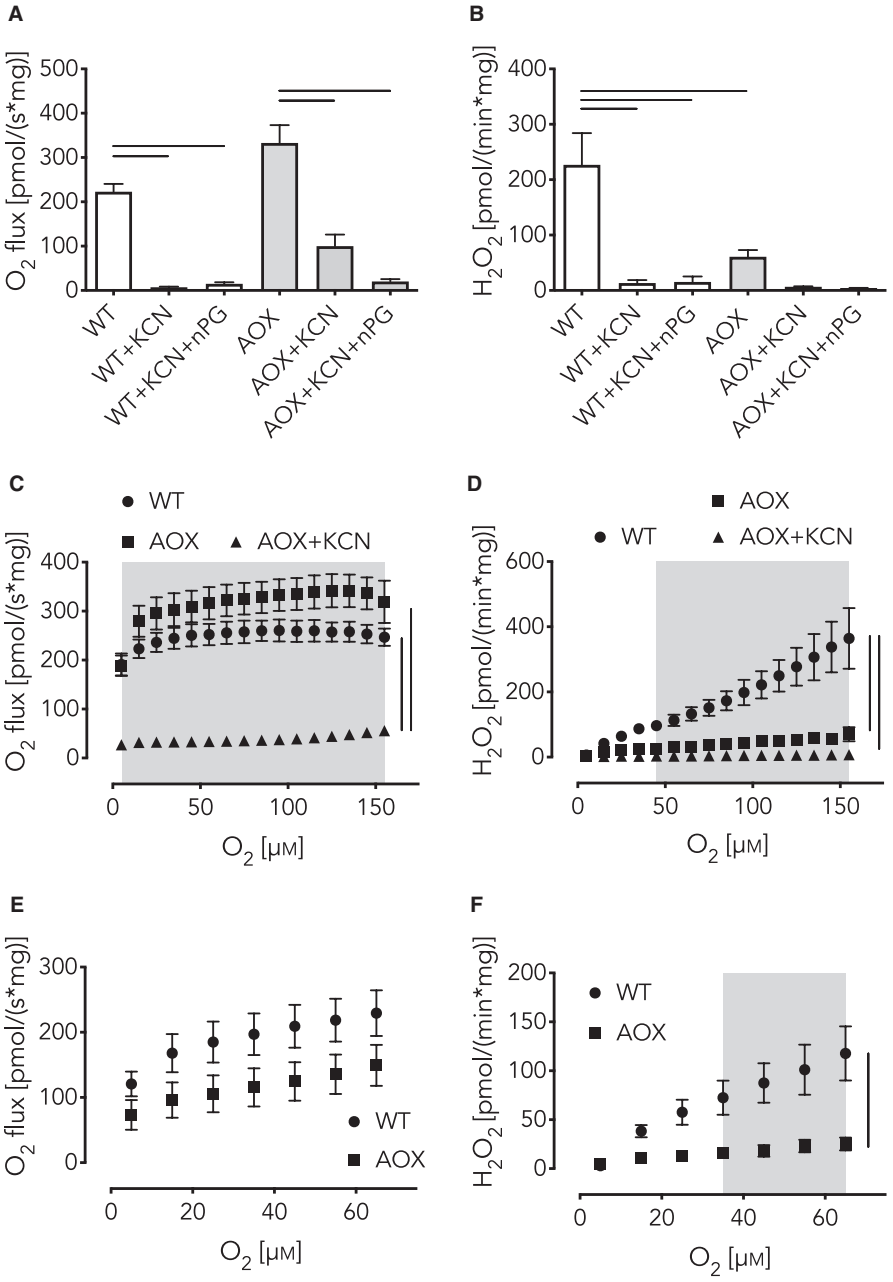

FIGURE 2 AOX is catalytically engaged in post-anoxic heart mitochondria and lowers mitochondrial ROS production. A-F, Isolated WT and AOX heart mitochondria energized with cII substrate succinate and addition of inhibitors as indicated. KCN, cIV inhibitor potassium cyanide; nPG, AOX inhibitor *n*-propyl gallate. A, Oxygen consumption. B, Hydrogen peroxide production. Data in (A, B) are shown as mean ± SEM of n ≥ 3 experiments. Horizontal bars in (A, B) indicate significant differences with $P < .05$ analysed by 1way ANOVA and Tukey's multiple comparisons test. C, Oxygen consumption in dependence of oxygen concentration. D, Hydrogen peroxide production in dependence of oxygen concentration. E, Oxygen consumption during reoxygenation after 20 min of anoxia. F, Hydrogen peroxide production during reoxygenation after 20 min of anoxia. Data in (C-F) are shown as mean ± SEM of n ≥ 3 experiments. Grey areas and vertical bars indicate significant differences with $P < .05$ analysed by 2way ANOVA and Tukey's multiple comparisons test in (C, D) and Sidak's multiple comparisons test in (F)

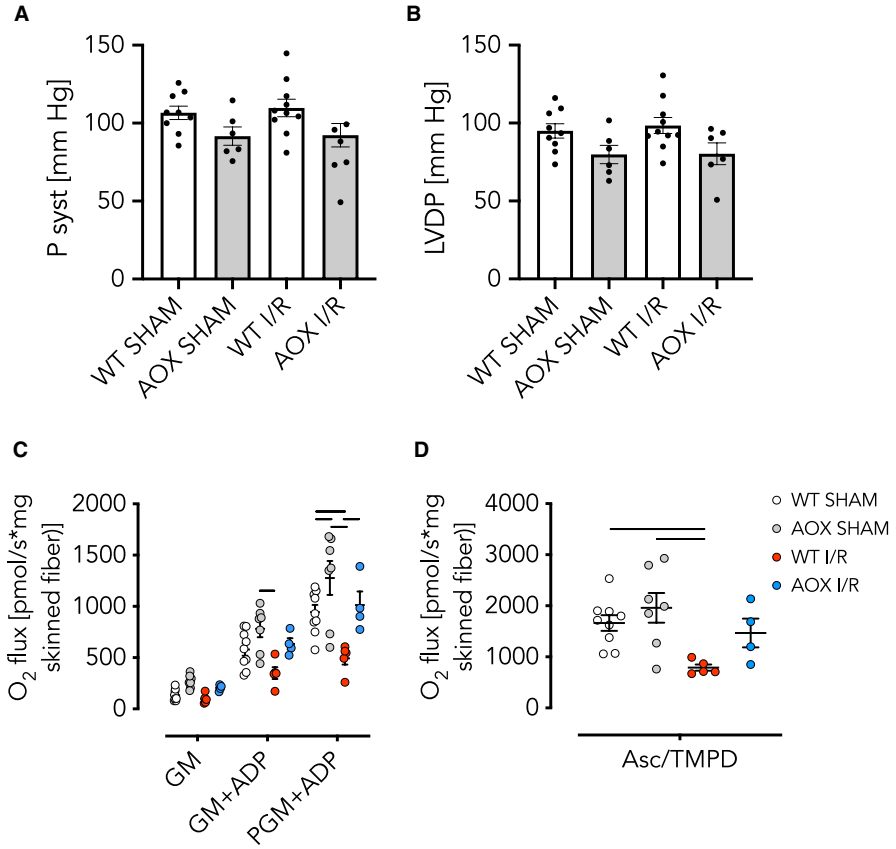

FIGURE 3 AOX expression does not affect cardiac contractility in vivo 3 wk after I/R despite improved respiratory function. A, B, Left ventricular pressures built up ex vivo in the isolated perfused Langendorff heart model of WT and AOX hearts subjected to 45 min of ischaemia or SHAM operation followed by 3 wk of reperfusion and remodelling in vivo. Data shown as mean ± SEM of n ≥ 6 experiments. A, Systolic pressure (P syst); B, left ventricular developed pressure (LVDP). C, D, Oxygen consumption of isolated skinned heart fibres. Data shown as mean ± SEM of n ≥ 4 experiments. C, Complex I (cI) activity driven by combinations of pyruvate (P), glutamate (G) and malate (M) as indicated, plus ADP. Horizontal bars indicate significant differences with $P < .05$ analysed by 2way ANOVA and Tukey's multiple comparisons test. D, Complex IV (cIV) activity driven by ascorbate (Asc) and *N,N,N′,N′*-tetramethyl-*p*-phenylenediamine (TMPD). Horizontal bars indicate significant differences with $P < .05$ analysed by 1way ANOVA and Tukey's multiple comparisons test

impairment of AOX is an unlikely explanation for the lack of cardioprotection against I/R injury, and that, therefore, all observed phenomena can mechanistically be attributed to catalytic AOX activity interfering with the mitochondrial respiratory chain and specifically to the restoration of the electron flux through the ETC.

3.3 | AOX improves mitochondrial functions 3 weeks after an ischaemic insult

We hypothesized that the restoration of electron flux by AOX and supposed decrease in RET-induced ROS, despite the lack of a measurable advantage during the acute phase, might yet be beneficial for the post-ischaemic remodelling process. We tested this assumption in WT and AOX mice 3 weeks after a transient (45 minutes) ischaemic insult followed by restoration of blood flow (reperfusion).[54] Functional left-heart parameters (P syst and LVDP) measured ex vivo, however, revealed no significant difference between WT and AOX (Figure 3A,B). Conversely, high-resolution respirometry using permeabilized heart fibres revealed that cI-linked respiration, driven by pyruvate, glutamate and malate (PGM) plus ADP (Figure 3C), as well as cIV activity driven by ascorbate/TMPD (Figure 3D) was significantly compromised in WT I/R but not AOX I/R hearts. The finding that cIV was impaired in WT I/R hearts came unexpected, since cIV lies downstream of the quinone pool and the ROS-producing complexes cI and cIII. Interestingly, electron microscopy revealed no evidence for an ultrastructural correlate of these biochemical differences, for example at the level of mitochondrial cristae density (Figure S2).

Typically, adaptive cardiac response to hemodynamic or metabolic stress is seen as myocardial hypertrophy concomitant with and triggered by an alteration of gene expression. To determine whether respiratory restoration by AOX induced a shift in gene expression in response to the ischaemic insult, we measured transcript levels of common marker genes. First, we measured that of the *atrial natriuretic peptide* (*Anp*), which is recognized as both a biomarker for the diagnosis of heart failure as well as a prognostic marker for cardiovascular risk.[55] Expression of the *Anp* was significantly increased by

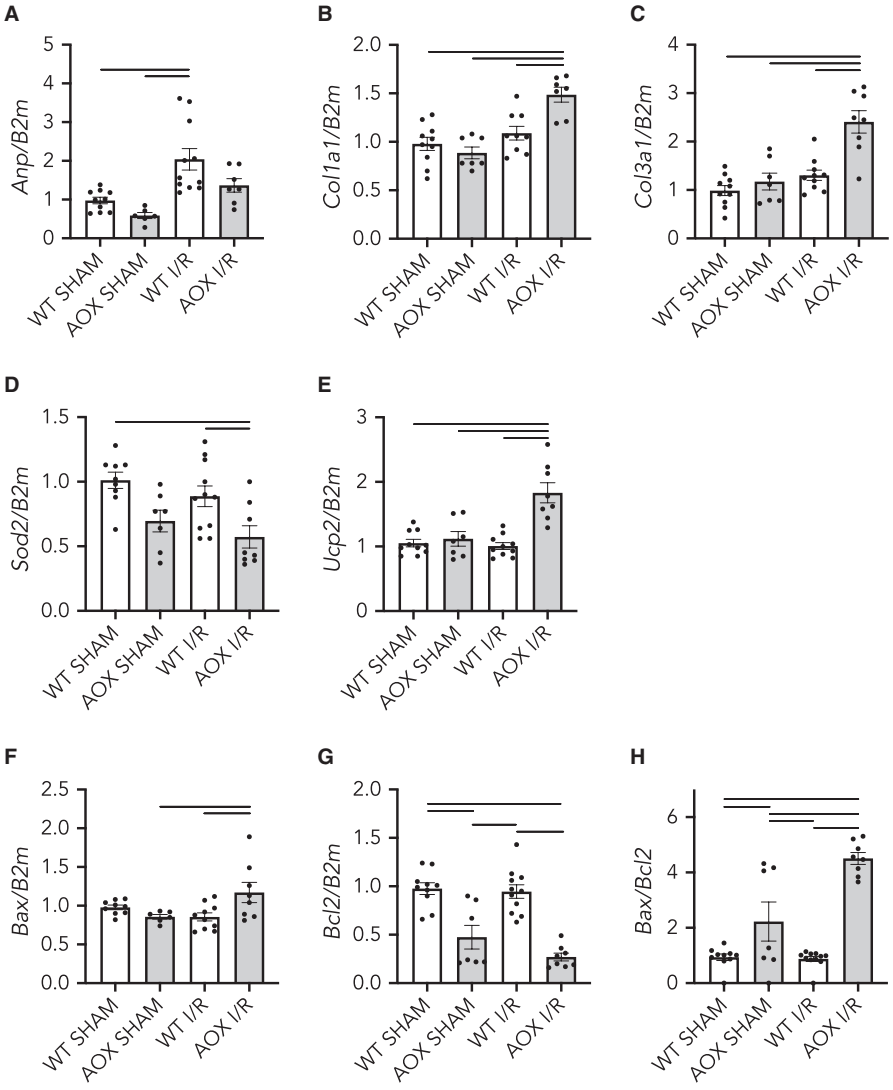

FIGURE 4 Relative transcript levels in total RNA from WT and AOX hearts subjected to 45 min of ischaemia or SHAM operation followed by 3 wk of reperfusion and remodelling in vivo, normalized to *B2m* (β_2 *microglobulin*), a reference housekeeping gene. Data shown as mean ± SEM of n ≥ 6 experiments. Horizontal bars indicate significant differences with $P < .05$ analysed by 1way ANOVA and Tukey's multiple comparisons test. A, *Atrial natriuretic peptide* (*Anp*); B, *Collagen 1* (*Col1a1*); C, *Collagen 3* (*Col3a1*); D, *Superoxide dismutase 2* (*Sod2*); E, *Uncoupling protein 2* (*Ucp2*); F, *Bcl2-associated X* (*Bax*); G, *B-cell lymphoma 2* (*Bcl2*); H, *Bax*/*Bcl2* expression ratio

I/R in WT hearts but, importantly, this increase was blunted in AOX animals (Figure 4A). Since ANP has been described as profibrogenic[56] and since excess cardiac collagen synthesis and deposition is known to negatively affect contractile function,[57] we measured transcripts of *collagen 1* (*Col1a1*) and *3* (*Col3a1*), which we found specifically increased in the AOX I/R group (Figures 4B,C). We also looked at the expression of mitochondrial genes involved in the response to oxidative stress. *Superoxide dismutase 2* (*Sod2*) is a mitochondrial protein that detoxifies superoxide generated as by-product of OXPHOS, by converting it to hydrogen peroxide and molecular oxygen. *Sod2* is induced as part of the cell-inherent ROS stress response,[58] which, when lacking, induces cardiac malfunctioning.[59] Transcript levels of *Sod2* appeared down-regulated in AOX hearts compared with WT, irrespective of any intervention (Figure 4D). Uncoupling proteins (UCPs), in contrast, are mitochondrial inner membrane proteins that act as proton leaks, thereby dissipating the proton gradient. *Uncoupling protein 2* (*Ucp2*) has previously been shown to be instrumental for protection against pressure overload-induced right heart failure.[60] Here, we found *Ucp2* specifically up-regulated in the AOX I/R group (Figure 4E). Finally, heart failure due to apoptotic loss of cardiomyocytes has been long discussed.[61] Bcl-2-associated X protein (BAX) is a pro-apoptotic member of the BCL2 protein family. Indeed, *Bax* transcript expression has been negatively correlated with cardiac function whilst *Bcl2* transcript expression has positive effects.[62] More specifically, an increased *Bax*/*Bcl2* ratio has been seen in cardiac fibrosis.[63] Of note, we found a significant increase in the ratio of *Bax* to *Bcl2* (Figure 4F-H), which is indicative for a cellular shift towards a pro-apoptotic phenotype.

3.4 | AOX impairs cardiac contractility 9 weeks after an ischaemic insult

The lack of any positive impact on post-ischaemic functioning, despite the prevention of *Anp* transcript induction, prompted us to investigate the effects of AOX at a later time point. Nine weeks after transient ischaemia (45 minutes), ex vivo functional measurements revealed a significant decrease in P syst (Figure 5A) and LVDP (Figure 5B) specifically in the AOX I/R group. High-resolution respirometry revealed a continuing, albeit much smaller, cI defect

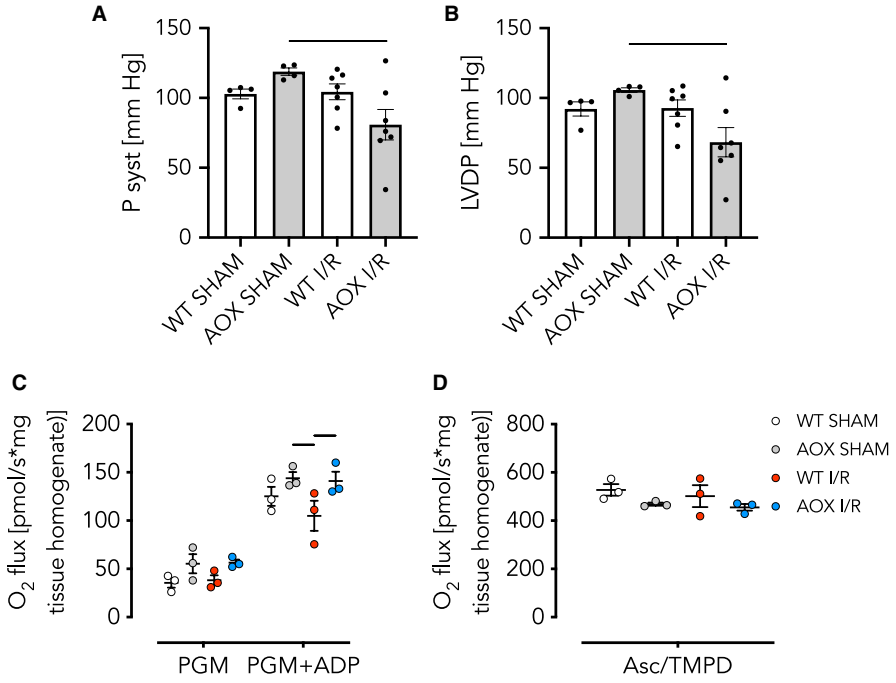

FIGURE 5 AOX expression decreases cardiac contractility 9 wk after I/R. A, B, Left ventricular pressures built up ex vivo in the isolated perfused Langendorff heart model of WT and AOX hearts subjected to 45 min of ischaemia or SHAM operation and 9 wk of reperfusion/remodelling. Data shown as mean ± SEM of n ≥ 4 experiments. Horizontal bars in (A) and (B) indicate significant differences with $P < .05$ analysed by 1way ANOVA and Tukey's multiple comparisons test. A, Systolic pressure (P syst); B, left ventricular developed pressure (LVDP). C, D, Oxygen consumption of heart tissue homogenate. Data shown as mean ± SEM of n = 3 experiments. C, Complex I (cI) activity driven by pyruvate (P), glutamate (G) and malate (M) plus ADP. Horizontal bars indicate significant differences with $P < .05$ analysed by 2way ANOVA and Tukey's multiple comparisons test. D, Complex IV (cIV) activity driven by ascorbate (Asc) and *N*,*N*,*N*′,*N*′-tetramethyl-*p*-phenylenediamine (TMPD)

in WT I/R but not in AOX I/R hearts (Figure 5C) whilst cIV activity was fully restored (Figure 5D). At this later time point, *Anp* transcript levels were even more elevated in WT I/R hearts than 3 weeks after ischaemia and AOX again prevented *Anp* induction (Figure 6A). Most other alterations of transcript level were less pronounced (Figure 6B-H).

3.5 | AOX fosters extracellular matrix remodelling in the post-ischaemic heart

To shed light on the mechanisms that may underlie the post-ischaemic functional deterioration of AOX I/R hearts, we initiated an unbiased, label-free quantitative proteome approach (data submitted to PRIDE database, identifier PXD014061) and used GOrilla, an online tool designed to discover and visualize enriched gene ontologies in ranked lists[64,65] (Tables S1 and S2). We revealed a pronounced expression of proteins involved in the reorganization of the extracellular matrix as a major feature in the post-ischaemic AOX heart. This is best exemplified by the expression of the protein periostin (POSTN, osteoblast-specific factor). Periostin was up-regulated almost fivefold in post-ischaemic compared with SHAM-operated AOX hearts at 3 weeks, and 17-fold at 9 weeks, whilst the increase in the corresponding WT hearts was <2- and approximately sevenfold after 3 and 9 weeks, respectively.

4 | DISCUSSION

In the present study, we tested how respiratory restoration by AOX affects the development of I/R injury and adaptive remodelling in the mouse heart. Our data demonstrate that AOX, despite being sufficiently expressed and catalytically active in the healthy and diseased mouse heart,[33,38,40] fails to confer either acute or chronic cardioprotection, despite respiratory restoration. Instead, AOX expression fosters long-term adverse remodelling and cardiac contractile impairment. Since one effect of AOX should be a decrease in mitochondrial superoxide production, the outcome of this study may seem surprising. Previous studies using mitochondrially targeted antioxidants under ostensibly comparable conditions did result in cardioprotection, as discussed in detail elsewhere.[66] Although ischaemic accumulation of succinate was shown to be instrumental for reperfusion injury through RET-induced ROS production[25] and despite recent findings that AOX can specifically decrease RET[34,36,37] the outcome of this study may be in accordance with another proposed mechanism, namely mitohormesis.[13] For instance, AOX may suppress mitochondrial signals, for example ROS, to a degree that adaptive cardiac remodelling is impaired. Indeed, a cardioprotective effect of low ROS levels has been shown.[14] Conversely, it may be that AOX, which like cIV requires oxygen as terminal electron acceptor, becomes only slowly

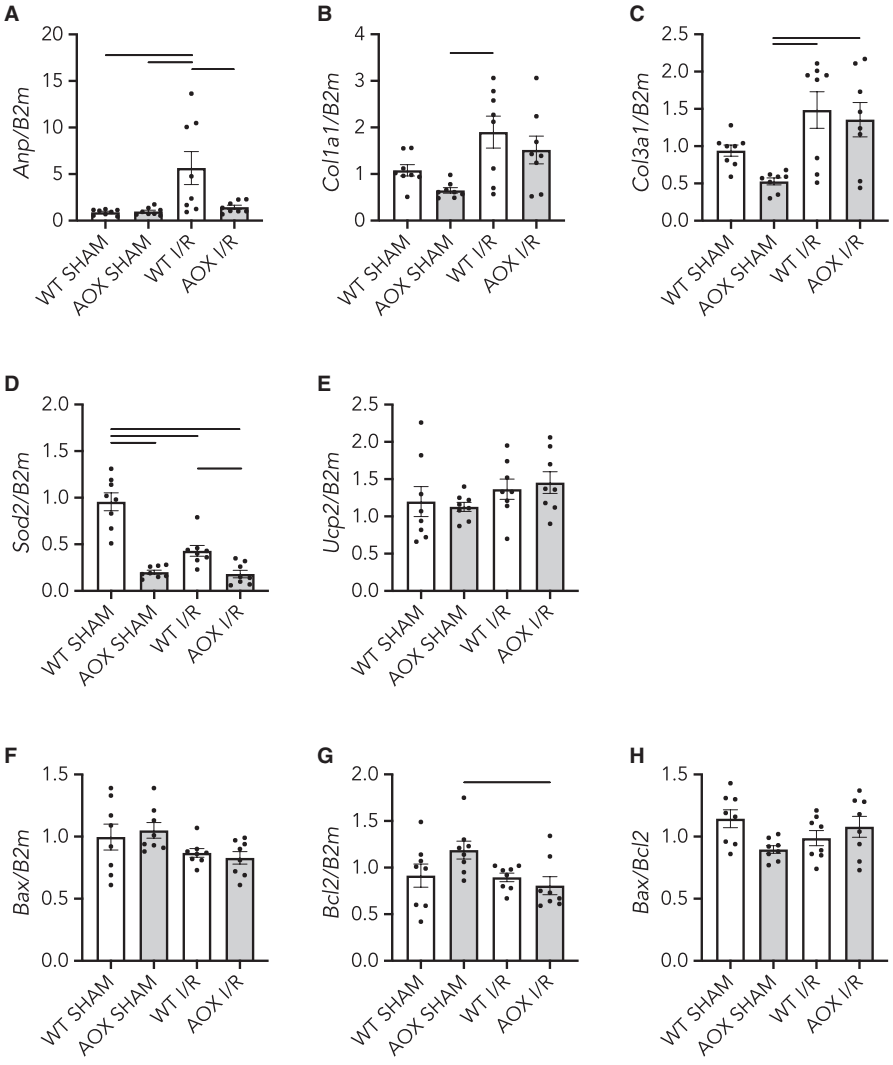

FIGURE 6 Relative transcript levels in total RNA from WT and AOX hearts subjected to 45 min of ischaemia or SHAM operation followed by 9 wk of reperfusion and remodelling in vivo, normalized to *B2m* (β_2 *microglobulin*), a reference housekeeping gene. Data shown as mean ± SEM of n = 8 experiments. Horizontal bars indicate significant differences with $P < .05$ analysed by 1way ANOVA and Tukey's multiple comparisons test. A, *Atrial natriuretic peptide* (*Anp*); B, *Collagen 1* (*Col1a1*); C, *Collagen 3* (*Col3a1*); D, *Superoxide dismutase 2* (*Sod2*); E, *Uncoupling protein 2* (*Ucp2*); F, *Bcl2-associated X* (*Bax*); G, *B-cell lymphoma 2* (*Bcl2*); H, *Bax*/*Bcl2* expression ratio

reactivated upon tissue reoxygenation. In such a case, cI and/or cIII may produce excess amounts of detrimental ROS in a small post-ischaemic time-window before AOX can exert any protective effect. However, our in vitro data indicate that AOX is catalytically engaged both before and after simulated ischaemic insults and prevents RET-induced ROS production under the conditions experienced in the post-ischaemic heart.[36,37] This would argue against a role for slow reactivation. Furthermore, respirometry after 3 weeks of reperfusion revealed that AOX did confer some protection from respiratory impairment, specifically of cI and cIV, despite the lack of any functional improvement. This makes a limitation on AOX catalytic activity in the post-ischaemic heart an unlikely explanation for the observed lack of acute cardioprotection.

One fundamental difference between the use of antioxidants targeted to mitochondria and genetically expressed AOX is that the former are not normally replenished beyond the acute post-ischaemic phase. In addition, antioxidants, unlike AOX, may exhibit antioxidant effects during transit to the mitochondria and may therefore not be entirely specific for mitochondrial ROS. An obvious follow-up study to test this idea would be the use of an inducible AOX strain to enable transient AOX expression during different phases of the I/R procedure. The use of AOX as a therapeutic, in the form of an mRNA mimetic or recombinant protein, may also address this issue. Both approaches would nevertheless suffer other shortcomings such as time- and/or organ-unspecific expression of relevant drivers, unwanted side effects of the same drivers in case of the genetic approach, and immune and inflammatory responses in case of the therapeutic use of AOX, necessitating cumbersome controls.

Despite its ability to maintain respiration and dampen RET-induced ROS in isolated mitochondria, we found that AOX not only fails to provide cardioprotection but actually promotes post-ischaemic maladaptation. An interesting aspect of our study is that the presence of AOX in the post-ischaemic heart restores cI-driven respiration. In fact, cI may be both, a ROS-producing complex for instance under conditions as seen in the post-ischaemic heart[24,25] or itself a target for ROS damage.[67] Previously, however, it was shown that supplementing rat hearts undergoing ischaemic insults with Ndi1, a single-subunit protein that in *Saccharomyces cerevisiae* serves as an NADH dehydrogenase, greatly decreases I/R injury and infarct size.[68,69] In the light of this and of our

findings showing that AOX can restore cI-driven respiration whilst decreasing ROS, it seems reasonable to conclude that other factors than ROS production or electron flow restoration through cI must contribute to the cardiac stress response.

The present findings have some similarity with another study in which AOX was found to disrupt skeletal muscle remodelling upon knock-out of cIV assembly factor COX15, a protein involved in the biosynthetic pathway of mitochondrial haem A, a prosthetic group of cIV.[58] In this model, co-expression of AOX exacerbated muscle dysfunction and accelerated premature death. The aggravated muscle phenotype was associated with decreased mitochondrial biogenesis and, most likely, impaired progenitor (satellite) cell recruitment. Due to the absence of cardiac progenitor cells, other mechanisms must be considered in the mouse heart, although the underlying mechanism, a failure of regular stress signalling and repair processes, may be similar. Our study also recapitulates a study showing that mitochondria-targeted overexpression of catalase does not prevent cardioskeletal myopathy in a mouse model of Barth syndrome.[70] It is important to note, however, that whilst catalase facilitates the turnover of hydrogen peroxide to water and oxygen, AOX prevents the production of superoxide at the impaired ETC and thus acts far upstream.

To provide some indication of the mechanism whereby AOX leads eventually to a maladaptive cardiac remodelling, we studied the expression of a small set of marker genes. Although the findings do not provide a definitive explanation, they reveal valuable clues that should be followed up by a more detailed characterization of the physiological and molecular changes in the AOX I/R model, as now discussed. First, AOX abrogated the up-regulation of *Anp* at the transcript level. ANP was originally found to be up-regulated in the failing heart, irrespective of the underlying cause[71] and was assumed to be compensatory in nature.[72] This view has subsequently been challenged.[73] ANP is now considered a diagnostic marker of maladaptive cardiac remodelling.[55,74-77] This notion may need further revision, in the light of our finding of increased expression of *Col1a1* and *Col3a1* in AOX hearts, despite the blunted *Anp* response. Whilst collagen decreases wall stress, it also impairs contractile function due to increased stiffness, and accompanies the development of heart failure.[57]

One consequence of *Anp* signalling, shown previously in rat pulmonary arterial smooth muscle cells, is the inhibition of TGFβ-induced extracellular matrix components.[78] We suggest that this might account for the observed up-regulation of periostin, consistent with another study where heart remodelling upon stress was associated with progressive extracellular matrix remodelling.[79] However, the role of periostin in cardiac repair remains unclear: whilst it has been found to initiate cell cycle re-entry of adult cardiomyocytes upon stress[80] it is also associated with myocardial fibrosis in some forms of heart failure.[81-83] Consistent with the idea that AOX interferes with a respiratory stress signal related to mitochondrial ROS, we observed downregulation of the oxidative stress marker *Sod2*, but up-regulation of *Ucp2*, previously observed in conditions of cardiovascular stress.[84]

In conclusion, we infer that mitochondrial respiratory restoration and the presumed decrease of mitochondrial ROS by AOX in the post-ischaemic heart are not sufficient to confer cardioprotection. Instead, AOX expression interferes with adaptive organ remodelling leading to contractile failure, implying an essential role for ETC-derived stress signals in this process.

ACKNOWLEDGEMENTS

The authors thank Pierre Rustin for valuable discussions, and Jana Meisterknecht and Nadine Woitasky for excellent technical assistance. This work was supported by ERC Advanced Grant 232738 and Academy of Finland grants 272376 and 256615 (to HTJ), grants from the Deutsche Forschungsgemeinschaft SFB 815/Z1 and the BMBF mitoNET-German Network for Mitochondrial Disorders 01GM1906D (to IW), a grant from the Deutsche Forschungsgemeinschaft SFB 1213 (to TB and K-DS), a core grant of the Medical Research Council (MRC) UK to the Mitochondrial Biology Unit (MC_UU_00015/5) (to CV), and a MRC grant (MC_U105663142) and a Wellcome Trust Investigator award (110159/Z/15/Z) (to MPM).

CONFLICT OF INTEREST

MSz has financial interests in developing therapeutics based on *Ciona intestinalis* AOX. All other authors declare no competing interests.

AUTHOR CONTRIBUTIONS

MSz, HTJ, K-DS, FNG, TK and MPM conceived and designed experiments and supervised parts of the work. MSz, RS, ZG, ED, MW, PKD, GD-V, JH, IW, TAN, UG, ARH, VP and CV performed experiments and analysed data. MSz, IW, TK, MPM, TB, FNG, K-DS and HTJ interpreted data and drafted the manuscript. All authors read and revised the manuscript and contributed substantially to the work.

DATA AVAILABILITY STATEMENT

All data needed to evaluate the conclusions in the paper are present in the paper and/or the supplements. Additional data related to this paper may be requested from the authors.

ORCID

Marten Szibor https://orcid.org/0000-0003-4029-160X
Zemfira Gizatullina https://orcid.org/0000-0003-2240-4471
Eric Dufour https://orcid.org/0000-0001-6690-5329
Praveen K. Dhandapani https://orcid.org/0000-0002-3486-4355
Grazyna Debska-Vielhaber https://orcid.org/0000-0002-6661-9821
Juliana Heidler https://orcid.org/0000-0003-2607-2849
Ilka Wittig https://orcid.org/0000-0002-9751-8054
Tuula A. Nyman https://orcid.org/0000-0001-8787-5886
Carlo Viscomi https://orcid.org/0000-0001-6050-0566
Thomas Krieg https://orcid.org/0000-0002-5192-580X
Frank N. Gellerich https://orcid.org/0000-0002-6550-4555
Klaus-Dieter Schlüter https://orcid.org/0000-0002-6093-4919
Howard T. Jacobs https://orcid.org/0000-0003-1895-6003

REFERENCES

1. Piquereau J, Caffin F, Novotova M, et al. Mitochondrial dynamics in the adult cardiomyocytes: which roles for a highly specialized cell? *Front Physiol*. 2013;4:102.
2. Otani H, Tanaka H, Inoue T, et al. In vitro study on contribution of oxidative metabolism of isolated rabbit heart mitochondria to myocardial reperfusion injury. *Circ Res*. 1984;55:168-175.
3. Ambrosio G, Zweier JL, Duilio C, et al. Evidence that mitochondrial respiration is a source of potentially toxic oxygen free radicals in intact rabbit hearts subjected to ischemia and reflow. *J Biol Chem*. 1993;268:18532-18541.
4. Peng Y-W, Buller CL, Charpie JR. Impact of N-acetylcysteine on neonatal cardiomyocyte ischemia-reperfusion injury. *Pediatr Res*. 2011;70:61-66.
5. Hao J, Li W-W, Du H, et al. Role of vitamin C in cardioprotection of ischemia/reperfusion injury by activation of mitochondrial KATP channel. *Chem Pharm Bull*. 2016;64:548-557.
6. Nishinaka Y, Sugiyama S, Yokota M, Saito H, Ozawa T. The effects of a high dose of ascorbate on ischemia-reperfusion-induced mitochondrial dysfunction in canine hearts. *Heart Vessels*. 1992;7:18-23.
7. Mickle DAG, Li R-K, Weisel RD, et al. Myocardial salvage with trolox and ascorbic acid for an acute evolving infarction. *Ann Thorac Surg*. 1989;47:553-557.
8. Klein HH, Pich S, Lindert S, Nebendahl K, Niedmann P, Kreuzer H. Combined treatment with vitamins E and C in experimental myocardial infarction in pigs. *Am Heart J*. 1989;118:667-673.
9. Goszcz K, Deakin SJ, Duthie GG, Stewart D, Leslie SJ, Megson IL. Antioxidants in cardiovascular therapy: panacea or false hope? *Front Cardiovasc Med*. 2015;2:29.
10. Bjelakovic G, Nikolova D, Gluud LL, Simonetti RG, Gluud C. Antioxidant supplements for prevention of mortality in healthy participants and patients with various diseases. *Sao Paulo Med J*. 2015;133:164-165.
11. Hegstad AC, Antonsen OH, Ytrehus K. Low concentrations of hydrogen peroxide improve post-ischaemic metabolic and functional recovery in isolated perfused rat hearts. *J Mol Cell Cardiol*. 1997;29:2779-2787.
12. Valen G, Starkopf J, Takeshima S, et al. Preconditioning with hydrogen peroxide (H2O2) or ischemia in H2O2-induced cardiac dysfunction. *Free Radical Res*. 1998;29:235-245.
13. Yun J, Finkel T. Mitohormesis. *Cell Metab*. 2014;19:757-766.
14. Antonucci S, Mulvey JF, Burger N, et al. Selective mitochondrial superoxide generation in vivo is cardioprotective through hormesis. *Free Radic Biol Med*. 2019;134:678-687.
15. Adlam VJ, Harrison JC, Porteous CM, et al. Targeting an antioxidant to mitochondria decreases cardiac ischemia-reperfusion injury. *FASEB J*. 2005;19:1088-1095.
16. Dare AJ, Logan A, Prime TA, et al. The mitochondria-targeted anti-oxidant MitoQ decreases ischemia-reperfusion injury in a murine syngeneic heart transplant model. *J Heart Lung Transplant*. 2015;34:1471-1480.
17. Ribeiro Junior RF, Dabkowski ER, Shekar KC, O´Connell KA, Hecker PA, Murphy MP. MitoQ improves mitochondrial dysfunction in heart failure induced by pressure overload. *Free Radic Biol Med*. 2018;117:18-29.
18. Szeto HH. Mitochondria-targeted cytoprotective peptides for ischemia-reperfusion injury. *Antioxid Redox Signal*. 2008;10:601-619.
19. Dai D-F, Chen T, Szeto H, et al. Mitochondrial targeted antioxidant Peptide ameliorates hypertensive cardiomyopathy. *J Am Coll Cardiol*. 2011;58:73-82.
20. Nickel A, von Hardenberg A, Hohl M, et al. Reversal of mitochondrial transhydrogenase causes oxidative stress in heart failure. *Cell Metab*. 2015;22:472-484.
21. Sabbah HN, Gupta RC, Kohli S, Wang M, Hachem S, Zhang K. Chronic therapy with elamipretide (MTP-131), a novel mitochondria-targeting peptide, improves left ventricular and mitochondrial function in dogs with advanced heart failure. *Circ Heart Fail*. 2016;9:e002206.
22. Rodriguez-Cuenca S, Cochemé HM, Logan A, et al. Consequences of long-term oral administration of the mitochondria-targeted antioxidant MitoQ to wild-type mice. *Free Radic Biol Med*. 2010;48:161-172.
23. Brand M, Goncalves R, Orr A, et al. Suppressors of superoxide-H2O2 production at site IQ of mitochondrial complex I protect against stem cell hyperplasia and ischemia-reperfusion injury. *Cell Metab*. 2016;24:582-592.
24. Chouchani E, Pell V, James A, et al. A unifying mechanism for mitochondrial superoxide production during ischemia-reperfusion injury. *Cell Metab*. 2016;23:254-263.
25. Chouchani ET, Pell VR, Gaude E, et al. Ischaemic accumulation of succinate controls reperfusion injury through mitochondrial ROS. *Nature*. 2014;515:431-435.
26. Granger DN, Kvietys PR. Reperfusion injury and reactive oxygen species: the evolution of a concept. *Redox Biol*. 2015;6:524-551.
27. McDonald AE, Origins VGC. Origins, evolutionary history, and taxonomic distribution of alternative oxidase and plastoquinol terminal oxidase. *Comp Biochem Physiol Part D Genomics Proteomics*. 2006;1:357-364.
28. Moore AL, Shiba T, Young L, Harada S, Kita K, Ito K. Unraveling the heater: new insights into the structure of the alternative oxidase. *Annu Rev Plant Biol*. 2013;64:637-663.
29. Hakkaart GAJ, Dassa EP, Jacobs HT, Rustin P. Allotopic expression of a mitochondrial alternative oxidase confers cyanide resistance to human cell respiration. *EMBO Rep*. 2006;7:341-345.
30. Dassa EP, Dufour E, Goncalves S, et al. Expression of the alternative oxidase complements cytochrome c oxidase deficiency in human cells. *EMBO Mol Med*. 2009;1:30-36.
31. Fernandez-Ayala DJM, Sanz A, Vartiainen S, et al. Expression of the Ciona intestinalis alternative oxidase (AOX) in Drosophila complements defects in mitochondrial oxidative phosphorylation. *Cell Metab*. 2009;9:449-460.
32. El-Khoury R, Dufour E, Rak M, et al. Alternative oxidase expression in the mouse enables bypassing cytochrome c oxidase blockade and limits mitochondrial ROS overproduction. *PLoS Genet*. 2013;9:e1003182.
33. Szibor M, Dhandapani PK, Dufour E, et al. Broad AOX expression in a genetically tractable mouse model does not disturb normal physiology. *Dis Model Mech*. 2017;10:163-171.
34. Mills EL, Kelly B, Logan A, et al. Succinate dehydrogenase supports metabolic repurposing of mitochondria to drive inflammatory macrophages. *Cell*. 2016;167:457–470.e13.
35. Giordano L, Farnham A, Dhandapani PK, et al. Alternative oxidase attenuates cigarette smoke-induced lung dysfunction and tissue damage. *Am J Respir Cell Mol Biol*. 2019;60:515-522.
36. Szibor M, Gainutdinov T, Fernandez-Vizarra E, et al. Bioenergetic consequences from xenotopic expression of a tunicate AOX in mouse mitochondria: switch from RET and ROS to FET. *Biochim Biophys Acta Bioenerg*. 2019;1861:148137.
37. Robb EL, Hall AR, Prime TA, et al. Control of mitochondrial superoxide production by reverse electron transport at complex I. *J Biol Chem*. 2018;293:9869-9879.
38. Rajendran J, Purhonen J, Tegelberg S, et al. Alternative oxidase-mediated respiration prevents lethal mitochondrial cardiomyopathy. *EMBO Mol Med*. 2019;11.
39. Kolattukudy PE, Quach T, Bergese S, et al. Myocarditis induced by targeted expression of the MCP-1 gene in murine cardiac muscle. *Am J Pathol*. 1998;152:101-111.

40. Dhandapani PK, Begines-Moreno IM, Brea-Calvo G, et al. Hyperoxia but not AOX expression mitigates pathological cardiac remodeling in a mouse model of inflammatory cardiomyopathy. *Sci Rep*. 2019;9:12741.
41. Schmidt K, Tissier R, Ghaleb B, Drogies T, Felix SB, Krieg T. Cardioprotective effects of mineralocorticoid receptor antagonists at reperfusion. *Eur. Heart J*. 2010;31:1655-1662.
42. Bøtker HE, Hausenloy D, Andreadou I, et al. Practical guidelines for rigor and reproducibility in preclinical and clinical studies on cardioprotection. *Basic Res Cardiol*. 2018;113:39.
43. Booty LM, Gawel JM, Cvetko F, et al. Selective disruption of mitochondrial thiol redox state in cells and in vivo. *Cell Chem Biol*. 2019;26:449–461.e8.
44. Scialò F, Sriram A, Fernández-Ayala D, et al. Mitochondrial ROS produced via reverse electron transport extend animal lifespan. *Cell Metab*. 2016;23:725-734.
45. Kadaja L, Eimre M, Paju K, et al. Impaired oxidative phosphorylation in overtrained rat myocardium. *Exp Clin Cardiol*. 2010;15:e116-e127.
46. Kuznetsov AV, Veksler V, Gellerich FN, Saks V, Margreiter R, Kunz WS. Analysis of mitochondrial function in situ in permeabilized muscle fibers, tissues and cells. *Nat Protoc*. 2008;3:965-976.
47. Gnaiger E. Bioenergetics at low oxygen: dependence of respiration and phosphorylation on oxygen and adenosine diphosphate supply. *Respir Physiol*. 2001;128:277-297.
48. Cox J, Mann M. MaxQuant enables high peptide identification rates, individualized p.p.b.-range mass accuracies and proteome-wide protein quantification. *Nat Biotechnol*. 2008;26:1367-1372.
49. Deutsch EW, Csordas A, Sun Z, et al. The ProteomeXchange consortium in 2017: supporting the cultural change in proteomics public data deposition. *Nucleic Acids Res*. 2017;45:D1100-D1106.
50. Perez-Riverol Y, Csordas A, Bai J, et al. The PRIDE database and related tools and resources in 2019: improving support for quantification data. *Nucleic Acids Res*. 2019;47:D442-D450.
51. Tyanova S, Temu T, Sinitcyn P, et al. The Perseus computational platform for comprehensive analysis of (prote)omics data. *Nat Meth*. 2016;13:731-740.
52. Yeap X-Y, Dehn S, Adelman J, et al. Quantitation of acute necrosis after experimental myocardial infarction. *Methods Mol Biol*. 2013;1004:115-133.
53. Katz LN, Feinberg H. The relation of cardiac effort to myocardial oxygen consumption and coronary flow. *Circ Res*. 1958;6:656-669.
54. Ebelt H, Jungblut M, Zhang Y, et al. Cellular cardiomyoplasty: improvement of left ventricular function correlates with the release of cardioactive cytokines. *Stem Cells*. 2007;25:236-244.
55. Pagel-Langenickel I. Evolving role of natriuretic peptides from diagnostic tool to therapeutic modality. *Adv Exp Med Biol*. 2018;1067:109-131.
56. Polyakova V, Loeffler I, Hein S, et al. Fibrosis in endstage human heart failure: severe changes in collagen metabolism and MMP/TIMP profiles. *Int J Cardiol*. 2011;151:18-33.
57. Querejeta Ramón, López Begoña, González A, et al. Increased collagen type I synthesis in patients with heart failure of hypertensive origin: relation to myocardial fibrosis. *Circulation*. 2004;110:1263-1268.
58. Dogan SA, Cerutti R, Benincá C, et al. Perturbed redox signaling exacerbates a mitochondrial myopathy. *Cell Metab*. 2018;28:764-765.
59. Loch T, Vakhrusheva O, Piotrowska I, et al. Different extent of cardiac malfunction and resistance to oxidative stress in heterozygous and homozygous manganese-dependent superoxide dismutase-mutant mice. *Cardiovasc. Res*. 2009;82:448-457.
60. Esfandiary A, Kutsche HS, Schreckenberg R, et al. Protection against pressure overload-induced right heart failure by uncoupling protein 2 silencing. *Cardiovasc. Res*. 2019;115:1217-1227.
61. Olivetti G, Abbi R, Quaini F, et al. Apoptosis in the failing human heart. *N Engl J Med*. 1997;336:1131-1141.
62. Liu W, Ru L, Su C, Qi S, Qi X. Serum levels of inflammatory cytokines and expression of BCL2 and BAX mRNA in peripheral blood mononuclear cells and in patients with chronic heart failure. *Med. Sci. Monit*. 2019;25:2633-2639.
63. Bernardo AF, Cortez E, Neves FA, et al. Overnutrition during lactation leads to impairment in insulin signaling, up-regulation of GLUT1 and increased mitochondrial carbohydrate oxidation in heart of weaned mice. *J Nutr Biochem*. 2016;29:124-132.
64. Eden E, Navon R, Steinfeld I, Lipson D, Yakhini Z. GOrilla: a tool for discovery and visualization of enriched GO terms in ranked gene lists. *BMC Bioinform*. 2009;10:48.
65. Eden E, Lipson D, Yogev S, Yakhini Z. Discovering motifs in ranked lists of DNA sequences. *PLoS Comput Biol*. 2007;3:e39.
66. Nickel A, Löffler J, Maack C. Myocardial energetics in heart failure. *Basic Res Cardiol*. 2013;108:358.
67. Kang PT, Chen C-L, Lin P, Zhang L, Zweier JL, Chen Y-R. Mitochondrial complex I in the post-ischemic heart: reperfusion-mediated oxidative injury and protein cysteine sulfonation. *J Mol Cell Cardiol*. 2018;121:190-204.
68. Mentzer RM, Wider J, Perry CN, Gottlieb RA. Reduction of infarct size by the therapeutic protein TAT-Ndi1 in vivo. *J Cardiovasc Pharmacol Ther*. 2014;19:315-320.
69. Perry CN, Huang C, Liu W, Magee N, Sousa Carreira R, Gottlieb RA. Xenotransplantation of mitochondrial electron transfer enzyme, Ndi1, in myocardial reperfusion injury. *PLoS ONE*. 2011;6:e16288.
70. Johnson JM, Ferrara PJ, Verkerke ARP, et al. Targeted overexpression of catalase to mitochondria does not prevent cardioskeletal myopathy in Barth syndrome. *J Mol Cell Cardiol*. 2018;121:94-102.
71. Lowes BD, Minobe W, Abraham WT, et al. Changes in gene expression in the intact human heart. Downregulation of alpha-myosin heavy chain in hypertrophied, failing ventricular myocardium. *Journal of Clinical Investigation*. 1997;100:2315-2324.
72. Ghosh N, Haddad H. Atrial natriuretic peptides in heart failure: pathophysiological significance, diagnostic and prognostic value. *Can J Physiol Pharmacol*. 2011;89:587-591.
73. Semenov AG, Katrukha AG. Analytical issues with natriuretic peptides—has this been overly simplified? *Ejifcc*. 2016;27:189-207.
74. Menezes Falcão L, Pinto F, Ravara L, van Zwieten PA. BNP and ANP as diagnostic and predictive markers in heart failure with left ventricular systolic dysfunction. *J Renin Angiotensin Aldosterone Syst*. 2004;5:121-129.
75. Langenickel T, Pagel I, Höhnel K, Dietz R, Willenbrock R. Differential regulation of cardiac ANP and BNP mRNA in different stages of experimental heart failure. *Am J Physiol Heart Circ Physiol*. 2000;278:H1500-H1506.
76. Moro C, Lafontan M. Natriuretic peptides and cGMP signaling control of energy homeostasis. *Am J Physiol Heart Circ Physiol*. 2013;304:H358-H368.
77. Wang D, Oparil S, Feng JA, et al. Effects of pressure overload on extracellular matrix expression in the heart of the atrial natriuretic peptide-null mouse. *Hypertension*. 2003;42:88-95.
78. Li P, Oparil S, Novak L, et al. ANP signaling inhibits TGF-beta-induced Smad2 and Smad3 nuclear translocation and extracellular matrix expression in rat pulmonary arterial smooth muscle cells. *J Appl Physiol*. 2007;102:390-398.
79. Rysä J, Leskinen H, Ilves M, Ruskoaho H. Distinct upregulation of extracellular matrix genes in transition from hypertrophy to hypertensive heart failure. *Hypertension*. 2005;45:927-933.
80. Kühn B, del Monte F, Hajjar RJ, et al. Periostin induces proliferation of differentiated cardiomyocytes and promotes cardiac repair. *Nat Med*. 2007;13:962-969.
81. Imoto K, Okada M, Yamawaki H. Periostin mediates right ventricular failure through induction of inducible nitric oxide synthase expression in right ventricular fibroblasts from monocrotaline-induced pulmonary arterial hypertensive Rats. *Int J Mol Sci*. 2018;20:62.

82. Zhao S, Wu H, Xia W, et al. Periostin expression is upregulated and associated with myocardial fibrosis in human failing hearts. *J Cardiol*. 2014;63:373-378.
83. Teekakirikul P, Eminaga S, Toka O, et al. Cardiac fibrosis in mice with hypertrophic cardiomyopathy is mediated by non-myocyte proliferation and requires Tgf-β. *J. Clin. Invest*. 2010;120:3520-3529.
84. Fukunaga Y, Itoh H, Hosoda K, et al. Altered gene expression of uncoupling protein-2 and -3 in stroke-prone spontaneously hypertensive rats. *J. Hypertens*. 2000;18:1233-1238.

SUPPORTING INFORMATION

Additional supporting information may be found online in the Supporting Information section.

How to cite this article: Szibor M, Schreckenberg R, Gizatullina Z, et al. Respiratory chain signalling is essential for adaptive remodelling following cardiac ischaemia. *J Cell Mol Med*. 2020;24:3534–3548. https://doi.org/10.1111/jcmm.15043

7.6 S. A. Dogan *et al.*, *Cell Metab.* **28**, 764-775.e5 (2018)

Article

Cell Metabolism

Perturbed Redox Signaling Exacerbates a Mitochondrial Myopathy

Graphical Abstract

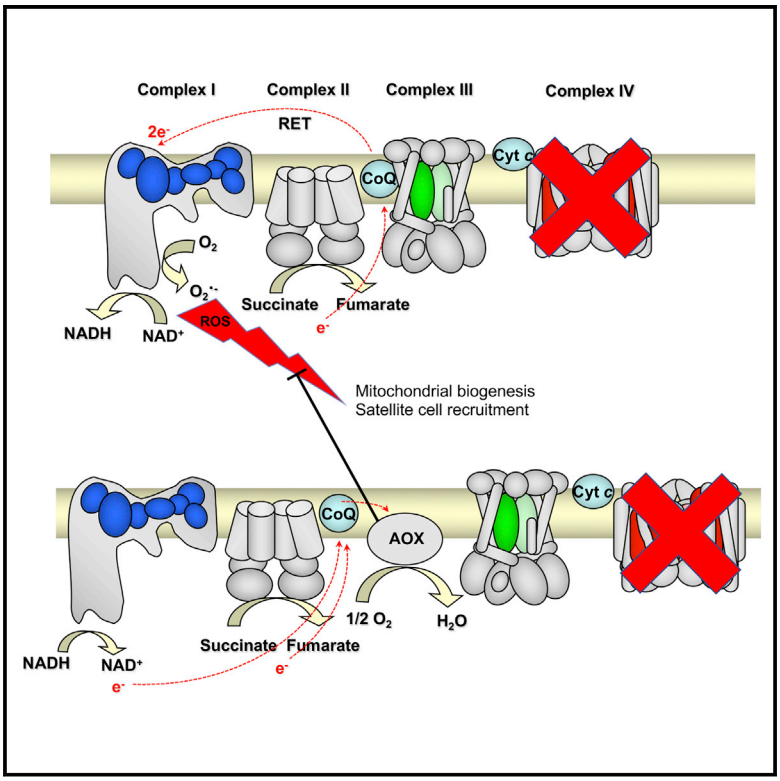

Highlights

- ROS trigger mitochondrial biogenesis in *Cox15*-deficient mice
- Satellite cell recruitment is ROS dependent in mitochondrial myopathy
- AOX and NAC interfere with ROS signaling
- The use of antioxidants in mitochondrial diseases should be carefully evaluated

Authors

Sukru Anil Dogan, Raffaele Cerutti, Cristiane Benincá, ..., Massimo Zeviani, Marten Szibor, Carlo Viscomi

Correspondence

marten.szibor@uta.fi (M.S.),
cfv23@mrc-mbu.cam.ac.uk (C.V.)

In Brief

Dogan et al. show that alternative oxidase attenuates ROS signaling in a COX-defective mitochondrial myopathy model, thus blunting ROS-dependent mitochondrial biogenesis and satellite cell recruitment. These findings must be considered in the treatment of mitochondrial myopathies, suggesting the need for careful assessment of antioxidant therapy.

Dogan et al., 2018, Cell Metabolism *28*, 764–775
November 6, 2018
https://doi.org/10.1016/j.cmet.2018.07.012

CellPress

CellPress

Cell Metabolism
Article

Perturbed Redox Signaling Exacerbates a Mitochondrial Myopathy

Sukru Anil Dogan,[1] Raffaele Cerutti,[1] Cristiane Benincá,[1] Gloria Brea-Calvo,[2] Howard Trevor Jacobs,[3,4] Massimo Zeviani,[1] Marten Szibor,[3,4,*] and Carlo Viscomi[1,5,*]

[1]MRC Mitochondrial Biology Unit, University of Cambridge, Wellcome Trust/MRC Building Hills Road, Cambridge CB2 0XY, UK
[2]Centro Andaluz de Biología del Desarrollo and CIBERER, Instituto de Salud Carlos III, Universidad Pablo de Olavide-CSIC-JA, Sevilla 41013, Spain
[3]Institute of Biotechnology, University of Helsinki, Viikinkaari 5, Helsinki 00790, Finland
[4]Faculty of Medicine and Life Sciences, University of Tampere, Arvo Ylpön katu 34, Tampere 33520, Finland
[5]Lead Contact
*Correspondence: marten.szibor@uta.fi (M.S.), cfv23@mrc-mbu.cam.ac.uk (C.V.)
https://doi.org/10.1016/j.cmet.2018.07.012

SUMMARY

Alternative oxidases (AOXs) bypass respiratory complexes III and IV by transferring electrons from coenzyme Q directly to O_2. They have therefore been proposed as a potential therapeutic tool for mitochondrial diseases. We crossed the severely myopathic skeletal muscle-specific COX15 knockout (KO) mouse with an AOX-transgenic mouse. Surprisingly, the double KO-AOX mutants had decreased lifespan and a substantial worsening of the myopathy compared with KO alone. Decreased ROS production in KO-AOX versus KO mice led to impaired AMPK/PGC-1α signaling and PAX7/MYOD-dependent muscle regeneration, blunting compensatory responses. Importantly, the antioxidant *N*-acetylcysteine had a similar effect, decreasing the lifespan of KO mice. Our findings have major implications for understanding pathogenic mechanisms in mitochondrial diseases and for the design of therapies, highlighting the benefits of ROS signaling and the potential hazards of antioxidant treatment.

INTRODUCTION

Oxidative phosphorylation (OXPHOS) is the process by which mitochondria convert the energy derived from nutrients into ATP. Electrons generated by intermediary metabolism in the form of reducing equivalents are transferred along the four complexes of the mitochondrial respiratory chain (complexes I–IV, cI–cIV) to eventually combine with molecular oxygen to produce water. This exergonic process, termed respiration, sustains the extrusion of protons across the inner mitochondrial membrane, carried out by proton pumps present in cI, cIII, and cIV. Proton translocation generates an electrochemical gradient, giving rise to a membrane potential, $\Delta\psi$, which is exploited by the ATP synthase (complex V, cV) to convert ADP and Pi to ATP. Mutations in a vast array of genes encoded by either the nuclear or mitochondrial DNA (mtDNA) disrupt the respiratory chain and lead to primary mitochondrial diseases. Several interconnected mechanisms account for the cellular consequences of OXPHOS defects, including decreased ATP synthesis, increased production of reactive oxygen species (ROS), altered ion trafficking, deranged metabolite levels, and abnormalities in mitochondrial-related cell death and turnover pathways such as apoptosis and autophagy.

In particular, ROS are by-products of normal respiration, but can increase dramatically when the respiratory chain is impaired. ROS are in fact thought to play a "hormetic" double role: in physiological conditions, low levels of ROS act as signaling molecules regulating homeostatic pathways related to mitochondrial bioenergetics, whereas at high levels they act as toxic agents damaging cellular components, including nucleic acids, proteins, and lipids (Yun and Finkel, 2014). Along the respiratory chain, ROS are generated at different sites with cI, cII, and cIII playing the main role (Brand, 2016). In particular, cI generates ROS through reverse electron transfer (RET), which exploits the electrons flowing back from coenzyme Q (CoQ) when this is over-reduced by electrons from cII (Chouchani et al., 2014) or in the presence of drugs or genetic defects that inhibit cIII and/or cIV (Guarás et al., 2016). Although the detrimental role of ROS has recently been challenged (Scialò et al., 2016), cells have evolved highly efficient ROS scavenging systems, which in mammals are mainly controlled by an antioxidant response program, based on the Kelch-like ECH-associated protein 1 (KEAP1) and nuclear factor erythroid 2-related factor 2 (NRF2/NFE2L2) (Holmström and Finkel, 2014).

In spite of recent progress, no specific therapy is currently available for OXPHOS disorders. Because of their huge genetic heterogeneity, an effective therapy should have the widest possible applicability or at least have the potential to be applied to more than a single disease entity.

Alternative oxidases (AOXs) are cyanide-resistant, membrane-bound mitochondrial enzymes present in plants, lower eukaryotes, and some specific metazoan phyla, consisting of just a single gene product. AOXs maintain electron flow when the respiratory chain is inhibited at the level of cIII and/or cIV, by directly transferring electrons from CoQ to O_2, thus bypassing cIII and cIV and preventing over-reduction of the CoQ pool. Notably, AOX activity is not associated with proton pumping across the inner mitochondrial membrane and thus does not contribute

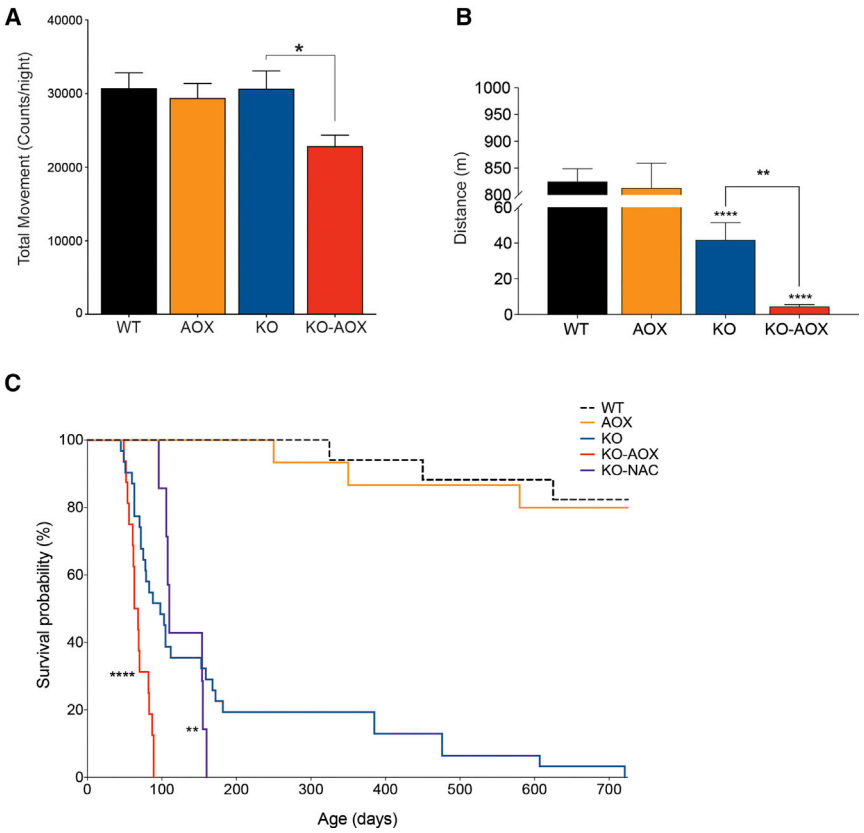

Figure 1. AOX Expression Exacerbates the Physical Properties and Lifespan of KO Mice

(A) Total movement of male 8-week-old WT, AOX, KO, and KO-AOX mice measured by CLAMS and indicated as counts per night (n = 8–10).

(B) Treadmill analysis of motor performance (n = 4).

(C) Kaplan-Meier survival curves (number of animals used are WT, 17; AOX, 15; KO, 31; KO-AOX, 16; KO-NAC, 8). Mean lifespans of KO-AOX and KO-NAC are compared with KO by one-sample t test. *N*-Acetylcysteine (NAC) was given to KO mice in the drinking water from 3 weeks of age.

Bars represent means ± SEM. Asterisks over the bars indicate statistical significance versus WT; over the brackets among indicated groups. *$p \leq 0.05$; **$p \leq 0.01$; ****$p < 0.0001$; unpaired Student's t test.

directly to the maintenance of $\Delta\psi$ and ATP synthesis. However, in the presence of cIII or cIV defects, the increase in proton pumping at cI, due to the re-activation of electron flow, should sustain the electrochemical gradient and ATP production. Importantly, the re-activation of electron flow by AOXs limits the excessive generation of ROS and maintains redox homeostasis, thereby maintaining tricarboxylic acid cycle activity (Mills et al., 2016). This has been exploited extensively to improve the phenotype of cellular and fly models with cIII and cIV defects (El-Khoury et al., 2014). However, its use in mammalian models has not been explored so far. Here, we report the *in vivo* effects of AOX expressed in a skeletal muscle-specific knockout mouse for *Cox15* (*Cox15*$^{sm/sm}$, hereafter designated KO), encoding the terminal enzyme of the biosynthetic pathway of *heme a*, an essential prosthetic group of cIV (cytochrome *c* oxidase [COX]).

RESULTS

AOX Expression Exacerbates the Phenotype of KO Mice

KO mice develop a profound, muscle-restricted COX deficiency leading to severe mitochondrial myopathy and early death (Viscomi et al., 2011). A mouse strain carrying *AOX* from the tunicate *Ciona intestinalis* inserted in the murine *Rosa26* locus has recently been described (AOX^{tg}, hereafter designated AOX), and was shown to be phenotypically indistinguishable from wild-type (WT) littermates (Szibor et al., 2016).

We crossed the KO and AOX lines to generate KO-AOX double mutants, to test whether AOX could alleviate the KO phenotype. Unexpectedly, KO-AOX mice showed a more severe phenotype, with earlier onset of symptoms than KO, characterized by decreased body weight (Figure S1A) due to diminished fat mass (Figure S1B) and decreased total spontaneous movements (Figure 1A) as well as treadmill motor performance in comparison with KO littermates (Figure 1B). The survival probability of the KO-AOX mice was markedly lower as well; its median lifespan was 60 days compared with 150 days for KO (log rank, $p < 0.0001$; Figure 1C). In fact, all the KO-AOX mice had to be euthanized by 90 days of age because of their poor condition.

Since the COX defect in KO mice is muscle specific, we reasoned that worsening of the myopathy might be responsible for the more drastic phenotype of KO-AOX mice. We thus analyzed the skeletal muscle from 8-week-old animals of the four genotypes, i.e., before KO-AOX mice start to die. COX/SDH histochemical staining confirmed the expected prevalence of COX-deficient fibers in KO versus WT and AOX animals. However, the defect was even more prominent in KO-AOX samples (Figure 2A). In addition, SDH staining was increased in KO muscles, but it was similar to the WT in KO-AOX mice (Figures S2A and S2B). Quantitative spectrophotometric assay of COX-specific activity in muscle homogenates confirmed this observation (10.29 ± 1.46 in KO versus 4.17 ± 0.47 in KO-AOX; $p < 0.01$; Figure 2B). Likewise, morphological analysis by hematoxylin and eosin (H&E) staining revealed significantly decreased cross-sectional area of KO-AOX versus KO myofibers (Figure 2C). The number of centralized nuclei, an index of skeletal muscle regeneration, was markedly increased in KO versus WT and AOX (8.55% ± 0.73% in KO versus 0.41% ± 0.13% in WT), but much less so in KO-AOX mice (Figure 2D). This finding prompted us to investigate the differentiation of satellite cells in the skeletal muscle of the different genotypes. The number of nuclei positive for PAX7, a marker of resident myoblasts, and MYOD, a marker of the differentiating satellite cells, was significantly increased in KO versus WT and AOX muscles, but it was expressed at normal levels in KO-AOX mice (Figures 3A and 3B).

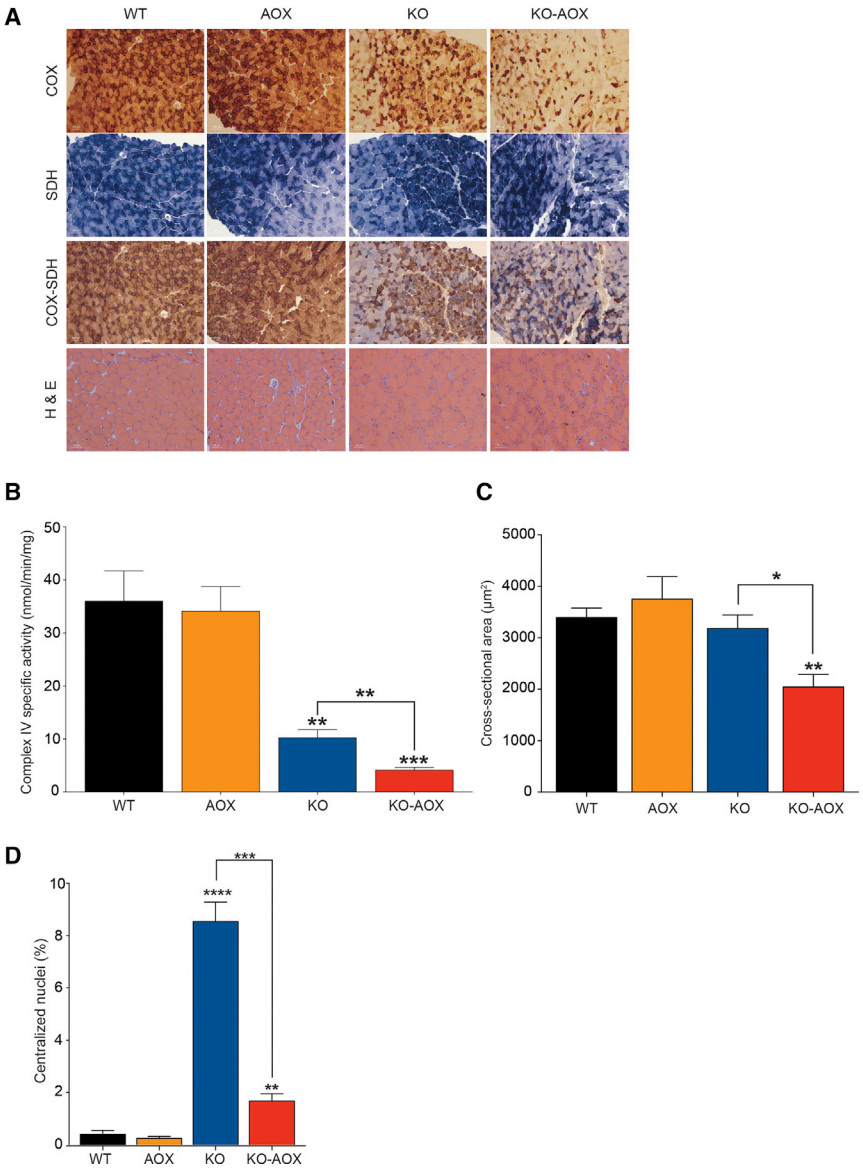

Figure 2. AOX Expression Worsens the Biochemical Muscle Phenotype of KO Mice

(A) Histochemical analyses of cytochrome *c* oxidase (COX), succinate dehydrogenase (SDH), double staining of COX-SDH, and H&E in 8-week-old WT, AOX, KO, and KO-AOX animals.

(B) Spectrophotometric specific activity of cIV in skeletal muscle of 8-week-old mice (n = 5).

(C) Analysis of the cross-sectional area of muscle fibers (n = 4).

(D) Analysis of the number of centralized nuclei in muscle fibers (n = 4).

Bars represent mean ± SEM. Asterisks over the bars indicate statistical significance versus WT; over the brackets among indicated groups. *p ≤ 0.05; **p ≤ 0.01; ***p ≤ 0.001; ****p < 0.0001; unpaired Student's t test.

Next, we investigated if AOX determined a switch in the fiber type by immunodecorating muscle sections with antibodies against the different myosin isoforms. However, no differences were observed (Figures S3A and S3B). Taken together, these data clearly indicate that the mitochondrial myopathy was significantly more severe in KO-AOX animals.

Next, we confirmed AOX expression and catalytic activity in KO-AOX individuals. Western blot immunovisualization showed robust expression of AOX in most tissues except brain of adult mice, as previously reported (Szibor et al., 2016) (Figure S4A). Oxygraphic analysis of isolated mitochondria in the presence of ADP (state III) demonstrated substantial cyanide-resistant respiration in muscle of both AOX and double recombinant KO-AOX mice (Figure S4B). State III O_2 consumption rate was markedly higher in WT and AOX mitochondria compared with KO and KO-AOX. In contrast, oligomycin-sensitive respiration was markedly increased in both AOX and KO-AOX muscle mitochondria compared with the corresponding naive models, WT and KO, respectively (Figure S4C). These results indicate that AOX-dependent respiration is active but insensitive to either cyanide or oligomycin inhibition.

AOX Expression Interferes with Mitochondrial Biogenesis in KO-AOX

In addition to SDH staining, CS activity was also increased in KO animals compared with controls and KO-AOX (Figure 4A). These data prompted us to evaluate other markers of mitochondrial biogenesis in skeletal muscle. The mtDNA copy number (Figure 4B) and the expression levels of mitochondrial transcription factor A (TFAM) (Figure 4C) were increased in the KO versus WT and AOX but were similar to WT values in the double recombinant KO-AOX animals. In addition, the amount of several subunits of the respiratory complexes was significantly increased in KO versus WT and AOX, but not in samples from KO-AOX mice (Figure 4D). Overall, these data suggest that AOX expression blunts the increased mitochondrial biogenesis observed in the muscle-specific *Cox15*-defective model.

We then investigated whether the main mitochondriogenic control pathways were affected by AOX in KO muscles. AMP-dependent kinase (AMPK) is an important sensor of cellular energetic status and is activated when the AMP/ATP ratio increases (Lin and Hardie, 2017). Under such energy-deficient conditions, AMPK is activated by phosphorylation of Thr_{172} (p-AMPK) by LK1 kinase and, in turn, p-AMPK phosphorylates a large number of targets, including the transcriptional co-activator PGC-1α, a master regulator of mitochondrial biogenesis. As previously reported (Viscomi et al., 2011), p-AMPK was upregulated in KO mice, but it was within the normal range in KO-AOX animals (Figure 4E). Moreover, PGC-1α protein amount was also increased in KO versus WT and AOX, while it was normal in KO-AOX muscle samples (Figure 4F). Finally, quantitative transcript

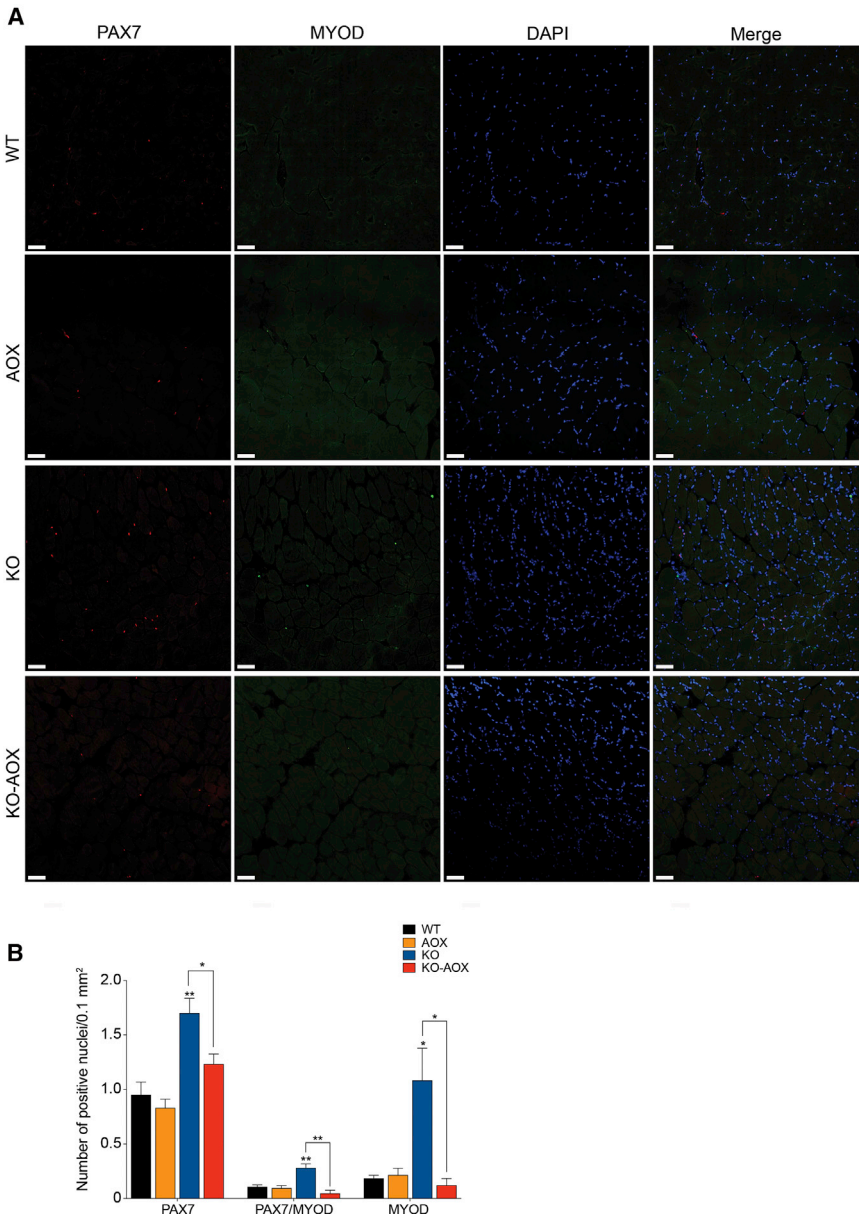

Figure 3. AOX Impairs the Regeneration Capacity of Myofibers

(A) Representative confocal 3D z stack image of 8-week-old muscle fibers labeled with PAX7 (red), MYOD (green), and DAPI (blue). The image represents a randomly chosen image from four samples. Scale bar, 50 μm.

(B) Quantification of the number of positive PAX7, PAX7/MYOD, and MYOD nuclei in muscles of WT, AOX, KO, and KO-AOX animals (n = 4). Bars represent means ± SEM. Asterisks over the bars indicate statistical significance versus WT; over the brackets among indicated groups. *p ≤ 0.05; **p ≤ 0.01; unpaired Student's t test.

analysis showed decreased expression of several genes related to the respiratory chain in KO-AOX versus KO mice, confirming that mitochondrial biogenesis is diminished in the presence of AOX (Figure 4G).

AOX Impairs ROS Signaling in KO Mice

Since AOX prevents excessive ROS production, we reasoned that it might interfere with ROS signaling in cIV-deficient muscle. Thus, we quantified ROS production in skeletal muscle mitochondria by measuring hydrogen peroxide (H_2O_2) production. Succinate-driven H_2O_2 production was significantly increased in KO compared with WT and AOX mitochondria but was lower in KO-AOX double mutants than in WT animals (Figure 5A). Accordingly, mitochondrial aconitase (ACO2) activity, which is inhibited by H_2O_2, was significantly lower in the KO compared with WT and AOX mitochondria but had normal values in the KO-AOX samples (Figure 5B). Altogether, these results are consistent with AOX being active only under stress conditions, as previously reported (Szibor et al., 2016).

Since AOX requires a highly reduced CoQ pool to be activated (Dry et al., 1989), we measured the amount of reduced and oxidized CoQ in frozen skeletal muscle of the mice. The relative amount of reduced CoQ was increased in KO versus WT and AOX mice but was comparable with WT in the double mutants, confirming that AOX efficiently oxidizes the CoQ pool (Figure 5C). These results support the idea that RET, which is promoted by over-reduction of the CoQ pool, is involved in generating ROS in the KO model, and that this phenomenon is blunted by AOX.

Increased ROS can trigger the oxidative stress response via KEAP1/NFE2L2 signaling. Accordingly, the transcripts for superoxide dismutase (*Sod2*) and glutathione peroxidase (*Gpx1*), two key enzymes of the antioxidant response that are NFE2L2 targets, were significantly increased in KO versus WT and AOX mice, but significantly decreased in KO-AOX versus KO animals (Figure 5D). A similar trend was detected for both *Cat*, encoding catalase, and *Sod1*, encoding the cytosolic isoform of superoxide dismutase (Figure 5D). A significant increase of the *Nfe2l2* transcript was also detected in KO but not in KO-AOX samples (Figure 5D).

Various retrograde signals from mitochondria can be activated under stress conditions associated with increased ROS, energy deficiency, and loss of $\Delta\psi$ (Quirós et al., 2016). As low levels of ATP can activate AMPK, as well as ROS (Rabinovitch et al., 2017), we assessed the ATP production rate. We found a strong but comparable impairment of ATP synthesis in both KO and KO-AOX skeletal muscle mitochondria, using either cI- or cII-linked substrates (Figure 5E). In addition, the ATP content was comparably lower than controls in KO and KO-AOX samples (Figure 5F). Likewise, $\Delta\psi$ was markedly but comparably lower than controls in both KO and KO-AOX muscle mitochondria

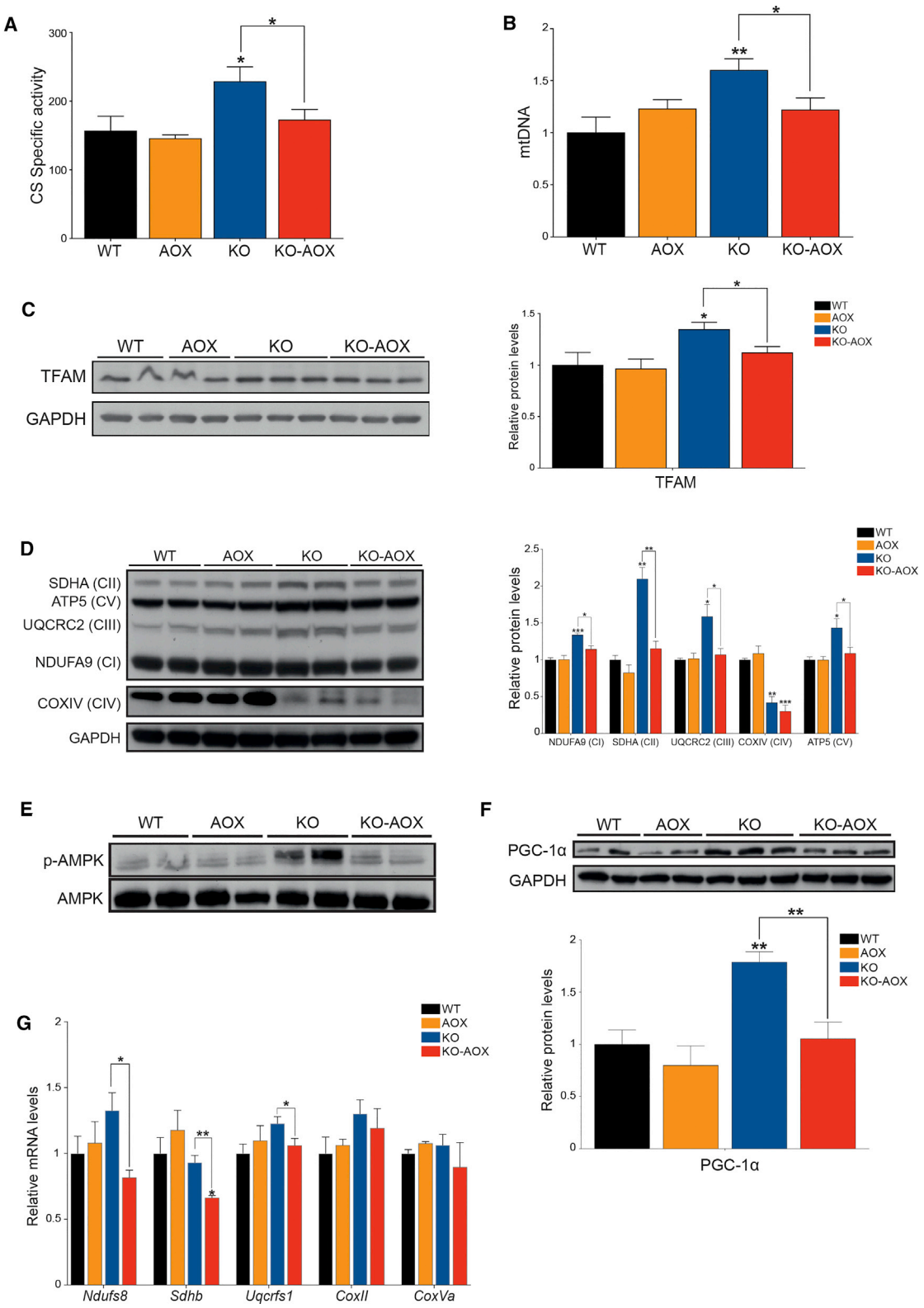

Figure 4. AOX Interferes with Mitochondrial Biogenesis in KO-AOX Mice

(A) Spectrophotometric activity of citrate synthase (CS)-specific activity (n = 5).

(B) mtDNA copy number by qPCR (n = 8–10).

(C) Western blot and quantification (n = 5) of TFAM.

(legend continued on next page)

(Figure 5G). The comparable decrease of ATP production rate, ATP steady-state levels, and $\Delta\psi$ in KO and KO-AOX indicates that impaired bioenergetics is not the main reason for the more severe phenotype of KO-AOX mice.

To further test the hypothesis that decreased ROS production underlies the aggravated phenotype, we supplemented the drinking water of eight KO mice after weaning with *N*-acetylcysteine (NAC), a cell-permeable precursor of glutathione (Viscomi et al., 2010). The mean survival was significantly shorter in treated versus untreated animals, and the maximal lifespan was grossly decreased in the NAC-treated cohort, although NAC supplementation also delayed the earliest deaths of KO mice (Figure 1A).

Autophagy Is Restored in KO-AOX Skeletal Muscle

Mitochondrial biogenesis and autophagy together regulate mitochondrial content (Peralta et al., 2016). We measured the amount of LC3, a marker for autophagosomes, and P62, a marker for autophagic cargoes, in skeletal muscle samples of the different models. The ratio between lipidated, autophagosome-associated LC3 (LC3-II) and non-lipidated, cytosolic free LC3 (LC3-I) was significantly decreased, whereas the amount of P62 was increased, in KO versus WT and AOX muscles, suggesting decreased autophagy (Figure 6A). Conversely, KO-AOX muscle showed a markedly increased LC3-II/LC3-I ratio while the levels of P62 were comparable with WT, indicating no decrease in autophagy.

Mitochondrial Stress Markers Are Comparably Increased in Both KO and KO-AOX

A number of mitochondrial pathways are activated in response to mitochondrial dysfunction. We measured the expression at the protein and/or mRNA level, of several components of this integrated stress response, including (1) key players of the mitochondrial unfolded protein response (UPR^{mt}) (Shpilka and Haynes, 2017), such as the bZIP transcription factors *Chop* (C/EBP-homologous protein), *Atf4*, and *Atf5* (Fiorese et al., 2016), and mitochondrial chaperones HSP60/HSPD1 and mtHSP70/HSPA9 (Dogan et al., 2014); (2) components of the one-carbon/mitochondrial folate cycle, e.g., methylene tetrahydrofolate dehydrogenase 2 (MTHFD2) (Khan et al., 2017; Kuhl et al., 2016), and enzymes of proline biosynthesis from glutamate, e.g., delta-1-pyrroline-5-carboxylate synthase (ALDH18A1) and mitochondrial pyrroline-5-carboxylate reductase 1 (PYCR1); and (3) the fibroblast growth factor 21 (*Fgf21*) and growth differentiation factor 15 (*Gdf15*) mitokines (Lehtonen et al., 2016). Increased amounts of these markers or their transcripts were detected in both KO and KO-AOX animals (Figures 6B–6D). In particular, *Fgf21* mRNA was highly expressed in KO muscles, and even more so (260-fold) in KO-AOX mice (Figure 6D). *Gdf15* was about 100-fold higher than controls in KO mice, but significantly lower in KO-AOX, although still increased relative to WT animals (Figure 6D). Other factors involved in the integrated stress response, including *Atf3* and *Atf6*, related respectively to cell death and ER-stress pathways, did not change (*Atf3*) or changed to a very small extent (*Atf6*). Interestingly, the activation of these stress-related pathways in our KO model takes place via EIF-2alpha and not via mTORC1 (Melber and Haynes, 2018). The levels of mTORC1 target eukaryotic translation initiation factor-binding protein 1 (EIF4EBP1), an important player in protein synthesis (Morita et al., 2013) was increased in both KO and KO-AOX compared with WT. However, phosphorylated versus unphosphorylated EIF4EBP1 ratio was decreased to the same extent in KO and KO-AOX versus WT and AOX mice, indicating that mTORC1 signaling, and thus protein synthesis and cell growth, was reduced in both KO and KO-AOX muscles. In contrast, we detected increased levels of phosphorylated EIF-2alpha in both KO and KO-AOX mice compared with both WT and AOX littermates (Figures S5A–S5C). These findings suggest that the induction of major mitochondrial stress responses correlates with mitochondrial myopathy and disease progression but AOX did not significantly modify these pathways, except insofar as it worsened the myopathy, affecting the expression of relevant endocrine markers, such as *Gdf15* (Figure 6E).

DISCUSSION

While the expression of an AOX xenogene on a murine WT background had hardly any consequences, we here showed that AOX entrains a dramatic worsening of the clinical and biochemical phenotype in a mouse model of COX-defective mitochondrial myopathy. Under stress conditions, including defects of cIII or cIV, AOX directly oxidizes CoQ, maintaining electron flow from NADH and $FADH_2$ but abolishing the contribution of cIII and cIV to the formation of the $\Delta\psi$. The unexpected outcome observed in the KO-AOX double mutant model suggested two possible mechanisms: a direct bioenergetic failure caused by the exclusion of the proton pumping activity of cIII and cIV, or an indirect effect consequent to decreased ROS signaling and blunting of mitochondrial biogenesis. We excluded the first possibility, since no difference was detected in the ATP production rate, ATP levels, or $\Delta\psi$ between KO and KO-AOX muscle samples, as expected since AOX does not translocate protons across the mitochondrial inner membrane. Conversely, ROS production was significantly decreased in KO-AOX muscle as were several indicators of mitochondrial biogenesis.

Redox signaling controls a large number of transcriptional pathways (Holmström and Finkel, 2014). However, its importance *in vivo* has not been adequately investigated. While our results argue against the general applicability of AOX as a therapeutic tool in mitochondrial disorders, they provide solid genetic

(D) Western blot and quantification (n = 5) for MRC complexes. Individual subunits and the complexes are indicated on the left.
(E) Representative western blot for phosphorylated and total AMPK.
(F) Western blot and quantification (n = 5) of PGC-1α.
(G) Relative expression levels of respiratory chain transcripts (n = 6). Results represent fold increase normalized against WT.
All experiments were performed on 8-week-old mice with western blots using skeletal muscle homogenates of 8-week-old mice and GAPDH as loading control. Bars represent means ± SEM. Asterisks over the bars indicate statistical significance versus WT; over the brackets among indicated groups. *$p \leq 0.05$; **$p \leq 0.01$; ***$p \leq 0.001$; unpaired Student's t test.

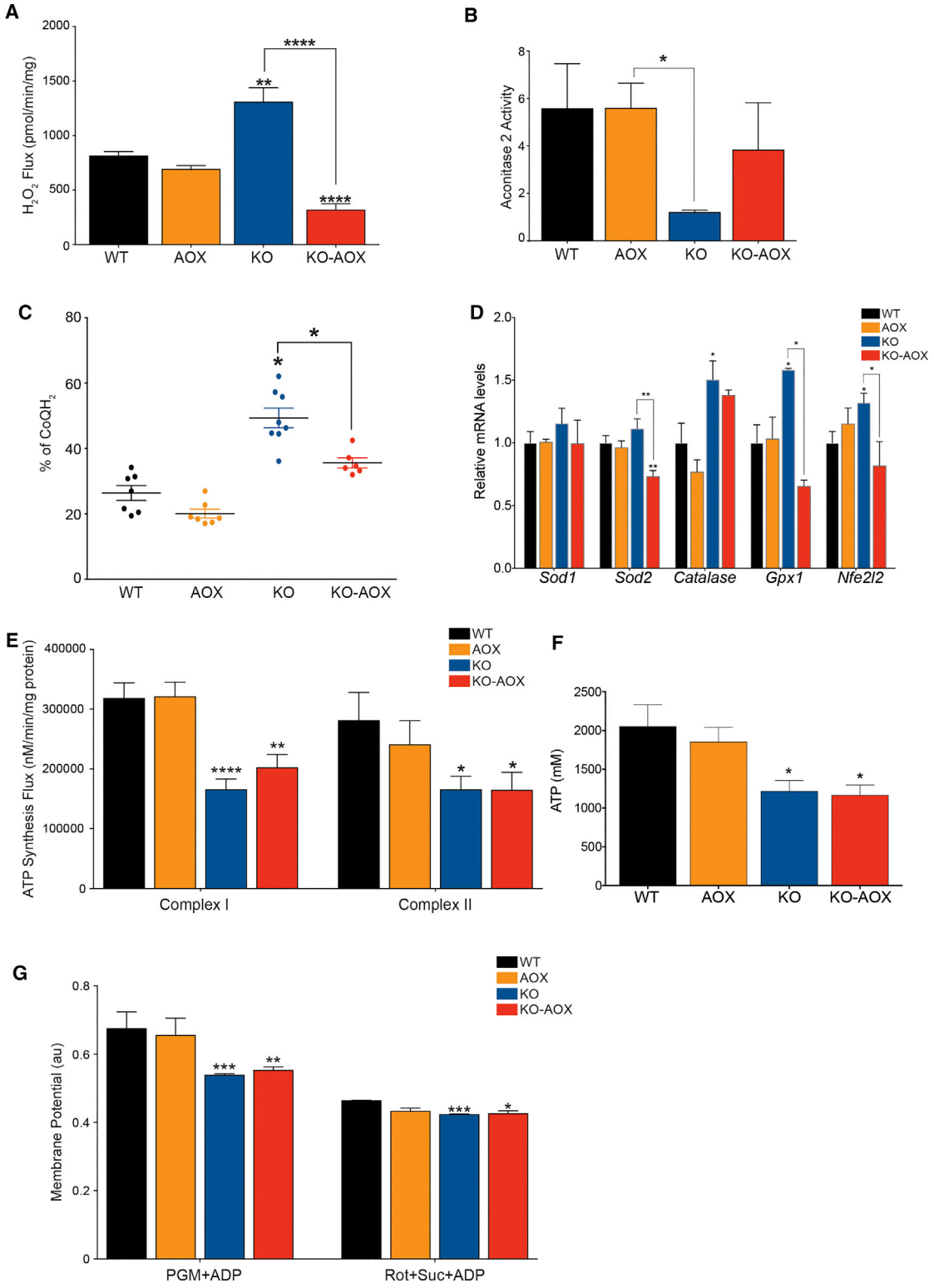

Figure 5. AOX Impairs ROS Signaling in KO Mice

(A) H_2O_2 production rate caused by RET in isolated skeletal muscle mitochondria (n = 4).

(B) Aconitase2 activity in frozen skeletal muscle samples (n = 5).

(C) Percentage of reduced CoQ in frozen muscle samples.

(D) Relative expression levels of antioxidant response transcripts (n = 6). Results represent fold increase normalized against WT.

(legend continued on next page)

evidence in a mammalian mitochondrial disease model of the crucial pathophysiological role of ROS-dependent pathways as compensatory responses to mitochondrial dysfunction, at least in skeletal muscle, as previously suggested (Horn et al., 2017; Reczek and Chandel, 2015). This has obvious implications in understanding some of the pathogenic mechanisms of mitochondrial diseases and can potentially be exploited to develop effective therapies. For instance, an ROS-based mechanism can underpin the formation of ragged-red fibers (RRFs), a morphological hallmark of mitochondrial myopathy. RRFs are determined by the segmental accumulation of dysfunctional mitochondria along the muscle syncytium, especially in the sub-sarcolemmal region. However, the mechanism leading to their formation is poorly understood. We propose that ROS can be a major signal inducing the local proliferation of mitochondria, in an attempt to compensate their functional defect through the activation of a mitochondriogenic program by the surrounding nuclei. Furthermore, our findings support the idea that the induction of mitochondrial biogenesis, for instance by activating the SIRT1-and/or AMPK-dependent PGC-1α axis, or other mitochondriogenic pathways, could be a rational and potentially effective approach in the therapy of mitochondrial diseases. Interestingly, there is increasing evidence that AMPK is directly regulated by ROS either through oxidation and S-glutathionylation of cysteines 299 and 304 in the α subunit, leading to the activation of the enzyme, or oxidation of cysteines 130 and 174 in the α subunit, resulting in its inactivation (Shao et al., 2014). An additional mechanism potentially contributing to the decrease of mitochondrial content is the maintenance of autophagic flux in KO-AOX, as suggested by an increased LC3-II/LC3-I ratio and normalization of the P62 level, which is impaired in KO muscle. Further investigation will be needed to understand whether this effect is directly related to decreased ROS production or is an indirect consequence of the activation of stress responses. The integrated stress response is indeed activated in both KO and KO-AOX mice. This seems to be controlled by the activation of the translation initiation factor EIF-2alpha by phosphorylation operated by GCN2 or other kinases under mitochondrial stress conditions (Melber and Haynes, 2018) and as observed in other mouse models of mitochondrial dysfunction (Seiferling et al., 2016). In contrast, mTORC1 signaling, which was shown to regulate mitochondrial integrated stress response in a model of impaired mtDNA replication (Khan et al., 2017), is inhibited in both KO and KO-AOX mice as indicated by reduced levels of phosphorylated EIF4EBP1. Interestingly, we found that two mitokines recently introduced as biomarkers for mitochondrial myopathies (Lehtonen et al., 2016) were both highly increased in KO and KO-AOX mice. However, while *Fgf21* was much higher in KO-AOX than in KO, *Gdf15* was reduced in KO-AOX compared with KO, implying a stress-dependent modulation of the latter, as suggested by previous work (Chung et al., 2017).

An intriguing finding of our study is the decrease in the number of centralized nuclei in KO-AOX versus KO muscle fibers. Centralized nuclei are a primary sign of muscle regeneration (Yin et al., 2013). During muscle regeneration, satellite cells, which constitute the resident pool of stem cells in skeletal muscle, undergo a process of activation, characterized by proliferation and migration to the site of damage, where they differentiate into myocytes and eventually fuse with the existing myofibers. Specific transcription factors are expressed during this process, including *Pax7*, *MyoD*, and *Myogenin*. Our data suggest that ROS influence this pathway, similar to what is observed in other populations of stem cells. Myogenic differentiation is associated with high ROS levels, mainly due to the concomitant induction of mitochondrial biogenesis (L'honoré et al., 2014). Antioxidant defenses are activated at the same time to prevent cellular damage (Latella and Puri, 2014). The decreased number of centralized nuclei and reduced PAX7- and MYOD-positive nuclei in KO-AOX muscles indicate that satellite cells are present but cannot differentiate into myotubes, thus impairing the capacity for repair/regeneration of the myofibers. This effect is likely to have an important role in the observed worsening of the phenotype in KO-AOX mice.

The majority of ongoing clinical trials for mitochondrial diseases are based on the use of antioxidants, stemming from the assumption that excessive ROS production causes oxidative damage to cellular components. However, there has hitherto been only a minimal investigation of the extent of ROS production and oxidative damage in mitochondrial diseases *in vivo*, and the available data are contradictory. For instance, in the mutator mouse (Trifunovic et al., 2004), no signs of oxidative damage have been detected in post-mitotic tissues (Trifunovic et al., 2005), while extensive ROS damage has been shown in replicating cells (Hamalainen et al., 2015). Our data using both AOX and NAC highlight a potential risk associated with antioxidant use, of interfering with compensatory ROS signaling, at least in mitochondrial myopathies. This observation is in agreement with previous reports showing that antioxidants can have deleterious effects on pluripotent stem cells with impaired mitochondrial function (Hamalainen et al., 2015). However, it should be noted that NAC and AOX act on redox homeostasis through different mechanisms, as AOX prevents excess ROS production by increasing electron flow along the respiratory chain and is expressed transgenically throughout embryonic development, while NAC, a glutathione precursor, was administered shortly after weaning, thus explaining the observed differences in their survival curves.

In our model, COX deficiency leads to accumulation of the reduced form of CoQ, and thus to excess production of superoxide anion via RET. By re-activating the electron flow along the respiratory chain, AOX normalizes the CoQ pool and abolishes the increases in RET and ROS production. Our data indicate that this effect, in turn, precludes the activation of a number of

(E) ATP synthesis flux in skeletal muscle mitochondria in the presence of cI-linked substrates (pyruvate, malate, glutamate) + ADP or cII-linked substrate (succinate, rotenone) + ADP (n = 4).

(F) ATP content in frozen skeletal muscle samples (n = 6–8).

(G) Analysis of mitochondrial membrane potential using safranin in isolated skeletal muscle mitochondria (n = 4).

All experiments were performed on 8-week-old mice. Bars represent means ± SEM. Asterisks over the bars indicate statistical significance versus WT; over the brackets among indicated groups. *$p \leq 0.05$; **$p \leq 0.01$; ***$p \leq 0.001$; ****$p < 0.0001$; unpaired Student's t test.

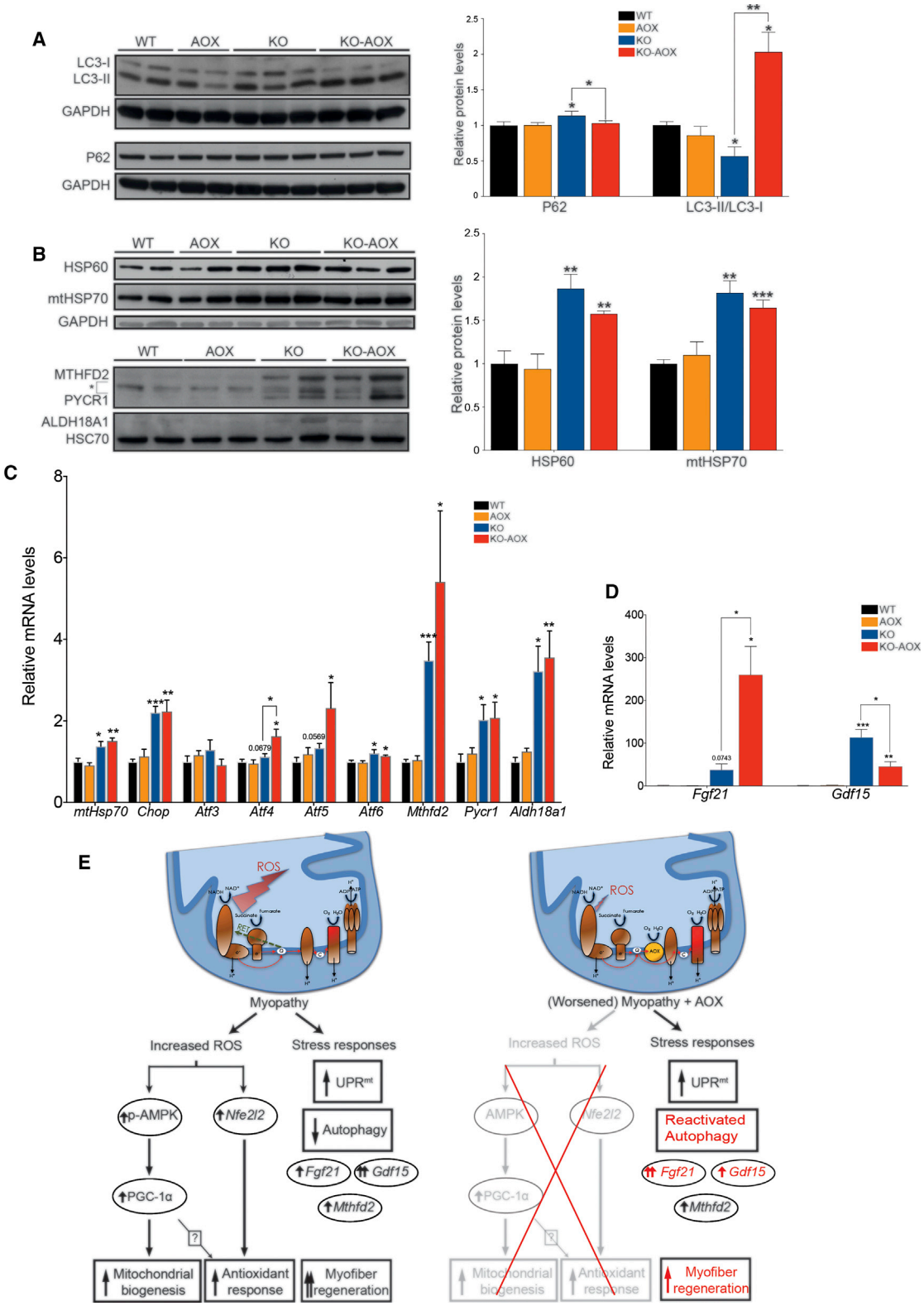

Figure 6. Mitochondrial Stress Responses Are Upregulated Regardless of AOX Expression, Except for Autophagy

(A) Western blots and quantification (n = 10) of autophagy markers (P62, LC3-I, and -II).

(B) Western blots and quantification (n = 10) of proteins involved in UPR^{mt} (HSP60 and mtHSP70) and mitochondrial metabolism (MTHFD2, PYCR1, and ALDH18A1). *Unspecific protein.

(legend continued on next page)

transcriptional response pathways and networks, as confirmed by real-time PCR data. Thus, AOX (or antioxidants) can block the homeostatic response to bioenergetic failure, exacerbating the pathological phenotype.

Our data do not rule out the possibility that AOX may be beneficial in other conditions affecting different organs and/or due to different mutations, which impair the activities of cIII and/or cIV or affect multiple respiratory complexes. It is also worth noting that not all mitochondrial diseases are associated with increased mitochondrial biogenesis. In addition, ROS produced at different sites may have different impact on whether their signaling or toxic role prevails (Sanz, 2016). In particular, it has recently been shown that ROS produced selectively via RET increases lifespan in *Drosophila*, whereas an opposite effect is observed when RET is prevented by increasing CoQ oxidation via AOX expression (Scialò et al., 2016), suggesting that over-reduction of CoQ generates an ROS signal important for homeostasis via RET. Along the same lines, we showed here that the accumulation of over-reduced CoQ increases ROS production via RET, triggering complex transcriptional cascades, which control mitochondria-related pathways to alleviate the pathology. Our findings thus have important consequences for the future treatment of mitochondrial disorders.

Limitations of the Study

Our work is limited to a single antioxidant compound in a single COX-defective myopathy. Antioxidants are widely used in the therapy of mitochondrial diseases and, although there is weak evidence of their efficacy, toxicity is usually not a major concern. We cannot exclude that in conditions associated with cIII or cIV deficiency in which ROS overproduction plays a major pathogenic role, the introduction of AOX may be beneficial.

STAR★METHODS

Detailed methods are provided in the online version of this paper and include the following:

- KEY RESOURCES TABLE
- CONTACT FOR REAGENT AND RESOURCE SHARING
- EXPERIMENTAL MODEL AND SUBJECT DETAILS
- METHOD DETAILS
  - Histochemistry, Immunofluorescence and Imaging
  - Analysis of Mitochondrial Enzyme Activities
  - Analysis of Body Composition
  - Real-Time Quantitative Polymerase Chain Reaction
  - Western Blot Analysis
  - Mitochondria Isolation and H_2O_2 Production
  - Mitochondrial Aconitase Activity
  - QH_2/Q Measurements
  - Measurement of ATP Synthesis Flux and ATP Content
  - Mitochondrial Membrane Potential Measurement
- QUANTIFICATION AND STATISTICAL ANALYSIS

SUPPLEMENTAL INFORMATION

Supplemental Information includes five figures and one table and can be found with this article online at https://doi.org/10.1016/j.cmet.2018.07.012.

ACKNOWLEDGMENTS

The authors wish to thank Ana Belen Cortes for technical assistance and Prof. Anthony Moore, University of Sussex, for helpful discussion. This work was supported by MRC-QQR Grant 2015-2020 (M.Z.), ERC Advanced Grants ERC FP7-322424 (M.Z.) and 232738 (H.T.J.), NRJ-Institut de France (M.Z.), and Academy of Finland grants 272376 and 256615 (H.T.J.). S.A.D. was supported by an EMBO Long-Term Fellowship (ALTF 856-2014) and EU (LTFCOFUND2013, GA-2013-609409). We are grateful to the personnel at ARES and Phenomics Animal Care Facilities for the support in managing our colonies. The BF-F3, SC-71, and BA-F8 monoclonal antibodies developed by Prof. Stefano Schiaffino, University of Padova, Italy, were obtained from the Developmental Studies Hybridoma Bank; created by the NICHD of the NIH; and maintained at The University of Iowa, Department of Biology, Iowa City, IA 52242.

AUTHOR CONTRIBUTIONS

S.A.D. performed all the experiments except histochemical and morphometric analyses (by R.C. and C.B.) and QH_2/Q measurements (by G.B.-C.). The study was conceived, planned, and supervised by C.V., H.T.J., M.S., and M.Z. All authors contributed to writing and commenting on the manuscript.

DECLARATION OF INTERESTS

The authors declare no competing interests.

Received: February 9, 2018
Revised: May 18, 2018
Accepted: July 18, 2018
Published: August 16, 2018

REFERENCES

Brand, M. (2016). Mitochondrial generation of superoxide and hydrogen peroxide as the source of mitochondrial redox signaling. Free Radic. Biol. Med. *100*, 14–31.

Bugiani, M., Invernizzi, F., Alberio, S., Briem, E., Lamantea, E., Carrara, F., Moroni, I., Farina, L., Spada, M., Donati, M.A., et al. (2004). Clinical and molecular findings in children with complex I deficiency. Biochim. Biophys. Acta *1659*, 136–147.

Chouchani, E., Pell, V., Gaude, E., Aksentijević, D., Sundier, S., Robb, E., Logan, A., Nadtochiy, S., Ord, E., Smith, A., et al. (2014). Ischaemic accumulation of succinate controls reperfusion injury through mitochondrial ROS. Nature *515*, 431–435.

Chowdhury, S., Djordjevic, J., Albensi, B., and Fernyhough, P. (2015). Simultaneous evaluation of substrate-dependent oxygen consumption rates

(C and D) Relative expression levels of mitochondrial stress response transcripts (n = 6). Results represent fold increase compared with WT that was normalized to 1.

(E) Proposed model for activation of mitochondrial biogenesis and different stress responses in *Cox15*$^{sm/sm}$ skeletal muscle. AOX expression worsens the myopathy. Some stress responses, emphasized in red, show differences compared with KO mice. The arrows correspond to the levels of induction of the specified markers (one arrow, moderate increase; two arrows, considerable increase).

Western blot were performed on skeletal muscle homogenates of 8-week-old mice. GAPDH and HSC70 were used as loading controls. Bars represent means ± SEM. Asterisks/p values over the bars indicate statistical significance versus WT; over the brackets among indicated groups. *$p \leq 0.05$; **$p \leq 0.01$; ***$p \leq 0.001$; unpaired Student's t test.

and mitochondrial membrane potential by TMRM and safranin in cortical mitochondria. Biosci. Rep. *36*, e00286.

Chung, H.K., Ryu, D., Kim, K.S., Chang, J.Y., Kim, Y.K., Yi, H.S., Kang, S.G., Choi, M.J., Lee, S.E., Jung, S.B., et al. (2017). Growth differentiation factor 15 is a myomitokine governing systemic energy homeostasis. J. Cell Biol. *216*, 149–165.

Dogan, S., Pujol, C., Maiti, P., Kukat, A., Wang, S., Hermans, S., Senft, K., Wibom, R., Rugarli, E., and Trifunovic, A. (2014). Tissue-specific loss of DARS2 activates stress responses independently of respiratory chain deficiency in the heart. Cell Metab. *19*, 458–469.

Dry, I.B., Moore, A.L., Day, D.A., and Wiskich, J.T. (1989). Regulation of alternative pathway activity in plant mitochondria: nonlinear relationship between electron flux and the redox poise of the quinone pool. Arch. Biochem. Biophys. *273*, 148–157.

El-Khoury, R., Kemppainen, K., Dufour, E., Szibor, M., Jacobs, H., and Rustin, P. (2014). Engineering the alternative oxidase gene to better understand and counteract mitochondrial defects: state of the art and perspectives. Br. J. Pharmacol. *171*, 2243–2249.

Fernandez-Marcos, P., Jeninga, E., Canto, C., Harach, T., de Boer, V., Andreux, P., Moullan, N., Pirinen, E., Yamamoto, H., Houten, S., et al. (2012). Muscle or liver-specific Sirt3 deficiency induces hyperacetylation of mitochondrial proteins without affecting global metabolic homeostasis. Sci. Rep. *2*, 425.

Fiorese, C., Schulz, A., Lin, Y., Rosin, N., Pellegrino, M., and Haynes, C. (2016). The transcription factor ATF5 mediates a mammalian mitochondrial UPR. Curr. Biol. *26*, 2037–2043.

Frezza, C., Cipolat, S., and Scorrano, L. (2007). Organelle isolation: functional mitochondria from mouse liver, muscle and cultured fibroblasts. Nat. Protoc. *2*, 287–295.

Guarás, A., Perales-Clemente, E., Calvo, E., Acín-Pérez, R., Loureiro-Lopez, M., Pujol, C., Martínez-Carrascoso, I., Nuñez, E., García-Marqués, F., Rodríguez-Hernández, M., et al. (2016). The CoQH2/CoQ ratio serves as a sensor of respiratory chain efficiency. Cell Rep. *15*, 197–209.

Hamalainen, R.H., Ahlqvist, K.J., Ellonen, P., Lepisto, M., Logan, A., Otonkoski, T., Murphy, M.P., and Suomalainen, A. (2015). mtDNA mutagenesis disrupts pluripotent stem cell function by altering redox signaling. Cell Rep. *11*, 1614–1624.

Holmström, K., and Finkel, T. (2014). Cellular mechanisms and physiological consequences of redox-dependent signalling. Nat. Rev. Mol. Cell Biol. *15*, 411–421.

Horn, A., Van der Meulen, J.H., Defour, A., Hogarth, M., Sreetama, S.C., Reed, A., Scheffer, L., Chandel, N.S., and Jaiswal, J.K. (2017). Mitochondrial redox signaling enables repair of injured skeletal muscle cells. Sci. Signal. *10*, https://doi.org/10.1126/scisignal.aaj1978.

Khan, N.A., Nikkanen, J., Yatsuga, S., Jackson, C., Wang, L., Pradhan, S., Kivela, R., Pessia, A., Velagapudi, V., and Suomalainen, A. (2017). mTORC1 regulates mitochondrial integrated stress response and mitochondrial myopathy progression. Cell Metab. *26*, 419–428.e5.

Krumschnabel, G., Fontana-Ayoub, M., Sumbalova, Z., Heidler, J., Gauper, K., Fasching, M., and Gnaiger, E. (2015). Simultaneous high-resolution measurement of mitochondrial respiration and hydrogen peroxide production. Methods Mol. Biol. *1264*, 245–261.

Kuhl, I., Miranda, M., Posse, V., Milenkovic, D., Mourier, A., Siira, S.J., Bonekamp, N.A., Neumann, U., Filipovska, A., Polosa, P.L., et al. (2016). POLRMT regulates the switch between replication primer formation and gene expression of mammalian mtDNA. Sci. Adv. *2*, e1600963.

L'honoré, A., Commère, P., Ouimette, J., Montarras, D., Drouin, J., and Buckingham, M. (2014). Redox regulation by Pitx2 and Pitx3 is critical for fetal myogenesis. Dev. Cell *29*, 392–405.

Latella, L., and Puri, P. (2014). Redox or death: checking on fetal myogenesis. Dev. Cell *29*, 373–374.

Lehtonen, J.M., Forsstrom, S., Bottani, E., Viscomi, C., Baris, O.R., Isoniemi, H., Hockerstedt, K., Osterlund, P., Hurme, M., Jylhava, J., et al. (2016). FGF21 is a biomarker for mitochondrial translation and mtDNA maintenance disorders. Neurology *87*, 2290–2299.

Lin, S., and Hardie, D. (2017). AMPK: sensing glucose as well as cellular energy status. Cell Metab. *27*, 299–313.

Melber, A., and Haynes, C.M. (2018). UPR(mt) regulation and output: a stress response mediated by mitochondrial-nuclear communication. Cell Res. *28*, 281–295.

Mills, E.L., Kelly, B., Logan, A., Costa, A.S.H., Varma, M., Bryant, C.E., Tourlomousis, P., Dabritz, J.H.M., Gottlieb, E., Latorre, I., et al. (2016). Succinate dehydrogenase supports metabolic repurposing of mitochondria to drive inflammatory macrophages. Cell *167*, 457–470.e13.

Morita, M., Gravel, S.P., Chenard, V., Sikstrom, K., Zheng, L., Alain, T., Gandin, V., Avizonis, D., Arguello, M., Zakaria, C., et al. (2013). mTORC1 controls mitochondrial activity and biogenesis through 4E-BP-dependent translational regulation. Cell Metab. *18*, 698–711.

Mourier, A., Motori, E., Brandt, T., Lagouge, M., Atanassov, I., Galinier, A., Rappl, G., Brodesser, S., Hultenby, K., Dieterich, C., et al. (2015). Mitofusin 2 is required to maintain mitochondrial coenzyme Q levels. J. Cell Biol. *208*, 429–442.

Peralta, S., Garcia, S., Yin, H., Arguello, T., Diaz, F., and Moraes, C. (2016). Sustained AMPK activation improves muscle function in a mitochondrial myopathy mouse model by promoting muscle fiber regeneration. Hum. Mol. Genet. *25*, 3178–3191.

Quirós, P., Mottis, A., and Auwerx, J. (2016). Mitonuclear communication in homeostasis and stress. Nat. Rev. Mol. Cell Biol. *17*, 213–226.

Rabinovitch, R., Samborska, B., Faubert, B., Ma, E., Gravel, S., Andrzejewski, S., Raissi, T., Pause, A., St-Pierre, J., and Jones, R. (2017). AMPK maintains cellular metabolic homeostasis through regulation of mitochondrial reactive oxygen species. Cell Rep. *21*, 1–9.

Reczek, C.R., and Chandel, N.S. (2015). ROS-dependent signal transduction. Curr. Opin. Cell Biol. *33*, 8–13.

Rodríguez-Aguilera, J., Cortés, A., Fernández-Ayala, D., and Navas, P. (2017). Biochemical assessment of coenzyme Q10 deficiency. J. Clin. Med. *6*, https://doi.org/10.3390/jcm6030027.

Sanz, A. (2016). Mitochondrial reactive oxygen species: do they extend or shorten animal lifespan. Biochim. Biophys. Acta *1857*, 1116–1126.

Schindelin, J., Arganda-Carreras, I., Frise, E., Kaynig, V., Longair, M., Pietzsch, T., Preibisch, S., Rueden, C., Saalfeld, S., Schmid, B., et al. (2012). Fiji: an open-source platform for biological-image analysis. Nat. Methods *9*, 676–682.

Scialò, F., Sriram, A., Fernández-Ayala, D., Gubina, N., Lõhmus, M., Nelson, G., Logan, A., Cooper, H., Navas, P., Enríquez, J., et al. (2016). Mitochondrial ROS produced via reverse electron transport extend animal lifespan. Cell Metab. *23*, 725–734.

Seiferling, D., Szczepanowska, K., Becker, C., Senft, K., Hermans, S., Maiti, P., Konig, T., Kukat, A., and Trifunovic, A. (2016). Loss of CLPP alleviates mitochondrial cardiomyopathy without affecting the mammalian UPRmt. EMBO Rep. *17*, 953–964.

Shao, D., Oka, S., Liu, T., Zhai, P., Ago, T., Sciarretta, S., Li, H., and Sadoshima, J. (2014). A redox-dependent mechanism for regulation of AMPK activation by Thioredoxin1 during energy starvation. Cell Metab. *19*, 232–245.

Shpilka, T., and Haynes, C. (2017). The mitochondrial UPR: mechanisms, physiological functions and implications in ageing. Nat. Rev. Mol. Cell Biol. *19*, 109–120.

Szibor, M., Dhandapani, P., Dufour, E., Holmström, K., Zhuang, Y., Salwig, I., Wittig, I., Heidler, J., Gizatullina, Z., Gainutdinov, T., et al. (2016). Broad AOX expression in a genetically tractable mouse model does not disturb normal physiology. Dis. Model. Mech. *10*, 163–171.

Trifunovic, A., Hansson, A., Wredenberg, A., Rovio, A., Dufour, E., Khvorostov, I., Spelbrink, J., Wibom, R., Jacobs, H., and Larsson, N. (2005). Somatic mtDNA mutations cause aging phenotypes without affecting reactive oxygen species production. Proc. Natl. Acad. Sci. USA *102*, 17993–17998.

Trifunovic, A., Wredenberg, A., Falkenberg, M., Spelbrink, J., Rovio, A., Bruder, C., Bohlooly-Y, M., Gidlöf, S., Oldfors, A., Wibom, R., et al. (2004). Premature ageing in mice expressing defective mitochondrial DNA polymerase. Nature *429*, 417–423.

Viscomi, C., Bottani, E., Civiletto, G., Cerutti, R., Moggio, M., Fagiolari, G., Schon, E., Lamperti, C., and Zeviani, M. (2011). In vivo correction of COX deficiency by activation of the AMPK/PGC-1α axis. Cell Metab. *14*, 80–90.

Viscomi, C., Burlina, A., Dweikat, I., Savoiardo, M., Lamperti, C., Hildebrandt, T., Tiranti, V., and Zeviani, M. (2010). Combined treatment with oral metronidazole and N-acetylcysteine is effective in ethylmalonic encephalopathy. Nat. Med. *16*, 869–871.

Yin, H., Price, F., and Rudnicki, M. (2013). Satellite cells and the muscle stem cell niche. Physiol. Rev. *93*, 23–67.

Yun, J., and Finkel, T. (2014). Mitohormesis. Cell Metab. *19*, 757–766.

8 Danksagung

Zuerst möchte ich Herrn Professor Jürgen Holtz danken, der mich ermuntert hat, eine wissenschaftliche Laufbahn einzuschlagen. Ohne ihn wäre mein Leben mit Sicherheit in ruhigeren Bahnen verlaufen. Vielen Dank auch an Herrn Professor Thomas Braun, bei dem ich lernen durfte, sehr komplexe Fragestellungen mithilfe genetischer Modelle zu untersuchen. Insbesondere die Generierung der AOX-Maus sollte meinen wissenschaftlichen Werdegang nachhaltig verändern. Meinem langjährigen Chef, Herrn Professor Howy Jacobs, danke ich für den nicht-endenden Strom an Ideen und für die Anleitung (oder vielleicht besser Aufforderung) stets außerhalb eingefahrener Muster zu denken. Meinen Dank richte ich auch an Herrn Professor Klaus-Dieter Schlüter. Ohne seine Unterstützung, seine kollegiale Art, sein positives Denken und seine Geduld mit mir wäre diese Arbeit nie vollendet worden.

Den verschiedenen Arbeitsgruppen mit denen ich arbeiten durfte, meinen engagierten Kooperationspartnern und Freunden in Wissenschaft, Wirtschaft und Freizeit danke ich für die vielen Anregungen, den kritischen Austausch, die Blickwinkel von außen und die enorme wissenschaftliche Expertise, die ich dadurch nutzen konnte.

Meinen lieben Eltern Karin und Günter Szibor gilt mein Dank für ihre fortwährende Unterstützung bei allen Wendungen, die mein Leben genommen hat. Ihr habt mir alle Möglichkeiten zur Entwicklung gegeben und Steine aus dem Weg geräumt, wo immer sie meinen Weg blockierten. Das gilt auch für meine Geschwister Barbara, Ursula und Florian und ihren inzwischen erwachsenen Großfamilien.

Mein ganz besonderer Dank gilt meiner lieben Ehefrau Annett Szibor sowie unseren großartigen Töchtern Martha, Greta und Frida. Es war sicherlich nicht immer leicht mit mir. Es hätte aber auch wesentlich schlimmer kommen können. Danke, dass es Euch gibt.

9 Ehrenwörtliche Erklärung

Hiermit erkläre ich, dass ich die vorliegende Arbeit bzw. die mir zuzuordnenden Teile im Rahmen einer kumulativen Habilitationsschrift, selbstständig und ohne unzulässige Hilfe oder Benutzung anderer als der angegebenen Hilfsmittel angefertigt habe. Alle Textstellen, die wörtlich oder sinngemäß aus veröffentlichten oder nichtveröffentlichten Schriften entnommen sind, und alle Angaben, die auf mündlichen Auskünften beruhen, sind als solche kenntlich gemacht. Ich versichere, dass ich für die nach §2 (3) der Habilitationsordnung angeführten bereits veröffentlichten Originalarbeiten als Erst-oder Seniorautor fungiere, da ich den größten Teil der Daten selbst erhoben habe, für das Design der Arbeiten verantwortlich bin und die Manuskripte maßgeblich gestaltet habe. Für alle von mir erwähnten Untersuchungen habe ich die in der „Satzung der Justus-Liebig-Universität zur Sicherung guter wissenschaftlicher Praxis" niedergelegten Grundsätze befolgt. Ich versichere, dass alle an der Finanzierung der Arbeiten beteiligten Geldgeber in den jeweiligen Publikationen genannt worden sind. Ich versichere außerdem, dass die vorgelegte Arbeit weder im Inland noch im Ausland in gleicher oder ähnlicher Weise einer anderen Prüfungsbehörde vorgelegt wurde oder Gegenstand eines anderen Prüfungsverfahrens war. Mit der Überprüfung meiner Arbeit durch eine Plagiatserkennungssoftware bzw. ein internetbasiertes Softwareprogramm erkläre ich mich einverstanden.

Jena, 8. Dezember 2021

Dr. med. Marten Szibor